UNIVERSITY OF THESSALY

SCHOOL OF ENGINEERING

DEPARTMENT OF MECHANICAL ENGINEERING

MEng Thesis

FAILURE DIAGNOSTICS AND RECYCLING OF METAL AIR BATTERIES

by

ANDREAS DIONYSOPOULOS

Supervisor

Prof. Panagiotis Tsiakaras

Submitted in partial fulfillment of the requirements for the degree of Master of Science in Mechanical Engineering at the University of Thessaly

Volos, September 2023

i

ΠΟΛΥΤΕΧΝΙΚΗ ΣΧΟΛΗ

ΤΜΗΜΑ ΜΗΧΑΝΟΛΟΓΩΝ ΜΗΧΑΝΙΚΩΝ

Διπλωματική Εργασία

ΔΙΑΓΝΩΣΗ ΒΛΑΒΩΝ ΚΑΙ ΑΝΑΚΥΚΛΩΣΗ ΤΩΝ ΜΠΑΤΑΡΙΩΝ

ΜΕΤΑΛΛΟΥ ΑΕΡΑ

υπό

ΑΝΔΡΕΑΣ ΔΙΟΝΥΣΟΠΟΥΛΟΣ

Επιβλέπων

Καθ. Παναγιώτης Τσιακάρας

Υπεβλήθη για την εκπλήρωση μέρους των απαιτήσεων για την απόκτηση του Μεταπτυχιακού

Διπλώματος Μηχανολόγων Μηχανικών του Πανεπιστημίου Θεσσαλίας

Βόλος, Σεπτέμβριος 2023

Approved by the Committee on Final Examination:

Advisor   Dr. Panagiotis Tsiakaras

                                           Professor

                                           Department of Mechanical Engineering

                                           University of Thessaly

Member   Dr. Athanasios Papathanasiou

                                           Professor

                                           Department of Mechanical Engineering

                                           University of Thessaly

Member   Dr. Angeliki Brouzgou

                                           Assistant Professor

                                           Department of Energy Systems

                                           University of Thessaly

Acknowledgements

I would like to express my deepest gratitude to my supervisor Professor Panagiotis Tsiakaras. His patience, support, guidance and overall insights, helped me complete this thesis and made this a unique experience for me.

I am also grateful to Professor Athanasios Papathanasiou and Assistant Professor Angeliki Brouzgou, both members of the Examination Committee, who generously provided knowledge and expertise. I feel that I could not have undertaken this journey without their feedback. In addition, I would like to extend my sincere thanks to the University of Thessaly for providing me with the opportunity to join the extremely topical MSc program "Analysis and Management of Energy Systems", through which I had the pleasure of collaborating with highly educated Professors, who have both academic and technical expertise.

Lastly, I would be remiss if I did not thank my wife Kyriaki, my children and my parents Spyros and Panagiota for their patience, unconditional support and encouragement, elements which contributed to the completion of my postgraduate studies. Therefore, this thesis is dedicated to them.

Ευχαριστίες

Θα ήθελα να εκφράσω την βαθύτατη ευγνωμοσύνη μου στον επιβλέποντα Καθηγητή κ. Παναγιώτη Τσιακάρα. Η υπομονή του, η υποστήριξή του, η καθοδήγησή του και οι γενικές του γνώσεις, με βοήθησαν να ολοκληρώσω την παρούσα διπλωματική εργασία, η οποία αποτέλεσε, για εμένα, μία μοναδική εμπειρία.

Είμαι, επίσης, ευγνώμων στον Καθηγητή κ. Αθανάσιο Παπαθανασίου και την Επίκουρη Καθηγήτρια κα. Αγγελική Μπρούζγου, αμφότεροι μέλη της Εξεταστικής Επιτροπής, που γενναιόδωρα παρείχαν γνώσεις και τεχνογνωσία. Αισθάνομαι ότι δεν θα μπορούσα να επιχειρήσω αυτό το ταξίδι, χωρίς τις υποδείξεις τους. Επιπλέον, θα ήθελα να εκφράσω τις ειλικρινείς μου ευχαριστίες στο Πανεπιστήμιο Θεσσαλίας, το οποίο, μου έδωσε την ευκαιρία να συμμετάσχω στο, εξαιρετικά επίκαιρο, μεταπτυχιακό πρόγραμμα «Ανάλυση και Διαχείριση Ενεργειακών Συστημάτων», μέσω του οποίου είχα τη χαρά να συνεργαστώ με Καθηγητές υψηλής μόρφωσης, οι οποίοι διαθέτουν, τόσο ακαδημαϊκή, όσο και τεχνική εμπειρία.

Τέλος, θα ήταν παράλειψη, αν δεν ευχαριστούσα τη σύζυγό μου Κυριακή, τα παιδιά μου και τους γονείς μου Σπύρο και Παναγιώτα, για την υπομονή τους, την άνευ όρων υποστήριξη και ενθάρρυνσή τους, στοιχεία τα οποία συνετέλεσαν στην ολοκλήρωση των μεταπτυχιακών μου σπουδών. Ως εκ τούτου, η παρούσα διπλωματική εργασία αφιερώνεται σε αυτούς.

Abstract

Metal air batteries have attached extensive interests, as they are considered one of the most promising next - generation electrochemical energy storage devices that have the potential to drastically increase the power density and decrease the cost of energy storage. Nevertheless, metal air batteries are complex systems that have numerous scientific and technical problems, such as the kinetics of redox mediators (a specific type of electrolyte additives) for oxygen reduction reactions, desolution of CO_2 , H_2O, etc from the air, high overpotentials and related side reactions on both anode and cathode. Problems also encountered with their electrolyte. These challenges should have to be properly addressed before metal air batteries be produced and deployed on a large scale.

Considering the rapid development and evolution of technology, this thesis summarizes the environmental consequences of energy production and emerging issues of this field. In addition, a variety of electrochemical devices for energy storage and conversion are mentioned. Technical characteristics of metal air batteries, their main materials and components, the operating principle and their applications are also covered. Furthermore, the challenges facing their commercialization, failures that occur, diagnostics and the proposed solutions are highlighted. Future trends and prospects of metal air batteries, the general technical issues confronting their developments and perspective on possible solutions are also discussed.

Finally, life cycle and recycling methods of metal air batteries are overviewed, focusing on benefits and drawbacks.

Περίληψη

Οι μπαταρίες μετάλλου αέρα έχουν προσελκύσει ευρέως το ενδιαφέρον, καθώς θεωρούνται από τις πιο υποσχόμενες ηλεκτροχημικές συσκευές αποθήκευσης ενέργειας, επόμενης γενιάς, οι οποίες έχουν τη δυνατότητα να αυξήσουν δραστικά την πυκνότητα ισχύος και να μειώσουν το κόστος αποθήκευσης ενέργειας. Ωστόσο, οι μπαταρίες μετάλλου αέρα είναι πολύπλοκα συστήματα που έχουν πολυάριθμα επιστημονικά και τεχνικά προβλήματα, όπως η κινητική των οξειδοαναγωγικών μεσολαβητών (ένας συγκεκριμένος τύπος πρόσθετων ηλεκτρολύτη) για αντιδράσεις αναγωγής οξυγόνου, διάλυση του CO_2, H_2O κλπ. από τον αέρα, υψηλές υπερτάσεις και σχετικές παράπλευρες αντιδράσεις, τόσο στην άνοδο, όσο και στην κάθοδο. Προβλήματα, επίσης, παρουσιάζονται και με τον ηλεκτρολύτη τους. Αυτές οι προκλήσεις θα πρέπει να αντιμετωπιστούν κατάλληλα, προτού οι μπαταρίες μετάλλου αέρα κατασκευαστούν και αναπτυχθούν σε μεγάλη κλίμακα.

Λαμβάνοντας υπόψη τη ραγδαία ανάπτυξη και εξέλιξη της τεχνολογίας, η παρούσα διατριβή συνοψίζει τις περιβαλλοντικές συνέπειες της παραγωγής ενέργειας και τα αναδυόμενα ζητήματα αυτού του τομέα. Επιπροσθέτως, γίνεται αναφορά σε μια ποικιλία ηλεκτροχημικών συσκευών αποθήκευσης και μετατροπής ενέργειας. Καλύπτονται επίσης, τα τεχνικά χαρακτηριστικά των μπαταριών μετάλλου αέρα, τα κύρια υλικά και εξαρτήματά τους, η αρχή λειτουργίας και οι εφαρμογές τους. Επιπλέον, επισημαίνονται οι προκλήσεις που αντιμετωπίζει η εμπορευματοποίησή τους, οι αστοχίες που προκύπτουν, η διάγνωση και οι προτεινόμενες λύσεις. Συζητούνται επίσης, οι μελλοντικές τάσεις και οι προοπτικές των μπαταριών μετάλλου αέρα, τα γενικά τεχνικά ζητήματα που προκύπτουν από την εξέλιξή τους και η προοπτική για πιθανές λύσεις.

Τέλος, εξετάζονται ο κύκλος ζωής και οι μέθοδοι ανακύκλωσης των μπαταριών μετάλλου αέρα, δίνοντας έμφαση στα οφέλη και τα μειονεκτήματα.

CONTENTS

CHAPTER 6

LIST OF TABLES

LIST OF FIGURES

7

CHAPTER 1

Introduction

Nowadays, energy is the power engine that sustains the operation of our society. In the energy field, we are confronted with a daunting challenge caused by the gradual depletion of fossil fuel. Renewable energies such as solar and wind have been developed in order a safe and sustainable energy supply to be secured. However, there is a geographical limitation and intermittent of these energies, thus calling for reliable Electrical Energy Storage (EES) to stabilize and make efficient power delivery [1].

It was Alessandro Volta who first invented the battery, although - even earlier - the first experiments had been conducted by Benjamin franklin in 1749. Finally, it was in 1890 that the first Pumped Hydro Storage facilities (PHS) were built in Italy and Switzerland. Their first intended use was to generate power and to improve the managing of the water resources. PHS facilities were mostly built in the 1960s, where they supported the rollout of nuclear power plants [2].

These days the role of energy storage is becoming crucial for the energy system [2]. There has been an increased focus on energy storage by both researchers and politicians, as the awareness of the environmental impacts that come with relying on fossil commodities and the reliability and long-term durability of electricity networks increases across the globe. Energy storage can aid in resolving the matter of intermittency related to wind and solar power. In some cases, this can react immediately to essential demand changes, allowing the grid to respond more rapidly and reducing the need to implement backup power plants [3].

Meanwhile, the development of reliable EES system has been a task of urgency, because of the increasing number of transportation vehicle. Among various EES systems, the ones that are the most promising to meet the needs, are rechargeable batteries and that is because of their high energy density and high energy efficiency [4]. Above all, the ones whose operation on the basis of intercalation mechanism has played an important role in our society in the past two decades, is the Lithium-Ion Batteries (LIBs) [5]. Nevertheless, the low energy density of LIBs was a restriction of being applied as the energy supplier of the generation to come. On this basis, there has been provided a solution by the development of Metal-Air Batteries (MABs) from their higher energy theoretically density than that of LIBs [1].

Undoubtedly, in order to develop electrode materials, electrolytes, and separators for energy storage devices, there has been made tremendous efforts, so as to meet the needs of emerging technologies such as electric vehicles, decarbonized electricity, and electrochemical energy storage. Nevertheless, the sustainability concerns of LIBs and following generation rechargeable batteries have received little consideration. Recycling plays a vital role in the overall sustainability of future batteries and is affected by battery features including environmental hazards. For that reason, recycling should be taken into account when developing battery systems [6]. Moreover, with little profit to be reaped from recycling, governments should step in regulations to save the environment from the toxic effects of used batteries.

In chapter 2, environmental implications and consequences of energy sources will be described. The environmental impacts of metal-air batteries will also be mentioned.

In chapter 3, life cycle assessment of lithium-air battery cells will be discussed.

In chapter 4, general points of electrochemistry will be mentioned and there will be a description of electrochemical energy systems, mainly for energy storage and conversion.

In chapter 5, the principle operation of metal-air batteries will be mentioned. Battery chemistry, basic components of a typical battery and their importance in the operation of metal-air batteries are topics that will be analyzed. In addition, different ways of the performance improvement of electrode materials and their results will be covered.

In chapter 6, failures, diagnostics and future prospects of metal-air batteries will be stated.

In chapter 7, the recycling process will be examined and methods of recycling, will be mentioned.

In chapter 8, material design targets and strategies of metal-air batteries will be analyzed.

Finally, in chapter 9, conclusions and perspectives on the future development of metal-air batteries toward practical applications will be pointed out.

CHAPTER 2

Environmental implications and consequences of energy sources

2.1 Introduction

During the last twenty years, the risk and reality of environmental deterioration have become more obvious, because of a combination of several factors since there has been a dramatic growth of the environmental implications of human activities due to the sheer increase of world population, energy/consumption, industrial activity, etc. During the 1970s most environmental analysis and legal control instruments focused on conventional pollutants such as SO_2, NO_x, particulates, and CO. Lately, there is a great environmental concern extended to the control of micro - or hazardous air pollutants, which are often toxic chemical substances and harmful in small doses, as well as to that of globally significant pollutants such as CO_2. Except from advances in environmental science, developments in industrial processes and structures have led to new environmental issues. For instance, in the energy sector, major shifts to the road transport of industrial goods and to individual travel by cars has come to an increase in road traffic and hence a shift in the attention paid to the effects and sources of NO_x and volatile organic compound (VOC) emissions [7].

Given these situations, it can be highlighted that energy is one of the main factors that can be achieved by contributing many factors, such as the requirement for a supply of energy resources that is fully sustainable. Moreover, a secure supply of energy resources is demanded and widely agreed for its necessity [7].

It is widely noticed around our universe that there is a continuous increase in sharing power generation by intermitted Renewable Energy Sources (RES). Simply connecting RES to the power grid does not always indicate that all the generated clean electricity will - at last - be delivered to final consumers. The power grid, connecting generation and demand, is a complex system constructed by physical laws. A common characteristic of many power systems is that RES replace conventional technologies, which demands significant changes in the patterns of electricity flows through the grid [8].

2.2 Environmental implications of the electricity system

The Environmental Protection Agency (EPA) describes the ways non-renewable energy affect climate change and the environment.

- Emissions of greenhouse gases and other air pollutants, mostly when a fuel is burned.

- Water resources usage so as a steam can be produced, offering cooling and serve other functions.

- Discharges of pollution into water bodies, including thermal pollution (water that is hotter than the original / actual temperature of the water body).

- Generation of solid waste, possibly including hazardous waste.

- Land use for fuel production, power generation, power transmission and distribution lines.

- Consequences on plants, animals, and ecosystems that result from the air, water, waste, and land implications above.

Emphasizing particularly on the first point, almost 62 % of electricity derives from burning fossil fuels, mostly coal and natural gas. Greenhouse gas emissions are released into the atmosphere, due to the above burning, which traps heat that would normally escape into space and in turn, warms the planet. There is an increasingly heat of globe at a historical high rate, which affects virtually every aspect of life on Earth. Higher temperatures cause warmer climate, water supply is decreased, weather patterns are becoming more and more extreme, sea levels are rising all the time and our ecosystem damage is irreparable. Characteristically, some areas such as Russia will possibly face warmer temperatures. On the other hand, the Middle East will probably become hard to be resident [9].

2.3 Environmental implications of non-renewable energy sources

2.3.1 Introduction

Non-renewable energies, such as coal, oil and natural gas, are those that do not self-sustain naturally. On the contrary, renewable energy sources like wind, water and sun - most of which are converted to power cleanly - the conversion of fossil fuels to usable energy can result in harmful emissions and may disrupt local wildlife. The processing of fossil fuels emits harmful greenhouse gases into the air, such as carbon dioxide, damage the ozone layer which protects humanity from the sun's radiation. The air pollution also negatively affects our respiratory health. Acid rain, which is created by the emission of sulfur and other chemicals into the atmosphere, corrodes the machinery and can disrupt local ecosystems. Energy sources are categorized as non-renewable because they do not form or replenish in a short period of time. On the other hand, renewable energy sources such as solar and wind replenish naturally in a short period of time [10].

2.3.2 Greenhouse gas emissions

Probably the most well-known implication of using non-renewable energy sources is the emission of greenhouse gases, in particular CO_2 and methane, which contribute to climate change. Coal is considered the worst to emit the highest percentage of CO_2. Natural gas emits 15-20 % fewer heat-trapping gases compared to gasoline when used to power a vehicle and it also emits 50-60 % less CO_2 compared to coal [10].

The concerns about climate change and greenhouse gas emissions include direct impact of rising temperatures and changing weather patterns which affect human livelihoods as dry seasons or floods or dry seasons grow. Climate change is affecting ecosystems, diminishing their capacity to adapt to changing climates and threatening biodiversity and the serious ecosystem services.

2.3.3 Air pollution

Non-renewable energy sources are not just changing Earth's atmosphere by proliferating the amount of greenhouse gas emissions. Additionally, they emit an amount of pollutants that are affect people's health and the environment. When mercury is emitted into the air, it goes on to settle on the ground or blends with water, it accumulates on organisms such as fish, passing through the food chain [10].

This has deep effects on our biodiversity and creates real risks for people as researchers have found that exposure to mercury may lead to neurological and neuro-behavioral effects in embryos and young children. Other air pollutants emitted due to fossil fuel combustion include nitrogen oxides, Sulphur dioxide and particulate matter.

2.3.4 Acid rain and water pollution

Dangerous pollutants that are emitted into the air may usually follow the water cycle, for instance, acid rain which is created due to the emission of Sulphur and other chemicals into the atmosphere [10]. Rain becomes mildly acidic, is corrosive to machinery and can disrupt local ecosystems. In addition, acid rain changes the acidity of lakes and streams which can be very noxious to fish and other aquatic organisms. It could also be harmful to trees therefore weakening forest ecosystems.

2.4 Environmental implications of renewable energy sources

2.4.1 Introduction

Renewable energy will be a vital source for power generation in the following years, because we can use these resources repeatedly to produce useful energy. The energy

resources are usually divided to renewable and nuclear energy resources and fossil resources. Other renewable energy resources, like wind, solar, hydropower, biomass, ocean energy, geothermal, biofuel etc., provide 15-20 % of the total world's energy. Due to fast growing population, which leads to the use of the fossil fuels such as gas, coal and oil to satisfy the energy requirement, which creates unsustainable situations and greenhouse effect, depletion of fossil fuels, global warming, environmental and geographical conflicts and fluctuation in fuel prices. Renewable energy is considered to be a sustainable energy, supported from economic, social and environmental dimensions of society. Renewable energy resources are able to complete the world's energy demand, provide energy security and protect the environment. However some failings also exist such as the variation of output because of seasonal change, which is the common thing for wind and hydroelectric power plant. The main renewable energy sources with their usage in different form are presented in **Table 2.1** and it is expected that renewable energy will be one of the important sources for the future.

Table 2.1 Main renewable energy sources with their usage form [11].

Energy resource	Energy conversion and usage option
Hydropower	Power generation
Biomass	Heat and power generation, pyrolysis, gasification, digestion
Geothermal	Urban heating, power generation, hydrothermal, hot rock
Solar	Solar home system, solar dryers, solar cookers
Direct solar	Photovoltaic, thermal power generation, water heaters
Wind	Power generation, wind generators, windmills
Wave	Numerous designs
Tidal	Barrage, tidal stream

The world's renewable energy sources scenario by 2040 is estimated as given below in **Table 2.2**.

Table 2.2 Global renewable energy scenario by 2040 [11].

	2001	2010	2020	2030	2040
Total consumption (million tons equivalent)	10,038	10,549	11,425	12,352	13,310
Biomass	1080	1313	1791	2483	3271
Large hydro	22.7	266	309	341	358
Geothermal	43.7	86	186	333	493
Small hydro	9.5	19	49	106	189
Wind	4.7	44	266	542	688
Solar thermal	4.1	15	66	244	480
Photovoltaic	0.1	2	24	221	784
Solar thermal electricity	0.1	0.4	3	16	68
Marine (tidal/wave/ocean)	0.05	0.1	0.4	3	20
Total RES	1365,5	1745,5	2964,4	4289	6351
Renewable energy contribution source (%)	13.6	16.6	23.6	34.7	47.7

6

2.4.2 Wind power

Harnessing power from the wind is one of the cleanest and most sustainable ways to generate electricity since it does not produce global warming emissions or toxic pollution. In addition, wind is inexhaustible, abundant and affordable, which makes it a viable and large-scale alternative to fossil fuels [12].

There are also an amount of environmental implications associated with wind power generation that must be recognized and mitigated, such as land use issues and challenges to wildlife and habitat.

2.4.3 Solar power

As wind power, sun provides an exceptional resource for generating clean and sustainable electricity.

The environmental implications related with solar power may include land and water use and habitat loss and the use of dangerous materials in manufacturing, thus the types of implications vary greatly depending on the scale of the system and the technology used-photovoltaic (PV) solar cells or concentrating solar thermal plants (CSP) [12].

2.4.4 Geothermal energy

Enhanced geothermal systems (or hot dry rock geothermal), which involve drilling into the earth's surface to achieve deeper geothermal resources, may allow broader access to geothermal energy.

In addition, geothermal plants differ in terms of the technology they use to convert the resource to electricity, such as direct steam, flash, or binary and the type of cooling technology they use, like water-cooled and air-cooled. Environmental implications have differences depending on the conversion and cooling technology used [12].

2.4.5 Biomass for electricity

Biomass power plants involve the combustion of a feedstock to produce electricity. Hence, biomass plants raise similar, but not identical, concerns about air emissions and water use as fossil fuel plants. Nevertheless, the feedstock of biomass plants may be sustainable produced, while fossil fuels are non-renewable. Sources of biomass resources for generating electricity have differences, ranging from energy crops (like switchgrass), to agricultural waste, forest products, manure and waste, and urban waste [12].

2.4.6 Hydroelectric power

Hydroelectric power includes massive hydroelectric dams. It also includes small run-of-the-river plants. Large-scale hydroelectric dams are constantly being constructed in many places around the world.

2.4.7 Hydrokinetic energy

Hydrokinetic energy, which involves tidal and wave power, encompasses an array of energy technologies, many of which still remain in experimental researches. While actual implications of large-scale operations have not been observed, a range of potential implications may be projected.

2.5 Environmental implications of Metal-Air Batteries (MABs)

2.5.1 Introduction

Nowadays, lithium-ion batteries (LIBs) are the preferred commercial technology available to satisfy the demanded requirements [13]. Nevertheless, this technology presents a variety of limitations like cost and safety issues [14]. Even though LIBs have been around for a long time, this technology still has many disadvantages to overcome through different strategies [15, 16]. It will be a notable growth in the consumption of some certain materials such as cobalt, manganese and nickel, used in their cathode [17].

2.5.2 Environmental implications

The growth of sustainable energy storage systems is an inexcusable goal that scientist and industry must undertake, especially given the actual concerns over the depletion of non-renewable resources, battery waste management and global warming issues. These days, LIB technology still has environmental sustainability concerns, mainly arising from the use of highly toxic and scarce materials [18]. In the sustainable energy storage landscape, MABs provide environmental benefits originating from their high energy efficiency that is 5 - 30 times greater than conventional LIBs. Additionally, MABs rarely use Co, Mn, V, Ni, or graphite materials, and when they do, smaller quantities are required [19, 20]. These strategies can mitigate the pressures over the extraction of CRMs for the battery industry, which encompasses serious environmental pressures, as for instance, 1900 tons of H_2O (diverted from essential agricultural activities) are consumed by evaporation for the extraction of 1 Li tone [21]. Nevertheless, it should be considered that the catalysts in MABs are usually composed by noble metals subjected to supply chain bottlenecks and environmental concerns. Battery recycling is a reasonable

approach to recover those scarce materials as the net implication of LIBs' production can be minimized when the materials are recovered after battery end-of-life (EoL) [22].

Apart from these considerations, the full comprehensive of the sustainability of MABs demands the determination of their environmental implications. If the environmental impacts of pure metals are considered, Ca-air, Zn-air, and Mg-air batteries should be preferred. The production of pure Li has a global warming potential (GWP) of 7.1 kg CO_2 equiv kg^{-1}, being the impacts of the other metals as follows: 8.2 kg CO_2 equiv kg^{-1} for Al, 5.4 kg CO_2 equiv kg^{-1} for Mg, 3.1 kg CO_2 equiv kg^{-1} for Zn, and 1.0 kg CO_2 equiv kg^{-1} for Ca. Considering cathode materials, pure cobalt shows a GWP of 8.3 kg CO_2 equiv kg^{-1}, while vanadium encompasses 33.1 kg CO_2 equiv kg^{-1}, manganese 1.0 kg CO_2 equiv kg^{-1}, iron 1.5 kg CO_2 equiv kg^{-1}, or nickel 6.5 kg CO_2 equiv kg^{-1} [23].

The fabrication of energy storage systems is subjected to large amounts of raw materials and energy consumption, together with the emission of different wastes [24]. Accordingly, battery sustainability should go beyond the mere determination of the global warming involved during the use of raw materials and should cover the different life cycle stages [25, 26]. Using the life cycle assessment (LCA) methodology, it is potential to quantify of environmental implications of a product or service through its life cycle, covering from the extraction and processing of the raw materials to the End-of-Life (EoL) and taking into consideration the use, manufacturing and distribution [27]. The main environmental burdens of MABs begin from the nature of cathode catalysts, which usually demand highly toxic and scarce elements. Aqueous electrolytes are environmentally preferred over aprotic solvents, which entail notable environmental burdens in terms of CO_2 emissions and toxicity [28].

Zn-based batteries are stable towards moisture, so no inert atmosphere is required during battery manufacturing. This simplifies the production process and results in lower energy and material (argon) consumption typically needed to ensure a moisture-free inert atmosphere during cell assembly of conventional LIBs or NIBs [29]. As presented in **Figure 2.1**, this is the general trend except for the resource depletion category, where the Zn powder anode has the largest contribution [30, 31]. Generally, notable implications in human toxicity (cancer and non-cancer effects), freshwater ecotoxicity and resource depletion are attained.
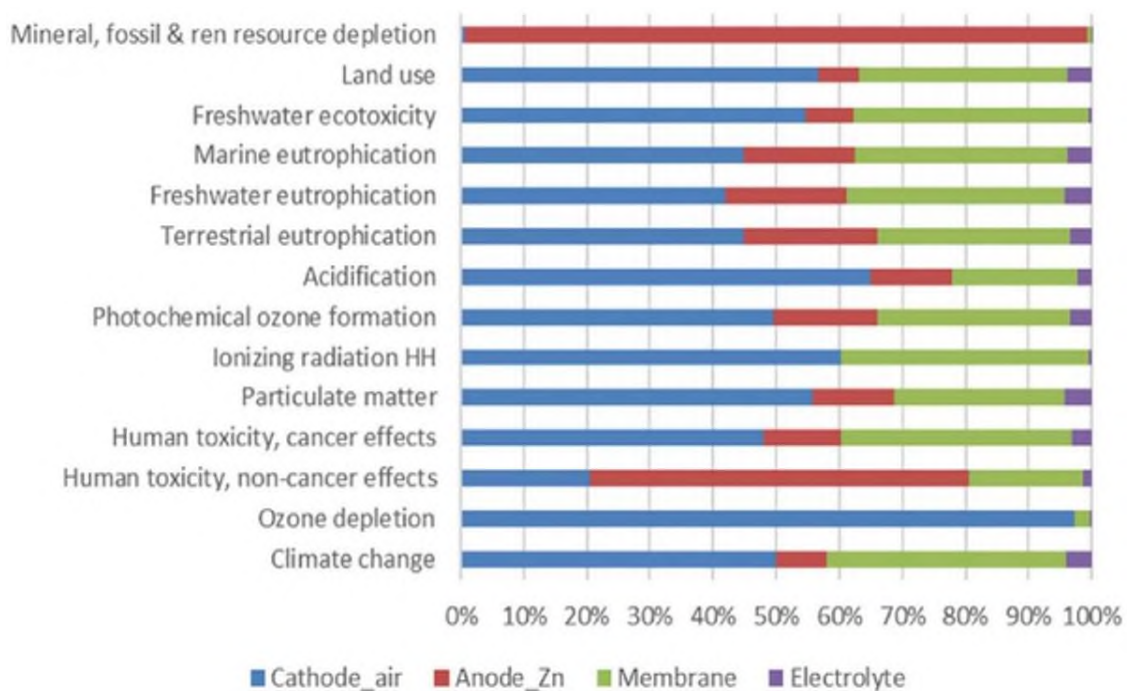
Figure 2.1 General trend of environmental implications and notable impacts in human toxicity [28].

A *cradle-to-grave* analysis (including production, use and recycling) has been performed on Li-air battery cell for EVs [32]. The battery has a Li foil anode, a PP separator soaked in $LiClO_4$ in TEGDME, a CNT/CO_3O_4 cathode, copper current collectors and PP housing. The cathode had a relative production-related CO_2 impact of 37 %, followed by the 28 % of the assembly energy and the 23 % of the Li foil. A notable abiotic resource depletion (89 % contribution) and ecotoxicity (67 % contribution) during production arising from copper was observed. Interestingly, 10 % - 30 % of production related environmental impacts could be avoided considering a recycling scenario [33]. The negative electrode (Li foil) takes the largest share in most of the categories, largely attributed to the copper current collector used. In contrast, the cathode contributes by less than 7 % in most of the categories. Overall, with 149 g CO_2 equiv km^{-1}, the Li-air battery system showed a 9.5 % reduction in life cycle climate change due to the avoidance of manganese, nickel, and cobalt in the cathode. An additional environmental benefit when implemented into an electric vehicle may arise from the weight of Li-air batteries, where decreases from 531 to 267 kg have been estimated by replacing a NMC (nickel, manganese, and cobalt) LIB [33]. Such weight saving can provide direct environmental benefits when implemented into an electric vehicle independently of the electricity grid type [34]. However, four orders of magnitude larger implications for ecotoxicity of earth potential and 8 times larger for ozone depletion potential are achieved, highlighting the need for a holistic design of this type of batteries.

At the end, *cradle-to-gate* impacts of 7 laboratory-scale aprotic Li-air battery cathode chemistries having 60 kWh have been analyzed [35]. As presented in **Figure 2.2**, the implications

vary depending on the battery type because of the variety of materials such as nickel, MnO_2, cobalt, ruthenium, graphene, MOFs, carbon nanotubes, CO_3O_4, Ag or AuNi.
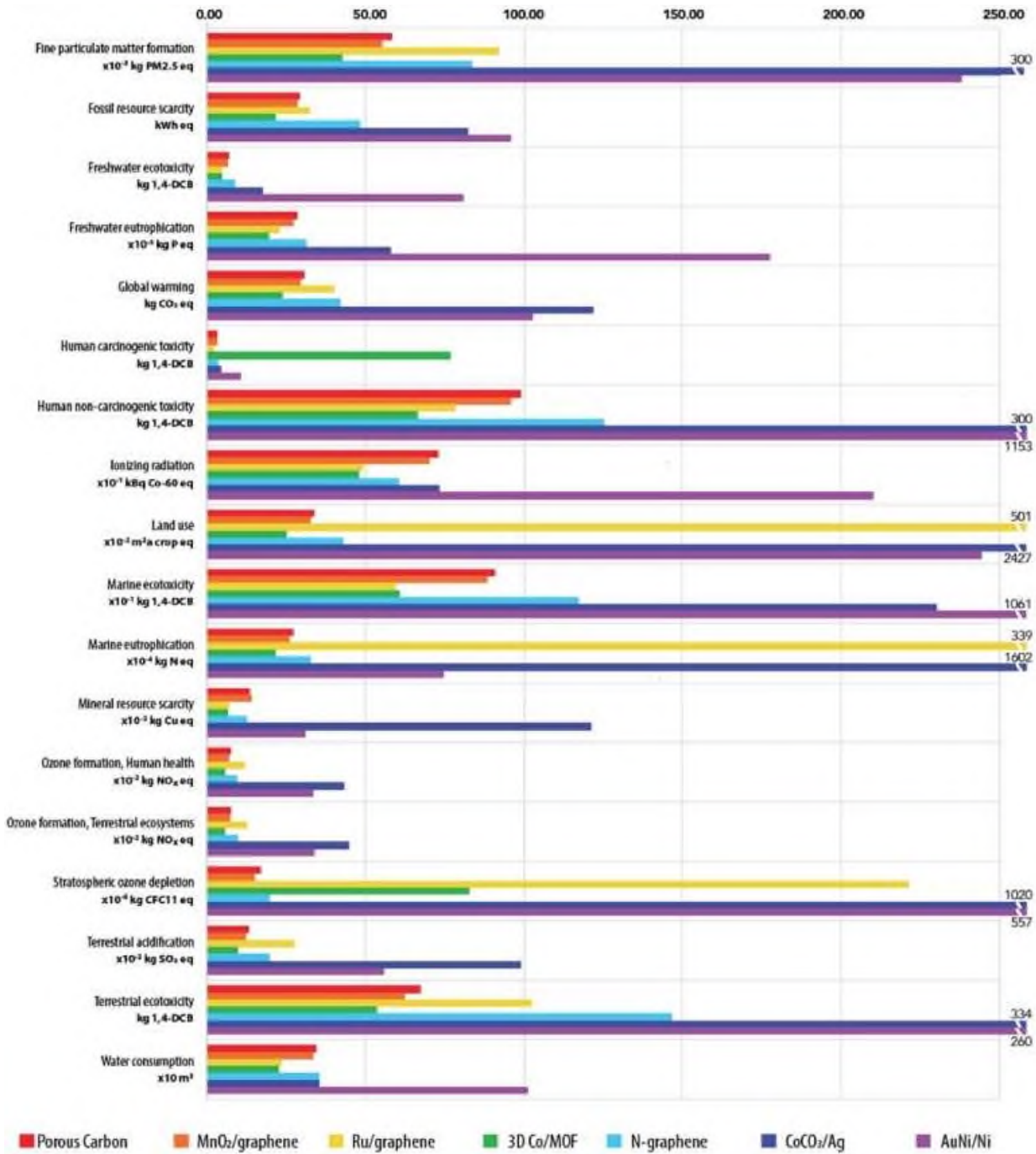
Figure 2.2 Impacts depending on the battery type due to the variety of materials [28].

On average, the cathode is the major contributor to the GWP with a relative weight of 44.5% [30]. Li-air batteries present an average value of 55.8 kg CO_2 equiv per 1 kWh, which remains below the 146.4 kg CO_2 equiv for NIBs, the 58.4 kg CO_2 equiv for LIBs, or the 130.6 kg CO_2 equiv for Li-S, having a similar energy density. The implications related to toxicological risks may be also minimized because of the efficiency/simplicity of the cathode fabrication, the use of abundant and safe materials, and limited amounts of electrolyte. Totally, reported LCA

researches highlight the potential of MABs as a promising choice to fabricate sustainable energy storage systems. It is crucial to keep in mind that battery performance (delivered energy) and lifetime are important variables determining the full sustainability. Environmentally sustainable MABs must be designed to avoid issues resulting in early failure of the cell, such as those including dendrite formation, component volumetric changes, current collector corrosion, anode detachment from the current collector, and loss of electrode's electronic conductivity or electrolyte contamination or decomposition. This could avoid the extraction of new resources demanded for new batteries, could limit the CO_2 emission originating from battery manufacturing and could delay the entering of the batteries in the waste stream [28].

CHAPTER 3

Life cycle assessment of lithium-air battery cells

3.1 Introduction

Lithium Air Battery (LAB) cells are currently being investigated for propulsion aggregates in vehicles as they theoretically can provide a 10-fold increase in energy density compared to the best battery technology (lithium-ion) of today [36]. The current state of research is however far from large scale implementation, and the technology must overcome many hurdles involving voltage stability, charge over potential, electrolyte stability, and many other physical-chemical factors that should ideally include full cell development that operates in ambient air [37].

Electric vehicles are seen as the main answer to the transport sector´s problems of climate impact and diminishing oil supplies. Provided that the electricity can be generated from renewable energy sources, considerable reductions of CO_2 emissions from the transport sector are possible [38]. However, development of battery performance is crucial in the transition from combustion engines to electric motors in automobiles [39].

3.2 Recycling and treatment processes and avoided processes

Data concerning the recycling processes is estimated based on an assumption regarding how much environmental burden can be avoided in total. It is assumed that legislation and resource supply concerns will drive recycling rate (including collection rate) to as much as 80 % [40], but at the expense of energy efficiency and cost to such an extent that only 50 % of environmental impacts of virgin material production is avoided. The reason for assuming only 50 % of the possible avoided burdens is partly because recycled materials are often of inferior quality and cannot fully replace virgin materials, and partly because the recycling processes need resources and cause environmental burdens.

Since the cell consists mainly of electrolyte (46 %) and sealing gasket (15 %), both assumed to be incinerated, only 3.4 grams or 20 % of the total cell weight will be recycled as material (copper, lithium, cobalt and polypropylene). The environmental impacts of lithium battery recycling are calculated as the sum of environmental impacts from the transportation and involved recycling processes and treatment processes minus environmental impacts from avoided production of virgin materials. By assuming that environmental impacts for recycling processes corresponds to 50% of Avoided virgin production, the environmental impacts of lithium battery recycling can be calculated as: Transports – 0.5 × Avoided virgin production [39].

13

3.3 Parameterized model

The life cycle of the lithium-air cell was built as a parameterized model enabling variation of influencing factors. Parameters are shown in **Table 3.1**, along with the values of the two scenarios: STABLE project achievement and Long-term lithium-air scenario.

Table 3.1 Model parameter settings for STABLE project scenarios [39].

Parameter	STABLE project achievement	Long term lithium-air scenario
Charge/discharge efficiency, η	0.66	0.8
Number of cycles until failure	50	200
Energy density (Wh/kg)	2700	10800
Share of total capacity that is cycled	0.2	0.8

The STABLE project did not reach its objective in one single cell configuration. The number of cycle target was reached with cells with very low energy density and cells with very high energy density did not achieve that many cycles. This is reflected in the STABLE project achievement scenario.

When comparing the energy density of the lithium-air cell to the current energy density of lithium-ion batteries (≈100 Wh per kg at best) it has to be considered that the above energy densities for the lithium-air cells are calculated per kg of active component and the 100 Wh are per kg of battery system. A rough estimation, and assumption in the calculations, is that a lithium-air battery system consists of 50% non-active materials, providing an estimated energy density of 1350 Wh per kg at the battery level for the STABLE project achievement [39].

3.4 Climate impact

The present "STABLE achievement" level of lithium-air cell performance, shown in **Figure 3.1**, comes with a large climate impact (almost 300 g CO_2 equivalents per km, compared with e.g. the EU 95 g CO_2 equivalents per km target). The production phase contributes most to climate impact. At the long-term goal level, the total climate impact is only 26 g CO_2 equivalents per km and dominated by losses in the use phase. Note that the presented use phase impacts only constitute battery-related losses. The vehicle operation-related (battery-to-wheel) climate impact is 89 g CO_2 equivalents per vehicle km with average European electricity mix at 594 g CO_2 equivalents per kWh and battery-to-wheel consumption of 0.15 kWh per km. Recycling avoids about 10% of production related climate impact in both scenarios [39].
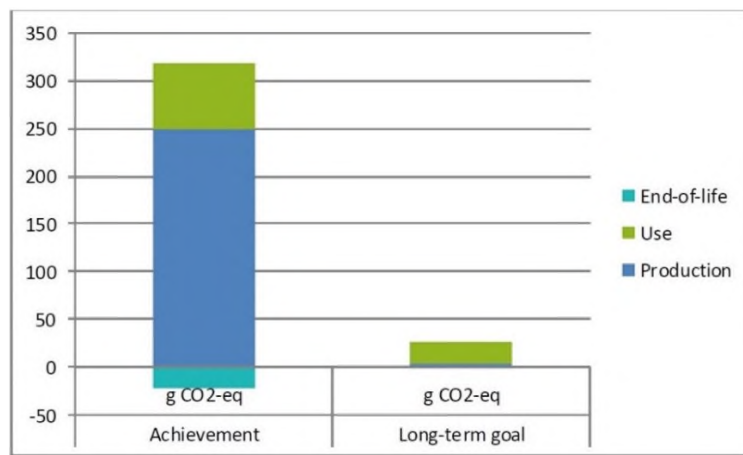
Figure 3.1 *Climate impact per vehicle km for the two scenarios [39].*

Detailed climate impact data per vehicle kilometer and per delivered kWh is given in **Table 3.2**. It can be seen that as performance of the cell develops, climate impact decrease altogether and is dominated by the use phase.

Table 3.2 *Climate impact per vehicle km and per delivered kWh for the two scenarios [39].*

Scenario	Achievement		Long-term goal	
Life cycle stage	g CO_2-eq/km	g CO_2-eq/kWh	g CO_2-eq/km	g CO_2-eq/kWh
Production	249	1100	3.2	17
Use *	69	296	23	124
Subtotal	318	1396	26	141
End-of-life	-22	-97	-0.29	-1.5
Total	296	1299	26	140
∗ The presented use phase impacts cover only battery related losses. The operation in terms of propelling the vehicle is not included.				

3.4.1 Production related climate impact

As pointed out, climate impact from the production phase is high per km or delivered kWh at the present level of development, but decreases rapidly with increasing energy density, efficiency, number of charge cycles and depth of discharge as fewer cells are needed per vehicle kilometer or delivered kWh. Production related climate impact is fairly evenly distributed among the cell components: 37% from the cathode of which 34% are attributed to electrical energy; 27% from the assembly energy use; 23% from the lithium foil and 5% from the electrolyte, accounting for 92% of production related climate impact [39].

3.4.2 Use phase climate impact

Climate impact from the use phase is dominating more and more as the cell develops, even though in absolute terms it also decreases (as the cell develops). The use phase climate impact stems mainly from battery internal power losses, which are defined by the internal efficiency of the battery. A lot of the power passing through the battery is lost as heat: 34% and

20% respectively in the achievement and long-term goal scenarios. The extra power needed to carry the weight of the battery provides a smaller but significant contribution, especially at lower energy density levels when more cells are needed.

3.4.3 Recycling related climate impact

Recycling avoids about 10% of production related climate impact in both scenarios. Almost all of the avoided climate impact stems from avoided virgin production of lithium foil. The climate impact of the recycling processes was assumed to be equal to 50 % of the avoided virgin production. The recycling transports give small but not insignificant contributions to climate impact.

3.5 Abiotic depletion

At the present level of lithium-air cell performance, the lithium-air cell has a relatively large abiotic depletion potential, see **Figure 3.2**. As performance of the cell develops abiotic depletion from Production and End-of-life decreases since less cells are needed. Use phase abiotic depletion driven by electricity use then becomes dominant. Recycling avoids about 30% of production related abiotic depletion in both scenarios.
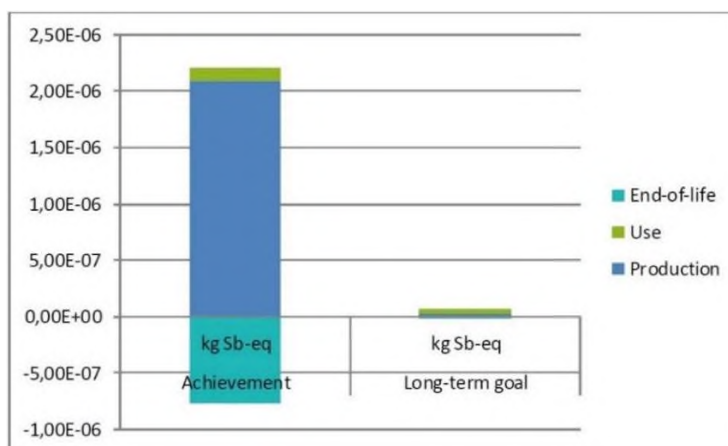
Figure 3.2 *Abiotic depletion, kg Sb (Antimony) equivalents per vehicle km for the two scenarios [39].*

Detailed data about abiotic depletion per vehicle kilometer and per delivered kWh is given in **Table 3.3**.

Table 3.3 *Abiotic depletion, kg Sb eq per vehicle km and per delivered kWh for the two scenarios [39].*

Scenario	Achievement		Long-term goal	
Life cycle stage	kg Sb-eq/km	kg Sb-eq/kWh	kg Sb-eq/km	kg Sb-eq/kWh
Production	2.10E-06	9.3E-06	2.7E-08	1.5E-07
Use ∗	1.1E-07	4.8E-07	3.6E-08	1.9E-07
Subtotal	2.2E-06	9.7E-06	6.3E-08	3.4E-07
End-of-life	-7.7E-07	-3.4E-06	-1.0E-08	-5.3E-08
Total	1.4E-06	6.3E-06	5.3E-08	2.8E-07
∗ The presented use phase impacts cover only battery related losses. The operation in terms of propelling the vehicle is not included.				

3.5.1 Production related abiotic depletion

Abiotic resource depletion from the production phase is relatively high per km or delivered kWh at the present level of development, but decreases rapidly with increasing energy density, efficiency, number of charge cycles and depth of discharge, as fewer cells are needed per vehicle kilometer or delivered kWh. Production related abiotic resource depletion stems mainly from copper, contributing 89 %. Lithium, the Tetra Ethylene Glycol Dimethyl Ether (TEGDME) electrolyte and electricity use (for processing) of the cathode and for assembly contribute from 5 to 1 % [39]. These relations between the production related abiotic resource depletion are the same for both scenarios since the same materials are assumed for both scenarios.

3.5.2 Use phase abiotic depletion

Abiotic resource depletion from the use phase is dominating more and more as the cell develops, even though in absolute terms also the use phase abiotic resource depletion decreases as the cell develops. The use phase abiotic resource depletion stems almost completely from electricity (99 %).

3.5.3 Recycling related abiotic depletion

Recycling is calculated to avoid ≈ 30 % of production related abiotic resource depletion in both scenarios. Almost all of the avoided abiotic resource depletion stems from avoided virgin production of copper. The recycling transports give insignificant contributions to abiotic resource depletion.

3.6 Ecotoxicity

At the present level of lithium-air cell performance, the cell shows relatively large ecotoxicity compared to the long-term goal, as shown in **Figure 3.3**. As performance of the cell is developing in the future, the use phase power losses become more dominant.
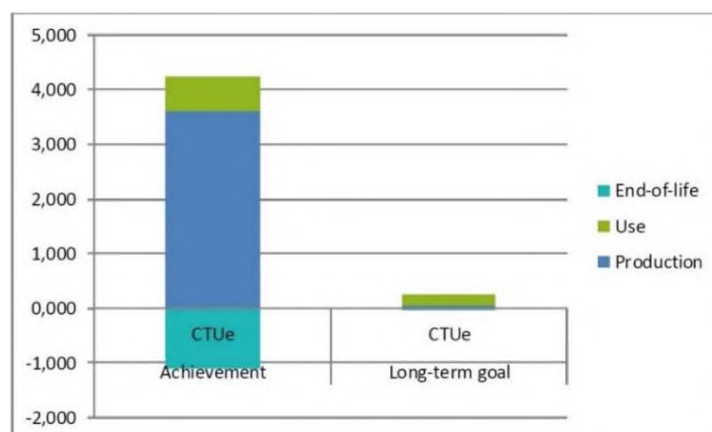
Figure 3.3 *Ecotoxicity, Comparative Toxic Unit for ecosystems (CTUe) per vehicle km for the two scenarios [39].*

Recycling avoids about 30 % of production related ecotoxicity in both scenarios. Detailed data is given in **Table 3.4**.

Table 3.4 Ecotoxicity, Comparative Toxic Unit for ecosystems (CTUe) per vehicle km and per delivered kWh for the two scenarios [39].

Scenario	Achievement		Long-term goal	
Life cycle stage	CTUe/km	CTUe/kWh	CTUe/km	CTUe/kWh
Production	3.6	16	0.0464	0.25
Use *	0.6	2.8	0.214	1.1
Subtotal	4.2	19	0.3	1.4
End-of-life	-1.1	-4.8	-0.0142	-0.076
Total	3.1	14	0.2	1.3
* The presented use phase impacts cover only battery related losses. The operation in terms of propelling the vehicle is not included.				

3.6.1 Production related ecotoxicity

Ecotoxicity from the production phase is high per km or delivered kWh at the present level of development, but decreases rapidly with increasing energy density, efficiency, number of charge cycles and depth of discharge as fewer cells are needed per vehicle kilometer or delivered kWh. Production related ecotoxicity is fairly evenly distributed among the cell components: 67% from the copper tab; 10% from the lithium foil, 9% from the electricity used for the cathode; 8 % from the assembly energy use; and 2 % from the electrolyte accounts for more than 90% of production related ecotoxicity [39].

3.6.2 Use phase ecotoxicity

Ecotoxicity from the use phase is dominating more and more as the cell develops, even though in absolute terms also the use phase ecotoxicity decreases as the cell develops. The use phase ecotoxicity stems mainly from electricity during the use phase (99 %).

3.7 Dominance analysis

In **Table 3.5** can be seen that electricity, copper and lithium dominate the Production phase and electricity completely dominate the Use phase in all impact categories. Toxicity was calculated as two human toxicity scores (cancer and non-cancer related) and one ecotoxicity score. Non-cancer human toxicity was found to give around ten times higher morbidity rate than cancer-related human toxicity. In this chapter, only ecotoxicity is presented. From a dominance perspective, ecotoxicity represents well in particular non-cancer human toxicity, see **Table 3.5**.

Table 3.5 Dominance analysis [39].

Life cycle phase impact category	Production	Use	End-of-life
Climate impact	Electricity (54%) Lithium (23%) Gas (8%) TEGDME (4%)	Electricity (99%)	Lithium (-105%) Copper (-6%) Polypropylene (-4%) Transport (15%)
Abiotic depletion	Copper (89%) Lithium (5%)	Electricity (99%)	Copper (-96%) Lithium (-5%) Transport (1%)
Toxicity-cancer	Copper (35%) Lithium (26%) Electricity (24%)	Electricity (99%)	Copper (-59%) Lithium (-44%) Transport (3%)
Toxicity non-cancer	Copper (79%) Lithium (8%) Electricity (8%)	Electricity (99%)	Copper (-92%) Lithium (-10%) Transport (2%)
Ecotoxicity	Copper (67%) Electricity (17%) Lithium (10%)	Electricity (99%)	Copper (-88%) Lithium (-14%) Transport (2%)

3.8 Toxicity considerations

From the dominance analysis can be seen that toxicity stems from production of electricity, copper and lithium. There is consensus that metals are not well modeled in LCA [41]. The lithium process scores high in toxicity due to emissions of chromium, nickel, arsenic and mercury associated with the lithium production. On the other hand, it is not that clear where emissions of lithium would happen, thus such emissions are not modeled fully. Volatility of some lithium-containing electrolyte may provide a source of lithium contamination, but there are no dedicated reports of lithium emissions during full battery pack operation for lithium-air systems [39].

Lithium-ion batteries in uncontrolled landfills would leach out metals above current US regulatory limits [42]. Impact assessment methods have not taken lithium and aluminum into account due to lack of toxicity data in the models, i.e. there is no data on lithium emissions from landfills nor are there characterization factors available to translate such emissions into toxicity impacts.

The TEGDME electrolyte and the organic N-Methyl-2-Pyrrolidone (NMP) solvent used in the manufacturing of the cathode are both considered toxic. Due to lack of data, potential emissions of these substances were not modeled in any phase. Both substances could potentially leak out in the working environment and TEGDME emissions might also occur during the use of the battery cell [39].

As pointed out above, tradeoffs between tailpipe emissions, material resource use and toxicological impacts need to be assessed in LCAs of vehicles.

In view of above, it seems reasonable to be extra cautious when interpreting LCA toxicity scores for lithium batteries. Until the recommended developments are achieved, known toxic materials should be considered also outside of the LCA.

3.9 Potential of Lithium Air cell

At the long-term goal level, production related climate impact is only 3 g CO_2 equivalent per km which is a factor of 4-9 lower than today's best battery technology. The potential gains in performance are so large that a battery with lithium-air cell functioning at the long-term goal level would most probably be very competitive, even if controlled oxygen supply is needed for its proper functioning [37, 43]. The *actual* environmental footprint of a distant industrial scale manufacturing of lithium-air batteries will probably be *higher* due to intentional exclusions, like cell electronics and oxygen supply, or unintentional exclusions because of lack of knowledge and *lower* due to improved, up-scaled and/or different manufacturing processes. In conclusion, the currently predicted environmental impact could be higher or lower or roughly equal to that of a fully functional commercial LAB in the future.

3.10 Recycling

By recycling the battery cell, 10-30 % of production related environmental impact could be avoided. However, it is important to point out that at present there is no dedicated recycling activity for lithium traction batteries and that the economic return for recycling is quite poor [44, 45]. Thus, recycling of lithium batteries will probably not happen unless it is legally enforced worldwide, as it currently is in Europe (EC 2006). In this respect, LCA may be important in guiding policy and providing a starting basis for quantitative assessment for possible lithium battery recycling. This emphasizes the need to develop LCA toxicity impact methods in order to properly assess lithium. Resource supply considerations will also be a motivation for recycling of scarce materials used in traction batteries. In view of the above, it is recommended that future battery cell development projects already at the design stage should consider how the battery and cell should be recycled.

CHAPTER 4

Electrochemical energy systems

4.1 Introduction

The enormous growth in world population, particularly in the developing world, coupled with technological developments are considered as the key factors behind the immense increase in electrical energy consumption over the past half century. Further increases in the world energy consumption are expected with its energy demand projected to be doubled by the middle and tripled by the end of the century [46] as a result of further population growth (with world population expected to reach 9 billion by 2048) and increased electrical energy demands in industrial and commercial sectors [47]. Currently, fossil fuels such as oil, gas and coal are the primary sources of energy, with more than 85% of the world's total energy generation achieved through these conventional sources [48]. Over-reliance on fossil fuels for production of energy has led to numerous environmental challenges including poor air quality, unexpected climatic variations, water/soil contamination and a colossal increase in greenhouse gas emissions [49, 50]. To contain or reverse these trends, deployment of more sustainable and low carbon or even carbon free renewable sources of energy such as wind, solar or tidal are essential. However, these renewable sources of energy are location - specific and, in some cases unpredictable in nature and therefore operational flexibility is key for their integration into the power systems. This flexibility is attainable when using appropriate energy storage technologies that can help in managing fluctuations and mismatches in energy supply and demands, ultimately improving the efficiencies in energy and power supply systems by reducing the gap between production and consumption. Furthermore, growth in energy proportion added to national grid through the integration of renewable sources such as wind and solar results in curtailments which can be addressed by using appropriate storage technologies [51]. There are a broad range of energy storage and conversion technologies available including chemical, thermochemical, mechanical, electrical and electrochemical storage systems. Among these, electrochemical energy storage and conversion systems such as electrochemical capacitors/ batteries and fuel cells respectively, have received the most intensive attention and have been adopted in everyday applications due to their high columbic efficiencies. Basically, energy storage devices perform two important tasks-(a) time shifting bulk energy from renewables production to time of energy demand (supplied by batteries + fuel cells) (b) production of clean, stable power and frequency, avoiding voltage spikes (important for digital economy) by supercapacitors and high power batteries. However, challenges related to their durability, high cost, environmental concerns,

and operability problems must be addressed in order to improve their effectiveness and further increase uptake [52, 53]. Environmental impact of lithium mining including human health, effect on biodiversity and availability of clean/fresh water for consumption and agriculture use are other key concerns. Since major lithium reserves are located in salt lakes and pans where lithium is extracted through evaporation and flooding of reserves with fresh water [54]. Similarly, electrochemical capacitors (ECs) have inferior energy densities whereas fuel cells have operability and system issues [55, 56].

A diverse range of energy storage and conversion devices is shown in **Figure 4.1** based on their energy delivery time varying with the type of mechanism involved in energy storage or conversion systems.
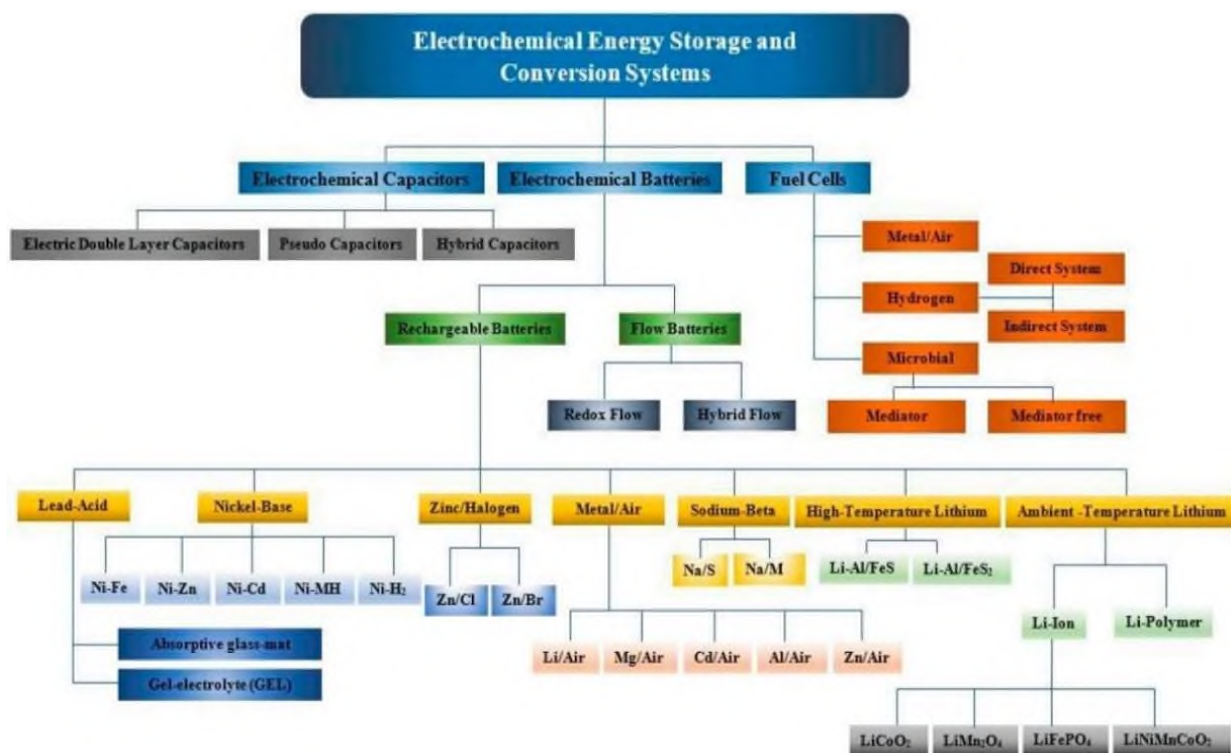
Figure 4.1 *Classification of electrical energy storage and conversion devices [57].*

For example, electrochemical capacitors are considered as high-power density devices and their delivery time is in the range of few seconds to minutes since these devices utilize only the material on the electrode surface unlike batteries or fuel cells where bulk of the material is involved in energy storage and conversion respectively. Other characteristics of these devices vary as well due to the fundamental difference in the mode of energy storage or conversion.

4.2 Electrochemistry at a glance

Electrochemistry involves chemical phenomena associated with charge separation. Often this charge separation leads to charge transfer, which can occur homogeneously in solution, or

heterogeneously on electrode surfaces. In reality, to assure electroneutrality, two or more charge transfer half-reactions take place, in opposing directions. Except in the case of homogeneous redox reactions, these are separated in space, usually occurring at different electrodes immersed in solution in a cell. These electrodes are linked by conducting paths both in solution (via ionic transport) and externally (via electric wires etc.) so that charge can be transported. If the cell configuration permits, the products of the two electrode reactions can be separated. When the sum of the free energy changes at both electrodes is negative, the electrical energy released can be harnessed (batteries). If it is positive, external electrical energy can be supplied to oblige electrode reactions to take place and convert chemical substances (electrolysis) [58].

4.3 The nature of electrode reactions

Electrode reactions are heterogeneous and take place in the interfacial region between electrode and solution, the region where charge distribution differs from that of the bulk phases. The electrode process is affected by the structure of this region. However, we first assume that there is no effect apart from charge separation. At each electrode, charge separation can be represented by a *capacitance* and the difficulty of charge transfer by a *resistance*. For the rest of this and the ensuing sections we consider only one of the electrodes [58].

The electrode can act as only a source (for reduction) or a sink (for oxidation) of electrons transferred to or from species in solution, as in

$$O + ne^- \rightarrow R \tag{4.1}$$
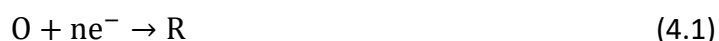
Where O and R are the oxidized and reduced species, respectively.

Alternatively, it can take part in the electrode reaction, as in dissolution of a metal M:

$$M \rightarrow M^{n+} + ne^- \tag{4.2}$$

In order for electron transfer to occur, there must be a correspondence between the energies of the electron orbitals where transfer takes place in the donor and acceptor. In the electrode this level is the highest filled orbital, which in a metal is the Fermi energy level, E_F. In soluble species it is simply the orbital of the valence electron to be given or received [58].

Thus:

- for a reduction, there is a minimum energy that the transferable electrons from the electrode must have before transfer can occur, which corresponds to a sufficiently negative potential (in volts)

- for an oxidation, there is a maximum energy that the lowest unoccupied level in the electrode can have in order to receive electrons from species in solution, corresponding to a sufficiently positive potential (in volts).

The values of the potentials can be controlled externally. In this way we can control which way an electrode reaction occurs and to what extent.

4.4 Electrochemical Energy Storage and Conversion Systems

4.4.1 Introduction

Electrochemical Capacitors (ECs)/batteries and fuel cells are key electrochemical energy storage and conversion technologies respectively, used in commercial applications with their particular selection dependent on performance limitations such as energy densities, power densities, and cycle life.

Electrochemical batteries and fuel cells are considered as high energy density devices with typical gravimetric energy densities in the range of 100-200 Wh kg^{-1} and 600-1200 Wh kg^{-1} respectively, whereas current ECs have significantly lower energy densities with typical values typically between 0.05-30 Wh kg^{-1} [59]. However, ECs are considered as high-power density devices with very short charge/discharge times (of the order of seconds) which is difficult to achieve by other electrochemical energy storage and conversion devices. **Figure 4.2** shows a comparison of specific energy, specific power and their delivery timescale for different energy storage and conversion devices.
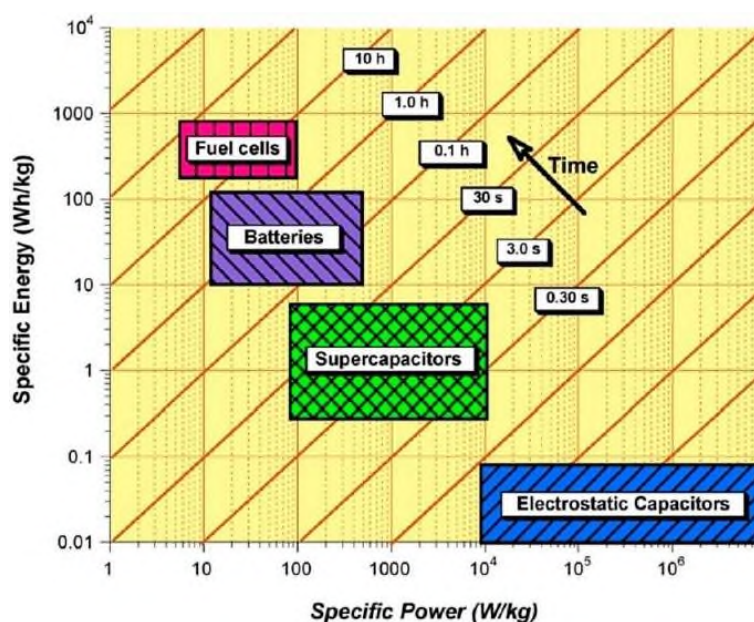
Figure 4.2 Energy density, power density and delivery timescale for different energy storage and conversion devices [60].

At present, none of these devices has the capability to meet the wide spectrum of requirements demanded by the diverse range of renewable energy sources such as wind, tidal

and solar. However, they can respond to a broad rang requirements such as fast charge/discharge, peak power demands and high energy storage needs over a longer period of time when used in a combination of two or more.

4.4.2 Electrochemical Capacitors

Electrochemical Capacitors (ECs), also known as Supercapacitors (SCs) or Ultra-capacitors (UCs), are electrochemical energy storage devices having Energy Densities (EDs) higher than electrostatic capacitors but lower than electrochemical batteries, as shown in **Figure 4.2**. ECs can bridge the energy gap in the range of 10^{-2} to 10 Wh kg^{-1} between electrochemical batteries and electrostatic capacitors as shown in **Figure 4.2**.

Their other distinctive properties include high power densities, remarkably long cycle life and good capacity retention. According to their charge storage mechanism, ECs can be further classified into three categories of Electric Double Layer Capacitors (EDLCs), Pseudo-Capacitors (PCs) and Hybrid Capacitors (HCs). Electric Double Layer Capacitors (EDLCs) store electric energy by storing electric charge through the formation of an electric double layer at the electrode/electrolyte interface upon polarization, where their capacitance is substantially higher than the capacitance of a conventional electrostatic capacitor due to very high specific surface areas and charge separation of only a few Ångstroms. In the case of ideal electric double layer behaviour, cyclic voltammograms are rectangular in shape with a voltage independent current and linear charge/discharge curves as shown in **Figure 4.3** (a–c) [61].
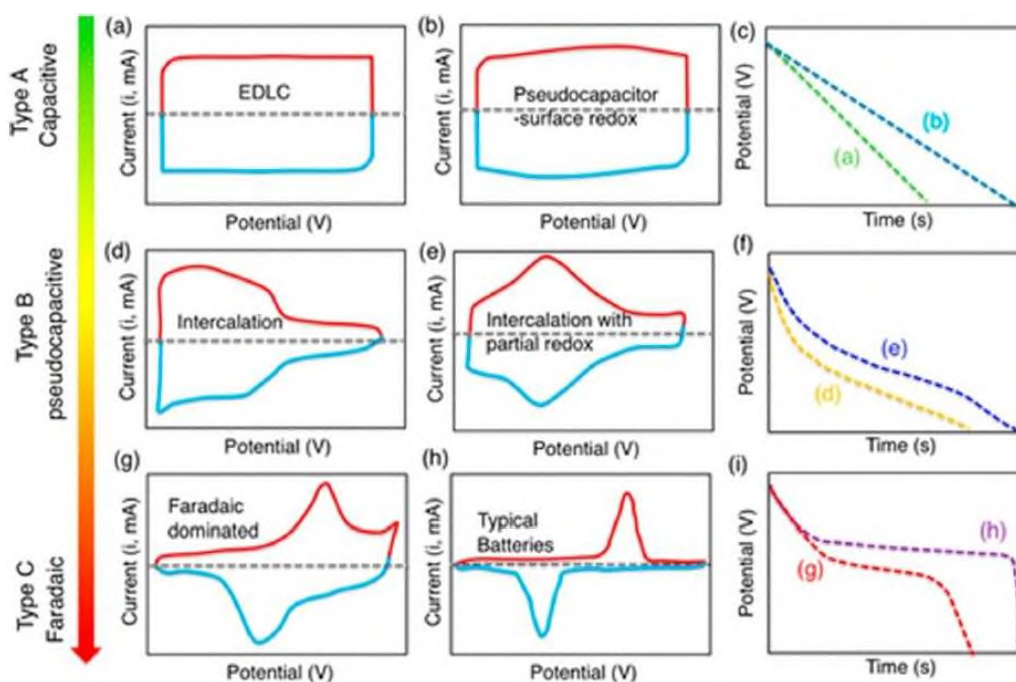
Figure 4.3 Schematic CV profiles (a, b, d, e, g, h) and corresponding galvanostatic discharge curves (c, f, i) for different type of electrode materials [64].

Capacitor-like behaviour involving electrochemical, rather than physical, charge storage has been demonstrated in so-called pseudo-capacitive materials in Ecs [62], which occupies the middle ground between EDLCs and battery like capacitor as shown in **Figure 4.3 (d–f)**. Pseudo-capacitive charge storage benefits from voltage-dependent electrochemical electronic transfer, which is known as Faradic charge storage [233] and is similar to that of battery storage, whereas, hybrid capacitors involve both physical and chemical (battery-like) charge storage mechanisms (with noticeable and separated peaks associated with the reduction and oxidation) as shown in **Figure 4.3 (g,h)**. The charge/discharge behaviour of batteries/battery like capacitors is non-linear and symbolized by plateaus of nearly constant potential corresponding to the potentials at which the Faradaic reduction or oxidation occurs as shown in **Figure 4.3 (i)** [63, 64].

Table 4.1 shows the material selection criteria and performance parameters for different types of electrochemical capacitors.

Table 4.1 Material selection and performance characteristics of ELDCs, PCs and HCs [57, 65-77, 78-80].

	Electric Double Layer Capacitors (EDLCs)	Pseudo-Capacitors (PCs)	Hybrid Capacitor (HCs)
Electrode material	Carbon-based materials: activated carbon, graphene, carbon nanotubes and polymeric carbons	MOs: MnO_2, NiO and RuO_2. CPs: PANI, PT and PPY	Combination of EDL material and pseudo-capacitive material
Specific capacitance ($F\ g^{-1}$)	200–300	200–1340	50–1893
Energy density ($Wh\ kg^{-1}$)	6.8–12	167–223	132–231
Power density ($kW\ kg^{-1}$)	98,000–165	21,000–220	2800–57
Cyclability (cycles)	100,000	5000	12,000
Capacitance retention (%)	60–100	52–96	80–95
Charge storage mechanism	Physical	Chemical	physical + chemical

EDLCs are the best performing devices in terms of power densities but they suffer from low energy densities when compared with PCs or HCs. The development of novel materials and new types of supercapacitor devices such HCs (symmetric, asymmetric and battery type) has potentially opened up new routes to address some of the deficiencies of EDLCs. However, these new generation devices are at their initial stages of development and require substantial further research and development efforts to respond to required energy/power densities in a wide range of practical applications [57].

4.4.3 Electrochemical Batteries

4.4.3.1 Rechargeable Batteries - Introduction

As the oldest technology for electrical energy storage (EES), rechargeable batteries are extensively used in everyday life and industrial applications [81]. An electrochemical battery consists of electrochemically active positive (anode) and negative (cathode) electrodes and liquid or solid electrolytes and stores energy in the form of electric charge and chemical energy in its electrodes'

electroactive materials. During the discharge cycle, electrochemical reactions occur at both cathode and anode simultaneously, a circuit is completed with the flow of electrons through external circuit where electrons originating from anode are collected at the cathode. Whereas during the charging cycle the reverse reaction takes place and the battery is recharged through the application of an external potential at both electrodes, as shown in **Figure 4.4** [82].
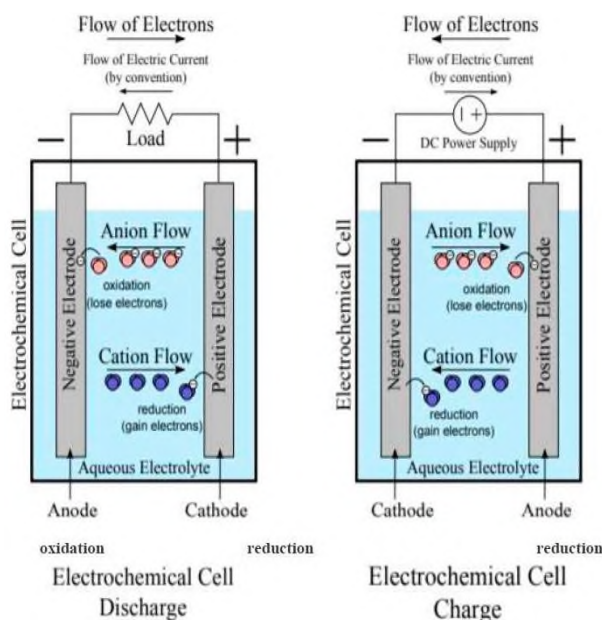
Figure 4.4 A typical charge and discharge cycle of an electrochemical battery cell [83].

Complete chemical reactions (anodic/cathodic) for some of the most widely commercialized battery systems are given in **Table 4.2**.

Table 4.2 Chemical reactions and single unit voltages of different battery systems [57, 84-86].

Battery Type	Chemical Reaction at Anodes and Cathodes	Voltage (V)
Lead-acid	$Pb + SO_4^{2-} \Leftrightarrow PbSO_4 + 2e^-$ $PbO_2 + SO_4^{2-} + 4H^+ + 2e^- \Leftrightarrow PbSO_4 + 2H_2O$	2.0
Lithium-ion	$C + nLi^+ \; ne^- \Leftrightarrow Li_nC$ $LiXXO_2 \Leftrightarrow Li_{1-n}XXO_2 + nLi^+ + ne^-$	3.7
Nickel-cadmium	$Cd + 2OH^- \Leftrightarrow Cd(OH)_2 + 2e^-$ $2NiOOH + 2H_2O + 2e^- \Leftrightarrow 2Ni\,(OH)_2 + OH^-$	1.0–1.3
Nickel-metal hybrid	$H_2O + e^- \Leftrightarrow \frac{1}{2}H_2 + OH^-$ $Ni(OH)_2 + OH^- \Leftrightarrow NiOOH + H_2O + e^-$	1.0–1.3

Commercially available rechargeable batteries are usually available in four different shapes i.e., coin, cylindrical, prismatic, and pouch cells as shown in **Figure 4.5**.

Electrochemical batteries can be used in a wide range of applications including energy management, transportation, power quality and ride-through power. Installation of battery storage is reasonably straightforward due to flexibility of location and short installation time [234]. Despite these benefits, there are major barriers for their applications in large-scale facilities. These obstructions include relatively low cyclability, comparatively high maintenance

cost and inferior power densities. Recycling of spent batteries is another factor which plays a key role for the selection of different battery systems for energy storage applications [88].
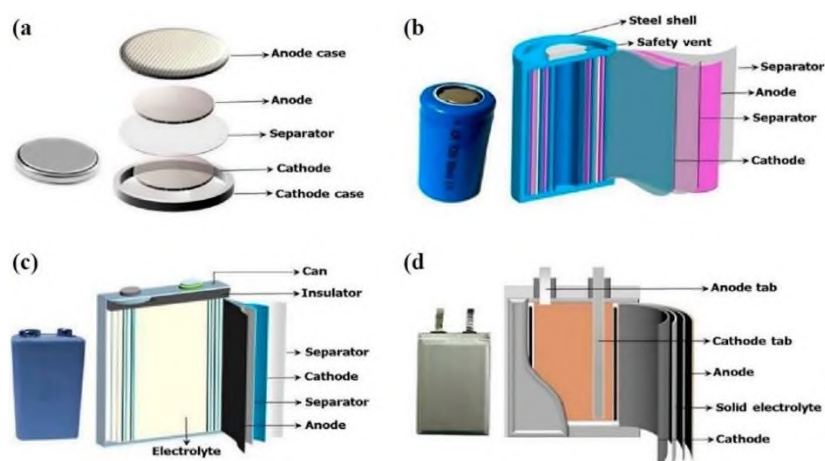
Figure 4.5 *Schematic illustration of a typical rechargeable battery cell in different configurations: (a) coin, (b) cylindrical, (c) prismatic and (d) pouch shaped [87].*

Batteries are subdivided into primary and secondary batteries. Non-rechargeable batteries, often called primary batteries, are designed not to be recharged once they discharge energy [89]. However, it has been reported [90, 91] that these batteries are tiny, light, cheap, and straightforward sources of electricity that are appropriate for a wide range of portable equipment. On the other hand, a secondary battery is rechargeable, since it may be electrically recharged after it has been discharged [92, 93]. This is because secondary batteries operate based on reversible redox reactions, and the reversible reactions realize the charge-discharge functions. Secondary batteries, like lithium-ion, lead-acid, zinc-air, nickel-cadmium, etc., can be recharged several times.

4.4.3.2 Lithium-Ion Batteries (Li-ion)

Lithium-ion batteries are currently the most frequently used electrical energy storage technology for a wide range of commercial applications. The main consumption of Li-ion batteries at present is the portable electronic sectors where their excellent properties such as exceptionally low maintenance, excellent cyclability, high voltage (~3.6 V), low self-discharge and very high specific energy led to the displacement of nickel-based battery systems (Ni-Cd and NiMH) which had previously predominated the battery market. Li-ion batteries are also becoming more common in applications such as electric/hybrid electric vehicles (EVs and HEVs), the military and aerospace industries [94-96].

Graphite, with its layered structure, is the key anode material for Li-ion batteries however, some acceleration in research activity around non-graphitic carbons, metal oxides and their composites has been witnessed recently [97-99]. Lithiated metal oxides (lithium cobalt oxide, lithium iron sulphates, lithium nickel cobalt aluminum oxide, lithium nickel manganese cobalt oxide and Li manganese oxide) are used as cathode materials for Li-ion batteries [100, 101].

Conventional Li-ion batteries use liquid electrolytes, which consist of lithium-based salts (e.g., $LiPF_6$, $LiClO_4$ and $LiAsF_6$) dissolved in an organic solvent (such as $C_4H_8O_3$, $C_3H_6O_3$, $C_4H_6O_3$ and $C_5H_{10}O_3$). Selection of appropriate organic solvents is crucial since they play a fundamental role in improving Li-ion mobility, which ultimately improves overall performance of the battery cell and is also crucial to the safety of the device [102]. New state-of-the-art all solid-state batteries, also known as Li-ion polymer batteries where Li salt containing highly conductive polymer gels replace the conventional liquid Li based salts as electrolyte are becoming commercially available [235]. Li-ion polymer batteries are mainly popular for portable electronics like mobile phones, ultra-slim laptops and wearable electronics due to their leakage free compact and light cell structure [103, 104]. Material composition by percentage weight of different commercially used Li-ion batteries used in various applications including Plug-In Hybrid Electric Vehicles (PHEV) where 20 and 40 are all electric range in miles, electric vehicles (EVs) and laptops is provided in **Table 4.3**.

Table 4.3 Composition of leading Li-ion batteries [57, 105].

Component	Typical Material	PHEV 20°	PHEV 40°	EV	Laptop
Cathode	$LiCoCO_2$, $LiMn_2O_4$ $LiNiO_2$	36	40	33	25
Anode	Graphite (LiC_6) $Li_4Ti_5O_{12}$, Cu	31	29	21	20
Electrolyte [b]	ECM [c] Propylene carbonate $LiPF_6$, $LiBF_4$, $LiClO_4$	11	12	7	12
Separator	PP	2	1	4	3
Case	Steel, PE/PP, Al, Cu, Fe	20	17	19	40
Others [a]	Cu, PE/PP, Steel			16	
[a] Other denotes materials like binders, recipe ingredients, and control circuitry, insulation. Includes solvent. [b] Argonne model; $LiNi_{0.8}Co_{0.15}Al_{0.05}O_2$ cathode and graphite anode batteries. [c] Ethyl-Methyl-Carbonate.					

Like other electrochemical battery systems, in Li-ion batteries the ions move from anode to cathode by passing through electrolyte and separator while electron flow through external circuit completes the electrochemical reaction. During the discharge cycle, the reaction proceeds in the reverse direction, as shown in **Figure 4.4**. A complete electrochemical reaction for Li-ion batteries is given in **Table 4.2**, based on the intercalation and de-intercalation of lithium ions [57].

Performance parameters such as energy/power densities, safety, stability and cyclability of lithium-ion batteries are continually improving as a result of the introduction of new materials (anode, cathode and electrolyte) and improvement in battery technology (stock design, reduced self-discharge and weight). Despite their outstanding characteristics, Li-ion batteries are still lagging behind in some key areas such as their high cost when compared with their counterparts such as lead acid or sodium ion batteries, which originates from the high lithium cost resulting from limited availability and sporadic geographical distribution of elemental lithium reserves. Moreover, at temperatures over 30 °C there is a considerable drop in capacity retention and

cyclability over longer period of time in Li-ion batteries. Another major issue which surrounds Li-ion batteries is their operational safety, since additional protection circuits are required to limit circuit currents and voltages for their safe operation to avoid overloading [87]. Currently research is under way to address these issues and improve battery technology even further in order to enhance the suitability of Li-ion batteries for a wider range of applications.

4.4.3.3 Lead-Acid Batteries (Pb-A)

The lead-acid (Pb-A) battery was invented by French physicist Gaston Planté in 1859. In a standard Pb-A battery cell PbO_2 is used as the cathode and Pb as the anode with sulphuric acid used as an electrolyte. The chemistry of this type of battery system is considered mature, robust and well understood, with Pb-A batteries considered one of the most technologically developed and commercially successful battery systems [106, 107]. The complete composition of the various constituents of these batteries by percentage weight is given in **Table 4.4**. Lead-acid batteries retain the largest market share both in terms of production capacity (MWh) and sales volume, the automotive industry being the principal user with secondary markets for other industries such as standby and emergency power sources, portable electronic devices and telecommunications/data networks applications, making it the market leader [108]. Lead acid battery systems are based on particularly complex primary and secondary electrochemical reactions. Cathode and anode are comprised of lead peroxide (PbO_2) and sponge lead (Pb) on lead lattice respectively using water and sulphuric acid solutions as electrolyte. During complete reversible charge/discharge reactions lead and lead peroxide are converted into lead sulphate ($PbSO_4$) [109], complete electrochemical reaction is given in **Table 4.2**.

Table 4.4 Composition (by percentage weight) of two leading Pb-A batteries [57, 110, 111].

Material (%)	Industrial	EV battery
Lead	25	69 ∗
Lead oxide	35	
Polypropylene	10	4
Sulphuric acid	10	11
Water	16	18
Glass	2	4
Antimony	1	
∗ 1:3 ratio of lead to lead oxides		

Lead-acid batteries can be further divided into two groups: valve regulated and sealed lead-acid batteries. Valve regulated batteries have valves installed in order to release excess pressure generated at positive electrode during oxygen reduction reaction whereas sealed lead-acid batteries with innovative and improved technology, known as Valve Regulated Lead Acid

(VRLA) based battery cells, were introduced between 196 and 1975 and are completely sealed [112, 113]. VRLA based battery systems are more compact in size than valve regulated cells making them more useful for small scale applications such as small portable devices. In contrast, valve operated battery systems can be readily scaled up, resulting in higher storage capacity leading to a broader application base such as in emergency lighting, uninterruptible power supplies (UPS) and as energy sources for power telecommunication. Although, VRLA technology did not improve the operating performance (energy/power densities) of Pb-A based battery systems they resulted in additional benefits due to lower electrolyte content, including a lower level of maintenance, improved reliability and most importantly it is easier for them to meet airfreight and transportation regulations. Other benefits of Pb-A batteries include fast response times, small daily self-discharge rates (< 0.3 %), relatively high cycle efficiencies (~ 63-90 %) and low capital costs [114-116]. Other advantageous properties of lead-acid batteries which make them a commercially attractive technology include cost-effectiveness, excellent rate capability, outstanding charge retention and good performance over wide temperature ranges.

Despite these beneficial properties, lead-acid batteries suffer from short life span (300-500 cycles), pose environmental concerns, possess a relatively poor energy density (40 Wh kg^{-1}) and suffer acid stratification [108, 117]. Moreover, VRLA based Pb-A batteries suffer from 'dry out' failures and perform poorly at low temperatures, requiring temperature controlled voltage management systems to address these issues which increases the overall cost of a battery system [118, 119]. In order to address the performance and operational issues of lead acid batteries, currently R&D in Pb-A batteries focuses on: (a) material innovation for battery performance enhancement such as cyclability and deep discharge capability improvements; (b) reduction in response time; (c) optimization of battery technology for their commercialization in a wide range of applications including transportation sector and photovoltaic power integration [120].

4.4.3.4 Nickel-Cadmium Batteries (Ni-Cd)

The Nickel-Cadmium battery system was first patented by Swedish engineer Waldemar Jungner in 1899 [121]. Metallic cadmium and nickel hydroxide are used as anode and cathode respectively along with an aqueous alkali solution such as potassium hydroxide (KOH) as an electrolyte which does not undergo significant changes during operation. Anode and cathode are separated by a three-layer porous polymeric separator which normally consists of nylon/polypropylene/nylon layers assisting in electrolyte diffusion [122]. The material composition of a typical nickel-cadmium battery is given in **Table 4.5**, where it can be seen that the fundamental material composition can vary substantially depending on application. In a Ni-

Cd Cell Ni is reduced (NiOOH → Ni(OH)$_2$) at the cathode during the discharge cycle and cadmium (Cd) is oxidized (Cd → Cd(OH)$_2$) at the anode. During charging the reverse reactions take place. However, during the discharge cycle oxygen and hydrogen are produced at the positive and negative electrodes, respectively requiring the addition of water and venting [123]. The complete chemical reaction scheme for the operation of a Ni-Cd battery system is given in **Table 4.2**. The composition of the various constituents of Ni-Cd batteries by percentage weight used for automotive and portable electronic applications is given in **Table 4.5**.

Table 4.5 Typical materials composition (by percentage weight) of the Nickel-Cadmium Battery types used for automotive and portable electronic applications [57, 110, 124].

Material (%)	Automotive	Portable Electronic
Cd	25	16.4
Ni powder	20	20.5
Ni(OH)$_2$	17	8.1
KOH	5	3.5
Plastic	3	3.7
Steel & copper	16	39
Water	12	8
Others	2	

Nickel-Cadmium batteries operate on the same working principle as other electrochemical battery systems but with two distinctive designs, one a completely sealed cell and other with a vent to release gases (oxygen and hydrogen) [125, 126]. Sealed cells are used in everyday life whereas vented Ni-Cd batteries are used in aircraft and diesel engine starters, where large energy per weight and volume are critical [127]. The Ni-Cd battery system offers advantageous properties including fast charge/discharge and long cycle life (they can complete up to 3000 cycles). They can tolerate deep discharge rates without any capacity loss and have good size flexibility (ranging from small portable devices to large vented cells) in comparison to other battery systems such as the lead acid batteries. Ni-Cd batteries were widely used and had the largest market share until the 1990s in applications such as standby power sources and portable applications, before losing market share to other, superior, rechargeable battery systems such as LIBs [128-129]. The disadvantageous characteristics of the Ni-Cd system, such as environmental concerns due to cadmium toxicity and their high production cost (nearly ten time higher than lead-acid batteries) limit their wider use. Another drawback of Ni-Cd batteries is that they suffer from 'memory' issues which limit their capacity if they are un-used for extensive periods or not discharge completely before charging [130, 131].

4.4.3.5 Nickel-Metal Hybrid Batteries (Ni-MH)

Nickel metal hydride (Ni-MH) battery technology is a further development of nickel-cadmium batteries with the key objective of addressing two fundamental issues-high cadmium cost and environmental concerns. Ni-MH batteries can be considered an improved form of Ni-Cd batteries since both have similar configurations, with identical cathode and electrolyte material. The primary difference is that the anode in Ni-MH is replaced with an hydrogen absorbing alloy [132]. Additionally, cell voltages and charge/discharge curves are also identical for both battery systems. As shown in **Table 4.2**, similar to lithium-ion batteries in which Li ions transfer between the electrodes during the operation of the battery, in the overall cell reaction of a Ni-MH batteries, hydrogen is transferred from one electrode to the other [133]. The very simple electrochemical reactions of Ni-MH batteries provide the basis for their long cycle life (~ 500 cycles) and fast kinetics (high power densities, typically ≥ 1000 W kg$^{-1/2}$). The typical material composition of leading Ni-MH batteries is outlined in **Table 4.6**.

Table 4.6 Composition (by weight percentage) of two leading Ni-MH batteries [57, 134].

Material	NiMH-AB$_2$ [a] Percentage	NiMH-AB$_5$ [b] Percentage
Ni	12	15
Ni(OH)$_2$	12	15
M: Ni, Ti, V, Zr	13	
M: La, Nd, Pr, Ce		8
KOH	3	3
PP	5	5
Steel	44	44
Others	11	10
[a] Anode materials consists of titanium (Ti), zirconium (Zr), Ni and vanadium (V). [b] Anode based on metals from lanthanum (La) to lutetium (Lu).		

NiMH batteries are inferior to Li-ion cells however, some of their key characteristics that make them preferable choice over Ni-Cd technology, particularly for applications in portable electronic devices include: an insignificant memory effect, outstanding performance over a wider temperature range, rapid charging (they can be fully charged within an hour) and a high energy density (50 % higher than the energy density of Ni-Cd batteries) [135, 136]. Electric/hybrid electric vehicles (EVs/HEVs) such as the Toyota Prius are significant users of Ni-MH batteries. Applications of Ni-MH batteries depend on the nickel-metal hydride cell's chemistry, where the cell offers tolerance to both overcharge and over-discharge through gas recombination reactions. This results in a maintenance free battery cell since there is no pressure build up even inside a totally sealed battery cell. This extraordinary capability of the Ni-MH cell eliminates the requirement for cell voltage

monitoring, which results in simplified battery management systems (BMS) as compared with other high energy density systems such as sodium-sulphur and lithium-ion systems [137, 138].

The applications of Ni-MH batteries are declining with time due to collective effects of the development of other efficient battery technologies (such as lithium-ion batteries) and the deficiencies of Ni-MH battery systems. The principal drawback of Ni-MH cells is their very high self-discharge rate (up to three times that of Ni-Cd batteries and even higher when compared with other rechargeable battery systems such as lead-acid or lithium-ion) which results in a Ni-MH battery losing up to third of its charge within a month even without being used. The self-discharge issue of the battery is less noticeable in applications such as EVs/HEVs due their frequency of use, but it becomes more prominent in occasionally used portable electronic devices. Other disadvantages include a high material cost which makes them less competitive to other rechargeable batteries such as lithium-ion in longer term [139, 140].

4.4.3.6 Comparison of different rechargeable battery types

The key objective of all rechargeable battery systems is to increase their energy densities without compromising on their power densities, while simultaneously restricting their mass and volume to allow the diversification of their applications. **Figure 4.6** illustrates the relationship between energy and power densities of various commercialized rechargeable battery systems among them the Li-ion battery shows the highest gravimetric and volumetric energy densities.
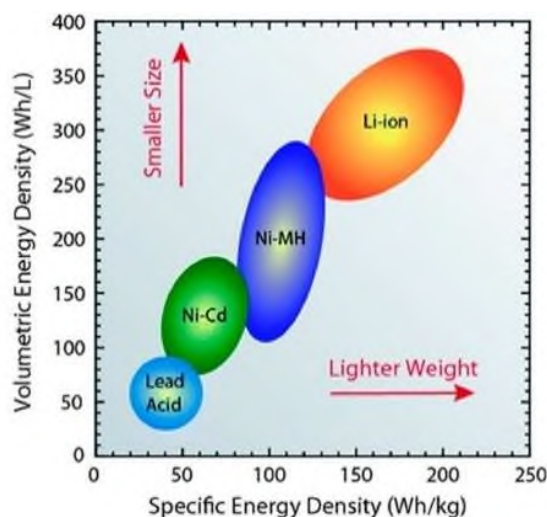
Figure 4.6 *Graphical comparison of different rechargeable battery technologies in terms of their volumetric and specific energy densities. The arrows indicate the direction of development to reduce battery size and weight [141].*

These are the main characteristics which make Li-ion batteries commercially successful electrical energy storage technology.

An ideal battery system needs to possess high energy/power densities coupled with fast charge/discharge rates, operational safety, and appropriate cyclability. The advantages and

disadvantages of the four rechargeable battery systems discussed above are summarized in **Table 4.7**, which gives a comprehensive understanding of the different characteristics of these rechargeable battery systems.

Table 4.7 Advantages and disadvantages of different battery systems [57, 142].

Battery Type	Advantages	Disadvantages
Lead-acid	1. Mature technology 2. Word wide production 3. Low material cost 4. No memory effect 5. Low self-discharge rate 6. Relatively low capital cost	1. Short cycle life 2. Modest energy/power density 3. Long charging time 4. Safety issues (gas discharge) 5. Temperature sensitive output 6. Poor reliability
Lithium-ion (Li-ion)	1. Long cycle life 2. High round trip efficiency 3. Global R&D efforts 4. Relatively fast charging 5. Highly reliable 6. Low discharge rates 7. Excellent energy/power density	1. High capital cost 2. Safety issues (Thermal runaway) 3. Material bottle concerns 4. Poor recovery/recycling 5. Advanced battery management systems required
Nickel metal hydride (NiMH)	1. Modest initial cost 2. Acceptable energy/power density 3. Modest round-trip efficiency 4. Highly reliable 5. Excellent safety record 6. Relatively fast charging 7. Eco-friendly materials 8. Low operational maintenance	1. Higher self-discharge rate 2. Memory effect 3. Relatively short cycle life 4. Poor recovery/recycling
Nickel-cadmium (Ni-Cd)	1. Comparatively low capital cost 2. Highly reliable 3. Mature technology 4. Superb safety record 5. Wide operating temperatures 6. Relatively fast recharge 7. Excellent cycle life 8. Low operational maintenance	1. Modest energy/power density 2. Memory effect 3. Relatively poor round trip efficiency 4. Reliance on hazardous cadmium

4.4.3.7 Flow Batteries

A flow battery system is comprised of two external liquid electrolyte tanks connected to a cell stack and separated by an ion selective membrane, as shown in **Figure 4.7**.

Electrolytes are pumped from electrolyte tanks to the cell stack where operation is based on reduction-oxidation reactions of the electrolyte solutions. Electrical energy is converted into chemical energy during charging, when one electrolyte is reduced at the cathode and the other electrolyte is oxidized at the anode. During the discharge phase the same process is completed in reverse direction [143].
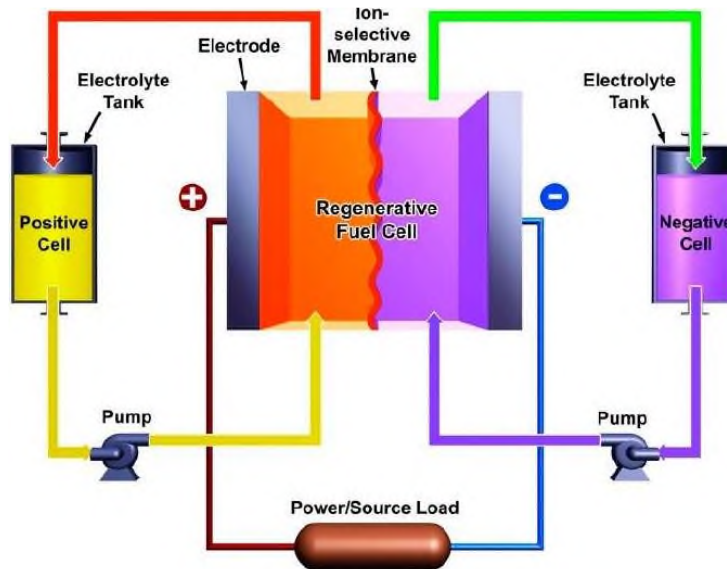
Figure 4.7 *Schematic representation of a redox flow battery [144].*

Flow batteries can be classified into two groups: *hybrid flow batteries* and *redox flow batteries*. Properties such as design flexibility and scalability, low toxicity, safety, durability and un-limited capacity make flow batteries a favorable option compared with currently available electrochemical energy storage technologies for energy storage in large scale applications [145-147]. The shortcomings of flow batteries include a comparatively high manufacturing cost, inferior performance resulting from non-uniform pressure drops and reactant mass transfer limitations and highly complicated system requirements when compared with other rechargeable batteries [148, 149]. Some of the most technologically mature flow battery systems include vanadium redox flow battery (VRB), zinc bromine (ZnBr) flow battery and polysulfide bromine (PSB) flow battery. These battery systems are still at research stages and have not seen widespread applicability and commercialization when compared with commercialized rechargeable batteries.

4.4.3.8 Lithium-air (oxygen) batteries

In its simplest form, the lithium-air cell brings together a reversible lithium metal electrode and an oxygen electrode at which a stable oxide species is formed. There are two variants of rechargeable Li-air technology - a non-aqueous and an aqueous form, both of which offer at least ten times the energy-storing capability of the present lithium-ion batteries [190-193]. **Figure 4.8** provides a schematic view of the two versions. In both, the cathode is a porous conductive carbon which acts as the substrate for the reduction of oxygen, while the anode is metallic lithium [236].

A
Li-air (non-aqueous)

B
Li-air (aqueous)
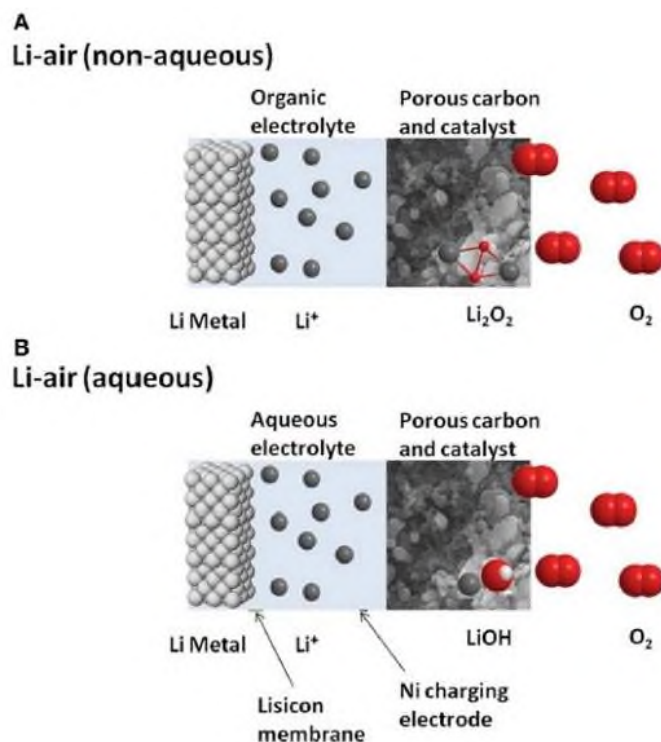
Figure 4.8 Schematic representation of two contemporary versions of the lithium-air battery - (A): non-aqueous version, similar to Li-ion and (B): aqueous, with Li^+-permeable membrane protecting the lithium anode [182].

For the non-aqueous system, the reduction of oxygen ends with formation of peroxide, so that the overall reaction follows Equation (4.3).

$$2\mathrm{Li(s)} + \mathrm{O_2(g)} \rightarrow \mathrm{Li_2O_2(s)} \qquad (4.3)$$

A cell based on this reaction has an open circuit voltage of 2.96 V and operates at specific energy values ranging between 3460 and 11680 Wh kg^{-1}. During discharging, the cell draws in oxygen and thereby gains mass, while it loses mass during charging, so that specific energy reaches a maximum when fully charged [237].

In the aqueous form of lithium-air battery, water is involved in the reduction of oxygen, while the lithium electrode must be protected from reaction with water, usually by means of a lithium-ion-conducting solid electrolyte such as LISICON. Typically the electrolyte solution is a saturated solution of LiCl and LiOH and the favored reduction product is a hydrated lithium hydroxide, according to Equation (4.4).

$$4\mathrm{Li(s)} + 6\mathrm{H_2O(l)} + \mathrm{O_2(g)} \rightarrow 4(\mathrm{LiOH.H_2O})(s) \qquad (4.4)$$

The involvement of water in the reaction complicates the operation of the cell and degrades the specific energy which is theoretically around 2000 Wh kg^{-1} and varies over $\sim$ 100 Wh kg^{-1} with state-of-charge [193]. While this is still an impressive level of performance, the main problem with the aqueous form of lithium-air is the difficulty of maintaining separation of lithium metal from the aqueous medium. Most of the Li$^+$-conducting solids tried to date do

37

not have sufficient long-term stability against aqueous solutions. In addition they contribute significantly to cell impedance - reducing the thickness of this protective layer ameliorates this effect but is limited by the poor mechanical strength of very thin layers [238]. For these reasons, most research effort in lithium-air batteries is focusing on the non-aqueous form.

Clearly a key aspect to the realization of the very high specific energy of lithium-air battery is that the lithium metal anode can be made to operate safely and at full utilization [239].

The positive electrode of a lithium-air cell represents a complex challenge in that it must provide for: (i) access to oxygen; (ii) wetting by the electrolyte; and (iii) displacement by reaction products [240, 241]. While allowing access to oxygen, the electrode must be able to block access to water, carbon dioxide, and nitrogen, which will all react with the electrode materials and/or products of reaction at the electrodes [242]. The properties of the main product of discharge, lithium peroxide, Li_2O, also pose a number of problems with regard to cell longevity. First, it is an insulating solid, which means that conditions must be adjusted to prevent the formation of massive deposits during discharging. Second, lithium peroxide is a strong oxidant that tends to react with electrolyte components, including any adventitious water, to form irreversibly a variety of materials that severely degrade the lifetime of a Li-air cell [243].

4.4.3.9 Sodium-air (oxygen) batteries

The reversible sodium electrode is well-known in the history of battery development as it is featured in some of the very earliest examples of high performance secondary batteries. Both the sodium-sulfur and the Zebra (sodium-nickel chloride) systems employ molten sodium electrodes which give reversible behavior at values of potential that are sufficiently negative for useful device voltages [194]. Recently, the sodium electrode has again become the focus of attention, now coupled with an oxygen electrode in the sodium-air cell. This, like all metal-air systems, benefits in energy terms from the inherently lightweight air-breathing cathode and offers theoretical values of specific energy that range from 1105 to 2643 Wh kg^{-1}, depending on the state-of-charge. These numbers are derived from the overall cell reaction shown in Equation (4.5).

$$Na(s) + O_2(g) \rightarrow NaO_2(s) \tag{4.5}$$

Many of the limitations on performance of the air cathode in Li-O$_2$ cells also define the behavior of this electrode in Na-O$_2$ cells. The use of carbonate and ether electrolyte solutions has been hampered by problems of insufficient stability during charging [195]. While the preferential formation of sodium superoxide during discharging clearly lowers the overpotential associated with charging, it is not clear whether this compound will be stable on the longer

timescale of a typical device service life, or whether the discharge product will gradually be converted to the more stable, and less easily recharged, sodium peroxide [244].

4.4.3.10 Zinc-air (oxygen) batteries

The main structure of a primary Zn-air battery, which is composed of a Zn anode, an electrolyte, an air cathode with active materials to promote the Oxygen Reduction Reaction (ORR) [245], and a gas diffusion layer that allows air to enter into the electrolyte, is illustrated in **Figure 4.9** (a) [246].
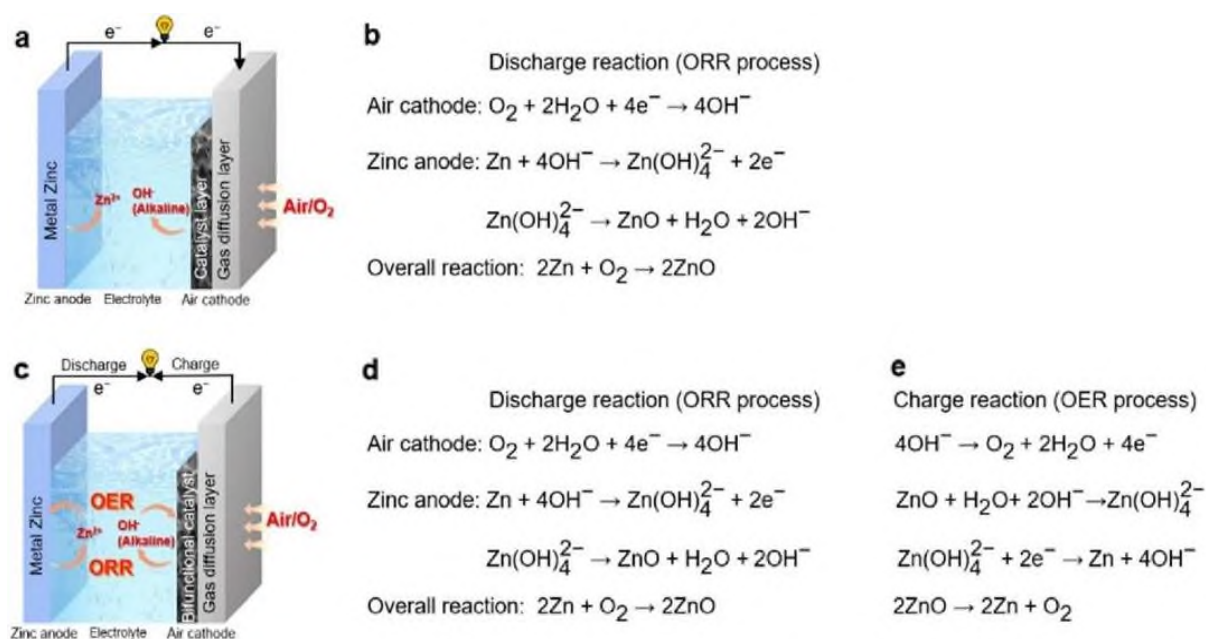
Figure 4.9 (a) Schematic working principle and (b) discharge reaction equations of a primary Zn-air battery in an alkaline medium. (c) Schematic working principle, (d) discharge reaction equations, and (e) charge reaction equations of a rechargeable Zn-air battery in an alkaline medium [246].

The basic working principle of a primary Zn-air battery during the discharge process in an alkaline electrolyte is illustrated in **Figure 4.9** (b) [247]. Specifically, the Zn anode first liberates two e⁻ and is oxidized to zinc ions (Zn^{2+}) [248]. The released e-migrates via an external circuit to the air cathode, where it contacts O_2 on the surface of the catalysts [249, 250]. Then, the O_2 is reduced through the ORR to form hydroxide ions (OH⁻) at the solid (active catalysts)-liquid (electrolytes)-gas (O_2) three-phase interface [251], and the full battery reaction is Zn+O_2 to ZnO. Theoretically, the ORR in a Zn-air battery is fully reversible. Therefore, a bifunctional [(ORR and Oxygen Evolution Reaction (OER)] oxygen-catalytic electrode will allow realization of a rechargeable Zn-air battery, where the charging process is promoted by the OER on the cathode, and ZnO is reduced back to Zn and deposited on the anode [252]. Generally, the properties of rechargeable Zn-air batteries are particularly dependent on the kinetics of both the ORR and the OER, which are closely related to the natural activities of the bifunctional catalysts, as well as the reactant diffusion efficiency at the

reaction interface [253]. The main structure of a rechargeable Zn-air battery, which is similar to that of a primary battery but with different electrolytes and catalyst layers, is illustrated in **Figure 4.9 (c)** [254]. The working principle of a rechargeable Zn-air battery during the discharging and charging processes in an alkaline electrolyte is illustrated in **Figure 4.9 (d,e)** [255].

4.4.3.11 Lithium-Sulfur batteries

A positive electrode comprised solely of elemental sulfur has a theoretical specific capacity of 1672 mAh g^{-1}. Assuming an equivalent amount of lithium for the negative electrode, complete reaction of Li and S to form Li$_2$S, and an average discharge potential of 2.2 V per cell, the electrode specific energy for Li-S is 2600 Wh kg^{-1} [196-198]. The overall discharge reaction, in its simplest form, is given in Equation (4.6), and a schematic view of the components and their role is provided in **Figure 4.10**.

$$2\text{Li}(s) + \text{S}(s) \rightarrow \text{Li}_2\text{S}(s) \tag{4.6}$$

Fully packaged, it is expected that Li-S batteries in real life will operate at up to 700 Wh kg^{-1}. This level of performance places lithium-sulfur well-clear of existing battery systems, and many view it as a logical intermediate step to the lithium-air battery.
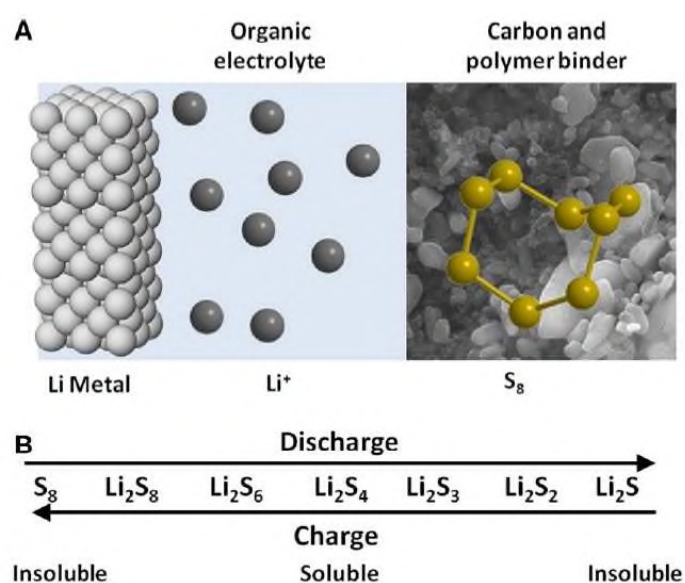
Figure 4.10 (a) A schematic view of the lithium-sulfur cell. (b) Summary of reactions that define Li-S and their relationship with solubility [182].

While not sharing the full range of difficulties of the air electrode, the sulfur electrode still represents a complex electrochemical system in which elemental sulfur, in the form of S$_8$ molecules, is successively reduced through a sequence of polysulfide dianions [196]. The solubility of the lithium salt of each successive reduction product decreases appreciably, with the end discharge product, Li$_2$S, being virtually insoluble in common organic electrolyte media

40

[256]. Overlaying this is the generally labile nature of exchange between intermediate members of the polysulfide series, which has the undesirable consequence of allowing significant loss of efficiency through a redox shuttle phenomenon [197].

4.4.4 Fuel Cells

The development of fuel cell technology can be traced back over 180 years to Sir William Grove's pioneering work experimentally demonstrating the electrolyzer / fuel cell in 1839 [150]. This was followed by construction of a full-scale device (initially called a gas battery which latter came to be known as fuel cell) in which electricity was produced by combining oxygen and hydrogen in a cell. The British engineer Francis Thomas Bacon has been credited with developing the first fully operational fuel cell in 1959, which was later adopted by NASA for space research [151]. NASA used both alkaline fuel cells (AFC) and polymer electrolyte membrane fuel cells (PEMFC) for space exploration missions such as Gemini and Apollo in the 1960s [257]. In the 1990s PEMFC and direct methanol fuel cells (DMFC) attracted worldwide interest, which resulted in further development in this field. Currently fuel cell technology is witnessing huge research drive, resulting in improvement in technology which will lead to widespread commercialization [258]. The fuel cell is an electrochemical energy conversion device where chemical energy is directly converted into electrical energy, resulting in high energy conversion efficiencies. This exchange of energy takes place within the core of the cell which comprises of an electrolyte in direct contact with the cathode (positive electrode) and anode (negative electrode) [259]. According to their fuels, operating temperatures and electrolytes, fuel cells can be classified into six main categories as follow [152, 153].

1. Solid oxide fuel cell (SOFC).
2. Proton exchange membrane or polymer electrolyte membrane fuel cell (PEMFC). These can be further subdivided into standard PEMFC (operating below 100 °C) or high temperature PEMFC or HT-PEMFC (operating in temperature ranges of up to 200 °C).
3. Molten carbonate fuel cell (MCFC).
4. Alkaline fuel cell (AFC).
5. Phosphoric acid fuel cell (PAFC).
6. Direct methanol fuel cell (DMFC).
7. Single layered fuel cell (SLFC).

Fuel cell technology has seen a limited use in nearly all types of power applications, ranging from the small scale such as personal computers and cell phones (up to 10 kW) to medium range applications such as transport applications (up to 100 kW) and lastly in large scale power applications (up to 10 MW) [154, 155].

4.4.4.1 Solid Oxide Fuel Cell (SOFC)

Solid oxide fuel cells (SOFCs) differ significantly from their counterparts since they are solid state devices without any moving components and have distinguishing characteristics such as combustion free operation, low emissions, inherently high conversion efficiencies and very high operational temperatures (in the range of 800-1000 ∘C). Efforts have been made to introduce new electrode materials to improve their thermal stability, electrical conductivity, catalytic activity, chemical compatibility and cost-effectiveness especially with the drop in operational temperature from 400 ∘C to 700 ∘C [260].

Selection of suitable anode materials is a key to maintain superior performance of SOFCs, since anode materials accounts for nearly 95% of the overall percentage of material in anode supported cell [261]. Most commonly used anode material in SOFCs is Ni-YSZ due to its high stability and excellent conductivity however, the materials is susceptible to carbon deposition when comes in contact with hydrocarbon fuels [160]. Song et al. improved the performance of a Ni-YSZ based SOFCs through doping of its anode by adding Al_2O_3 to Ni-YSZ which resulted in improved electrical conductivity, decreased anode activation polarization and nearly 39% improvement in performance of the cell [161]. Other anode materials used in SOFCs include $CrTi_2O_5$, $Cu-CeO_2$, $CrTi_2O_5$ $La_{0.8}Sr_{0.2}Fe_{0.8}Cr_{0.2}O_3$ and $Sc_{0.1}Y_{0.1}Zr_{0.6}Ti_{0.2}O_{1.9}$ [162].

The cathode is another fundamental component of a SOFC system and has different selection criteria when compared to the anode since the cathode in a SOFC requires distinctive operational properties such as high level of porosity and stability in oxygen environment. Also due to their elevated operating temperatures, SOFCs use more cost-effective and widely available transition metal oxides such as Cu, Co, Ce, Sr and Ni as an alternative to costlier metals such as Pt as cathode since high temperature operations of the cell result in sufficiently improved kinetics and thermodynamics of the chemical reactions underpinning fuel cell operation [262]. Moreover, SOFCs can be used as a substitute for electrochemical batteries due to their high efficiencies even in in reverse mode as solid oxide electrolysis cells (SOEC) in which steam is electrolyzed into hydrogen by feeding water and electric current into the cell to produce hydrogen and oxygen [156, 163]. Owing to these excellent properties and their modularity, fuel adaptability, diverse scale of application (small, medium and large scale) and vibration free, quiet operation, SOFC are promising candidates for use in the field of energy storage and conversion in the future [164].

The basic structure of a SOFC consists of a porous anode and cathode sandwiched around a ceramic based solid electrolyte such as yttria-stabilized zirconia (YSZ) or gadolium-doped ceria (GDC), as shown in **Figure 4.11**.
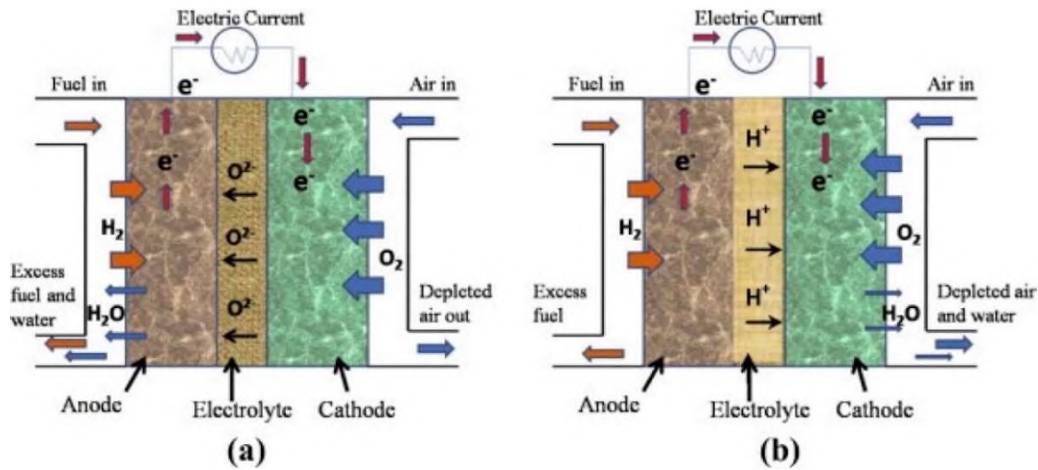
Figure 4.11 *Schematic representation of solid oxide fuel cell (SOFC) (a) oxide-ion conducting electrolyte, (b) proton conducting electrolyte [178].*

Electrons are generated at the anode through oxidation and are accepted at the cathode for oxygen reduction, resulting in circuit completion with the production of electricity due to the flow of electrons from anode to cathode through an external circuit [165, 263-270]. The chemical reactions are given by Equations (4.7) - (4.10).

$$H_2 \rightarrow 2H^+ + 2e^-$$ (4.7)

$$\frac{1}{2}O_2 + 2e^- \rightarrow O^{2-}$$ (4.8)

$$H_2 + \frac{1}{2}O_2 \rightarrow H_2O$$ (4.9)

$$H_2 + O^{2-} \rightarrow H_2O + 2e^-$$ (4.10)

SOFC technology has the potential to transform the overall electrical energy generation landscape with insignificant environmental impact if it is more extensively commercialized. Their commercialization has nonetheless been limited by several disadvantages such as high material costs, the requirement of high operating temperatures (800-1000 ∘C), safety issues and the complex stack and cell assembly. Furthermore, high operating temperatures have added issues including catalyst poisoning, electrode sintering, electrode/electrolyte interfacial diffusion and thermal/mechanical stability [271]. These issues, and particularly the need for high operating temperatures, has forced research towards low temperature SOFC technology . The benefits of lowering operating temperatures include widening the area of application and improving the life span of the SOFCs, technical improvements (i.e., reducing the likelihood of cermet anode's redox degradation) and economic advantages (i.e., using more cost effective cell components) [167].

4.4.4.2 Direct Methanol Fuel Cell (DMFC)

Direct methanol fuel cells are considered as a subcategory of proton exchange membrane (PEM) fuel cells and can also be considered as low operating temperature PEM,

where methanol is used as fuel [272]. DMFCs work on the principle of directly converting the chemical energy of high energy density liquid methanol fuel to electric power via electrochemical processes with carbon dioxide and water as by products [168, 169]. The potential for adoption of DMFCs as a key energy conversion device is predominately a result of the high specific energy of pure methanol (up to 6000 Wh kg^{-1}) [170]. A schematic representation of a DMFC system is shown in **Figure 4.12**, illustrating its basic working principles (e.g., reactants/products gasses and ion conduction flow direction).
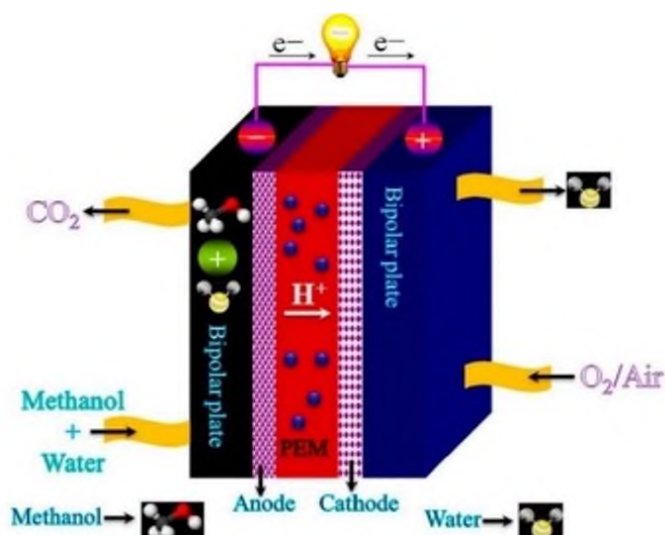
Figure 4.12 *Schematic diagram of a DMFC with PEM polymer electrolyte membrane [179].*

The electrochemical reaction between oxygen and methanol occurs at cathode and anode respectively whereas the complete electrochemical reaction of DMFC is given by Equations (4.11) - (4.13):

Anode:

$$CH_3OH + H_2O \rightarrow CO_2 + 6H + 6e^- \qquad (4.11)$$

Cathode:

$$\frac{3}{2}O_2 + 6H + 6e^- \rightarrow 3H_2O \qquad (4.12)$$

Complete reaction:

$$CH_3OH + \frac{3}{2}O_2 \rightarrow CO_2 + 2H_2O \qquad (4.13)$$
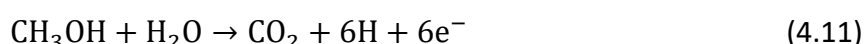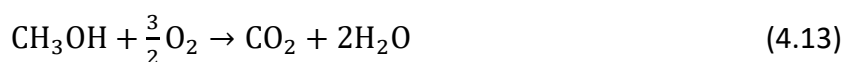
Methanol is a fuel with an excellent conversion efficiency, reaching around 96.5 % which is much higher than internal combustion engine, the latter being restricted by Carnot cycle. The maximum achievable theoretical operating voltage in a methanol-air cell is ~ 1.21 V [273], although this cannot be attained in practical operation due to sluggish reaction kinetics and ohmic losses in the electrolyte [172, 173].

One of the benefits of using methanol as fuel in DMFC is the storage and transportation of methanol, which is much easier than fuels such as hydrogen [274, 275]. Moreover, there is the added benefit of the high energy density of methanol, which is three orders of magnitude higher than hydrogen [276]. Direct methanol fuel cell technology is considered promising due to characteristics such as high-power density, low operating temperatures and easy start up [277].

4.4.4.3 Polymer Electrolyte Membrane Fuel Cell (PEMFC)

The working principle of polymer electrolyte membrane fuel cell (PEMFC) is similar to that of other fuel cells. Its structure consists of a gas diffusion layer (GDL), polymer electrolyte membrane (PEM), bipolar plate and catalyst layer (CL), as shown in **Figure 4.13**.
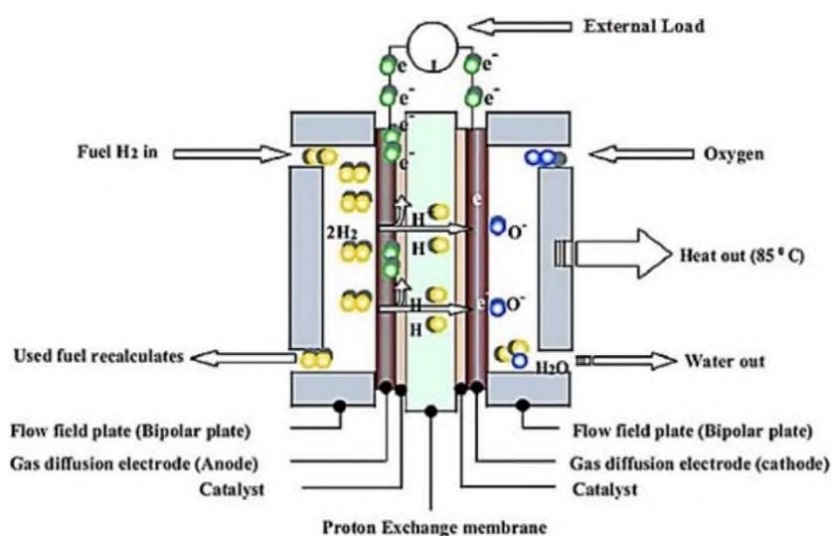
Figure 4.13 Schematic of working principle of polymer electrolyte membrane fuel cell [174].

Electrochemical reactions occur in the CLs while reactant gases flow through the GDL with hydrogen supplied to the anode and air or oxygen to the cathode. The chemistry of these cells leads to water being the only by-product, making the operation of PEMFCs completely environmentally friendly [278].

Advantageous properties such as low noise, lower operating temperature, high power density and excellent dynamic properties make PEMFCs a promising power source for automotive applications [279]. In addition, the simultaneous generation of both heat and power with high efficiency makes the PEMFC highly suitable for residential power generation applications [171]. In this case, additional heat generated during fuel cell operation can be used by households, which ultimately increases the overall efficiency of the cell especially high temperature HT-PEMFCs [280]. HT-PEMFCs operate at temperature range of 100-200 ∘C which is considerably higher than 60-80 ∘C for low temperature LT-PEMFCs which provides wider range of thermal energy usage [175].

4.4.4.4 Single Layer Fuel Cell (SLFC)

A new type of fuel cell, the single layer fuel cell (SLFC), has been reported recently based on semiconductor and an ionic conductor material. In contrast to a conventional fuel cell, the single layer fuel cell merges all three functional layers into one and is therefore also known as an electrolyte free fuel cell. Material composition and microstructure can be adjusted within the cell in order to reach a balanced ion/electron-conductivities and to reduce the lattice mismatch inside the fuel cell, hence enhancing the efficiency and performance. In a single layer fuel cell, the mixture of ionic and semiconducting materials provides the electrochemical reaction sites and charge transport medium respectively. The functional layer of a conventional fuel cell is the electrolyte layer whereas in a SLFC the nanocomposite material inside the single layer acts as a complete fuel cell [176].

The SLFC structure is presented schematically in **Figure 4.14**.
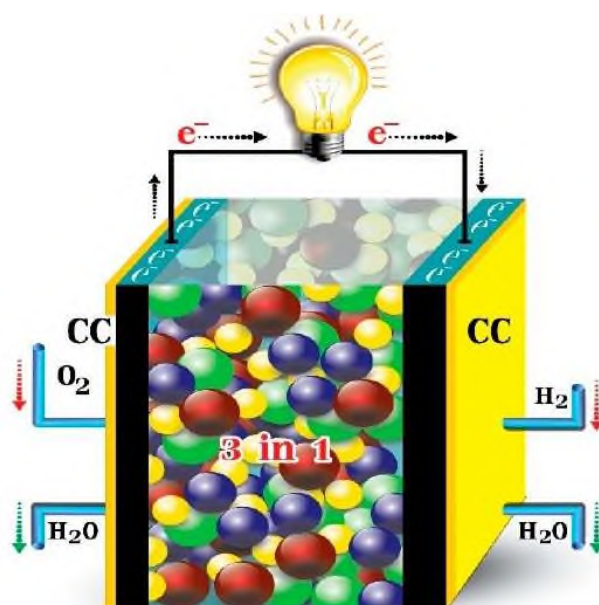
Figure 4.14 *The single component fuel cell, which is compromised of mixed conducting materials inside the layer [57].*

Mixed ionic and semiconductor materials are used to assemble the cell, both sides of this composite single layer is pasted by current collector (CC) for the current collection during the electrochemical operation. During this process, the side of SLFC which comes in contact with the hydrogen fuel becomes the anode while the side coming in contact with oxygen becomes the cathode. The anode side releases electrons by creating H^+ ions while the cathode side receives electrons, hence generating electricity and water.

The full reaction scheme for the SLFC can be described into two steps, given by Equations (4.14) - (4.16) [177].

Reaction at hydrogen-contacting (fuel) side:

$$H_2 \rightarrow 2H^+ + 2e^-$$

(4.14)

Reaction at the air contacting side:

$$\frac{1}{2}O_2 + 2e^- \rightarrow 2O^{2-}$$ (4.15)

Complete electrochemical reaction:

$$H_2 + \frac{1}{2}O_2 \rightarrow H_2O + electricity + heat$$ (4.16)
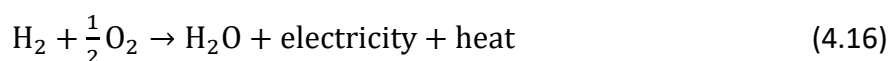
Table 4.8 summarizes the operational parameters, applications, advantages, and shortcomings of the different fuel cell systems, where it can be seen that different fuel cells technologies should be matched to specific projected applications for optimal use.

Table 4.8 Operational parameters, applications, advantages and disadvantages of different fuel cell technologies [57, 157-159].

Fuel Cell Type	Operating Temperature (°C)	Output (kW)	Efficiency (%)	Applications	Advantages	Disadvantages
Alkaline	900–100	10–100	60	(i) Military/Space	(i) Faster cathode reaction in alkaline electrolyte (ii) Variety of catalysts used	(i) Costly removal of CO$_2$
Molten Carbonate	600–700	1–1000	≥40	(i) Electric utility (ii) Distributed generation (large scale)	(i) High efficiency (ii) Fuel flexibility (iii) Variety of catalysts used	(i) Complex electrolyte management (ii) High operating temperature (iii) Slow start up
Polymer electrolyte membrane	50–100	1–250	53–58	(i) Backup power (ii) Portable power (iii) Transportation (iv) Distributed generation (small scale)	(i) Solid electrolyte: reduced electrolyte and corrosion issues (ii) Quick start up (iii) Low temperature	(i) Expensive catalyst requirement (ii) Highly sensitive to fuel impurities (iii) Low temperature (Heat wastage)
Direct methanol	60–200	0.001–100	40	(i) Portable devices	(i) Reduced cost due to the absence of fuel reformer	(i) Methanol high toxic and flammable (ii) Low efficiency
Phosphoric acid	150–200	50–1000	40	(i) Distributed generation	(i) Higher overall efficiencies (ii) Increased impurity tolerance	(i) Platinum catalysts required (ii) Low power output (iii) Large size
Solid Oxide	600–1000	1–3000	35–45	(i) Electric utility (ii) Auxiliary power (iii) Distributed generation (large scale)	(i) High efficiency (ii) Fuel flexibility (iii) Suitable for CHP (iv) Hybrid GT/Cycle (v) Variety of catalysts used	(i) High temperature enhances cell breakdown and corrosion (ii) Slow start up
Single layered	550–750		97–98	(i) Transportations (ii) Portable devices	(i) High efficiency (ii) Low cost (iii) Low emissions	(i) Un-tested technology

Although the working principle of all types of fuel cells is similar, their outputs, stack designs and working parameters are very different. For example, an alkaline fuel cell is the most efficient, with electrical efficiency around 60 % whereas a molten carbonate has the lowest efficiency (of around 40 %) with polymer electrolyte membrane fuel cells lying in the middle with intermediate efficiencies of around 55 %. Although, PEMFCs are not highly efficient, nevertheless they are ideal for transport applications due to their small size and low operating temperatures, while PAFCs and DMFCs are most cost-effective but suffer from low efficiencies [57].

4.4.5 Water Electrolysis

4.4.5.1 Low Temperature (LT) Water Electrolysis

Hydrogen can be generated by electrolyzing water at low temperatures (LTs) (< 100 °C) or electrolyzing steam at high temperatures (HTs) (> 700-800 °C) [281]. The LT electrolysis systems employ either an alkaline (hydroxyl ion conducting) solution as the electrolyte or a polymer membrane (proton conducting) as the electrolyte (**Figure 4.15**) [180, 181]. The hydrogen generation by utilizing a LT electrolyzer compared to that produced by natural gas (NG)

reforming or coal gasification, offers a number of advantages such as on-site, on-demand (distributed) generation, high purity hydrogen and unit modularity. Furthermore, such systems offer fast start-up and shutdown and good load following capability that makes them suitable for integrating with intermittent renewable energy sources such as solar PV and wind generators [282]. In LT systems, polymer electrolyte membrane (PEM)-based systems offer additional advantages over alkaline systems [283] such as higher current densities (small foot print in terms of kgs per hour hydrogen generation capacity per unit stack volume) [284], all solid state system requiring no alkaline solutions or electrolyte top-up, and higher purity hydrogen and hydrogen generation at significantly higher pressures [285, 286].
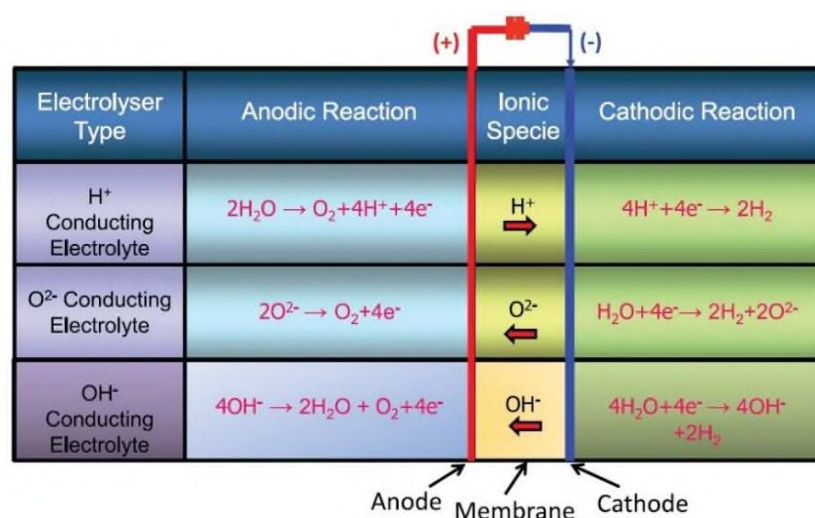
Figure 4.15 *Operating principles of low and high temperature water electrolysis with different electrolytes [182].*

The hydrogen generation by electrolysis is an energy intensive process and most commercial electrolyzers require an electric power input of 6.7-7.3 kWh/Nm^3 ($\approx$ 50-55 % efficiency based on High Heating Value) of hydrogen [181], and this increases the cost of hydrogen production and advantages of hydrogen as a clean fuel are lost if the electricity is supplied from fossil fuel resources. However, if the electric energy input can be supplied from renewable sources of energy and the electrolyzer system efficiency increased to 75-80 %, then the technology becomes more attractive [287-291]. The LT electrolyzers can easily operate with a large load variation and thus are highly suitable for integration with intermittent renewable energy sources [182].

4.4.5.2 High Temperature (HT) Water Electrolysis

As discussed above, hydrogen can be readily produced via LT electrolysis at almost any scale using only water and electricity as the inputs. This process is well-established but requires a high input of electrical energy in order to produce the hydrogen. From a thermodynamic perspective at 25 °C, 1 liter of hydrogen requires a minimum 3.55 kWh of electrical energy as an

input. This increases to around 4.26 kWh when electrochemical cell losses are taken into account. If the electrolysis process is carried out at HT then it is possible to utilize some of the heat for the production of hydrogen [292, 293]. This contribution can be high with up to a 1/3rd of the energy required to produce the hydrogen coming from thermal energy at around 1000 ^{o}C (**Figure 4.16**) [180-181, 183-185]. In **Figure 4.16**, the thermal energy input under cell operation may be slightly different due to internal heating of the cell resulting from current passage, however, due to the difficulty in making an estimate, it has been assumed to be the same as that under open circuit cell conditions. The HT electrolysis systems use an oxygen ion (O^{2-}) or proton conducting (H^+) ceramic as the electrolyte (**Figure 4.15**) [180-181, 183-185]. The process is the reverse to that of a solid oxide fuel cell (SOFC) with many similar materials used for cell construction [294-298]. The thermal input required for HT systems can be supplied from different sources including renewable or sustainable energy sources or nuclear energy [300].
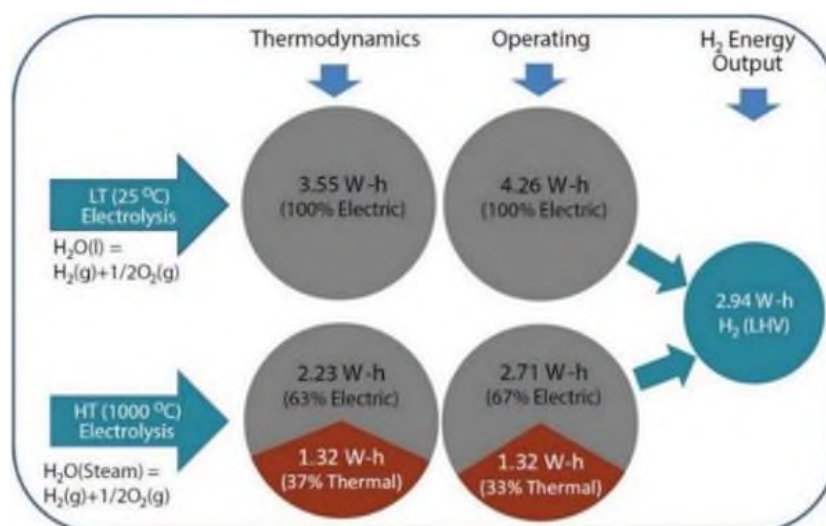
Figure 4.16 *Break down of energy input for the production of hydrogen from electrolysis at 25°C and 1000°C [181-182].*

A number of different systems have been proposed including the co-locating of the electrolyzer with a solar thermal source, nuclear power stations, or supplying heat produced from the burning of low grade fuels such as coal [181, 183, 186].

4.4.5.3 Carbon-assisted hydrogen production

The use of hydrogen as a transport fuel in fuel cell or internal combustion engine vehicles is likely to increase due to the concerns over oil shortage and rising greenhouse gas and other pollutant emissions. Hydrogen is generated mainly from Natural Gas (NG) and coal involving three major steps requiring separate reactors, all operating at temperatures in excess of 500 ^{o}C: (i) NG reforming or coal gasification to produce syngas (a mixture of hydrogen and carbon monoxide) at temperatures close to 800 ^{o}C; (ii) water gas shift reaction to convert carbon monoxide to hydrogen and carbon

dioxide at around 500 °C; and (iii) H_2/CO_2 separation and gas cleaning. Hydrogen production by water or steam electrolysis in which the electricity is drawn from the grid is overall a highly inefficient process, in that it requires electric input of 4.2-5 kWh per Nm^3 and 6.7-7.3 kWh per Nm^3 of hydrogen for the electrolysis cell stack and system, respectively [182, 299].

The participation of carbon in the anodic reaction of the electrolysis results in a drop in the thermo-neutral voltage from 1.48 to 0.45 V required for electrolysis of water near room temperature [187], which can translate into reduction in electric energy input to 1/3rd compared to normal electrolysis. Thus, the remaining 2/3rd of the energy would be supplied from the chemical energy of carbon. The carbon- assisted electrolysis carried out at higher temperatures can result in further reduction in the required electric energy input due to increased thermal energy contribution into the process by lowering the thermo-neutral voltage further [188, 189]. **Figure 4.17** schematically shows the electrochemical reactions involved for carbon-assisted electrolysis carried out at temperature < 100 °C (LT) employing a proton conducting electrolyte membrane, and at HTs (> 800 °C) employing an oxygen ion conducting ceramic electrolyte such as yttria or scandia stabilized zirconia.

In addition to a substantial reduction in the electric energy input by the involvement of carbon, this concept for hydrogen generation combines all three steps mentioned above for hydrogen from NG or coal in a single reactor.
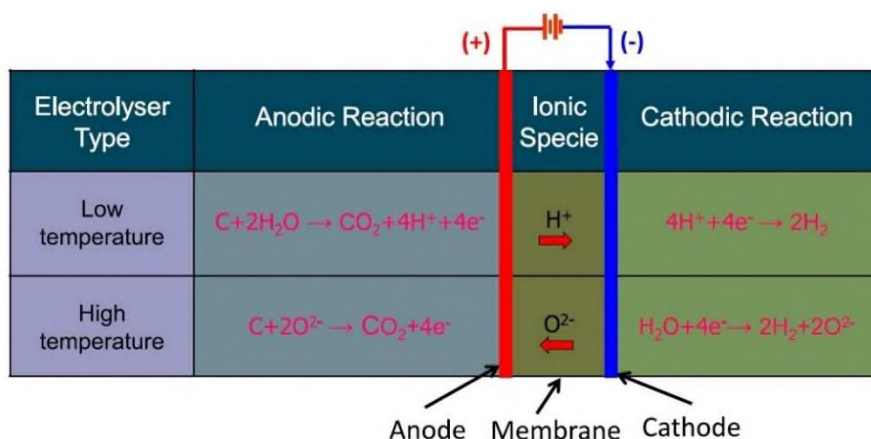
Figure 4.17 Electrochemical reactions involved in low and high temperature carbon-assisted electrolysis process for hydrogen generation [182].

The operating temperature is expected to be low (for proton conducting electrolyte membrane used) with the overall reaction being:

$$C + 2H_2O \rightarrow CO_2 + 2H_2 \qquad (4.17)$$

Furthermore, the process would generate pure hydrogen and CO_2 in separate compartments of the electrochemical cell separated by the impervious electrolyte membrane.

Thus, the substantial cost and the 20-25 % energy penalty for CO_2 capture / separation, as is the case with other routes above, can be avoided. Carbon source can be coal or biomass. All these advantages directly translate into a highly efficient process with low overall cost and substantially reduced CO_2 emissions [182].

4.4.6 Conversion of CO_2 to fuels with renewable energy

4.4.6.1 Introduction

Another emerging area under development energy conversion and storage involves the utilization of CO_2 as the feedstock to electrochemically synthesize fuels and certain specialty chemicals such as carbon monoxide, methanol, formic acid, methane, ethylene, and oxalic acid [199]. The utilization of electricity from renewable sources to convert CO_2 to high energy density fuels can help in alleviating the challenges of intermittent nature of the renewable sources by storing energy in the form of high energy density fuels, as well as addressing the liquid fuel shortage for the transport sector [301]. Apart from the production of fuels, some products formed by CO_2 conversion may also be suitable as a feedstock for the chemical, pharmaceutical, and polymer industries [302]. A number of review articles provide details on the methods of CO_2 reduction, electrode/electrolyte systems under consideration, various chemical products that can be produced and current status of the technology [199-207].
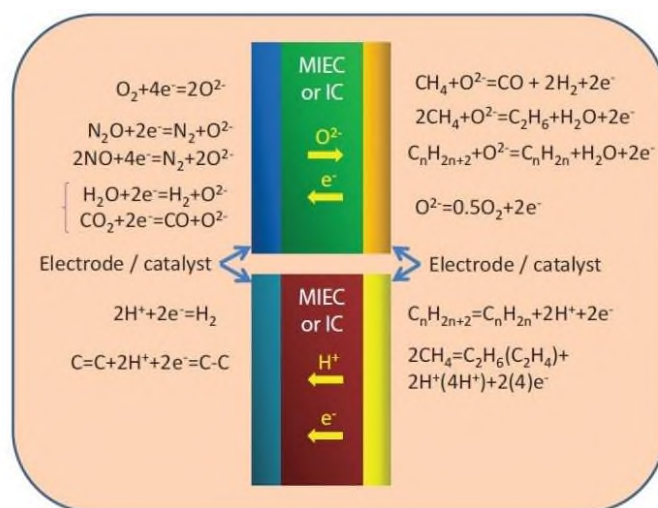
Figure 4.18 *Basic operating principle of O^{2-} and H^+ electrochemical reactors for chemical production [182].*

The processes employed for the electrochemically conversion of CO_2 include electro-catalysis (direct electrochemical conversion), photo electro-catalysis and bacteria-assisted electro-catalysis [303, 304] shown schematically in **Figures 4.18, 4.19**.

Waste	Anodic Reaction	Ionic Specie	Cathodic Reaction / Fuels produced
Biomass, Industrial & Municipal waste – (Bacterial catalysis-MEC)	Organic matter → $CO_2 + 2H^+ + 2e^-$	H^+ →	$2H^+ + 2e^- \rightarrow H_2$
CO_2 emissions (Electro-, photo electro- or bacterial- catalysis, MES)	$H_2O \rightarrow$ ½ $O_2 + 2H^+ + 2e^-$	H^+ →	$CO_2 + 2H^+ + 2e^- \rightarrow CO, CH_3OH, C_2H_5OH, HCOOH$ or C_2H_4 (Direct or in presence of photo-electrode cathode or bio-cathode)

Anode   Membrane   Cathode

Figure 4.19 *Electrochemical reactions involved in various processes for producing fuels and value-added chemicals from waste [182].*

4.4.6.2 Direct electrochemical conversion

The main electrolyte systems under consideration for the direct electrochemical conversion of CO_2 are divided into low or ambient temperature systems (aqueous, non-aqueous [199, 208-211] and PEM-based [212-213] electrolytes) and HT systems (molten carbonate [214] and solid oxide [215-223] electrolytes - in the 700-1000 ∘C range). In the direct electrocatalysis process, CO_2 is supplied as a feedstock to the cathode chamber of the cell for reduction. In case of LT electrolyte systems (aqueous and PEM electrolytes), water is supplied to the anode as a source of protons for reaction at the cathode [211-213]. The protons transported through the electrolyte to the cathode are made to react with CO_2 to produce fuels or chemicals (**Figures 4.18, 4.19**). The competing reaction in aqueous - and PEM-based electrolytes is the hydrogen evolution that should be avoided, otherwise it results in wastage of energy input to the process if hydrogen is not the required chemical.

4.4.6.3 Photo electrochemical conversion

In a photo electro-catalysis process, a photo-reduction electrode that consists of a semiconductor and a photo-catalyst is used as a cathode [205]. The photons from the solar radiation, absorbed by the semiconductor cause the excited electrons transfer from valence to conduction band, that results in transfer of electrons to photocatalysts. This electron transfer assists in the CO_2 reduction reaction involving protons transported through the electrolyte to produce CO and other organic compounds (**Figure 4.19**).

4.4.6.4 Bacterial-assisted electrochemical conversion

In bacteria-assisted electrosynthesis, the microorganisms at the cathode of the electrochemical cell assist in the reduction of CO_2 to fuels or value added chemicals. This process

is also called microbial electrosynthesis (MES) [224]. As depicted in **Figure 4.19**, the process involves protons transported through the electrolyte, electrons delivered to cathode and CO_2 supplied to the cathode camber. It is claimed that with electric input from renewable energy sources, the microbes can harvest the solar energy at 100 times the efficiency of a biomass-based fuel/chemical production [224].

4.4.7 Photoelectrochemical water splitting

Photoelectrochemical water splitting, which utilizes semiconductors to transform water and solar light into hydrogen, is one of the most efficient methods of solar energy consumption [305]. In their initial study published in 1972, Fujishima and Honda established the fundamental of solar energy photoelectrochemical conversion into chemical energy using semiconductors [306]. The electrons and holes were generated and transferred between energy levels by the semiconductor working electrode in the presence of sunlight [307]. At the semiconductor-water contact, a catalytic redox reaction of oxygen and hydrogen occurs.

There are three types of photoelectrochemical systems: n-type semiconductor as photoanode, p-type semiconductor as the photocathode, and tandem system involving both photoanode and photocathode (**Figure 4.20**).
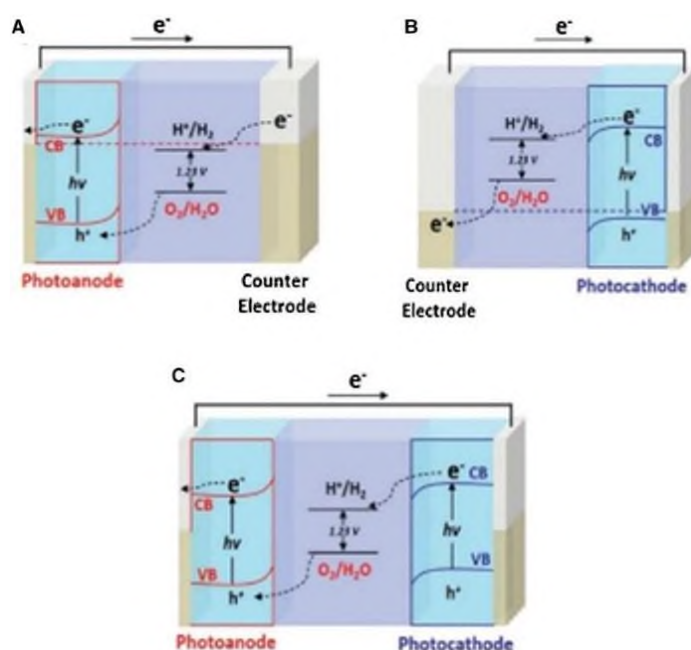
Figure 4.20 *Photoelectrochemical water splitting systems with (A) a photoanode, (B) photocathode, and (C) tandem system. For n-type, the photogenerated electrons are transferred to platinum as the counter electrode through the outer circuit, and the hydrogen is produced from water reduction. In contrast, the photogenerated holes are transferred to the working electrode, and then oxygen is produced from water oxidation. Meanwhile, for p-type, water reduction on the surface semiconductor, while water oxidation on the platinum. For tandem cells, it is made up of both n-type and a p-type semiconductor electrode that is acceptable [308, 309].*

For n-type semiconductors, electrons and holes are generated when light is penetrated by the semiconductor, which absorbs photons [**Figure 4.20** (A)]. The photogenerated electrons pass over the outer circuit to a counter electrode. Then hydrogen is produced from water reduction, while the photogenerated holes are transferred to the working electrode, and then oxygen is produced from water oxidation. For efficient charge separation, an external bias supplied by a power supply is frequently required due to the resistance established between the two electrodes in the solution produced at the interfacial [310]. As a result, the photoanode and counter electrode have two half-reactions:

Oxidation evolution reaction

$$H_2O \rightarrow \frac{1}{2}O_2 + 2H^+ + 2e^- \tag{4.18}$$

Hydrogen evolution reaction

$$2H^+ + 2e^- \rightarrow \frac{1}{2}H_2 \tag{4.19}$$

$$H_2O \rightarrow H_2 + \frac{1}{2}O_2 \bullet \Delta G^0 = +237.2 \text{ kJ mol}^{-1} \bullet E^0 = 1.23 \text{ eV} \tag{4.20}$$
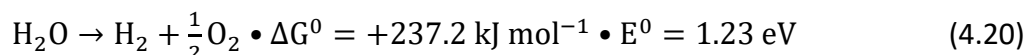
As observed, photoelectrochemical water splitting is an endothermic process that requires a Gibbs free energy of about 273.2 kJ mol^{-1}, or 1.23 electron volt per electron transported, which is thermodynamically unfavorable; thus, this reaction needed external energy to surpass the reaction energy barrier [311]. As a result, sunlight and bias voltage drive the water redox process. In theory, the difference between the semiconductor's Fermi level and the electrolyte's water redox potential causes band bending in the semiconductor's space charge layer, which is then accelerated by the bias to speed up the separation and transfer photogenerated electron-hole pairs [312]. Finally, the photoanode undergoes oxidation evolution via photogenerated holes, whereas the counter electrode undergoes hydrogen evolution [313].

The photogenerated electron-hole pairs' water redox ability is evaluated via the valence band and conduction band position versus the water redox potential that is strongly connected to the semiconductor's energy band structure [314]. An oxidation revolution reaction can be accomplished when the valence band energy of an n-type semiconductor is greater than the oxidation potential E^0 (H_2O/O_2) (1.23 V versus reversible hydrogen electrode). Similar to the reduction potential E^0 (H^+/H_2) (0 V versus reversible hydrogen electrode), the conduction band energy of p-type semiconductors is more negative, facilitating the hydrogen evolution process [315]. In p-type semiconductor materials, water is reduced on the surface of the semiconductors, whereas water is oxidized on the platinum surface [316] [**Figure 4.20** (B)]. The introduction of "tandem" systems, which involves both n- and p-type semiconductor, is one of

the most appealing approaches to collect a wide-ranging wavelength range of visible light in a photoelectrochemical system without introducing an external bias [**Figure 4.20** (C)].

The optimal use of visible light is also required for efficient hydrogen synthesis by photoelectrochemical water splitting in the presence of solar light. As a result, developing a stable photoelectrode material which works well in visible light has received a lot of attention [317]. Photocorrosion resistance is often strong in oxide semiconductors [318]. As a result, they have been used as photoanodes for water oxidation in conjunction with platinum to generate hydrogen. Creating effective anodic electrodes capable of overcoming the enormous over-potential needed to complete the four-electron water oxidation reaction, which is liable for the slow kinetics of such a photoelectrochemical system, is the greatest difficulty of this technology [316].

4.5 Electrochemical Sensors

A chemical sensor is defined by the IUPAC [225] as "a device that converts chemical data, ranging from the concentration of a single sample component to complete composition analysis, into an analytically usable signal". For the most part, a chemical sensor is constituted of two essential functional units: a receptor and a physicochemical transducer. The receptors are variable and can range from activated or doped surfaces to complex (macro)molecules that create highly specific interactions with the analyte [230].

If the receptor is of biological origin (e.g., DNA, antibodies, and enzymes), the device is referred to as a biosensor. The receptor interacts with the analyte, converting the recognition event into a predetermined output signal. One of the primary requirements of sensors is to maintain a high degree of specificity for the intended analyte in the presence of potentially interfering chemical species to avoid false-positive outcomes [319-324]. Another critical component of sensors is the transducer, which is responsible for converting the signal created by the receptor–analyte interaction into a readable value [325, 326]. Thus, both chemical and biosensors can be classified into catalytic or affinity-based devices. Whereas catalytic sensors utilize catalytic activity to generate the signal, as in the case of enzymatic, DNAzyme, or functionalized surfaces that can perform redox reactions under certain conditions, affinity-based devices rely on highly specific interactions between the receptor and analyte, e.g., using the specific affinity of nucleic acids (i.e., ssDNA and aptamers), antibodies–antigens, or host–guest interactions. The monitoring of the recognition events can be performed using several methods (e.g., optical, gravimetric, or electrochemical) depending on the type of transducer utilized [226].

Being the market leaders, electrochemical sensors are, by far, the most frequently employed type of sensor due to the fact of their advantages associated with low detection limits,

as low as picomoles, rapidness, and the low-cost equipment utilized for sensing. Electrochemical sensors come in a variety of form factors ranging from the top-bench to fully integrated wearable devices [227]. The utility of a chemical sensor is to deliver accurate real-time information regarding the chemical composition of its surroundings [327-329]. In an ideal scenario, such a device would be able to respond constantly and reversibly without interfering with the sample. In such devices, a biological or chemical identification layer is coated on a transduction element. In electrochemical sensors, the analytical information is taken from the electrical signal produced by the interaction of the target analyte and the recognition layer [330, 332-335]. Various electrochemical devices can be employed for environmental monitoring depending on the nature of the analyte, the character of the sample matrix, and the sensitivity or selectivity requirements [336, 337]. The bulk of these devices fall into several categories such as amperometric and potentiometric electrochemical sensors (depending on the device's nature) [228, 229, 331]. Electroactive species that are involved in chemical or biological identification are detected using amperometric sensors [338-340].

Electrochemical sensors can be classified into several categories including amperometric, potentiometric, impedimetric, photoelectrochemical, and electrogenerated chemiluminescence [230]. For potentiometric sensors, as a result of specific sensor–analyte interactions, a local Nernstian equilibrium is formed at the sensor interface, when no current is allowed to flow in the system giving information about the analyte's concentration [231]. Amperometric sensors employ a voltage placed between a reference and working electrodes to initiate electrochemical oxidation or reduction, measuring the resulting current as a quantitative indicator of the analyte's concentration [232].

CHAPTER 5

Principle Operation of Metal-Air Batteries

5.1 Introduction

From the beginning of human civilization, energy has played a vital role in maintaining the operation of our society. Nowadays, the growing number of transportation vehicles has made the development of reliable Electrical Energy Storage (EES) system a task of urgency. Among various EES systems, rechargeable batteries are the most promising to meet the demands of safe and sustainable energy supply, thanks to their high energy density and high energy efficiency [341]. Among them, Lithium-Ion Batteries (LIBs), have played an exceptional role in our society in the last twenty years [342]. Nevertheless, the low energy density of LIBs has restricted its application as the energy supplier of next generation. Therefore, the development of Metal-Air Batteries (MABs) have offered a solution benefitting from their much higher theoretical energy density than that of LIBs.

Generally, MABs consist of metal anodes porous (air) cathode and electrolyte. The MABs' cathode uses oxygen from ambient air, which leads to significant battery weight reduction, which has unprecedented advantages for many applications. In comparison with other batteries, particularly LIBs, MABs are cheap, because the cathode source (oxygen from air) is abundant and the anode can be made using low-cost metals, such as Li, Zn, Na, Fe, Al, etc. **Figure 5.1** illustrates the application of MABs as the energy storage system for a variety of technologies.
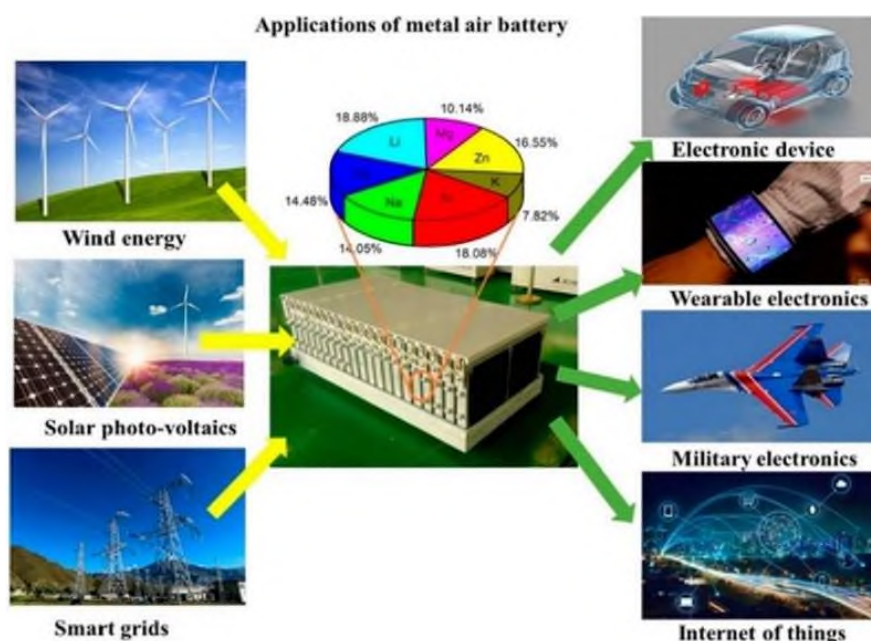
Figure 5.1 *Applications of MABs as energy source and storage systems [343].*

MABs are attractive due to their compact power sources for portable electronics and electric automobiles and also for their amazing energy transfer stations or energy storage devices.

Theoretical energy density is a significant sector in evaluating the performance of various battery configurations. **Figure 5.2** demonstrates theoretical energy density, specific energy, and nominal cell voltage of different MABs [344].
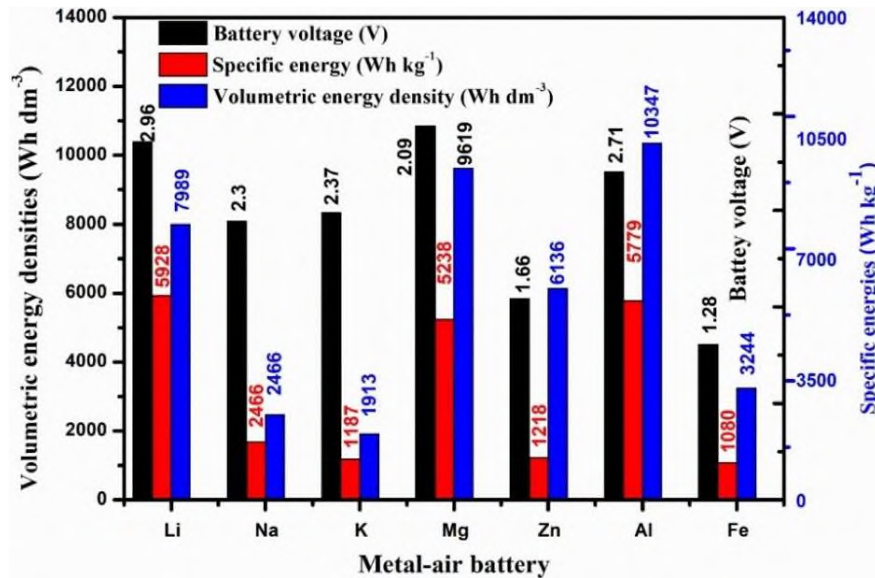
Figure 5.2 Theoretical specific energies, volumetric energy densities and nomimal battery voltages of various MABs [343, 344].

As oxygen, directly supplied from the surrounding environment, is involved in the cathode as an oxidant during the discharge period, MABs show significantly higher energy density. Even though, lithium-air batteries (LABs) provide the best combination of the highest theoretical energy density (5928 Wh kg^{-1}) and high cell potential (nominally 2.96 V), iron-air batteries (FABs) holds the smallest theoretical energy density and cell voltage (nominally 1.28 V). Al-, Zn-, and Fe-air batteries are also the studies hotspots due to their economic and safety considerations.

It has been proved that in specific non-ideal circumstances, the precipitation of the solid discharge product can consume active electrolyte components, lowering the energy density that can be achieved [347]. Mg-air systems are attractive due to the uniform deposition of Mg metal [348-350], but the corrosion of the Mg electrode severely restricts aqueous Mg-air batteries. Many ionic liquid electrolytes have been proposed for use in magnesium-air systems. Yet, they all face electrochemical instability problems [351], particularly noticeable during charging, and the cell's reversibility is limited. On the other hand, aluminum is used in the production of Al-air batteries, which provides both a high theoretical energy density and high specific energy values [352-354]. A combination of sodium's abundant natural supply and safety, as well as its features that are similar to lithium, has led studies into Na-air batteries [355-357]. Si-air batteries have

also gained a lot of attention these days [358]. They have a high theoretical energy density and are stable in electrolytes, including aqueous solutions. Nevertheless, the reversibility of the solid discharge product, pore blockage and precipitation are all issues that are presently being examined in experimental researches of Si-air systems in both ionic liquid and alkaline electrolytes. Zn-air and Li-air are two of the most promising metal-air systems now under research [359, 360], with Li-air being the most promising. Lithium-air batteries (LABs) have been under research for many years, but they have only lately emerged as a highly and scientifically explored subject. The electrolyte has proven to be a stumbling block in the advancement of LAB technology. The aprotic (non-aqueous) and aqueous electrolyte combinations used in Li-air systems are the most often seen. The use of mixed electrolyte systems has been proposed. Using the aprotic Li-air system (LiPF$_6$ in ethylene carbonate (EC)), Abraham et al. [362] proposed an overall reaction resulting in the formation of Li$_2$O$_2$ or Li$_2$O, which was announced in 1996. It has been proved that carbonate solvents are unstable, releasing lithium carbonates during discharging and emitting CO$_2$ during charging [363]. In recent years, carbonate electrolytes have mainly been phased out in favor of ether and ester solvents in conjunction with lithium salts. The precipitation of Li$_2$O$_2$ brings a second obstacle for LABs in aprotic electrolytes, which presents the third barrier. If this solid precipitates in the cathode, it can create a thick layer over the carbon surface, preventing electrons from transferring between it and the anode. Whole pores in the cathode may become closed as precipitation proceeds, resulting in the electrode being passivated and reducing the cell's capacity. At the end, it has been proved that oxygen transport in aprotic electrolytes may be a difficult component to control in LAB effectiveness, mostly at higher current densities [364]. It is commonly known that Li metal interacts strongly with water, which has typically restricted aqueous electrolytes in Li-air systems. Nevertheless, the usage of aqueous electrolytes has lately been enlarged [365]. In alkaline aqueous electrolytes, the discharge product is LiOH H$_2$O rather than Li$_2$O$_2$, indicating that the electrolyte is alkaline. These systems allow for LiOH to precipitate at the separator-anode interface, which minimizes the hazard of pore-clogging in the cathode, which has been seen in aprotic laboratory systems. While in the presence of air, dissolved CO$_2$ interacts with OH$^-$ to create carbonates, which gradually decreases the conductivity of the electrolyte and shortens its lifespan. When exposed to water, dissolved CO$_2$ reacts with OH$^-$ to form carbonates, which furthermore minimizes the cell's lifetime. Although there are still great obstacles difficulties [365-367], the future of LABs seems brilliant. Zinc-air batteries (ZABs) are the unique completely developed metal-air system nowadays available, and they have been successfully released as primary cells

for many years. Hearing aids, for example, are a low-current application that they are particularly suited for. However, their lifespan and electrical rechargeability, are both restricted [368]. One major benefit of Zn as an electrode material is that it is stable in water, unlike Li, which is a significant advantage. Alternative near-neutral aqueous [369] and ionic liquid electrolytes have been proposed in an attempt to enhance the rechargeability of ZABs. Resent studies continues to be concentrated on material development to overcome the lifespan limits of these systems and cell engineering to enhance the effectiveness of the system. Nevertheless, the progress of secondary ZABs has come to the point where they can be achievable for stationary storage applications. Zn-air systems provide one of the most rapid and dependable routes to today's practical secondary metal-air battery systems [370].

5.2 Theoretical Considerations and Mechanisms of MABs

Due to the fact that oxygen is being kept outside the battery, MABs are a sustainable choice among many other types of energy storage devices. The oxygen-reduction reaction (ORR) and the oxygen-evolution reaction (OER) are the two processes related to oxygen and MABs function in an open system [371]. The components are illustrated in **Figure 5.3**.
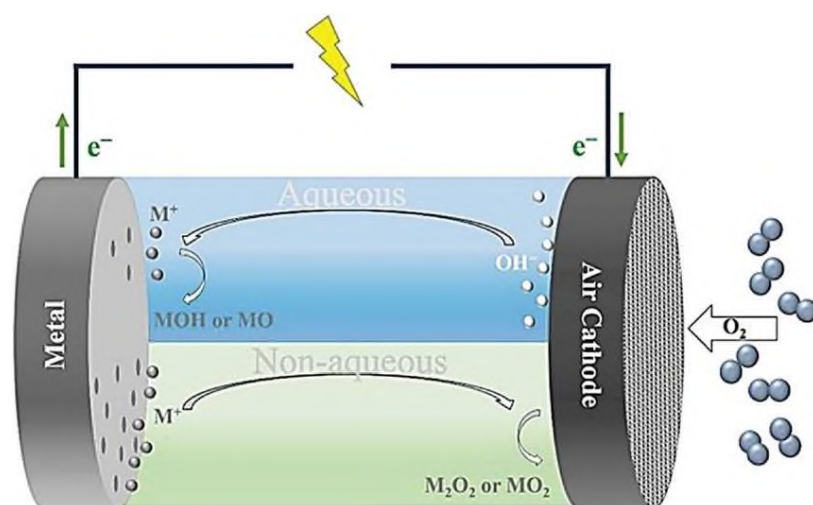
Figure 5.3 Diagram of MABs [345, 373].

MABs include three basic parts: a metal anode, a porous air cathode and an electrolyte that separates the two electrodes from one another. The anode material of MABs consists of metals like lithium Li, zinc Zn, sodium Na, iron Fe and other elements. There is a variety of types of electrolytes available [372] that include aqueous electrolytes, non-aqueous (aprotic), solid-state and hybrid electrolytes. Due to their exceptional sensitivity to water, lithium-air, potassium-air and sodium-air batteries were usually used in non-aqueous systems. Even though anodes composed of zinc, aluminum, magnesium and iron are compatible with aqueous

electrolytes, these aqueous systems demand the addition of a hydrophobic protective layer to prevent electrolyte leakage [371].

In MABs, metal changes into ions on the anodic electrode and at the same time oxygen transforms into hydroxide ions at the cathodic electrode, on the contrary to the operation of conventional ionic batteries, in which metallic ions are being transferred from the anode to cathode. The diffusion of oxygen into the MABs takes place via a layer known as the gas diffusion layer. The behavior of oxygen in an aqueous electrolyte medium is different from that of oxygen in a non-aqueous electrolyte, as illustrated in **Figure 5.4**.
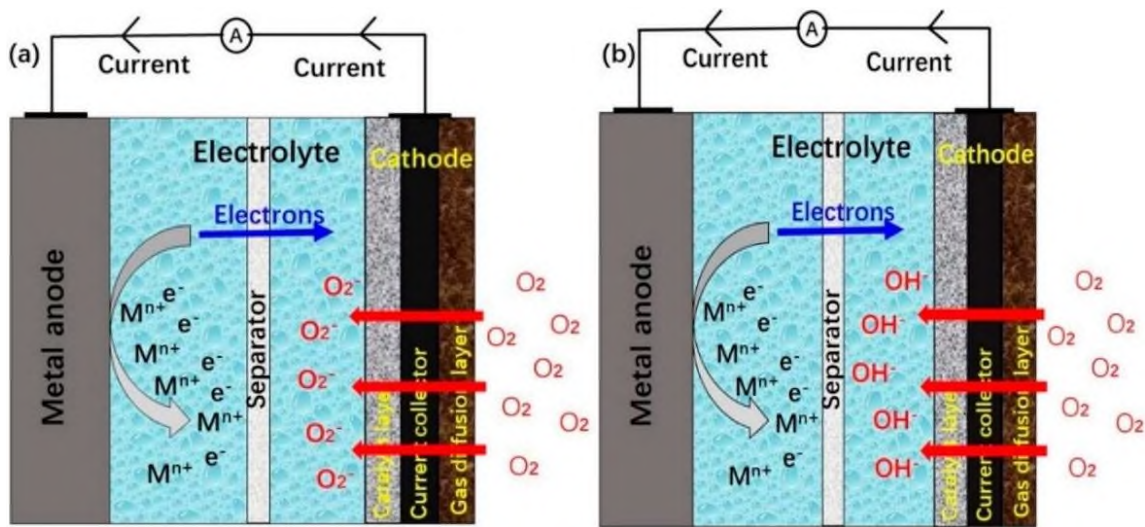
Figure 5.4 *MABs operational characteristics in (a) non-aqueous and (b) aqueous electrolyte [345, 346].*

During the transition of the metal into metallic ions, electrons are produced and the metallic ions afterwards dissolve into the electrolyte. During a charging operation, the above steps are reversed. The reaction formulas for several MABs are presented in **Table 5.1**.

Table 5.1 *Cathode, anode, and overall reactions of metal-air batteries [345, 346, 355, 374-376].*

Metal Anode	Electrolyte	Anode Reaction	Cathode Reaction	Overall Reaction
General		$M \rightleftarrows M^{n+} + ne^-$	$O_2 + 2H_2O + 4e^- \rightleftarrows 4OH^-$	
Iron Fe		$Fe + 2OH^- \rightleftarrows$ $Fe(OH)_2 + 2e^-$ $3Fe(OH)_2 + 2OH^- \rightleftarrows$ $Fe_3O_4 + 4H_2O + 2e^-$		$2O_2 + 3Fe \rightleftarrows$ Fe_3O_4
Aluminum Al	Alkaline aqueous	$Al + 4OH^- \rightleftarrows$ $Al(OH)\ 4 - +3e^-$	$O_2 + 2H_2O + 4e^- \rightleftarrows 4OH^-$	$3O_2 + 2Al \rightleftarrows$ Al_2O_3
Zinc Zn		$Zn + 4OH^- \rightleftarrows$ $Zn(OH)_4^{2-} + 2e^-$ $Zn(OH)_4^{2-} \rightleftarrows$ $ZnO + 2OH^- + H_2O$		$O_2 + Zn \rightleftarrows ZnO$
Lithium Li	Non-aqueous	$Li \rightleftarrows Li^+ + e^-$	$O_2 + e^- \rightleftarrows O_2^-$ $O_2^- + Li^+ \rightleftarrows LiO_2$ $LiO_2 + Li^+ + e^- \rightleftarrows Li_2O_2$	$O_2 + Li \rightleftarrows Li_2O_2$

5.2.1 Cell Potential

The cell potential is specified by calculating the potential difference between the anodic and cathodic electrodes, as presented in the following equation [377, 378]. The resulting value is expressed as a volt unit (V), as presented in Equation (5.1).

$$E^0_{cell} = E^0_{Red,Cathode} - E^0_{Red,Anode} \text{ (1 M and 1 bar)} \tag{5.1}$$

If the standard circumstances are altered, the Nernst equation can be used as a guideline to calculate:

$$E = E^0 - \frac{RT}{nF} \ln Q \tag{5.2}$$

which is derived from Gibbs free energy

$$\Delta G^o = -nFE^o = \Delta H^o - T\Delta S^o \tag{5.3}$$

This is calculated using the balanced reaction equation and thermodynamic tables. When ΔG is a positive value, it implies the reaction demands external energy (nonspontaneous reaction), while when it is a negative value, the reaction may take place in the absence of external energy (spontaneous reaction) [377-379].

5.2.2 Energy Efficiency

The energy efficiency of rechargeable batteries is subdivided into three parts. Firstly, the charging energy efficiency η_{charg}, which is equal to the net energy ΔQ_n divided by charge energy Q_{in}, as calculated as follows

$$\eta_{charge} = \frac{\Delta Q_n}{Q_{in}} \tag{5.4}$$

$$Q_{in} = \int_{SOC(0)}^{SOC(t)} U_{charge} C_n dSOC \tag{5.5}$$

$$\Delta Q_n = \int_{SOC(0)}^{SOC(t)} U_{OCV} C_n dSOC \tag{5.6}$$

$$SOC(t) = SOC(0) - \frac{\int I dt}{C_n} \text{ (I is positive when discharging the battery)} \tag{5.7}$$

which SOC refers to the state of charge, U is the battery voltage and C_n is the battery standard capacity. Secondly, the discharging energy efficiency;

$$\eta_{disch} = \frac{Q_{out}}{\Delta Q_n} \tag{5.8}$$

where the discharge energy is

$$Q_{out} = \int_{SOC(0)}^{SOC(t)} U_{disch} C_n dSOC \tag{5.9}$$

62

Thirdly, the charge-discharge energy efficiency is expressed as

$$\eta_{battery} = \frac{Q_{out}}{Q_{in}} \qquad (5.10)$$

The charge energy Q_{in} and discharge energy Q_{out} may be calculated from the automatically recording data of the current, time and voltage [380].

5.3 Electrochemical Performance of MABs

A variety of metal utilized in MABs, such as Zn-air, Li-air, Si-air, Fe-air and Al-air batteries, can provide good specific energy and medium-specific power. Moreover, as illustrated in **Figure 5.4**, the prospective efficiency of MABs was contrasted with that of LIBs. The specific energy provided by prospective MABs and LIBs ranges from 500 to 1500 Wh/kg$_{Me}$, up to 500 Wh/kg, and 200 to 300 Wh/kg, respectively, in terms of specific energy. While the specific power supplied by prospective MABs and LIBs range from 0.1-1 kW/kg$_{Me}$, up to 1 kW/kg, as well as up to 10 kW/kg. The specific power provided by MABs and LIBs ranges from 0.1-1 kW/kg$_{Me}$. **Figure 5.5** presents possible future effectiveness of certain MABs [381], which are not yet available.
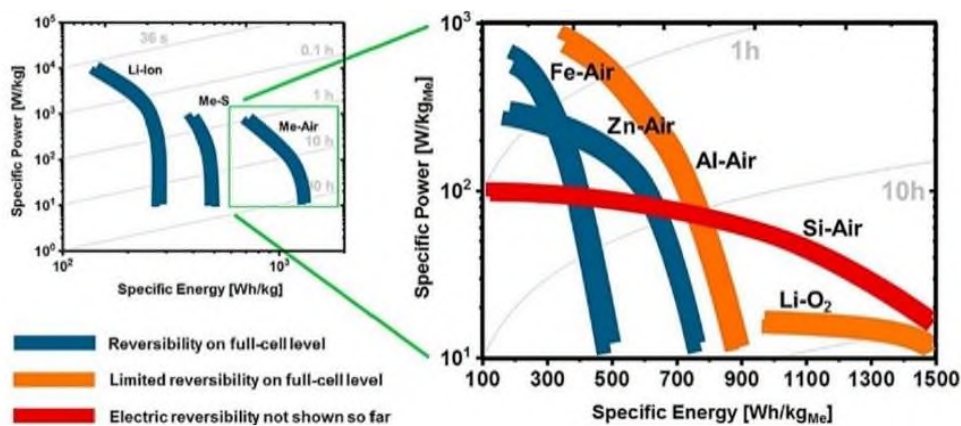
Figure 5.5 Ragone diagram for various types of batteries [345, 381].

Even though Li-air batteries achieved a high OCV of 2.91 V and high theoretical energy density, its lifetime was short, as it failed after two cycles because of the corrosion of the lithium anode by the electrolyte. Na-air batteries fabricated using a 3D tin sulfide nano-petals cathode presented a high-power density of 300 W/kg, a high round trip efficiency of 83 %, good rechargeability (40 cycles) and a low overpotential gap of 0.52 V [382]. Al-air batteries had an OCV of 1.2 V, theoretical energy density of 2.98 Ah/g, and specific energy of 200 Wh/Kg [354, 383]. Moreover, Mg-air batteries achieved a specific energy density of 3.9 kWh/Kg and a theoretical volumetric density of 14 kWh/L [351, 384]. Metal Zinc is cheap, so the cost of ZABs is quite low. Zn-air batteries showed a theoretical energy density of 0.82 Ah/g and with Co-MOF as cathode catalyst presented a power density of 86.2 mW/cm^2 and extraordinary charge-discharge performance

[385, 386]. Fe-air batteries showed a specific charge capacity of 300 Ah/Kg, energy efficiency of 35 %, theoretical open-circuit voltage of 1.28 V, voltage efficiency of 40 % and charge efficiency of 96 % [374, 387]. Sn-air batteries are another type of MABs, with an OCV of 0.95 V and 860 Wh/Kg specific energy. Sn-air batteries operated at room temperature with an electrolyte of methane sulfonic acid and polyacrylamide gel showed a maximum power density of 5 mW/cm^2 at 12 mA/cm^2 for 24 h [388]. **Table 5.2** presents the main differences between the reported MABs.

Table 5.2 Shows a comparison among the different available metal-air batteries [345, 351, 354, 374, 375, 389-397].

Type	Calculated OCV (V)	Practical Energy Density (Wh/kg)	Metal Cost (€/kg)	Efficiency (Discharge) (%)	Capacity Density (mAh/g)
Fe/Air	1.28	50-75	0.4	96	300-786
Zn/Air	1.65	350-500	1.85	-	300-875
Mg/Air	2.93	400-700	2.75	-	737-2131
Al/Air	2.71	300-500	1.75	70	260-2777
Na/Air	2.27	1600	1.7	-	-
Li/Air	2.96	1700	68	68-94	3842
Sn/Air	0.95	-	21	70-90	-

5.4 Anode of MABs

5.4.1 Introduction

Chemical activity of the metal anode specifies the discharge capacity. Due to high metal activity, an unavoidable side reaction with various components in the electrolyte can take place. The battery performance and the incidence of side reactions may vary, depending on metal's purity.

From the invention of the first MAB, the zinc-air battery, in 1878, a great deal of development and research has been carried out, and **Figure 5.6** demonstrates a summary of these advancements [398].
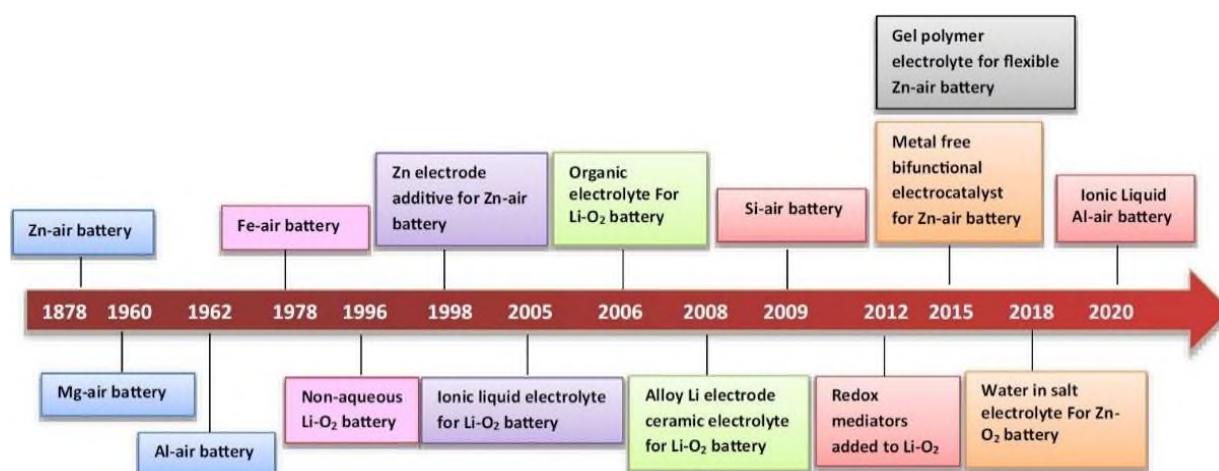
Figure 5.6 The evolution and modification of different types of MABs [450].

Many metals, such as lithium, zinc, aluminum, magnesium, iron, sodium and potassium, can be used as anodes in MABs. Every metal has its own advantages and disadvantages when are being

used as anode electrodes. The energy density of LABs is the greatest theoretically possible (11,140 Wh/kg) among the many kinds of MABs even though, obtaining rechargeable LABs is difficult. In addition, metals like zinc (0.82 Ah g^{-1}), magnesium (2.20 Ah g^{-1}) and aluminum (Al) are commercially viable, plentiful and safe. Moreover, Al is always available for recycling, it has a higher energy density (8.1 kWh kg^{-1}) and a significant theoretical voltage (2.7 V).

Chemical activity of the anode determines the discharge capacity of the anode. Due to the high activity of the metal, a side reaction with various components of the electrolyte can take place that cannot be avoided. The above reactions can take place at a variety of rates and have different effects on battery efficiency, according to the purity of metal and the storing conditions [351]. Theoretical specific energies for each kind of MABs is demonstrated in **Table 5.3**, with the specific energy calculated using the following formula:

$$W_{Me/MeOx} = n \bullet F \bullet M_{Me/MeOx}^{-1} \bullet U_{cell} \tag{5.11}$$

where W refers to the specific energy of the material, n refers to the number of atoms that have been transported, M refers to the molar mass, while Ucell is the cell voltage.

Table 5.3 *Various types of MABs have different theoretical specific energies [345, 375, 381, 390, 392, 401-408].*

MAB	Energy (Wh kg^{-1})		Voltage (V)	Electrolyte
	Including O$_2$	Without O$_2$ (Metal)		
Li/Air (Li$_2$O product)	5220	11,238	2.91	Non aqueous
Al/Air	2784	8091	2.7	Aqueous
	3311	6258	2.1	Non aqueous
Si/Air	3947	8461	2.21	Non aqueous
	2334	8001	2.09	Aqueous
Ca/Air (CaO product)	2996	4186	3.13	Non aqueous
Mg/Air	2848	6098	2.77	Aqueous
	3919	6493	2.95	Non aqueous
Na/Air (Na$_2$O$_2$ product)	1601	2716	2.33	Non aqueous
Fe/Air	764	1229	1.28	Aqueous
Zn/Air	1086	1352	1.65	Aqueous
K/Air	935	1700	2.48	Non aqueous
Sn/Air (at 1000 K)	860	6250	0.95	Non aqueous

Table 5.4 shows experimental findings [381], representing the most relevant results published.

Table 5.4 *The recent experimental results of various MABs [345, 381].*

MAB	Discharge Product	Experiment Specific Energy (Wh kg^{-1})	Condition	Reversibility Cycles	Voltage (V) Ref.
Fe/O$_2$	Fe(OH)$_2$	453 Wh/kg$_{Fe}$	[b,c,d,e]	3500 [b,d]	1.28
Zn/O$_2$	ZnO	>700 Wh/kg$_{Zn}$	[a,c,d]	>75 [a,c]	1.65
K/O$_2$	KO$_2$	~19,500 Wh/kg$_{Carbon}$	[a,c,d]	>200 [a,c]	2.48
Na/O$_2$	Na$_2$O$_2$	~18,300 Wh/kg$_{carbon}$	[a,c,d]	>20 [a,c]	2.33
	NaO$_2$				2.27
Mg/O$_2$	Mg(OH)$_2$	~2750 Wh/kg$_{cathode}$	[a,c,d,f]	<10 [a,c,d]	2.77
	MgO				2.95
Si/O$_2$	Si(OH)$_4$	~1600 Wh/kg$_{Si}$	[a,c,d]	Not yet	2.09
	SiO$_2$				2.21
Al/O$_2$	Al(OH)$_3$	~2300 Wh/kg$_{Al}$	[a,c,d]	Limited	2.71
	Al$_2$O$_3$				2.1
Li/O$_2$	Li$_2$O$_2$	>11,050 Wh/kg$_{carbon}$	[a,c,d]	>250 [a,c]	2.96
	Li$_2$O				2.91

Conditions: a is anode sheet/foil, b is porous/particulate anode, c is full-cell measurements, d is 100% deep discharge, e is repeated charge/discharge, and f is elevated temperature.

5.4.2 Progress done in the Anode

Al-air batteries are cheap, environmentally friendly, present high energy density, good recyclability and are having light weight. Additionally, the electrolyte may be an alkaline, salty, and non-aqueous solution [409].

The performance of an ultrafine-grain (UFG) aluminum anode produced by equal channel angular pressing (ECAP) in three distinct electrolytes (NaOH, KOH, and NaCl) was researched at a constant discharge current of 10 mA cm^{-2}. The cathode was an air electrode with gas diffusion and catalyst (Ag powder) layers as a double-layer structure, laminated with a current collector (Ni mesh). The UFG was also compared with coarse-grained (CG) aluminum. The results presented in **Table 5.5** prove that the grain with finer sizes enhanced the battery's performance in alkaline electrolytes due to the active dissolution of the aluminum anode.

Table 5.5 The characteristic performance of Al-air battery using different Al anodes at a current density of 10 mAcm^{-2} [345, 410].

Electrolyte Solution	Aluminum Anode	Average Discharge Voltage (V)	Capacity Density (Ah/kg)	Efficiency (%)	Energy Density (Wh/kg)
2 M NaCl	CG	0.398	2751	92.3	1097
	UFG	0.387	2726	91.6	958.4
4 M KOH	CG	1.38	2439	81.7	3363
	UFG	1.44	2475	83.1	3593
4 M NaOH	CG	1.397	1647	55.2	2428
	UFG	1.532	2307	77.3	3524

Nevertheless, because of the oxide film blockage in NaCl electrolyte and the local corrosion, the research results demonstrate that changing the Al anode grain to a fine size has no effect on performance. The anode efficiency of CG and UFG in NaOH is 55.3 % and 77.4 %, similarly. Additionally, the energy density improved by 55.5 % with a finer grain size relative to CG, however the effect in NaCl and KOH solutions is not clear [410].

Two aluminum anodes with different purity percentages were compared to study the effect of the impurity on the performance of the AABs. The examined anodes were a 2N5 purity 99.5 % and a 4N purity 99.99 % grade aluminum anode. The research results demonstrate that the 2N5 grade Al presented a lower battery performance than the 4N grade Al because of the impurities that shaped the complex layer consisting of cupper, silicon, iron and other elements. This impurity layer of 2N5 aluminum reduces the battery's voltage on standby status and depletes the battery efficiency and the discharge current at 1 volt. Nevertheless, lower voltages of 0.8 volts lead to the layer dissolving, and hence the performance enhanced. The results at the two different applied potentials are demonstrated in **Table 5.6**. In conclusion, the impurity

complex layer reduced with a declining discharge voltage. This situation improves battery efficiency and discharges current density by reducing the self-corrosion reaction. Thus, there is a possibility of using the cheaper 2N5 grade aluminum anode instead of 4N Al at the condition of high-power discharge for AABs [411].

Table 5.6 *Characteristics of 2N5 and 4N grade aluminum-air batteries at 1 and 0.8 V applied potentials [345, 411].*

Voltage (V)	Anode	Electric Capacity (C)	Electric Capacity/ Discharge (C)	Performance (%)
1	4N grade Al	1467.23	751.30	50.92
	2N5 grade Al	1991.22	377.47	18
0.8	4N grade Al	2211.13	1590.70	71.76
	2N5 grade Al	2151.14	1625.61	75

Zinc is believed to be an effective alloying element for the anode of AABs to raise the nominal cell voltage and reduce the self-corrosion rate. Nevertheless, a research showed that Zn added to Al 99.7 % purity anode reduced its discharge performance because of the formation of Zn oxidation film. In addition, indium (In) was added to an aluminum-zinc anode, which found improvement in the discharge performance of AABs by decreasing the resistance of zinc oxidation film via In ions, to overcome this formation. Furthermore, an Al-Zn-In alloy anode that is made of commercial-grade aluminum (99.7 % purity) is cheaper than 4N grade aluminum (99.99 % purity) [412].

5.5 Electrolyte of MABs

An electrolyte is a medium to transport ions and electrons to ensure the continued oxidation - reduction reaction. As illustrated in **Figure 5.7**, the electrolyte for MABs can be aqueous, non-aqueous, solid-state, or hybrid in nature [346].
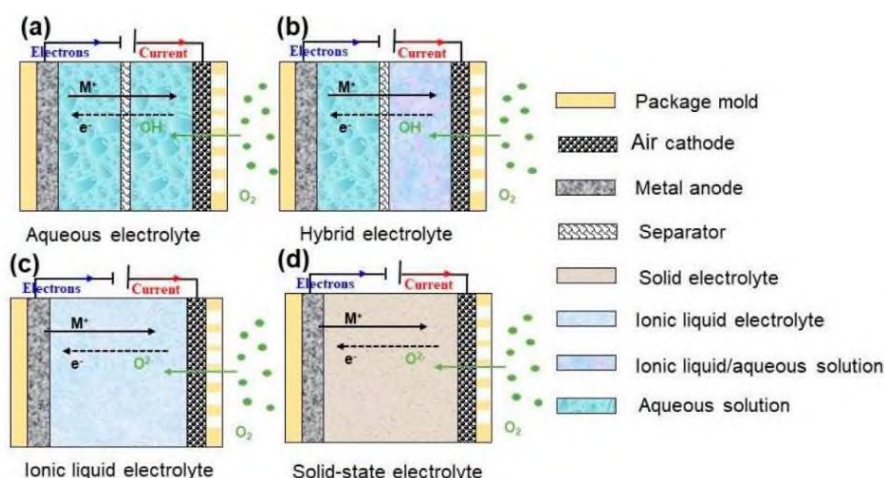
Figure 5.7 *Schematic diagrams of various electrolytes of MABs [345, 346].*

5.5.1 Aqueous Electrolyte

5.5.1.1 Introduction

Aqueous electrolytes provide highly ionic conductivity and attract batteries with high power density. Furthermore, water-based electrolytes are cheap and non-flammable. Nevertheless, aqueous electrolytes are more corrosive than organic solutions, but they have limited water thermodynamic electrochemical window. As their performance at low temperatures is limited by the freezing point, the range of their thermal application is narrower [413]. Aqueous electrolytes may be categorized into three solutions based on the pH number [346].

5.5.1.2 Alkaline

The alkaline electrolyte solution has a pH value higher than 7 and below or equal to 14 and is the most common electrolyte in the aqueous-based MABs compared to an acidic electrolyte, because of its favorable ORR with reduced overpotential and quicker reaction kinetics. Nevertheless, whenever CO_2 from the air environment interacts with this electrolyte, it creates a carbonate surrounding the cathode. A high quantity of carbonate decreases the cathode's efficiency as it obstructs the pores of the positive electrode [346]. Furthermore, the use of strong alkaline electrolytes damages the environment. ZABs and AABs commonly use aqueous alkaline electrolytes. MABs with alkaline electrolytes may achieve higher electrocatalysis activity of oxygen and better resistance to metal corrosion compared to neutral and acidic electrolytes. Among alkaline electrolytes such as NaOH, KOH and LiOH, the most preferable in MABs is the concentrated KOH solution, because it has the minimum viscosity and greatest ionic conductivity [398].

The discharge behavior of the lately announced Si-air batteries in the alkaline electrolyte has been studied using separate concentrations of KOH electrolyte. Silicon-air cell of refill type illustrated in **Figure 5.8** was used.
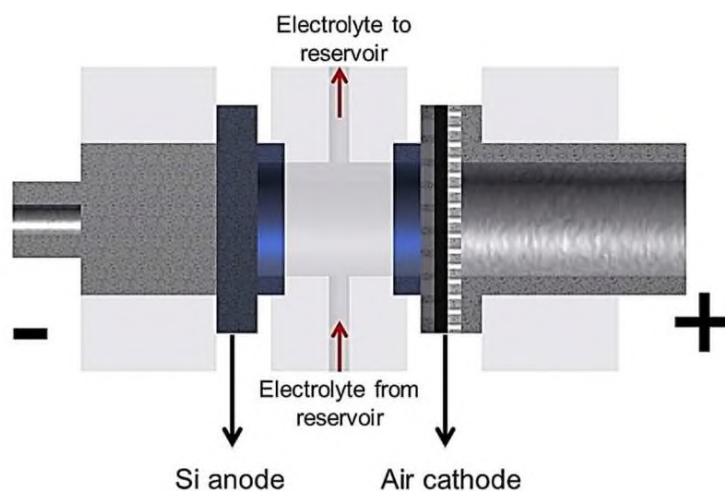
Figure 5.8 *A refill type of Si-air cell [345, 403].*

Whenever the KOH concentration fluctuates from 2 M to 5 M, the discharge potential according to the concentration is nearly constant, while it reduces significantly only at lower considerably up to 1 M, with the difference in discharge potential between a variety of concentrations being 100 mV. On the contrary, there was no effect on the KOH concentration on the open cell potential in this research. Due to the fact that OH^- changes the activity and conductivity of the electrolyte, raising the KOH concentration up to 6 M led in a linear ascent in ionic conductivity. The application of discharge current and the concentration of KOH, can cause an effect on the roughness of the Si surface [403].

Anode:

$$Si + 4OH^- \rightleftarrows Si(OH)_4 + 4e^- \qquad (5.12)$$

Cathode:

$$O_2 + 2H_2O + 4e^- \rightleftarrows 4OH^- \qquad (5.13)$$

Corrosion:

$$Si + 2OH^- + 2H_2O \rightarrow SiO_2(OH)_2^{2-} + 2H_2 \qquad (5.14)$$
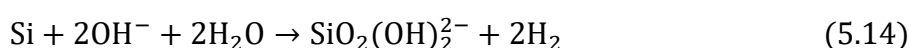
5.5.1.3 Neutral

Neutral solution which pH value is 7, has been proved to raise the lifespan and the cycle stability of secondary ZABs. Nevertheless, no modeling researches have calculated the performance of neutral ZABs in a laboratory setting yet. The pH stability of neutral ZABs is a crucial factor in cell function. Furthermore, AABs can be discharged with greater activity and reduced corrosion rate in a neutral salt solution than in an alkaline electrolyte [346].

5.5.1.4 Acidic

Acidic solution has a pH that ranges from 2 to less than 7. It is infrequently applied in aqueous-based MABs because of the decreased battery efficiency via a large amount of H^+ in the solution that reacts directly with metal. An Al-Zn alloy anode's performance is being changed by separate types of acids at the same pH, concentration change and operation temperature [346]. Acidic solution suppressed the formation of both dendrite on the anode and byproducts on the cathode. Nevertheless, it may lead to corrosion problems for some types of MABs [414].

5.5.1.5 Electrolyte Additives

The metal electrode in an aqueous electrolyte, suffers from crucial failures, such as dendrite formation, electrode corrosion, hydrogen evolution and passivation. The electrolyte material design may reduce a few of these failures by different electrolyte additives and increase the metal electrode's performance. The additives used for neutral salt water solution are Zn^{2+},

In^{3+} and Sn^{3+}. For alkaline solutions, the additives used may be ZnO and carboxymethyl cellulose (CMC) or ZnO and polyethylene, as illustrated in **Figure 5.9**.
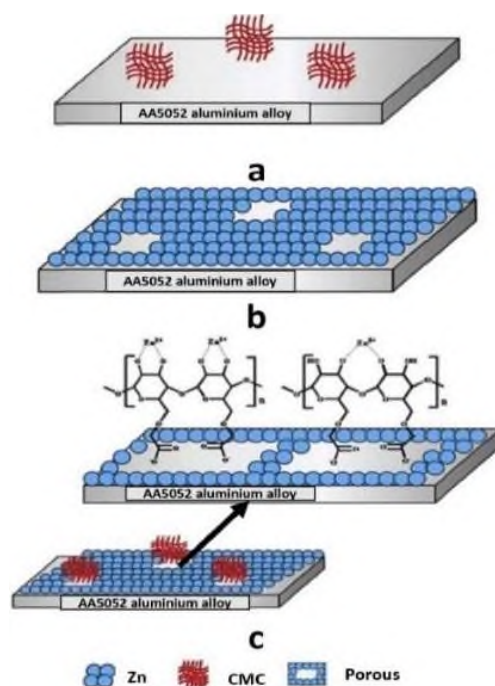
Figure 5.9 *Corrosion protection for Al anode in NaOH containing (a) carboxymethyl cellulose (CMC), (b) ZnO, and (c) CMC/ZnO [345, 414].*

Furthermore, a few aromatic carboxylic acids are preferred in alkaline conditions and show similar effects under acidic solutions. In acidic circumstances, is preferable the use of imidazole group N atoms [398, 414].

5.5.2 Non-Aqueous Electrolyte

Solid-state electrolytes tend to maintain both thermal stability and robustness and at the same time, reduce electrolyte leakage. In addition, they have the potential to disappear failures of gas crossover and electrolyte evaporation, to achieve the growth in the energy density of MABs and to create reusable and bendable gadgets. However, solid-state electrolytes, tend to decrease battery's capacity and increase its resistance. For MABs, solid-based electrolytes have higher OH$^-$ interfacial transporting resistance than aqueous system because of the poor wetting property that limits the three-phase interface reaction, however, using alkaline gel electrolyte (AGE) could reduce these failures [346, 398, 414].

Ionic liquid electrolytes have two types of cations. Firstly, ions of alkali metal in an organic solvent and secondly, large organic cations with inorganic/organic anions. These electrolytes face problems because of the carbonate formation that consumes the electrolyte and blocks the electrode pores [346]. Ionic liquids display high ionic conductivity, low volatility, no flammability and they can resist moisture in LABs. Ionic liquids that may be stored at room temperature (RTILs) are a

kind of salt that has a melting point below 100 °C and consists of large organic cations and organic/inorganic anions. Due to the fact that MAB electrolytes can be excessively nonvolatile, very conductive and may enhance the electrochemistry of some metals, researchers have turned their importance to expensive RTILs as MAB electrolytes as a result of the drying out problem [398, 415]. The aprotic organic electrolyte is widely used in MABs with metal electrodes that are unstable in water, like Li, Na [398] and this leads to the formation of a solid electrolyte interphase (SEI) at the surface of the anode. Nevertheless, it presents environmental, economic, toxicity and flammability issues. Furthermore, an organic electrolyte leads in a discharge product with nonconductive and insoluble characteristics that block the air cathode pores [416].

5.5.3 Hybrid Electrolyte

The name of mixed or hybrid electrolyte indicates that it is constituted of two distinct electrolytes separated by a solid electrolyte barrier that prevents gas and water diffusion while transferring cations. NASICON, for instance, is a solid electrolyte membrane and it implies sodium super ionic conductor [416]. The anode electrolyte in a hybrid battery system is mentioned as anolyte, while the cathode electrolyte is mentioned as catholyte. With the use of an alkali metallic ion (Na^+ or Li^+) solid-state electrolyte (SSE) separator, a novel aqueous iron-air battery was evolved, involving alkaline anolyte and acidic catholyte. With the exposition of anode and cathode to oxidation-reduction processes (redox reactions), the alkali metallic ion operates as a mediator of ionic transport [346, 417]. Hybrid Na-air cell is another example of a hybrid electrolyte battery system, which uses aqueous and organic electrolytes, with a membrane to separate them.
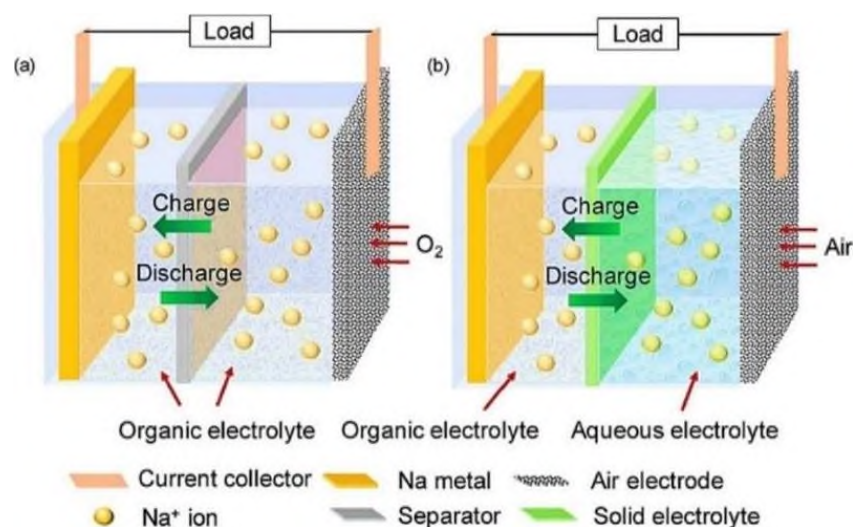
Figure 5.10 *Representation of (a) non-aqueous Na-O$_2$ battery, (b) hybrid Na-air battery [345].*

Figure 5.10 illustrates each cell compared to non-aqueous Na-O$_2$ batteries, with the comparative conclusions presented in **Table 5.7**.

Table 5.7 *Comparison between non-aqueous Na-O$_2$ cell and hybrid Na-air cell [345, 416].*

	Na-O$_2$	**Na-air**
Barrier	Polymeric like Celgard 3501	NASICON
Discharge products	NaO$_2$ and/or Na$_2$O$_2$	NaOH
Product solubility	Insoluble	Soluble
Overpotential gap	Higher	Lower
Overall performance (%)	≥ 75	≤ 75
Stability	No recommendable	Recommendable
Safety	Satisfactory	Reasonable

5.5.4 Selecting the Electrolyte

Most of the times, electrolytes are selected via a trial-and-error procedure based on rules of thumb connecting a variety of specifications of the electrolyte. Therefore, time is spent in testing with separate electrolytes to achieve the required performance. It has been proved that in non-aqueous Na-air, Li-air and K-air cells, there is a connection between the solvent reorganization energy and the ORR rate constant k and the oxygen diffusion coefficient D (O$_2$), as presented in **Figure 5.11**.
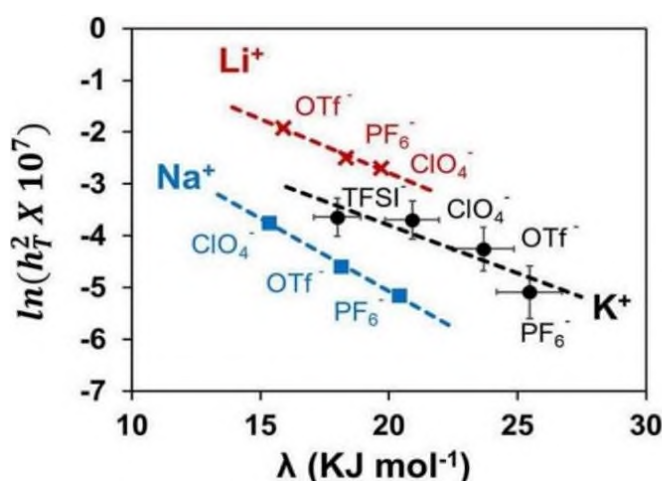
Figure 5.11 *Correlation graph between solvent reorganization energy λ, the diffusion coefficient of oxygen D$_{O2}$, and the ORR rate constant k [345, 418, 419].*

The study shows the basic associations that exist in the membrane between the salt and the solvent and the effect that these interactions have on the total battery's performance. It has been studied that, with growing cation size, the rate of ORR in the presence of alkali metal ions is intensely dependent on the selection of salt anion as the size of the cation increases. For non-aqueous alkali MABs [418, 419], the selecting of the electrolyte is made more accessible with the use of the graph presented in **Figure 5.11**.

Because of the difference on MABs' operation, each type of electrolyte has advantages and disadvantages that need to be considered. The advantages and disadvantages associated with each kind of MAB electrolyte are presented in **Table 5.8**.

Table 5.8 *Comparison of different types of membranes for metal-air batteries [345, 346, 381, 398, 414, 416, 420].*

Membrane		Types	Merits	Demerits
Aqueous	Alkaline	Potassium Hydroxide. Lithium Hydroxide. Sodium Hydroxide	Non-corrosive. Zn has rapid electrochemical kinetics as well as intrinsic electrochemical reversibility. Higher ionic conduction. ZAB has excellent performance at low temperatures. The solubility of zinc salts is very high.	CO_2 sensitivity is a concern. Alkaline solutions are harmful to the environment. Dissolution of Zn, precipitation of insoluble CO_3^{2-} hydrogen evolution, and electrolyte evaporation.
	Neutral	Potassium Chloride Lithium Chloride Zinc Dichloride Magnesium Dichloride	Secondary ZABs have excellent cycle stability as well as a long calendar life. Less corrosion and discharge due to high activity of Al alloy Carbonization of the electrolyte should be avoided. Dendrite formation may be reduced. Reduce the solubility of zinc in ZAB. CO_2 absorption is very low.	In industrial applications, this is a rare occurrence.
	Acidic	HCl HAc H_2SO_4 H_3PO_4 HNO_3	Reduced the development of byproducts on the cathode and the formation of dendrites on the anode.	Rarely utilized in industrial applications. Some kinds of MABs are prone to corrosion issues.
Non-aqueous	Ionic liquid	RTILs Lithium salts	Low volatility. Inflammability. High ionic conductivity. Excellent moisture resistance.	Carbonate crystallization. High purity is required. Synthesis is harmful to the environment.
	Organic	Sodium-based salts	Sodium and lithium-air batteries are among the most often used types of batteries. Contributes to the development of SEI at the anode.	Costly. Combustible. A certain degree of toxicity is present. The discharge product is preventing air cathode pores from opening.
	Solid-state	ZrO_2	Work in all MABs kinds without exception. Electrolyte leakage prevention, thermal stability, as well as robustness, are all important considerations. It is advantageous for increasing the energy density of MABs. Making wearable and flexible gadgets possible is made possible by this technology.	Increased resistance of the battery will result in a reduction in battery capacity. The wetting property is poor.
Hybrid		Alkaline anolyte and acidic catholyte.	Higher performance. Cycling stability is excellent.	In industrial applications, this is a rare occurrence.

5.6 Cathode of MABs

5.6.1 Introduction

The active material for the cathode is oxygen from the surrounding environment. Additionally, it does not demand a heavy shell to keep it contained, which raises the energy density of the device [420, 421]. The oxygen evolution reaction (OER) and the oxygen reduction reaction (ORR) are the cathode reactions, with OER taking place during the charge cycle and ORR taking place during the discharge cycle [346, 422].

5.6.2 Air Cathode Components

The air cathode consists of a gas diffusion layer (GDL), a catalyst and a current collector, as demonstrated in **Figure 5.12**.
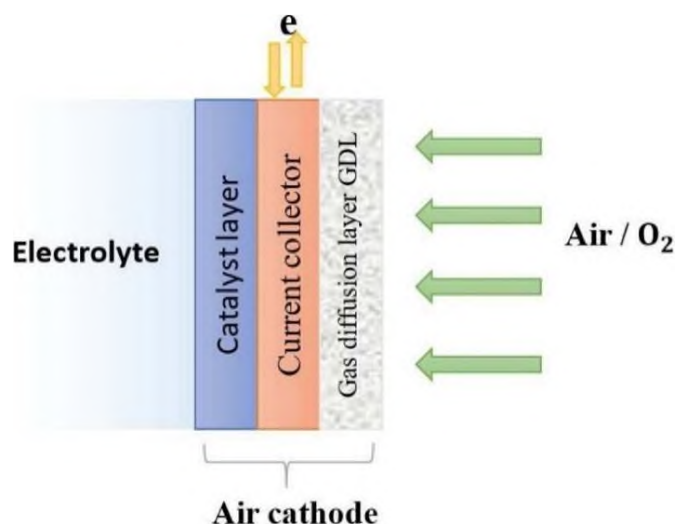
Figure 5.12 Air cathode components of MABs [345].

It may impact the attributes of MABs significantly, therefore it should be optimized by improving ORR, decreasing the formation of carbonate and byproducts, preventing flooding in the air cathode, and avoiding evaporation of the electrolyte [414].

The main tasks of a current collector are connecting to external electrical circuits to form a closed circuit and transmit electrons between them. It can be made of metal or non-metal, with the metal current collector being made of porous foam - like metals such as Ni mesh, stainless steel and Cu. However, non-metal current collectors, like conductive carbon paper, carbon cloth and graphitic fiber, are made of carbon-based materials [346, 414].

The gas diffusion layer (GDL) accomplishes several tasks. It performs as a conductor between the catalyst layer and the air atmosphere, allowing oxygen to diffuse into the atmosphere. Furthermore, it prevents both leakage of the electrolyte out of the battery and water entrance into the battery and it supports the catalyst layer of the battery. GDL ought to be highly porous, light, hydrophobic and thin. Gas diffusion layers usually consist of catalytic or carbon materials and hydrophobic binders like polytetrafluoroethylene PTFE (Teflon) and the catalytic materials are commonly combined with the binders before being put or imprinted onto current collectors [414].

The catalyst layer provides a significant impact on the MABs' characteristics. The bifunctional catalyst is needed to enhance the OER and ORR reactions, as the natural kinetics of the oxygen reactions is typically sluggish and rising the kinetics of these reactions increases the electrochemical performance of MABs and meanwhile reducing overpotentials. The electrocatalysts can be categorized into [351, 360, 372, 373, 414, 422, 423]:

1. Noble metals and their alloys, like platinum Pt, iridium Ir oxides and ruthenium Ru oxides, presenting exceptional performance in both OER and ORR tests.

2. Metal oxides that are single, binary, or ternary in nature, such as MnO, NiO, and CoO.

3. Carbonaceous materials, like doped carbons and nanostructured carbons.

4. Transition metals and metal macrocyclic complexes.

5.6.3 Oxygen Electrochemical Reactions in MABs

Due to the fact that oxygen performs uniquely in both aqueous and nonaqueous electrolytes (reaction pathways are presented in **Table 5.9**), it has been required to develop a numerous of catalysts that correspond to distinct reaction processes.

Table 5.9 Pathway reactions for the different electrolytes of MABs [345, 424, 425].

Electrolyte	Oxygen Reaction	Reaction Pathway	
		Two-Step	Four-Step
Aqueous MABs	ORR (Alkaline)	$O_2 + H_2O(l) + 2e^- \rightarrow O^* + 2OH^-$ $O^* + 2OH^- + H_2O(l) + 2e^- \rightarrow 4OH^-$	$O_2 + H_2O(l) + e^- \rightarrow OOH^* + OH^-$ $OOH^* + e^- \rightarrow O^* + OH^-$ $O^* + H_2O(l) + e^- \rightarrow OH^* + OH^-$ $OH^* + e^- \rightarrow * + OH^-$
	OER (Alkaline)		$OH^- + * \rightarrow OH^* + e^-$ $OH^* + OH^- \rightarrow O^* + H_2O(l) + e^-$ $O^* + OH^- \rightarrow OOH^* + e^-$ $OOH^* + OH^- \rightarrow * + O_2(g) + H_2O(l) + e^-$
	ORR (Acidic)		$O_2(g) + H^+ + e^- \rightarrow OOH^*$ $OOH^* + H^+ + e^- \rightarrow O^* + H_2O(l)$ $O^* + H^+ + e^- \rightarrow OH^*$ $OH^* + H^+ + e^- \rightarrow * + H_2O(l)$
	OER (Acidic)		$H_2O(l) + * \rightarrow OH^* + H^+ + e^-$ $OH^* \rightarrow O^* + H^+ + e^-$ $O^* + H_2O(l) \rightarrow OOH^* + H^+ + e^-$ $OOH^* \rightarrow * + O_2(g) + H^+ + e^-$
Non-aqueous MABs	ORR (e.g., LAB in non-aqueous electrolyte)	$O_2 + e^- \rightarrow O_2^-$ $O_2^- + Li^+ \rightarrow LiO_2$ $2LiO_2 \rightarrow Li_2O_2 + O_2$	
	OER	$Li_2O_2 \rightarrow 2Li^+ + O_2 + 2e^-$	

* is the active site on the surface, (l) is a liquid phase and (g) is a gas phase, O^*, OH^* and OOH^* are adsorbed intermediates.

Both processes can take place on an air cathode electrode without using catalysts. Nevertheless, since the natural kinetics of oxygen are slow, the use of electrocatalysts may speed up the reactions. ORR and OER are the two processes that take place with the presence of oxygen. This occurs during the discharge process in MABs and consists of a variety of stages, with the following most important:

1. Oxygen diffuses into the surface of the catalyst from the environment.

2. The surface of the catalyst absorbs oxygen.

3. The electrons from the anode are transferred to the oxygen molecules via an external circuit.

4. The oxygen connection is broken, and the oxygen bond becomes weaker.

5. The hydroxyl-ion t is removed from the catalyst's surface and transferred to the electrolyte.

All the above processes are reversible in OER, which takes place during the charging process. Due to the relative stability of the intermediates created following oxygen adsorption on the catalyst,

either a four-step or a two-step route can be used in ORR and OER processes. The superoxide intermediate generated by the two-electron mechanism is a reactive oxygen species.

$$O_2 + H_2O + 2e^- \rightarrow HO_2^- + OH^- \tag{5.15}$$
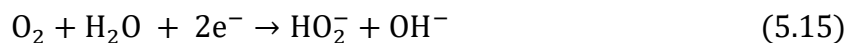
The hydroxide OH^- generated in the four-electron process in an alkaline medium is displayed in Equation (16).

$$O_2 + 2H_2O + 4e^- \rightarrow 4OH^- \tag{5.16}$$
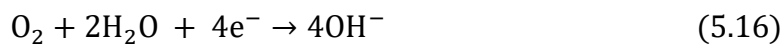
The process of four electrons is highly demanded for energy densities and high power. Feeding purified air or employing an O_2-permeable membrane is necessary for alkaline media to avoid accumulating carbonate ions in the liquid electrolyte with time [423-425].

5.6.4 Progress done in the Cathode

Despite the fact that they have exceptional performance, the electrocatalytic activity of noble metal-based electrocatalysts is restricted by their high cost and poor durability [426, 427]. In order to overcome these restrictions, a research created a graphene quantum dot/graphene hydrogel GH-GQD that has good durability and extraordinary electrocatalytic activity in alkaline solution in primary ZABs. The GQD results in greater ORR electrocatalytic activity. After that, different concentrations of GQD were compared, and it was found that the GH-GQD-90 exposed high ORR activity and extraordinary durability in alkaline primary MABs, and high performance as an ORR catalyst in primary ZAB. When used in MABs and fuel cells, the GH-GQD presents tremendous promise for ORR as an alternative to noble materials [428].
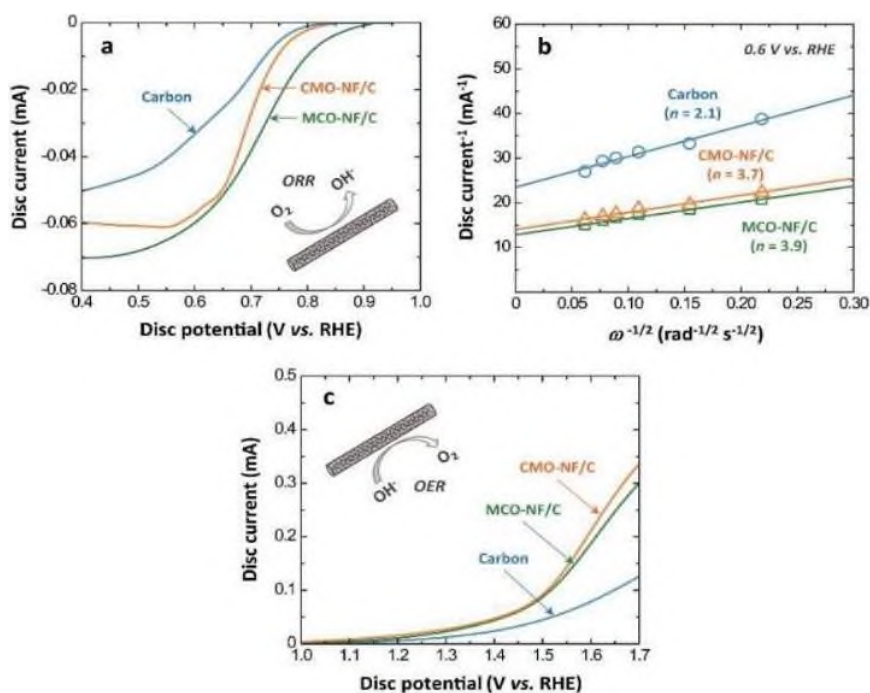
Figure 5.13 (a) Cathodic polarization curves at ω = 1200 rpm for the ORR measured, (b) K-L plots at 0.6 V vs. RHE and (c) anodic polarization for the OER [345, 429].

A research into rechargeable MABs generated a spinel-type manganese-cobalt oxide, $MnCo_2O_4$ (MCO), and $CoMn_2O_4$ (CMO) nanofiber that served as bi-functional cathode catalysts for the devices. As presented in **Figure 5.13**, these both have a high catalytic activity for both ORR and OER in an alkaline condition.

Then, they were tested in ZABs as catalysts and as a result, the round-trip efficiency was increased as compared to a cathode without a catalyst. A comparison of the electrochemical performance of ZABs utilizing the nanofiber catalysts that were manufactured with the performance of Pt/C and catalyst-free carbon cathodes is depicted in **Figure 5.14**.
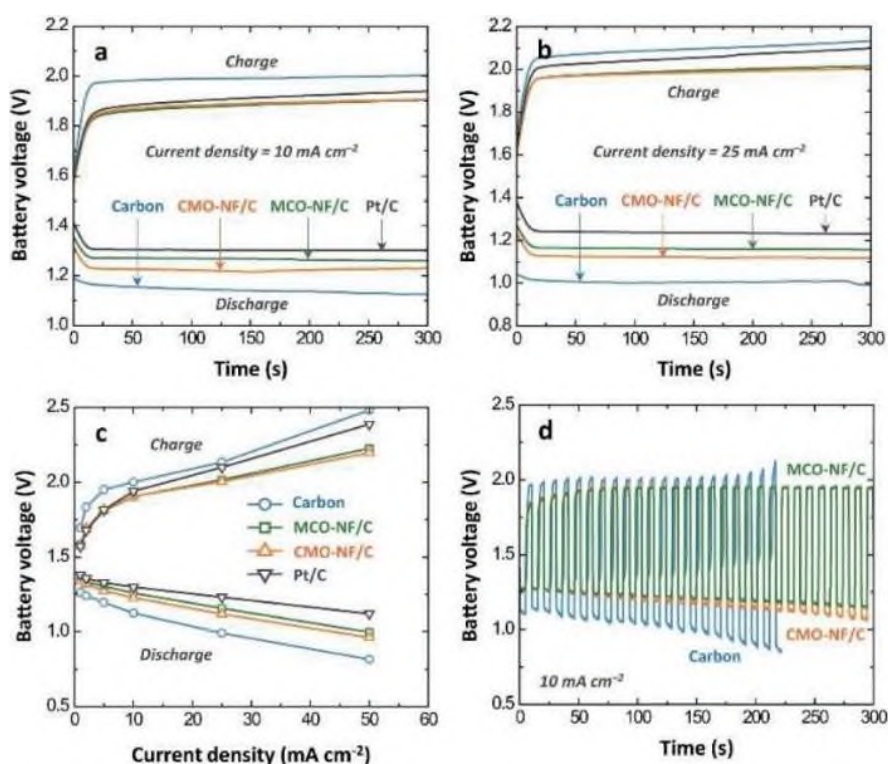
Figure 5.14 *Galvanostatic discharge-charge plots **(a)** at 10 mA cm^{-2} and **(b)** 25 mA cm^{-2}, **(c)** battery voltages at different current densities and **(d)** cycling performance at 10 mA cm^{-2} of rechargeable alkaline ZABs with various catalysts [345, 429].*

To receive Pt-based alternative electrocatalysts, a research mixed Ni, S and Co, to improve the electrochemical performance. Mixing sulfides and metal oxides containing transition metals frequently demonstrated useful electrochemical efficiency due to transition metal elements' synergy with single sulfide or metal oxide. The porous structure of $NiCo_2S_4$ can aid in the diffusion of oxygen and hydroxyl reactants, and it usually has a high surface area for oxygen reactions because of its porous nature. When $NiCo_2S_4$ microspheres are examined in an alkaline medium, they exhibit good electrocatalytic activity for OER and ORR and improved stability, making them a suitable catalyst for aqueous AABs and rechargeable ZABs. $NiCo_2S_4$ microspheres can be evaluated for aqueous MABs as an advanced electrocatalyst [430].

In another research, a PdCo/C bimetallic nanocatalyst was prepared as a potential air cathode catalyst. The prepared catalysts went through a heat treatment process at 200 °C in H_2/Ar atmosphere from 4 to 24 h. A clear correlation was found between the heat treatment and the total catalyst performance. As a result, the HT-8 h PdCo/C catalyst was examined in rechargeable Zn-air and Mg-air batteries. The resulting performance of each battery is depicted in **Figures 5.15** and **5.16**, respectively, to demonstrate its effectiveness.
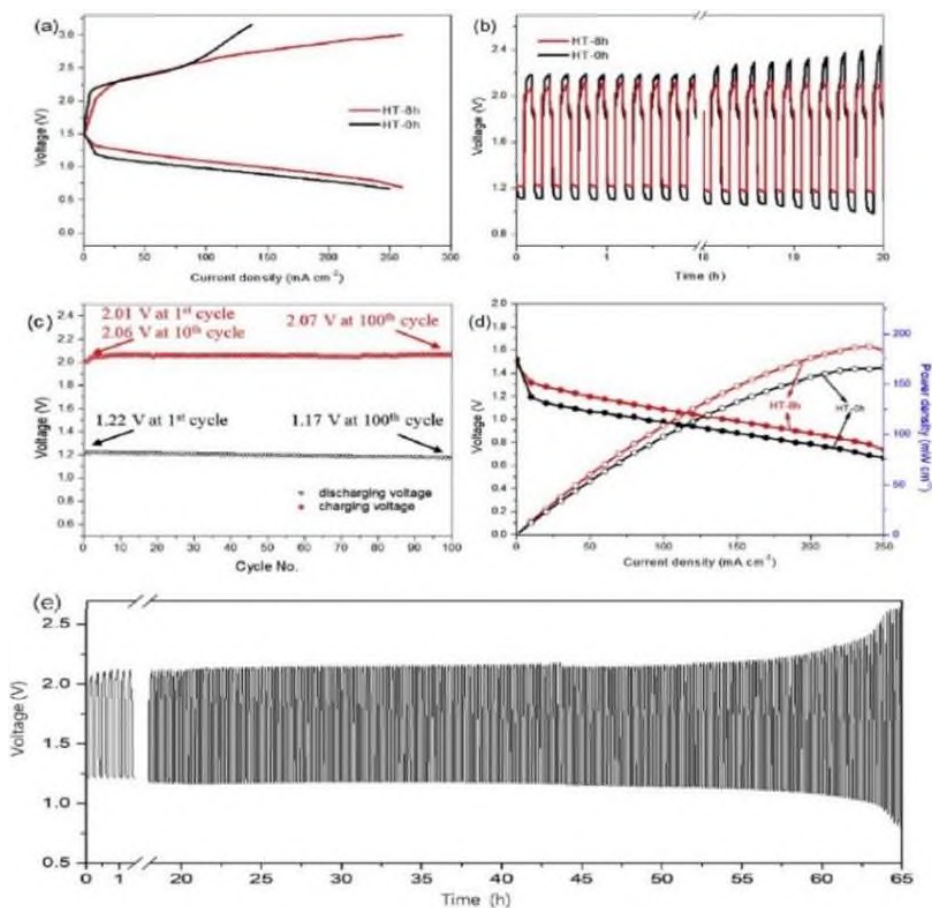
Figure 5.15 ZABs performance with PdCo/C catalysts. (a) Polarization curves, (b) discharge and charge voltage profiles for the first 20 h, (c) discharge and charge state end voltages for the consecutive 100 cycles of the HT-8 h through the first 20 h, (d) discharge polarization, and power densities curves and (e) battery long-term cycling stability using HT-8 h catalyst [431].
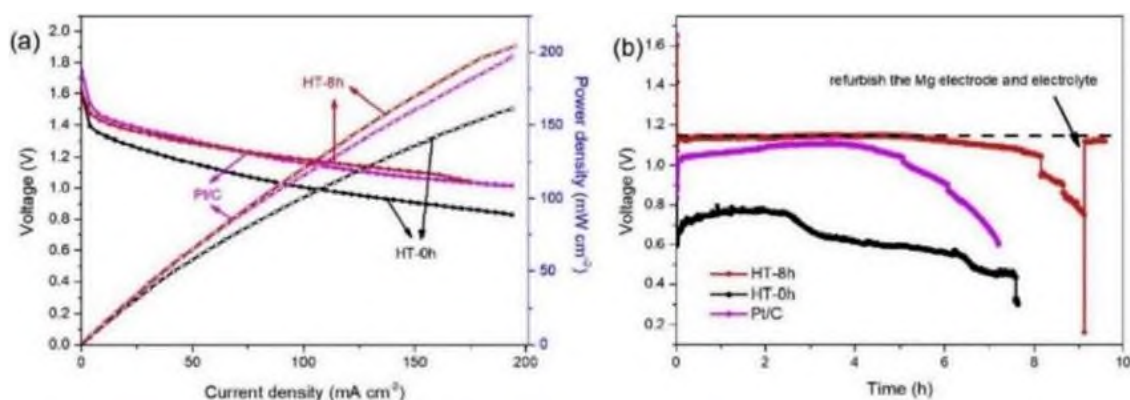
Figure 5.16 (a) Discharge polarization and power densities curves and (b) discharge stability curves of the HT-8 h, HT-0 h, and Pt/C in MABs [345, 431].

When the HT-8 h PdCo/C catalyst is used, the stability and activity of ZABs and Mg-air batteries are enhanced, and the activity is improved [431].

The impact of temperature on the manufactured in-house air cathode may be seen in the polarization curves presented in **Figure 5.17** and **Table 5.10**, respectively.
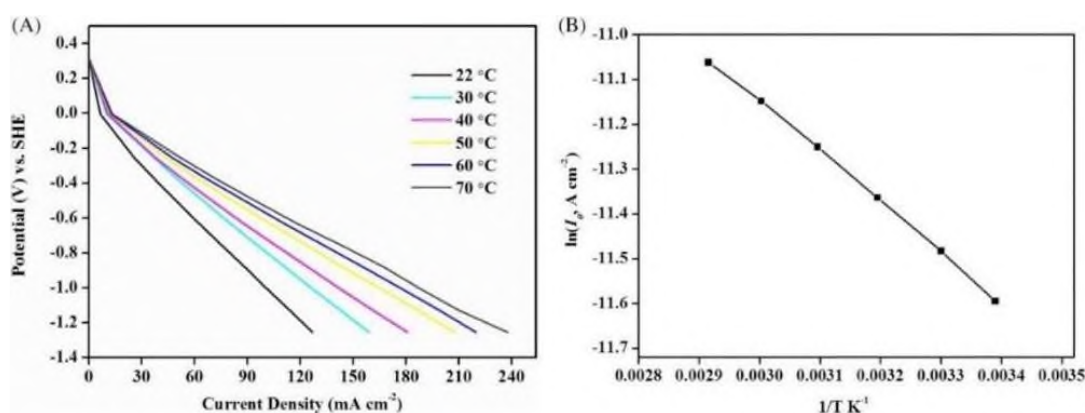
Figure 5.17 (A) LSV curves of developed air cathode in NaCl solution at different temperatures and (B) In I_0 of the cathodic ORR plot as a function of the temperature reciprocal (data from Table 5.10) [345, 432].

Researchers utilized various characterization methods to further understand the performance and characteristics of the newly created air cathode, which was then compared to commercial air cathodes for comparison.

Table 5.10 The ORR performance of advanced air cathode in air-saturated 10 wt% NaCl solution at a different temperature [345, 432].

Temperature (^{o}C)	Current Density (mA cm^{-2}) at -1.55 V (vs. SHE)	Geometric Exchange Current Density (mA cm^{-2}) at Ambient Pressure
22	127	9.21×10^{-3}
30	158	1.03×10^{-2}
40	182	1.16×10^{-2}
50	205	1.30×10^{-2}
60	224	1.44×10^{-2}
70	238	1.55×10^{-2}

The gas flow limitation and internal electrical resistance of the system are reduced, allowing an increase both in water transportation to reaction sites and in air permeability. As depicted in **Figure 5.18**, the performance of the magnesium-air single cell utilizing manufactured air cathodes is comparable to that of a commercial air cathode [432].

However, the newly designed air cathode, is both cost-effective in terms of production and materials and appropriate as a cathode for an MAB in a neutral or alkaline electrolyte.
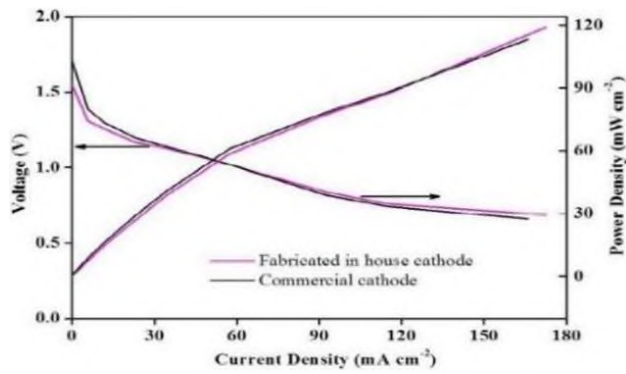
Figure 5.18 Mg-air single cell performance with the commercial cathode and fabricated in-house air cathode in neutral solution [345, 432].

The non-aqueous LAB was used to examine the impact of the operating temperature on the morphology of the discharge product produced. The solid discharge product Li_2O_2 clogs the cathode pores, hence stopping the discharge process. The product should be oxidized before it can be used in the charging process. Following the application of a variety of operating temperatures at varying discharge current densities, the performance of the Li_2O_2 discharge product is presented in **Figure 5.19**.
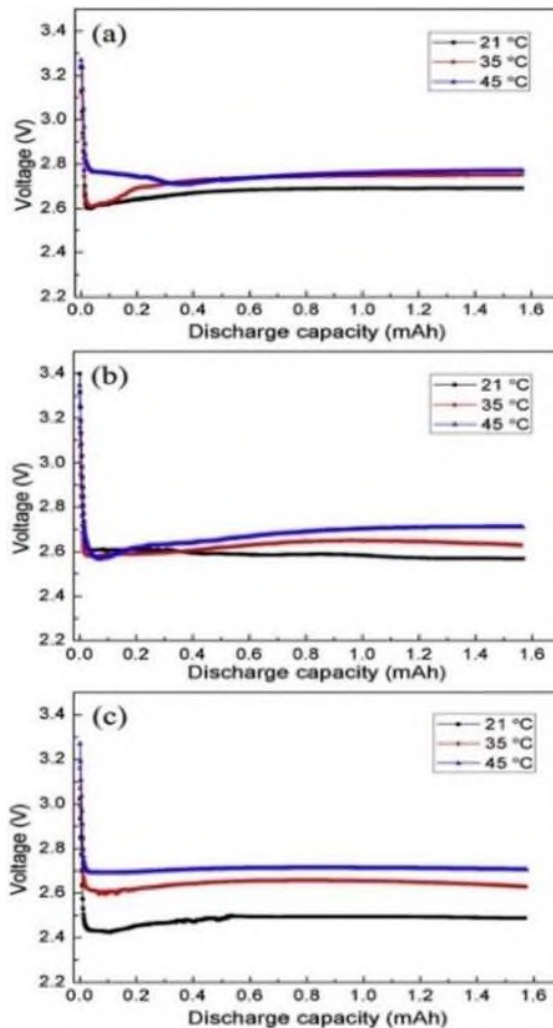
Figure 5.19 Discharge curves at different temperature and at current density (**a**) 0.1, (**b**) 0.2, and (**c**) 0.3 mA cm^{-2} [345, 433].

This is in addition to **Figure 5.20**, which demonstrates the voltage-capacitance graphs at numerous temperatures.
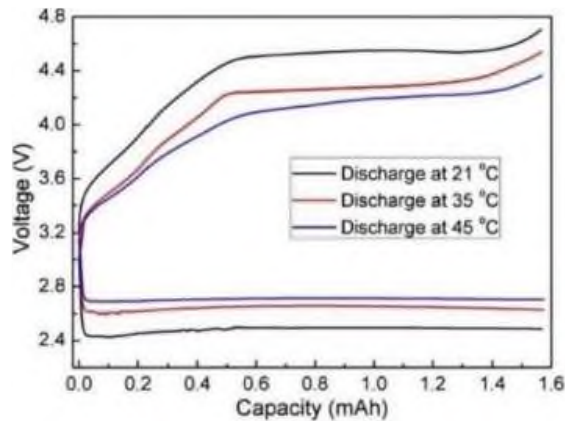
Figure 5.20 *Charge curves at the battery operating temperature of 21 °C with discharge at different temperatures [345, 433].*

In conclusion, changing the operating temperature at a specific discharge current density does not affect the form of Li_2O_2, while increasing the operating temperature leads to a reduction in the size of the discharge product. In addition, the operating temperature affects the charge voltage, cyclability, and capacity of a particular non-aqueous LAB [433].

5.7 Progress in the Design of MABs

5.7.1 Introduction

The two kinds of MABs are primary and secondary, as depicted in **Figure 5.21 (a–c)**.
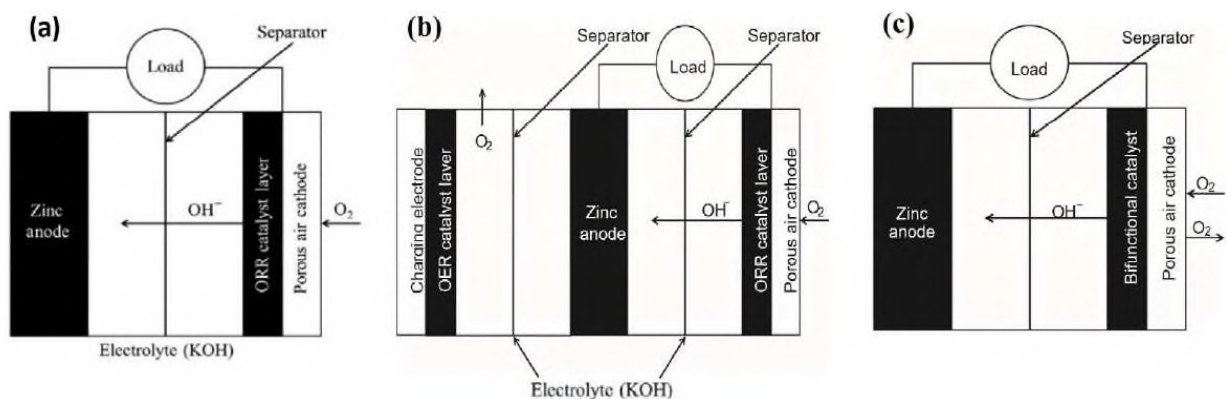
Figure 5.21 *(a) Primary Zn-air cell; secondary Zn-air cell in (b) three-electrode design and (c) two-electrode design with a bifunctional catalyst layer [345, 434].*

Primary MABs are non-rechargeable, while secondary MABs are rechargeable. The basic MABs have two electrodes, each with an ORR catalyst, while the rechargeable MABs have two or three electrodes, each with an ORR and OER catalyst, depending on the model. In the three-electrode arrangement, the metal electrode is located between the charging electrode for the OER and the air cathode electrode. The air cathode is electrically separated during the charging process,

which extends its lifespan by preventing it from being exposed to the high OER potential during the charging phase. On the contrary, the two-electrode design of rechargeable MABs, presented in **Figure 5.21 (c)**, consists of a metal electrode and a bifunctional air electrode that contains catalysts for ORR and OER and other functions [422]. Additionally, it has less mass (resulting in higher specific energy) and fewer interfaces, which decreases the possibility of kinetic rate losses [434].

5.7.2 Classifications Cell Structure

Figure 5.22 depicts the three configurations of MABs, the conventional static battery, the flow battery, and the flexible battery.
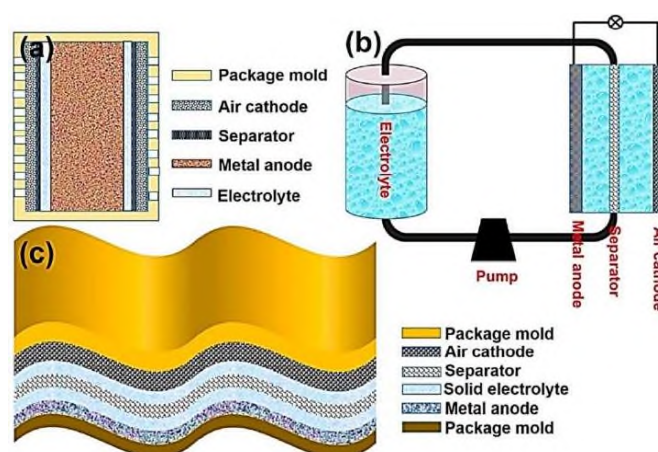
Figure 5.22 Configurations of MABs in a (*a*) multi-cell static battery, (*b*) flow battery and (*c*) flexible battery [345, 346].

The first configuration is the traditional static air battery, which consists of the three primary components (anode, cathode, and electrolyte) and a separator. In this configuration, the kinetics of the anode reaction are quick in comparison with the cathode reaction, and it demands highly efficient catalysts to assist the reactions, in addition to the challenge of the by-products that deposit insolubly on the surface of the electrodes during charge-discharge cycles, resulting in reducing the battery's performance because of the blocking of the pores of the electrode, limiting the air diffusion step. The second configuration is the flow battery, which consists of an anode, cathode, electrolyte bank, electrolyte, separator and it is commonly installed with a pump in order to maintain the electrolyte flow. The configuration of the electrolyte flow reduced the volume density and energy efficiency. The third configuration is the flexible battery, which gained the attention of researchers due to the increasing requirement for flexible, portable electronics in last years which demands a flexible energy storage device. This type of battery consists of a thin metallic plate anode to decrease battery weight, a highly conductive electrolyte, a cathode such as carbon fiber and a separator. Nowadays, the ideal flexible batteries are ZABs and AABs, because of their high energy density, safe operation and low cost [346].

5.7.2.1 Static MABs

MABs with a static structure can be used for large-scale electronics and have been studied widely. Nevertheless, their performance is limited regarding practical power/energy density and energy efficiency. Furthermore, the integration of static cell structure with other energy technologies is difficult and complicated [435].

- Parallel-Plate Electrode Configuration

The arrangement of the parallel-plate electrode configuration presented in **Figure 5.23** allows mass transport rates and high heat dissipation.
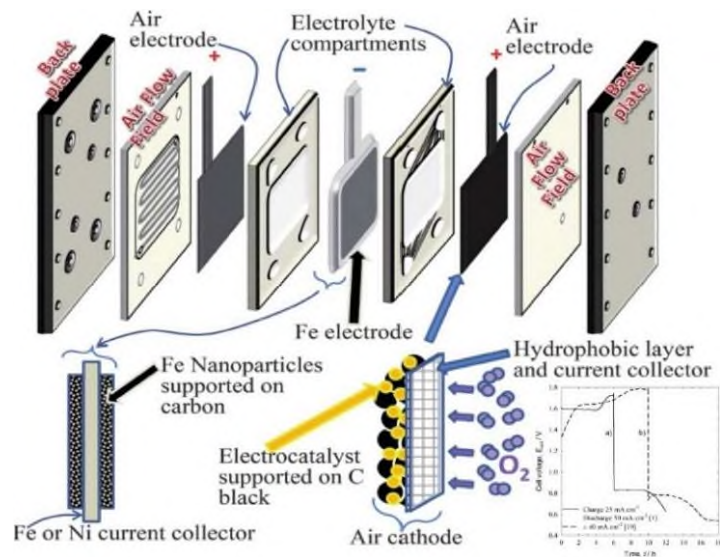
Figure 5.23 Parallel-plate electrode configuration of Fe-air battery [345, 374].

For laboratories, small cells are preferable because of the low demands of power and volume. Nevertheless, the heat produced in large cells during the charge and discharge cycles has to be taken into account. The cross-section of a unit cell and the stack connecting several cells together to form a battery are illustrated in **Figure 5.24**.
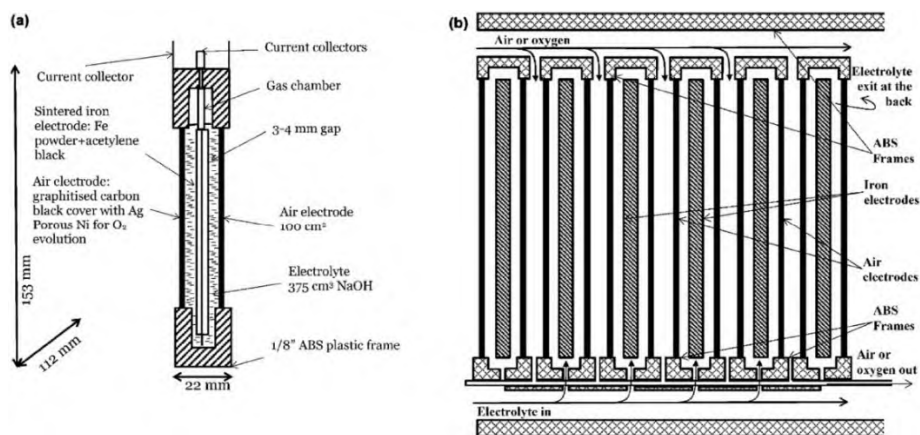
Figure 5.24 Fe-air unit cell. (a) Single-cell cross-section and (b) stack of 6 Fe-air cells [345, 374].

A variety of materials are examined in air cathodes such as Pt/C combined with Ir/C, and urchin-like NiO_2S_4 microspheres covered by a sulfur-doped graphene nanosheet, S-GNS (S-GNS/NiO_2S_4) [436].

- Coin-Type

A coin cell type and its components are presented in **Figure 5.25**.
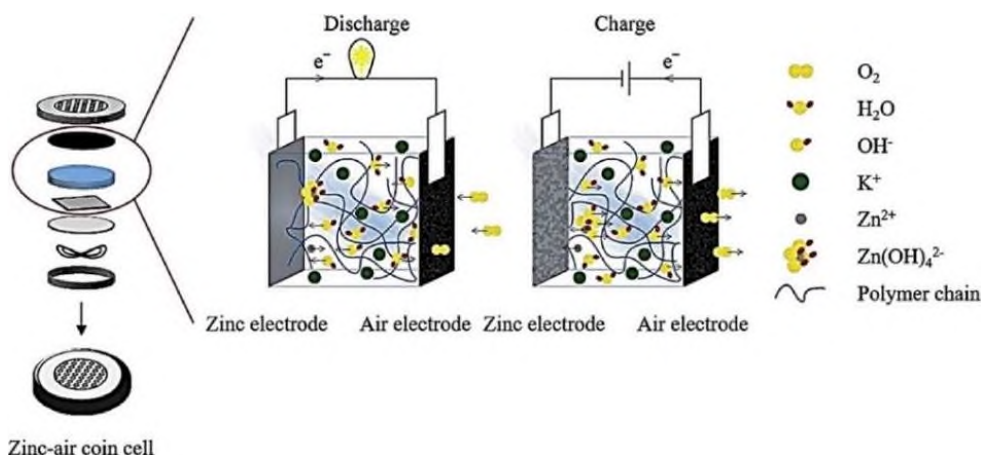
Figure 5.25 Schematic diagram of a coin cell [345, 437].

Figure 5.26 shows the performance of this configuration using electrolytes at 6 M concentration, such as poly vinyl alcohol (PVA), potassium hydroxide (KOH), PAM and poly-acrylic acid (PAA) [437].
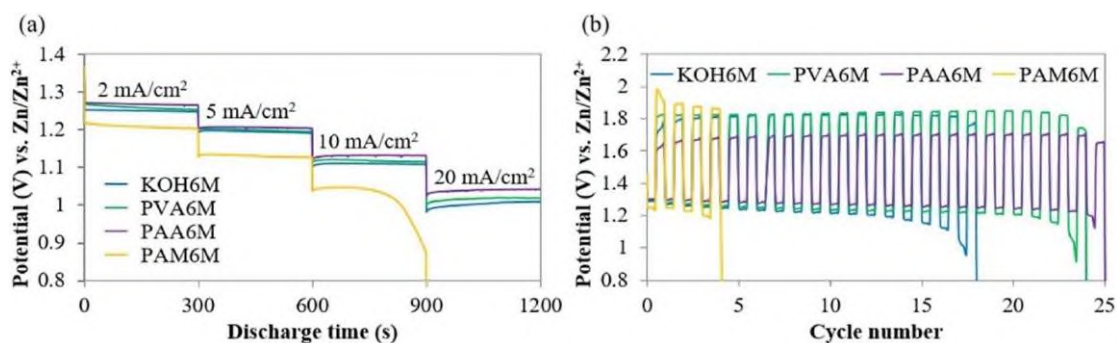
Figure 5.26 Zn-air coin cell: (a) discharge curves at different current densities and (b) discharge-charge cycling performance at 0.5 mA cm^{-2} using various electrolytes [345, 437].

- In Situ Cell

Numbered components of an in situ cell are depicted in **Figure 5.27**.
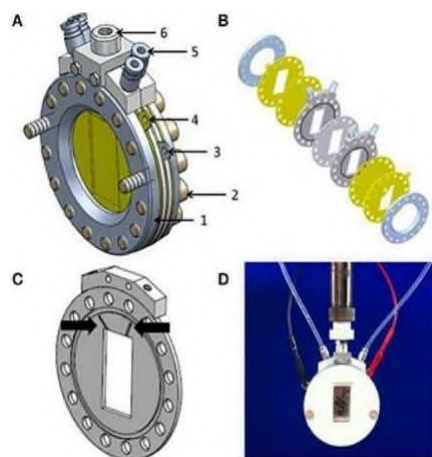
Figure 5.27 (A) Schematic diagram of in situ cell. *(B)* The cell components sketch. *(C)* Close-up view of the separator module (the black arrows represented the apertures which connect the battery inner compartment with the cell exterior). *(D)* Real assembled cell [345, 438].

The alloy clamp rings and PEEK screws, used to close the cell after assembly, are numbered 1 and 2, respectively. The thin sheets of Ni metal (used as positive and negative electrodes) are numbered 3 and 4, respectively. The tubing connections for pumping gas fuel or the electrolyte are numbered 5 and the thyristor is numbered 6.

5.7.2.2 Flexible MABs

The stability of the flexible MABs must be confirmed when subjected to frequent mechanical strain over an extended time period, and the security of the battery must also be confirmed when subjected to a variety of deformation situations. The electrodes in flexible MABs should have the ability of adaptation to changing conditions. Metal ribbons, rods and foil, or a flexible metal substrate covered with a metallic powder can be used as anodes, as can metal rods coated with a metallic powder. Complementary characteristics of a cathode current collector include high conductivity, great flexibility and air permeability. These characteristics should be combined with an active material coating to construct a flexible air cathode. The carbon materials with the greatest potential as active materials are nanotubes and graphene, which are distinguished by their high tensile strength and high Young's modulus. The exceptional performance of the flexible MABs is attributed to the close contact that exists between the cell components [346, 439].

- Fiber - Type

The configuration of this type of flexible MAB and the progress made in its development are presented in **Figure 5.28**.

Figure 5.28 Schematic showing the progress made in the development of fiber-shaped metal-air batteries [345, 440].

The cell structure of this type of MAB is usually a polymer electrolyte, such as gelatin gel polymer electrolyte GGPE, around the central metal anode and flexible air cathode coated with the electrolyte and it may operate efficiently under external strain. Moreover, other researches

depicted the marvelous mechanical stability and electrochemical performance of this configuration type [439].

- Sandwich - Type

The components in sandwich-type MAN are produced in plan form, then assembled as in **Figure 5.29**.
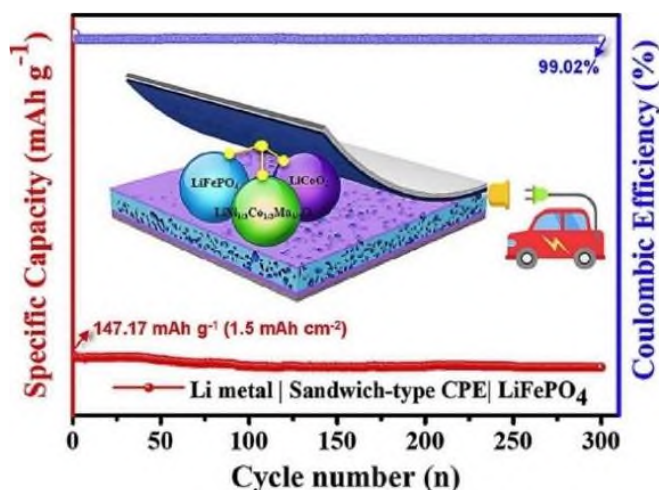
Figure 5.29 *Stability of sandwich-type Li metal battery (inset shows schematic of the cell) [345, 441].*

This configuration exhibited high volumetric and gravimetric energy density and exceptional electrochemical and cycling performance under bending conditions even at a high current density [439, 441].

- Array

A planner multilayer MAB array configuration is showed in **Figure 5.30**.
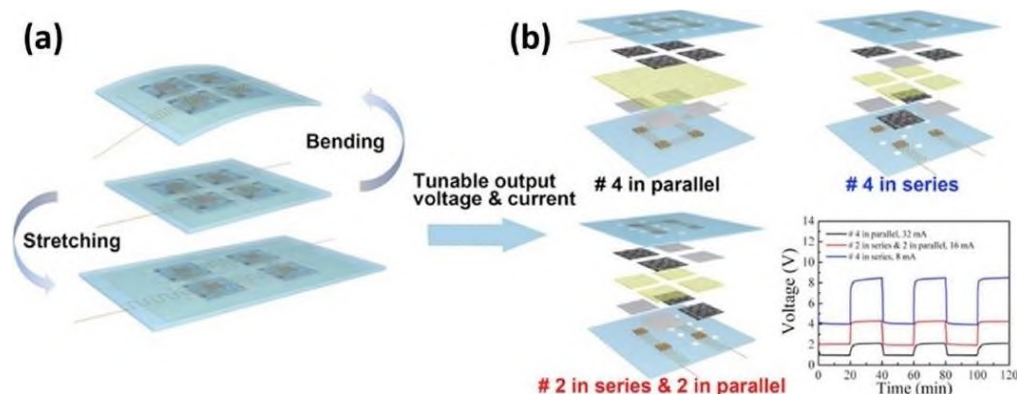
Figure 5.30 *(**a**) Multilayered structure of a flexible/stretchable rechargeable ZAB array and (**b**) bending and stretching the battery and different array connections series and parallel [345, 442].*

It possesses flexible and stretchable characteristics, a thickness of nearly 3 mm and exposes extraordinary stable and rechargeable battery performance. This array may be connected in series and parallel, or in a combination between them and it may be used in wearable devices [392].

5.7.2.3 Flow MABs (MAFBs)

The flow system is adaptable and can be easily combined with a variety of energy technologies when it comes to cell construction. It is safe and has a long operational life due to the flow of the anolyte/electrolyte, reducing side reactions. It can be used for large-scale energy storage as well as stationary power plants. The anolyte circulation is demonstrated in **Figure 5.31**.
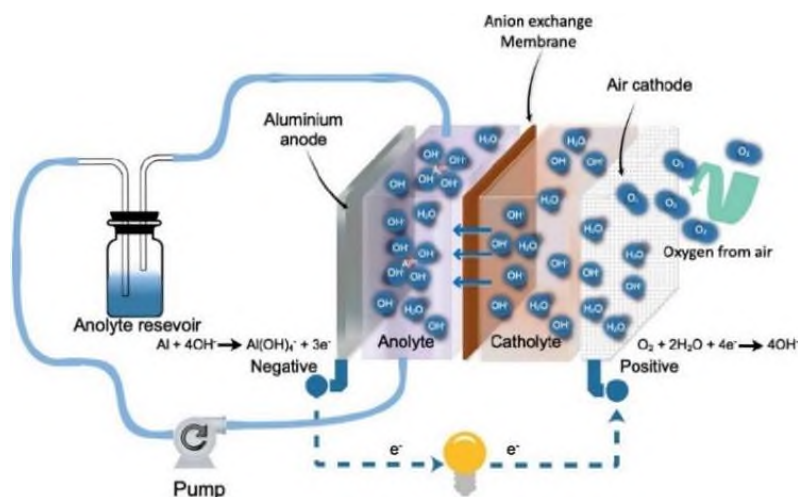
Figure 5.31 Schematic diagram of MAFBs' anolyte circulation [345, 443].

- Anolyte Circulation

The system consists of an anode electrode, a casting air electrode, two current collectors, an ion transport membrane and catalysts. The cell in **Figure 5.31** uses a flow of a redox couple at the negative electrode and air (or oxygen) at the positive electrode. The flow rate of the anolyte should be controlled to prevent any possible concentration polarization. Replacing the positive electrolyte tank that used conventional redox flow batteries REBs with an oxygen GDE decreases the total weight and volume, hence improving energy densities and power. An example of this approach are Zinc-air and Vanadium-air flow batteries (ZAFB, VAFB) towards metal-air flow batteries [435, 443].

- Electrolyte Cycling

This approach is depicted in **Figure 5.32 (A)**, where the fresh electrolyte constantly supplies the flow through the electrochemical cell.
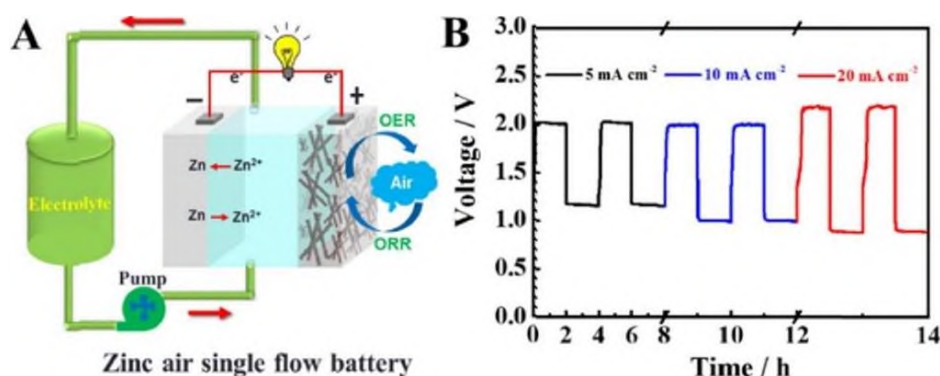
Figure 5.32 (A) Schematic diagram and (B) charge-discharge curves of the assembled ZAFB [345, 444].

It improves the metal anode charge and discharges efficiency, while eliminates the by-products and the side reactions. Hence, the cathode becomes less blocked, which is favorable for oxygen access. Lithium-air, Zinc-air and Sodium-air flow batteries can be constructed using this approach, and **Figure 5.32 (B)** presents the efficiency of zinc-air flow batteries using a NiSx-FeOy/sulfur-doped carbon fiber paper SCFP catalyst [435].

- Hybrid Electrolyte Flow Battery

Due to the fact that certain metals, like Na and Li, are water-sensitive, hence their use is questionable in aqueous media. Organic and inorganic hybrid electrolytes separated by a plate that is a superionic conductor are preferred in their flow configurations. Furthermore, this concept has been commonly improved in static sodium and LABs to protect the aprotic electrolyte and protect the extremely reactive the Na/Li metal anode from oxygen crossover or water and carbon dioxide impurities in ambient air [435].

- Bidirectional Flow Battery with a Two-Layered Cayhode

The bidirectional flow battery components of vanadium-air flow battery (VAFB) are presented in **Figure 5.33**, where it used an interchangeable gas diffusion electrode with a different catalyst for both charging and discharging processes.
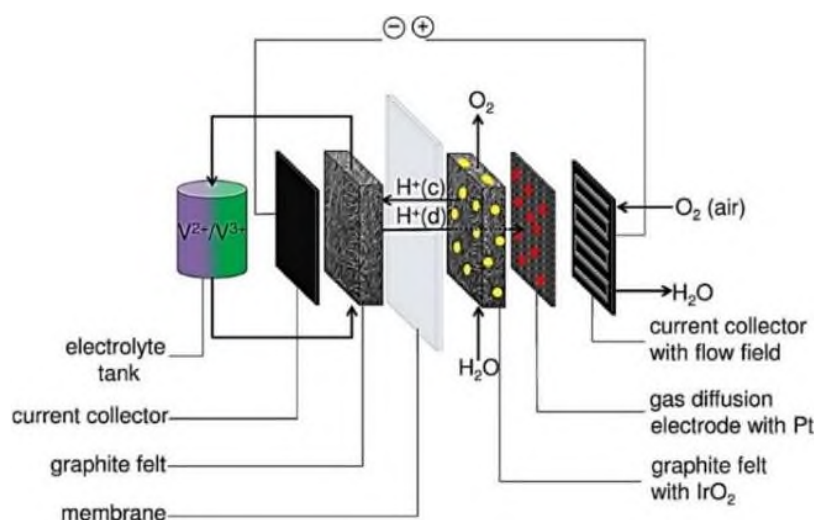
Figure 5.33 *A bidirectional VAFB based on a two-layered cathode [345, 448].*

Involving this developed cathode in VAFB resulted in 44.5 % voltaic efficiency and 87.6 % coulombic at 40 mA cm^{-2} (used catalyst Pt/C and IrO$_2$), but highly active electrocatalysts and crossover-minimizing membranes need to be collectively improved [435]. To reduce this problem, tungsten oxide nanofiller with a variety of mass loadings (0-20 % wt.) was announced in the Nafion matrix [445]. The coulombic efficiency, energy efficiency, and capacity retention were improved by 93 %, 75 % and 62 %, respectively, as compared to 88 %, 65 %, and 42 %, respectively, in the case of using pristine Nafion 212. Additionally, the electrode materials and

their cost have a great impact on the development and commercialization of flow batteries. As an example, in addition to the selection of mechanically and thermally stable electrodes, the cathode structure must be porous to facilitate the ORR reaction [446]. The treatment of graphite felt with polyacrylonitrile (PAN-GF) or rayon (R-GF) was performed to examine the impact of a precursor on the polarization effect [447]. The PAN-GF has higher conductivity because of the higher degree of graphitization and hence more negligible ohmic polarization.

CHAPTER 6

Failures - Diagnostics of Metal-Air Batteries

6.1 Failures of MABs

6.1.1 General description

The energy content of the MABs' cell is theoretically specified by the amount of available anode material, as the cathode uses oxygen from ambient air. Nevertheless, the application of oxygen from ambient air demands a partially open battery casing, which increases the risk for the electrolyte of drying or leaking out. Furthermore, the entrance of CO_2 and moisture can result in harmful side reactions such as the carbonation of alkaline electrolytes or the decomposition of the anode material because of the reactions with water, which needs to be resolved in order to avoid early failure of MABs. Therefore, the design of the air electrode by the application of suitable membranes has proven to be effective, but still there is enough space for improvements [456, 457].

For aqueous electrolytes, which mostly apply to Si-, Zn-, Fe-, and Al-air batteries, great failures for MAB cathodes exist in applying cheap, non-noble, but, high-performance, ideally, bifunctional, catalysts for the oxygen reduction / evolution reaction (ORR/OER). The ORR is a slow reaction, which decreases the availability of suitable non-noble catalysts already and reduces the choice of material even further once high-performance OER is demanded for the same material. Nevertheless, the application of bifunctional catalysts eliminates the risk of rapid catalyst degradation and, therefore, the demand for two separate air electrodes for charge and discharge operation. Catalyst degradation during repeated electrochemical cycling of MABs takes place when two different catalysts are chosen for the individual functionality of ORR and OER on the same electrode. Hence, extended catalyst study with respect to bifunctional materials is of great concern for MABs in order to decrease the complexity of the battery [459, 463].

In case of aqueous MAB-anodes, three great failures are appeared in the reprecipitation and dissolution of the anode material as a metal oxide or hydroxide on the metal electrode surface during repeated electrochemical cycling, the tendency of most metals towards corrosion and the hydrogen evolution because of the water splitting upon recharge of the battery. The first above failure can result in dendrite formation, which is extremely obvious for Zn-air batteries and sometimes leads to internal short circuits in the battery, if the applied current

density during the recharge is very increased. The second failure can lead in discharge capacity losses because of the dissolution of the anode material in the electrolyte. Especially in concentrated alkaline electrolytes, which are desirable for most aqueous MABs because of their marvelous ionic conductivity, most anode materials demonstrate severe corrosion unless a passivating layer forms on the electrode surface and prevents the metal from progressive dissolution on standby. The third failure should be avoided in order to prevent the battery from drying out and to improve the coulombic efficiency by the prevention of a parasitic side reaction during the recharge of the battery [465, 469].

For non-aqueous electrolytes, which particularly apply to Li-, Mg-, K-, Na-, Ca- and Si-air batteries, a significant failure in comparison to aqueous MABs is the quite different reaction zone for the discharge products. In non-aqueous MABs the discharge products typically accumulate on the air electrode, which demands the air electrode to offer both large storage capacity and decent oxygen permeability to be effective for long-lasting battery discharge. Else, the discharge of the cell will stop early, as the battery dies from oxygen starvation once the discharge products clog the pores of the air cathode and prevent the influx of additional oxygen into the battery. Furthermore, in non-aqueous MABs, an appropriate way to decrease the cathode-related overpotential during the recharge has to be determined, in order to sustain the performance and achieve long-term cycling stability [470, 471].

In addition, depending on the individual anode material, an appropriate electrolyte that is stable against decomposition by all of the occurring charge-/discharge (by-)products has to be determined, which is a necessary task because of the reactivity of the individual chemicals. Moreover, for non-aqueous electrolytes, another possible degradation mechanism may be the corrosive reactions with the applied electrode material, which lead into capacity losses of the battery and a possible development of a passivation layer on the metal surface. Additionally, for rechargeable MABs, the non-uniform re-deposition of the metal upon recharge can result in dendrite formation, which, finally, causes short-circuits and shedding of the electrode. In case of highly reactive metals as anode materials, for safety reasons, it is crucial to prevent water and oxygen access to the metal itself while forming stable Solid Electrolyte Interphase (SEI) in order to avoid electrolyte decomposition on the metal surface [472, 473].

6.1.2 Metallic Anode Failures

One of the crucial problems facing MABs is the corrosion, passivation, and dendritic formation of the metallic anode. Corrosion is one of the most critical side reactions between a metal and an electrolyte, as presented by the following process.

$$M + (2 + x)H_2O \rightleftarrows 2M(OH) + H_2 \qquad (6.1)$$

$$M + H_2O \rightleftarrows MO_x + H_2 \qquad (6.2)$$
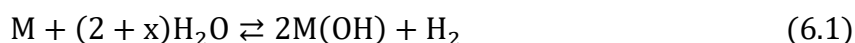
Hydrogen evolution is naturally favored in almost all MABs because the standard voltage of M/MO is under the level of hydrogen evolution. The rate of corrosion caused by the Hydrogen Evolution Reaction (HER) can be computed using the equations above. The HER can reduce the columbic efficiency of a metal anode, which may lead in a battery explosion. Corrosion can occur in FABs, ZABs, AABs and LABs, among other types of batteries. **Table 6.1** demonstrates some methods for decreasing the HER rate while, at the same time, increasing charging efficiency.

Table 6.1 Reducing corrosion strategies [345, 346].

Metal	Reducing Corrosion or HER Rate by
ZnO surface	Increasing ZnO reduces the self-discharge rate.
Al	Changing purity, properties and temperature of the alkaline electrolyte. Utilization of ionic membrane.
Fe	Using an alloy as an anode instead of pure metal and additives such as sulfur or bismuth is a good way to save money.

Passivation is the growth of an insulating layer on the electrode surface, which prevents the discharge product from moving around. Electrode discharge is prevented by the layer that develops. This can be seen in ZABs, LABs and AABs batteries, among other things. Depending on the system, the passivation layers in MABs are ZnO, LiOH and Al_2O_3, respectively. In the presence of an air cathode, the produced soluble species turned to a non-conductive layer on the surface of the metal. They increase the cell's internal electric resistance, which prevents the dissolving of metal. The use of porous electrodes to avoid the development of a passivation layer is an effective approach [346].

Dendritic formation and deformation result in gradually modification of the shape of the metal electrode, meaning that the surface roughness becomes uneven as dendrites form. This takes place because of the accumulation of metal ions during metal electrode cycling in alkaline electrolytes and may lead in an unstable battery system, or it can cause a shortcut [346].

6.1.3 Electrolyte Failures

Dissolving CO_2 from the air in the aqueous KOH electrolyte is an important failure for a few types of MABs, as for example ZABs, because CO_2 reacts with OH^- and forms CO_3^{2-}, hence decreasing both the electrolyte conductivity and the cell reaction. Appling a CO_2 filter could solve this issue, however it will enhance the complexity and the cost of the system [449].

The development of hydrogen gas could be a failure for electrolytes with a metal electrode with a lower potential than hydrogen development because the electrolyte becomes

thermodynamically unstable [449]. When using an active electrolyte, the insoluble by-products' deposition on both electrodes' surfaces during the charge-discharge cycles is a failure that must be taken into account. These by-products decrease the battery's performance because they block the electrode pores and restrict air diffusion [346, 450].

The absorption of moisture from the environment and the evaporation of electrolytes both shorten the life of aqueous MABs. As a result of the accumulation of water, air electrode flooding can happen, which may weaken oxygen delivery to the active areas of the catalyst. Nevertheless, water loss increases the electrolyte concentration in the body, which has a detrimental effect on the discharge response. Furthermore, if the electrolyte is diluted, the ionic conductivity will be reduced, resulting in higher internal resistances in the system. When designing the battery, there is a possibility of optimizing the internal water balance by considering the quantity of metal used, the composition and volume of the electrolyte and the degree of gas diffusion. The polymerization of the electrolyte can assist to reduce the amount of moisture that is lost. Additionally, the use of a siloxane membrane prevents from flooding and drying out [410].

6.1.4 Air Cathode Failures

Different types of materials including noble and transition metals, MOFs, Perovskites and carbon-based materials are effectively utilized as cathode catalysts for bifunctional (ORR/OER) activity. It is a great challenge to develop a bi-functional air catalyst that is active, stable, inexpensive and is appropriate for both ORR and OER [449]. A perfectly designed catalyst may:

1. enhance the catalyst's effective surface area with exposed electroactive sites,
2. facilitate the smooth charge-discharge process by restricting the agglomeration process,
3. control the porosity of the structure and
4. increase the electrical conductivity.

Therefore, the development of facile and operational approaches for the fabrication of binder-free thermally and mechanically stable catalysts with controlled morphologies, size, conductivity, surface area, and dense electroactive sites may resolve this issue, however this area demands deep research work to achieve astonishing efficiency and stability.

The precipitation of solid products such as Li_2O_2 in the cathode leads in a thick layer that restricts electron transport and can even lead in the blocking of cathode pores, decreasing the entire capacity of the cell. The transfer of oxygen is an issue for certain types of MAB when operating at high current densities [449].

Furthermore, the link between electroactive active sites, by the development of mesostructure/microstructure, catalytic mechanism atomic/molecular modeling may be entirely understood by Density Functional Theory (DFT) and other simulation techniques.

6.1.5 Failures of Zinc-air batteries and future prospects

Nowadays, there is major progress in the field of ZABs, but still there are extensive failures such as the intensive work required for the synthesis of new flexible and self-supporting cathodes, insight into electrocatalytic mechanisms, and recognition of suitable materials for the synthesis of the flexible electrode with outstanding catalytic performance.

A great development in the field of bifunctional ORR/OER electrocatalysts has been accomplished till now. However, there is an imminent need for advanced synthetic methods which can effectively (a) enhance the electroactive surface area of the catalyst with exposed catalytic active sites (b) control the porous structure (c) enhanced electrical conductivity, and (d) smooth charge-discharge process with restricted agglomeration problem, especially the latter part is mainly urgent because the nanoparticles agglomeration on the catalyst-GDL interface block the diffusion pathways and in turn limit the catalytic activity. So, the development of binder-free or direct growth of air electrodes is a promising solution to the above-mentioned problem as the electroactive nanoparticles, directly grown or deposited on the framework of the highly porous and conductive substrate prevent the particle's rapid agglomeration [450-455].

A reversible Zn electrode should (a) possess a high proportion of functional active material, (b) recharge with high efficiency, and (c) sustains its electrochemical activity over several hundred charge-discharge cycles. The structural modification via advanced casting and electrodeposition techniques as well as compositional modification through the addition of additives or chemical doping were found to be feasible solutions for all the above-mentioned requirements. Furthermore, the additives should be added in small amounts because a large proportion of additives affect the overall Zn capacity. Further research on the development of new additives is required to improve the electrochemical performance of the Zn-air battery [458, 460-462, 464].

New electrolyte technologies are required that allow the long-term operation of zinc-air batteries. Until now, the most popular electrolytes are aqueous alkaline electrolytes but the issue of electrolyte drying out and carbonate formation required to be addressed for better battery performance. Ionic liquids are a better alternative to aqueous alkaline electrolytes due to their limited electrolyte evaporation and resistance towards CO_2 poisoning and hydrogen evolution, thereby improving the battery efficiency and life cycle. However, their instant use as

a potential electrolyte in Zn-air batteries is restricted due to several limitations like high viscosity, high cost, and slow reaction kinetics for Zn and oxygen reactions. For flexible devices, electrolyte solidification is vital for the maintenance of battery structural integrity under various deformations. However, the electrode-electrolyte interfacial properties need to be emphasized while replacing the unavoidable liquid electrolyte with a flexible solid-state electrolyte [466-468].

In the case of the novel and cost-effective bifunctional electrocatalysts there is a need for an in-depth understanding of complicated ORR and OER reaction mechanisms, the development of novel catalysts capable of working in a wide range of voltage, temperature, and electrolytes, and introduction of new incorporation techniques, widespread adaption, and their scalability. Moreover, to develop a link between laboratory results with commercial applications, the catalysts should be tested under practical conditions [475, 476].

The current air electrode design in many Zn-air batteries is identical to that implemented in alkaline fuel cells; the catalysts are deposited on C-based gas-diffusion electrodes. But, the carbon materials are easily corroded in harsh conditions enforced by a repetitive charge-discharge process in alkaline electrolytes. Moreover, the preparation of air-electrode is normally tedious and its main disadvantage is the use of auxiliary materials. So, the advanced design of air-electrode needs to focus on such new strategies to use corrosion-repellent carbon-based materials or metallic foams/meshes should be used as a support for the catalyst [474, 477].

The optimal stack and cell design need to work out such as the provision of purified atmospheric air by the addition of extra components in the air-electrode [478].

6.1.6 Failures of Lithium-air batteries and future prospects

Although lithium-air batteries offer attractive prospect as a future electric power source, various scientific and technical limitations need to be overcome before they can become practical. In particular, the low practical capacity, low round-trip efficiency, and poor cycling life need to be addressed. Electrolytes are considered as the most critical components to achieving a long cycling life [450]:

1. For non-aqueous electrolytes, one of the main failures at the current stage is the search for stable solvents and lithium salts. In addition, functional additives in electrolytes, aiming at stabilizing the electrolyte and/or promoting electrochemical reactions, need to be deeply investigated.

2. For solid-state electrolytes, search for the one with a high lithium-ion conductivity, a very low diffusion coefficient for the other species, and a high stability towards both

electrolyte and lithium metal is in great need. In addition, polymer electrolytes with the promising applications in flexible LABs should draw more research interests.

3. For aqueous electrolytes, choosing the suitable one with a high energy density and a high stability towards the solid-state electrolyte membrane is significant.

In addition to electrolytes, air electrodes, which provide the place for electrochemical reactions, represent major challenges [450]:

1. To obtain a high practical capacity, the reaction pathways among oxygen, lithium ions, and electrons should be maintained as long as possible. Consequently, the structure in different types of lithium-air batteries should be well designed. Specifically, for solid-state lithium-air batteries, the reaction boundaries should be enlarged; for non-aqueous lithium-air batteries, detailed investigations on the correlations between the cathode microstructures and the synergy transport in the electrolyte are required; for liquid-based (including non-aqueous, aqueous, and hybrid) lithium-air batteries, facilitating the transport of species in the liquid electrolytes (e.g., optimizing the electrolyte distribution inside the cathode, or developing a flow system) is important.

2. To facilitate the electrochemical reactions in the discharge and charge processes, catalysts are introduced. In aqueous electrolytes, finding inexpensive alternatives to noble metals, especially with bifunctional catalytic activities for both ORR and OER, should be the ultimate target. For non-aqueous and solid-state LABs, understanding the roles of catalysts in the formation and decomposition of the solid product is essential to develop effective catalysts. In addition, advanced characterization approaches for monitoring the discharge and charge processes should be applied.

3. To ensure a long cycling life, the instabilities of carbon materials should be well addressed. Effective approaches include applying a protective layer onto the carbon surfaces and applying catalysts with activities towards the decomposition of carbonate species. Besides, stable non-carbon cathodes have attracted great research interests, but achieving a large practical discharge capacity is challenging.

4. To operate the battery in ambient air instead of pure oxygen, developing an oxygen-selective membrane with high oxygen selectivity and permeability, or applying catalysts with activities for the decomposition of side products (e.g., Li_2CO_3 and LiOH) are required. Meanwhile, a membrane that can suppress the evaporation of liquid electrolytes is needed for long-term operation of non-aqueous, aqueous, and hybrid LABs.

Metallic lithium is typically chosen as the anode material in most studies of lithium-air batteries, which is expected to achieve the highest capacity and energy. The challenges for using lithium include [450]:

1. In non-aqueous LABs, the reactions on the interface between the lithium anode and electrolytes are far more complicated due to the oxygen/water/side products crossover. Consequently, protecting the lithium electrode through suitable membranes or passivation films is important.

2. Although lithium dendrite formation (**Figure 6.1**) in LABs has been few reported in the current stage, the suppression approaches are important in further research.
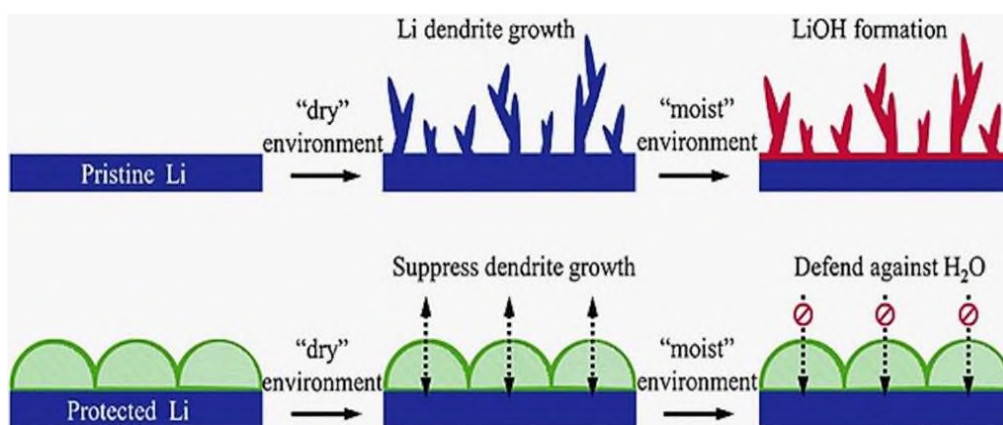
Figure 6.1 *Schematic representation of Li stripping / plating on original lithium electrode and sheltered lithium electrode [450].*

3. Given the stability issues associated with safety concerns, alternative materials of metallic lithium with a high stability, safety, as well as a high theoretical energy density are necessary.

The electrode material's future development also needs to be a great concern with the following features [450]:

1. Fast charging is a highly valued feature of portable electronics and EVs due to remarkably shortened charging time. Unfortunately, the structure devastation of electrode materials and performance decay rapidly occur under high current density, thus appropriate materials need to be designed [479-482].

2. Safety of material as changes in the crystal structure, chemical composition, and electrode morphology may activate side reactions and may release heat/gas. Thereby, internal failure mechanisms, safety issues, and triggering circumstances need additional investigation [484, 486-488, 492-496].

3. Temperature tolerance as external temperature difference caused by seasons and regions can touch 50 ∘C, which strongly affects the movement of metal ions and the

electrode material stability. High discharge rate at low temperatures along with maximum safety at high temperatures are requisite for electrode materials and need to be further worked out [483, 485, 489, 490, 498-500].

4. Scale-up fabrication with affordable cost is the point of attention concerning commercialization. Manufacture art, cost accounting, and process flexibility are very important as the process started practically [491, 497].

6.1.7 Failures of Aluminum-air batteries and future prospects

Besides the current progress of AABs, there is a need of

1. some noteworthy approaches to fabricate the economical (non-noble metal) metal catalysts and to explore the influence of physio-chemical properties such as valence state, structure, composition, structure, morphology, surface area, conductivity, and size, etc. on the inherent catalytic activity of the material [507].

2. Designing novel electrocatalysts equipped with advanced structures and a large number of active sites [510, 513].

3. Optimizing the synthetic conditions and strategies like temperature, precursor, reaction time, atmosphere, and reaction procedures to attain better activity and durability [517, 519].

4. Understanding of the link between the microstructure, electroactive active sites, and ORR response through theoretical calculations by using the DFT and other simulation techniques [505, 509, 514].

5. There is an utmost requirement for the development of facile and operational approaches for the synthesis of controlled morphologies and structures to encounter the requirements of ORR catalytic activity and durability [502, 511, 512, 515].

6. Mostly the preparations of catalysts are reported at the laboratory level. So, there is a need for simple and scalable methods for practical applications [516, 518].

7. Regarding the electrolytes, the non-aqueous systems avoid electrode corrosion and hydrogen evolution as compared to aqueous electrolytes. Especially the polymer electrolytes are the potential candidate for practical applications in AABs owing to their flexibility, thermal stability, superior electrochemical response, and lightweight nature. Thus, solid-state aluminum-air batteries with polymer electrolytes can be an important research area as they can address the issue of stability and electrolyte evaporation, and even can limit the dendrite's growth. But the comparatively low ionic conductivity of

these electrolytes under ambient conditions is the main challenge to overcome [501, 503, 504, 508].

8. The introduction of corrosion inhibitors into electrolytes can lessen the self-corrosion of Al anodes in turn enhancing the practical efficacy of AABs. The selection of effective corrosion retarders with appropriate concentration is a main investigation area for the future advancement in Al-air batteries [506].

9. Some advanced characterization methods e.g. synchrotron radiation particularly the in-situ techniques can be applied to disclose the various reaction mechanisms. Furthermore, computational studies must be used to investigate and predict the failure features and E0 value of new electrode materials [450].

6.1.8 Failures of Magnesium-air batteries and future prospects

The Mg-air batteries exhibit the second uppermost specific energy density and cell voltage value. However, this battery system is currently in evolving stages and its efficiency is not yet fully realized owing to failures regarding cathode, anodes, and electrolytes. These failures need to be properly addressed before the large-scale deployment of Mg-air batteries. The development of appropriate air cathodes in all types of batteries is particularly challenging because of the sluggish kinetics of OER and ORR. So, the development of electroactive catalysts to speed up the oxygen reactions kinetics and the designing of appropriate electrode material is the utmost requirement. Moreover, Mg-air batteries use alkaline electrolytes where air cathodes perform much better than acidic and neutral electrolytes. So, the issues related to electrodes including the creation of passivate films of $Mg(OH)_2$ on anodes and the carbonate precipitation at cathodes due to atmospheric CO_2 can develop interfacial films at anodes and block the pores of catalysts and in turn terminate the discharge processes as a result of high interfacial resistances [450].

Several failures restricting the commercialization of Mg-air batteries that need to be addressed are mentioned below:

1. Inadequate fundamental understanding of synergies and the reactions mechanisms of oxygen reactions, particularly the role of supports on the native N_2 coordination atmosphere of catalyst electroactive sites and elucidation of catalyst electroactive sites for O_2 stimulation and catalyst-support interactions [526, 528].

2. Inadequate strategies for designing the catalyst, selection of raw material, high yield synthesis, and optimization of catalyst performance [524, 531].

3. Un-optimized fabrication and designing of cell/electrode which is mismatched with novel catalysts in which catalytic reactions at the triple-phase boundary are complicated [530].

To overcome the above-mentioned failures, several research directions are favorable, including:

1. The combination of theoretical research with experimental characterization techniques. Inclusively a thoughtful approach to a better understanding of the connection between catalyst composition/structure and reaction mechanism [529].

2. The proper selection of raw materials to get optimized synthesis, design, and performance. Furthermore, the combination of atomic/molecular modeling and characterization through experimental techniques is essential for understanding the relationship of catalyst electronic structures and compositions with ORR catalytic mechanisms to further improve the oxygen catalytic reactions in MABs. For instance, the Density Functional Theory (DFT) calculations are used to study the ORR kinetic, containing the electrocatalytic reaction mechanism of each step, particularly the rate-determining steps, activated states, activation energies, and the comparison of the catalytic behavior of different catalysts. Moreover, in-situ spectroscopy (IRAS), X-ray absorption spectroscopy, Raman spectroscopy, and X-ray photoelectron spectroscopy, etc. can be used for a better understanding of structure and property relationships by determining the reaction intermediates, and local reaction environment [521, 523].

3. The detailed study of the electronic structure and geometric configuration structure of catalysts like the coordination environment of centrally electroactive metal sites including coordination numbers, adjacent atomic species, and distance between them is required as it can help to guide the design of anode and cathode material along with other battery components to optimize the conditions and parameters of electrode thickness, composition, and fabrication as well as the catalyst morphology [527].

4. The invention of innovative methods for the synthesis of carbon/ composite materials for advanced electrocatalysts. The composite material can also be optimized via a careful selection of materials and innovative designs. Additionally, the synergistic effects between different components further help to counteract the limitations of individual components and to generate more electroactive sites. Consequently, deep insight and development of morphology-controlled fabrication techniques to get high surface areas, appropriate pore sizes, and disseminations are required to augment the stability and

catalytic activity. Moreover, the controlled porous structure leads to facilitated reactant transport and charge transfer processes [520, 522].

5. Since the advanced structures with related air cathode constituents play an important role in battery efficiency. So, the innovative design and optimized air-cathode and catalyst based on multi-physics simulation and experimental techniques are needed to accomplish high-performance Mg-air batteries for practical applications [525, 532].

6.1.9 Failures of Iron-air batteries and future prospects

The iron-air batteries were introduced first of all in 1960. The complicated reactions at the Fe electrode, limited understanding of their kinetics, and the modest data availability from a process carried out under controlled conditions have strictly restricted the improvement in mathematical models of the Fe-air batteries, regardless of their potential utilization in prediction, performance rationalization, and optimization. To develop more proficient Fe-air batteries, the critical research areas include the following points [450]:

1. The Fe electrode supports the complex electrochemical reactions without any shape-change problems taking place due to the deposition/stripping process as in zinc-air batteries. The synthesis of robust nanostructured electrocatalysts having a stable response to the charge-discharge process without corrosion or HER problems remains a significant research endeavor [533].

2. Development of more proficient and medium-cost bifunctional oxygen electrodes [534].

3. Fabrication of negative electrodes with economical and easily scalable techniques needs more attention [534].

4. Utilization of improved engineering while designing the cell by using additive manufacturing technology [536].

5. Implementation of proven and accessible mathematical models to effectively demonstrate and simulate the battery performance by using aqueous, non-aqueous electrolytes with robust electrodes [537].

6. The progress of practical multi-physics simulations to rationalize the performance of the Fe-air cell and the presentation of its response by operational parameters should be deliberated in a critical research area.

6.1.10 Failures of Silicon-air batteries and future prospects

The most commonly used anode material is Si wafers but the high corrosion rate is the major drawback of this anode material. So, there is a need for Si anode material, capable of

sustaining its capacity even after a large number of charge-discharge cycles. Therefore, nano-structured Si, as well as doped silicon, is used to improve the response of the Si anode. Structural modifications like electrodeposition and chemical modification by the addition of a small number of additives prove to be an ideal solution to this issue. More efforts are required to properly figure out the charge-discharge mechanisms to get optimized discharge time. A more practical methodology is needed to address the problem of corrosion or passivation of Si-air batteries [538, 539].

The most important part of the metal-air battery is the air cathode but its sluggish kinetics for ORR hampers its performance. So, the electrocatalysts perform an important part in the activity of the cathode. Noble metals like Pt and Pt composites-based catalysts are extensively utilized as electrocatalysts for air electrodes. To make this process cost-effective, different types of electrocatalysts e.g. high spin state transition metal compounds and organic-inorganic hybrid can be effectively used as an efficient alternative. The research output is that the air cathode-specific capacity depends on multiple factors. Thus, a choice of suitable air electrodes with a very thin and exceedingly porous graphitic nano-sheet with optimized pore size is the best option. Further improvement of economical catalysts with upgraded activity and stability is requisite to improve the air cathode sluggish kinetics. The most appropriate option that needs to be further worked out is an inexpensive bi-functional electrocatalyst, active for both ORR and OER [540].

Novel and remarkably stable electrolyte technologies for the long-term operation of silicon-air batteries require further advancement. Currently, ionic liquids are the most potent option for Si-Air batteries. However, mechanically and thermally stable gel-polymer electrolyte seems to be viable electrolyte for advanced research. In addition, electrolyte solidification is important for safe operation and easy handling of Si-air batteries and structural stability under innumerable deformations. It is of utmost importance to study the silent features of the electrolyte-electrode interface of the battery [541].

Simulations/modeling are needed for an optimal design of Si-air batteries for the structural design of electrodes, as well as dispersion of electrocatalyst, electrolyte, current collector & depolarizers to provide a corrosion-resistant contact between the electrolyte and electrodes. Furthermore, the deep insight into Si dendritic growth is still in its infancy and needs to explore further [450].

6.1.11 Summary of MABs' failures and future prospects

All MABs have their specific merit and demerits, limitations, and potential applications. The nature of the electrolyte, electrode materials, separator, pH as well as temperature are different parameters affecting the efficiency of metal-air batteries while silent features reflecting proficiency of the metal-air batteries are power density, current density, life cycle, discharge capacity, and resistance. Nanostructured carbonaceous materials reformed by doping/metal-nitrogen complexes are auspicious, abundant, and economical electrocatalysts applicable to oxygen reactions [535]. However, the development of new strategies to study the synergistic interaction between carbon and dopant for improved stability and catalytic activity via Density Functional Theory (DFT) and other simulation techniques, extensive revision regarding the catalyst structure/design, the effect of atomic doping, internal connection between the electronic configuration of the catalyst and its performance towards oxygen reactions still required further attention. Among these carbon-based materials, the Carbon Nanotubes (CNTs) show certain limitations like the undefined toxicity of CNTs, deprived repeatability on different substrates, and higher cost as compared to other flexible electrocatalysts which need to work out.

Besides the considerable progress in this field, the growth of metal-air batteries is considerably hindered due to their mediocre rate capability, corrosion and dendrites formation during electrochemical reactions, sluggish kinetics of oxygen reactions at the cathode, and less improvement in the field of strategies of electrode material design, electrolyte modification, good selection of separator and limited understanding of the reaction mechanism. A reversible metal electrode (anode) with (a) multiple functional electroactive active sites (b) high recharge efficiency, and (c) long-term stability is the requirement of the efficient system and this area can be improved further by structure and composition modification through novel synthetic techniques and addition of the suitable amount of proper additives/chemical doping. The incorporation of effective corrosion retarders in appropriate concentration is also the main exploration area for future advancement. In addition, the hydrogen evolution makes the electrolyte thermodynamically unstable which needs to address further. The deposition of insoluble by-products on the electrode surfaces during the charge-discharge process must be taken into consideration as these by-products diminish the battery's performance owing to blockage of the electrode pores, and limited air diffusion. In the case of aqueous electrolytes, the problem of stability, leakage, and thermodynamic limitations need more investigation. Ionic Liquids and polymer electrolytes are comparatively better options than aqueous electrolytes but

this area needs further advancement. Flow MABs are a safe and reliable option with long operational life as the flow of anolyte/electrolyte minimizes the side reactions. Flow MABs can be effectively utilized for both stationary power plants and large-scale energy storage purposes but it deserves further work.

6.2 Diagnostics of MABs - *In Situ* Spectroelectrochemical Techniques

6.2.1 Raman Spectroscopy

6.2.1.1 *In Situ* Raman Spectroscopy for MABs

In situ Raman spectroscopy of MABs has established mechanistic detail about the fundamental reactions at the oxygen cathode interface. This includes the characterization of species present on the formation of reduced oxygen species (ROS) and electrolyte-electrode component degradation products.

An example of an *in situ* Raman cell is shown in **Figure 6.2**. The cell body was made from quartz glass with vacuum grade seals to allow removal, positioning, and cleaning of the electrodes.
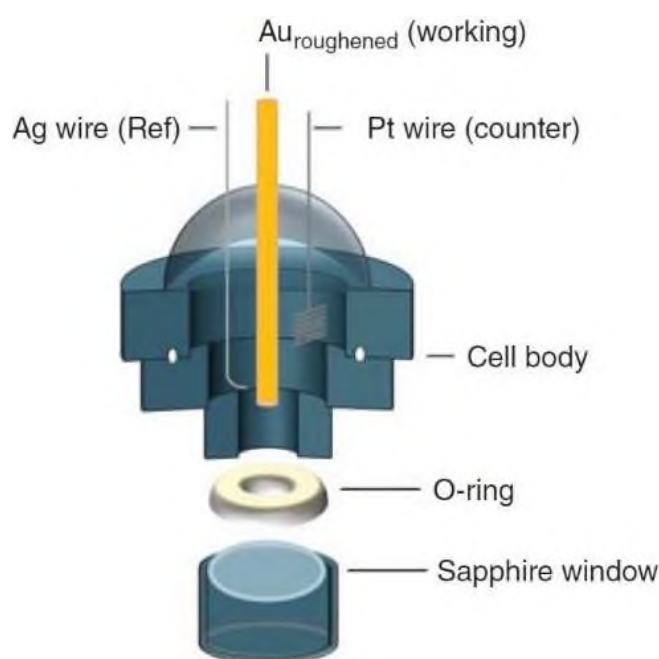
Figure 6.2 Schematic of an example in situ electrochemical Raman cell [542].

6.2.1.2 Background Theory

The Raman effect corresponds to the excitation of a molecule, to a real or virtual, excited electronic state and a subsequent emission to a different vibrational state in the electronic ground state [543]. This results in scattered lines either side of the incident frequency scattered light (Rayleigh scattering). These lines are known as *Stokes* (u=0-1) and *anti-Stokes* (u=1−0) lines (**Figure 6.3**).
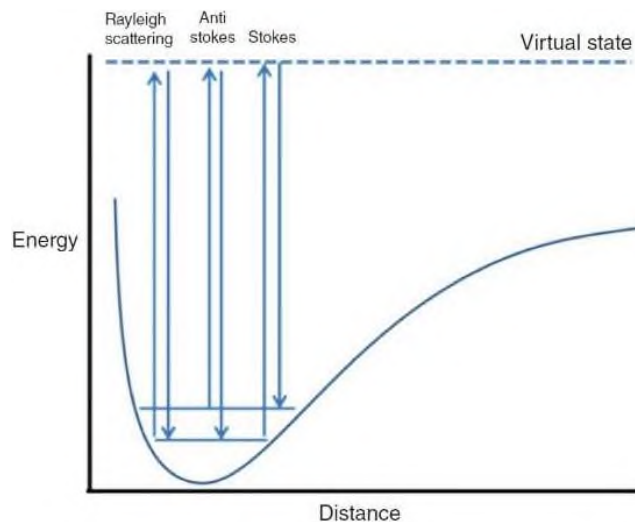
Figure 6.3 *Comparison of Raman scattering processes [542].*

Raman spectroscopy is based on scattering processes that are intrinsically weak when compared with optical processes like absorption and fluorescence [544]; therefore, it requires an amplification of the signal [544]. Approximately 1 in 10^7 photons is inelastically scattered, and the enhancement of Stokes and anti-Stokes scattering processes is required to provide sufficient signal from these excitations, and the vibrations they correspond to, in order to gain adequate sensitivity and to observe adsorbed species at electrode interfaces.

A method to achieve signal increase by up to 10^{14} times has been surface-enhanced Raman spectroscopy (SERS) [545]. 2017 was the 50th anniversary of the discovery of the surface enhancement phenomena [546]. Two independent groups after an initial finding of the SERS effect of pyridine on electrochemically roughened silver noted that the concentration of species at the interface did not account for the enhanced signal [546, 547]. The mechanisms used to explain the SERS effect were the electromagnetic [547] and charge transfer [546] enhancement of the Raman signal. There is still debate as to the mechanism of SERS, but it is generally accepted that contributions from both of these proposed mechanisms are apparent. The field of Raman signal enhancement is growing in terms of studies understanding the fundamental mechanism and in developing reproducible SERS-active substrates [548, 549].

Two subsets of techniques can be employed to enhance the Raman effect. The majority of nonaqueous *in situ* MABs work in this area has used nano-structuring of the surface, usually gold, to employ SERS. These methods include electrochemical roughening [550-559], Au metal deposition [560], and shell-isolated nanoparticle-enhanced Raman spectroscopy (SHINERS) [561]. This is to enhance the signals detected corresponding to electrochemically surface-active species such as oxygen (O_2), superoxide (O_2^-), and peroxide (O_2^{2-}) and their subsequent interactions with alkali metal cations (Li^+ and Na^+).

6.2.2 Infrared Spectroscopy

6.2.1.1 Background

Infrared (IR) spectroscopy is a vibrational spectroscopy technique that relies on the absorbance of the IR light by a molecule when a beam of IR light falls on it. The interaction of IR radiation is associated with molecular vibrations; only those molecules whose electric dipole moment changes during vibration can absorb IR light. The frequency of the absorbed IR radiation coincides with the vibrational energy levels of the molecule. The exact frequency at which a given vibration occurs is determined by the strengths of the bonds as well as the mass of the atoms involved. Knowing these absorption frequencies and their intensities would help to get *fingerprint information* about the structure and composition of the molecule. Traditionally dispersive IR spectrometers (which emerged in the 1940s) were used to obtain IR spectra that used a grating that was scanned through the wavelength range of interest. By contrast Fourier transform instruments simultaneously illuminate the sample with a broad spectral band of IR radiation. A moving interferometer modulates the IR light, and the resulting intensities as a function of the interferometer mirror position form an interferogram, which is transformed into the frequency domain spectrum through Fourier transformation. Fourier transform infrared (FTIR) spectrometers convey throughput advantage since the grating is dispensed of, and also with rapid scanning interferometers (or *step-scan* methods), the speed of spectral acquisition can be used for time-resolved studies. As such modern FTIR spectrometers have improved the acquisition of IR spectra so dramatically that FTIR spectrometers have, to a very large extent, replaced dispersive instruments.

6.2.2.2 IR Studies of Electrochemical Interfaces

Transmission-mode IR spectroscopy has been popular for conventional IR analyses, whereas IR characterization of electrode−electrolyte interfaces normally adopts reflectance methods. Over the past few decades, various designs utilizing internal, specular (external), or diffuse reflection of IR radiation at the metal-solution interface have been developed. A few examples are infrared reflection-absorption spectroscopy (IRRAS) employing specular reflectance, attenuated total internal reflection infrared spectroscopy (ATR-IR) utilizing total internal reflectance, and diffuse reflectance infrared spectroscopy (DRIFTS). There are three different acronyms used for IRRAS in the literature, viz. IRRAS, IRAS, and RAIRS, but IRRAS is more prevalent. The absorption of IR radiation by the medium through which an IR beam passes before and after the reflection can hamper the sensitivity to the interfacial region. External reflection spectroelectrochemistry methods (e.g. IRRAS) have to address the problem of

attenuation of IR signal by an overwhelming absorption by the electrolyte, while internal reflectance (ATR) techniques have to consider absorption of the radiation by the internal reflection element (IRE) that limits/determines the spectral range. The polarization modulation infrared reflection-absorption spectroscopy (PM-IRRAS) has proved successful for studying surface reactions on well-polished and reflective surfaces, and polarization modulated techniques also benefit from the surface selection rules.

The simplicity of ATR techniques and their applicability on nonreflective surfaces make them more appealing. In fact, ATR-IR is currently very popular for the *ex situ* characterization of battery electrodes. There are two possible optical geometries in the ATR mode, the Otto [562] configuration and Kretschmann [563] configuration; surface sensitivity of ATR techniques is also dependent on the configuration. The Kretschmann configuration is generally preferred for *in situ* studies; the Otto configuration is widely adopted for *ex situ* analyses where the electrode is analyzed after it is removed from the electrochemical cell.

In 1980 Hartstein et al. [564] found that very thin discontinuous films (∼10 nm thick) of gold or silver coated on an ATR prism with molecular layers resulted in signal enhancement. This approach has been named *surface-enhanced infrared absorption spectroscopy* (SEIRAS). Using a metal film deposited on a silicon ATR prism, Osawa et al. [565] demonstrated the scope of ATR-SEIRAS for *in situ* electrochemical studies [565-567]. A schematic representation of the external and internal reflection IR spectroscopy setups is shown in **Figure 6.4**.
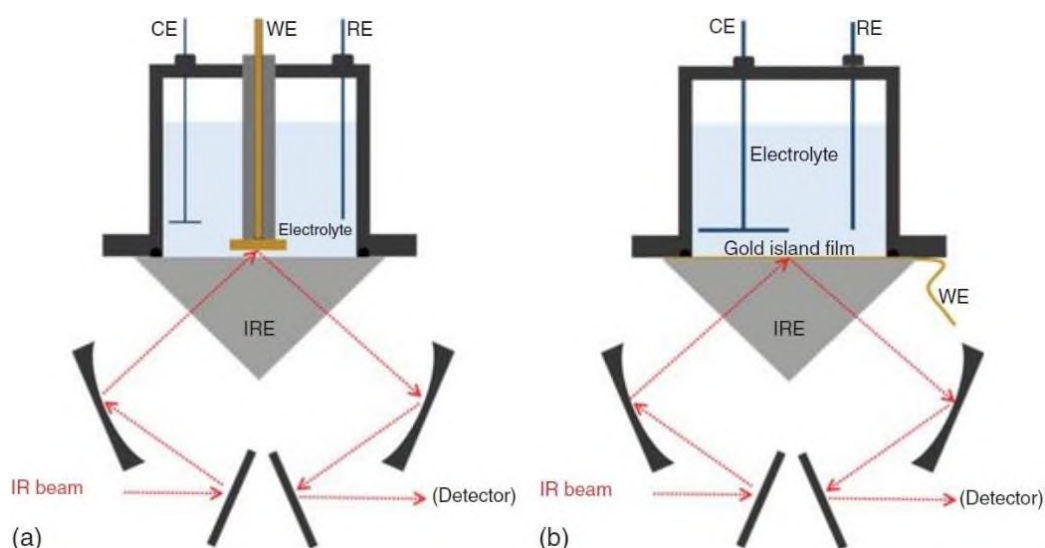
Figure 6.4 Schematic showing typical in situ setups used for IR reflection-absorption spectroscopy (a) as well as internal reflection SEIRAS spectroscopy (b) [542].

Each of the IR spectroscopy approaches listed above has its own associated advantages and limitations; external reflection ATR-IR techniques are being widely used for *ex situ* analyses of battery electrodes as they can be applied virtually to any electrode material.

IR spectroscopy is widely being used for *ex situ* analyses of the precipitates or decomposition products on metal-air battery electrodes. While *ex situ* analyses can be easily carried out on more practical MABs systems, *in situ* approaches are necessary to obtain information regarding the reaction pathways or intermediary species.

6.2.3 UV/Visible Spectroscopic Studies

UV/Vis spectroscopy is a characterization tool that is becoming increasingly utilized in MAB studies for the study of reactive intermediates formed during the discharge or charge process. The setup of a practical nonaqueous system in conjunction with standard spectrometers can provide challenges for researchers such as in the design of bespoke sealed cells capable of sufficient transmission of light or reflection of light within given space restrictions. UV/Vis spectroscopy allows the study of the UV range (190-400 nm), visible range (400-780 nm), and NIR (spectrometer dependent). From the absorption and luminescence spectra related to the electronic and vibrational transitions (generally molecular overtone and combination vibrations) of interest, this technique can be applied to battery electrolyte systems [568].

6.2.3.1 UV/Vis Spectroscopy

UV/Vis spectroscopy is the study of the excitation from the ground state to the electronically excited state. Original measurements on O_2 reduction in these systems utilized reflection modes, but the battery-related literature has typically utilized transmission modes only (**Figure 6.5**) [569].
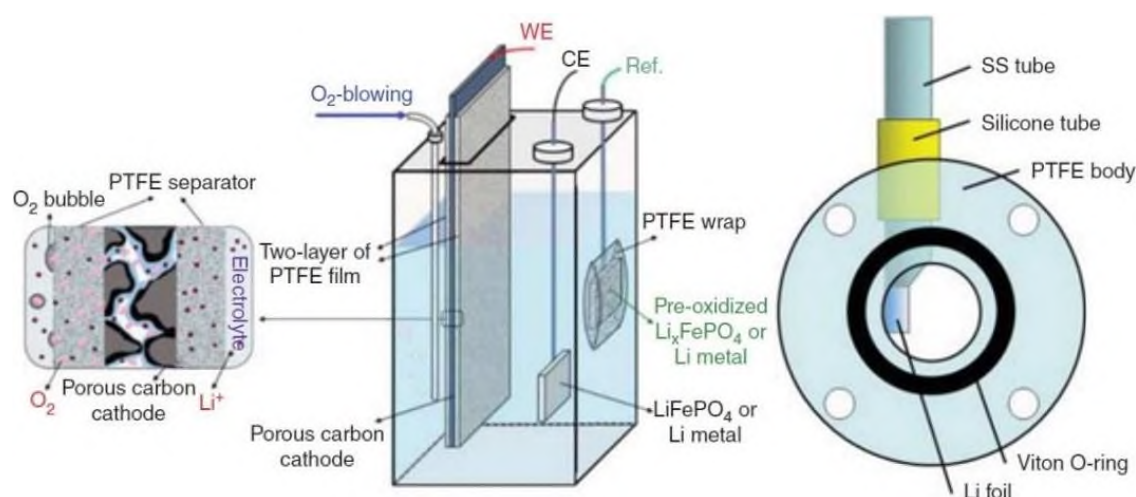
Figure 6.5 *Schematics of UV/Vis cells [542, 557, 570].*

A common problem with MABs is the passivation of the electrode surface, and precipitation of large crystalline discharge products can quite easily decrease the transparency of the electrode throughout the discharge process. Careful consideration in the appearance and

disappearance of signals when utilizing these measurements is critical to gaining accurate representations of the model processes being carried out in these cells.

6.2.4 Electron Spin Resonance

Electron spin resonance (ESR) or electron paramagnetic resonance (EPR), which can be considered as broadly comparable in principle with nuclear magnetic resonance (NMR), excites electron spin instead of the spin of magnetic nuclei. Although not as widely used in chemistry as NMR, it nevertheless holds an important place in the detection and study of unpaired electron spins, for instance, in organic free radicals, in paramagnetic inorganic metal complexes, or in solid-state materials, and it can also detect free electrons in metals. It is becoming an increasingly present technique across battery research including lithium-ion and MABs. In the latter case its ability to detect unpaired electrons enables analysis of radical species produced during battery charge or discharge such as superoxide and ROS and other side products arising from unwanted ancillary chemical or electrochemical processes.

ESR was discovered by Zavoisky in 1945 and since the late 1950s it has been used to study electrochemical processes [571]. **Figure 6.6** shows a cell used by Wandt et al. [573] for the study of MABs electrochemistry [572].
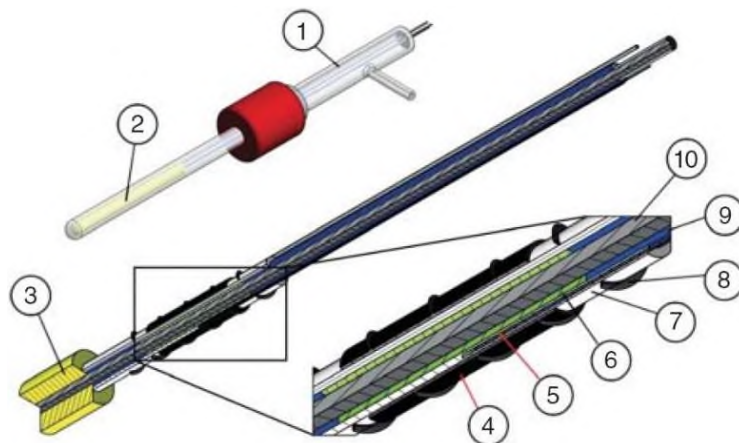
Figure 6.6 In operando EPR cell design for the detection of O_2 in an aprotic LAB. Top left: cell housing with (1) lid containing a connection for gas purging and three feedthrough wires for contacting of working, counter, and reference electrodes and (2) EPR tube containing the electrochemical cell. Center: tubular electrochemical cell with (3) poly(tetrafluoroethylene) (PTFE) spacer. Bottom right: cut-through electrochemical cell, (4) Vulcan working electrode coated on Celgard separator, (5) reference electrode, (6) LiFePO$_4$ counter electrode coated on Al wire (10), (7) glass fiber separator, (8) Al wire (0.1 mm diameter) as working electrode current collector, (9) PTFE tube, and (10) Al wire (2.0 mm diameter) as counter electrode current collector [542,572].

The components are those commonly found in MAB testing, but these are housed in a cell capable of being analyzed within an ESR spectrometer. The main difference in cell design in this case is the tubular shape required for these types of spectroscopies, similar to an NMR tube.

CHAPTER 7

Recent Advances in Recycling of Metal-Air Batteries

7.1 Introduction

Disposal of spent batteries represents an environmental problem because of heavy metals that can be dispersed in the environment; as a matter of fact, some types of batteries, like the alkaline and zinc–carbon ones, can be thrown away together with unsorted municipal wastes. Current community legislation is Council Directive 91/157/EEC (and subsequent amending acts of Directives 93/86/EEC and 98/101/EC) on batteries and accumulators containing certain dangerous substances. The Directive 2006/66/EC has been applied to all batteries and accumulators, whereas the ultimate disposal of portable, industrial and automotive batteries and accumulators by incineration or landfilling is strictly prohibited. Best Available Technique (BAT) defined in the IPPC Directive 2008/1/EC, which defines the best, i.e, the most effective in terms of environmental protection, available techniques, i.e, the techniques developed on a scale, which allows implementation in the relevant industrial sector under economically and technically viable conditions (EU Commission, 2009). Mandatory collection started in Austria in 1991 followed by many other Countries, which have arranged a financing system that enables to cover all the costs related to the recycling activities, such as collection, transportation to the plant, process net costs, information campaigns and so on. The European Battery Recycling Association (EBRA) members recycles (a) primary (non-rechargeable) batteries (Alkaline, Zinc-Carbon, Li primary and some types of button cells) and (b) secondary batteries (NiCd, Lead-acid, Nickel Metal Hydride, Li-ion and some types of button cells of Zinc-air batteries (the only type of metal-air batteries).

Zinc-air batteries are promising energy storage devices with high energy density, safety, and economic feasibility [575]. Most of the volume in the zinc-air battery is occupied by the anode, and hence, it provides up to five times more capacity and three times the energy of common alkaline batteries in a compact package [576-578]. Primary zinc-air batteries are implemented for medical (hearing aids, cardiac telemetry monitors), military, telecommunication (pagers, wireless messaging), and railway signaling/navigation applications [576]. Due to their low power output capability, zinc-air batteries are commercialized for hearing aid applications (< 10 mW, ~ 1300-1400 Wh/L) [579].

The zinc-air batteries are promising alternatives to lithium-ion batteries as zinc is highly stable, inexpensive (almost two orders of magnitude lower than lithium-ion) and has a higher energy density (~ 1353 Wh/kg) [580, 581].

Zinc is the major constituent of zinc-air batteries, which is primarily mined from underground (80 %) and open-pit mines (8 %) [582]. The most abundant mineral source is sphalerite (ZnS), while non-sulfide zinc deposits cover 10 % of the world's metallic zinc production [583, 584]. The world's zinc reserves (250 million tons) are majorly concentrated in Australia (27 %), China (18 %), Russia, Mexico (9 % each), Peru (8 %), Kazakhstan (5 %), USA (4 %), and India (3 %) [585].

7.2 Need for recycling

According to the United States Geological Survey (USGS), zinc is proposed as a critical element due to (a) site-specific concentration of primary zinc sources with 50 % consumption realized by few countries, (b) mineral competency, and (c) supply risk (0.48, above the threshold of 0.4) [586]. However, zinc is not listed as a critical element per the European Union's (EU) list of critical metals [587]. The declining ore quality [585], limited reserve life (14 ~ 17 years) [588, 589], and supply risk associated with zinc calls for the inevitable recycling of secondary sources.

A comparison of various zinc anode-based primary batteries is shown in **Table 7.1**.

Table 7.1 Comparison of cell chemistries and performances of various zinc-based batteries [574, 579].

Battery type	Theoretical specific energy (kWh/kg)	Volumetric energy density (Wh/l)	Capacity (g(Ah)$^{-1}$)	Theoretical operating voltage (V)	Self-discharge rate (%/day)	Lifespan Sealed (years)
Zinc alkaline	0.35	450	4.46	1.5	0.009	5.1
	$Zn + 2MnO_2 + 2H_2O \rightarrow Zn(OH)_2 + 2MnO(OH)$					
Zinc-carbon	0.35	156	4.46	1.5		2-3
	$Zn + 2MnO_2 + 2NH_4Cl \rightarrow ZnCl_2 + 2NH_3 + Mn_2O_3 + H_2O$					
Zinc- air	1.3	1300-1400	1.22	1.4	0.007	3
	$Zn + \frac{1}{2} O_2 \rightarrow ZnO$					

It was calculated that 1 ton of zinc-air batteries contains zinc concentration equivalent to 8 tons of primary ore (% Zn ~ 5.85 %), while zinc-carbon and alkaline batteries contain only ~ 2 tons, ~ 3 tons, respectively *[Primary ore equivalents = % Zn in 1 ton of battery ÷ % Zn in primary ore]*. Therefore, it is worth examining zinc-air batteries as a secondary zinc source compared to other zinc batteries.

As per the EU directives, landfilling, incineration, or improper disposal of spent batteries is illegal; therefore, they must undergo recycling. Every year 160,000 tons of consumer batteries enter the EU, ending in municipal solid; however, without specific mention of zinc-air [590, 591]. ZABs are generally not considered for recycling because of the non-existence of recycling rules/targets, non-hazardous stature, abandonment, and lack of technical know-how.

A circular economy is a sustainable approach to recycling, wherein the product should be extended for maximum use, and at the end of life, it becomes a potential secondary source. A circular economy aims at reducing the economic disparity due to limited and depleting natural resources. A circular recycling model suggested for the ZABs (**Figure 7.1**) is aimed at resource conservation and mitigation of primary production. The circular economy model interweaves the processing and consumption stages, where the recovered zinc is recycled and consumed in the primary processing of new batteries [574].
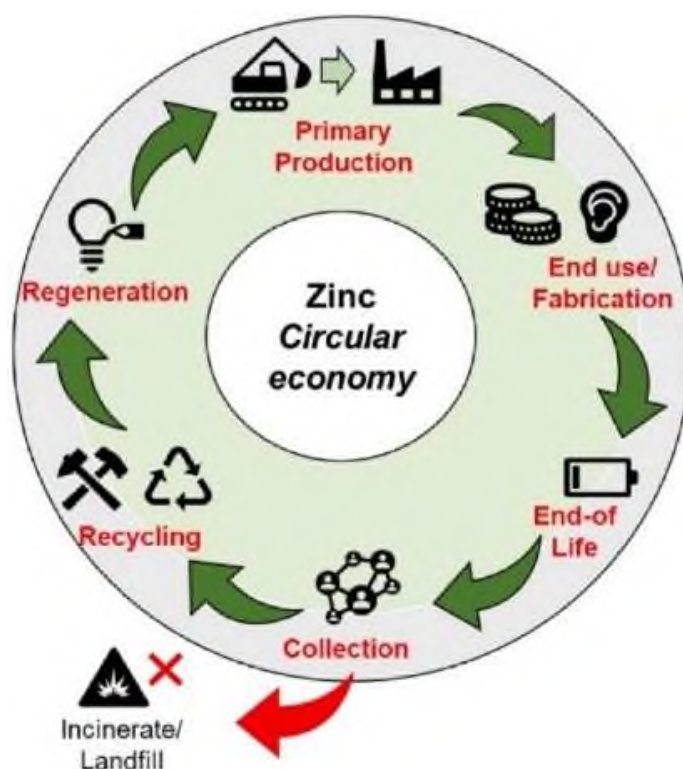
Figure 7.1 Circular recycling model for ZABs [574].

Herein, zinc-air batteries used in hearing aids are evaluated and considered because of their rich zinc source (~ 88 %), higher volumetric zinc (due to minimal cathode area), easy availability, and growing user demand. For recycling considerations, evaluating the economic value, mineralogy, and complexity of contained valuables in discarded zinc-air batteries is important.

7.3 Technologies for extracting metals from battery active materials

7.3.1 Pyrometallurgy

Pyrometallurgy is a branch of metallurgy also known as thermal metallurgy where heat is used for extraction and purification of metals followed by condensation. In this technology, the major operations are roasting, smelting, and refining. The roasting is performed to transform sulfide ores into oxides as SO_2 gas in the presence of air without fusion, whereas smelting is the process usually employed in the blast furnaces to reduce iron from ores. This technology is used to recover metals from waste battery by introducing higher temperature into it. Due to higher temperature, several reactions would occur in the battery recycling, viz., decomposition of compounds and reduction and evaporation of metals [574].

7.3.2 Hydrometallurgy

The hydrometallurgy is a part of extractive metallurgy where aqueous solutions are used to recover metals from ores and waste materials. This technology includes pre-treatment followed by leaching, solvent extraction, ion exchange, and electrowinning process for selective recovery of metals [574].

After the collection of spent batteries and before their chemical treatment, some mechanical/physical pre-treatments are required. These may include shredding or cut-crashing, thermal procedures, separation of ferrous metal from inert compounds (paper, plastic, ferrous and non-ferrous scraps) by the use of magnets as well as powder sieving. Subsequently, hydrometallurgical processes may be applied, usually in small scale plants, which involves leaching, separation and metal recovery steps. Due to the complex nature and numerous parameters that might affect the efficiency of leaching and the subsequent separation step(s), these processes still remain an important research avenue [574].

7.3.3 Direct recovery

Instead of hydrometallurgical degradative recovery of metals in spent batteries to prepare electrode materials, recent efforts have focused on the direct utilization of recycled active materials to prepare electrode materials without losing the energy embedded in the battery particles. However, the performance of the materials is low [574].

7.4 Characterization of zinc-air batteries

Discarded zinc-air batteries of various sizes (1 unit ~ 0.3-1.8 g) used in hearing aids (**Figure 7.2**) were procured from hearing aid users.
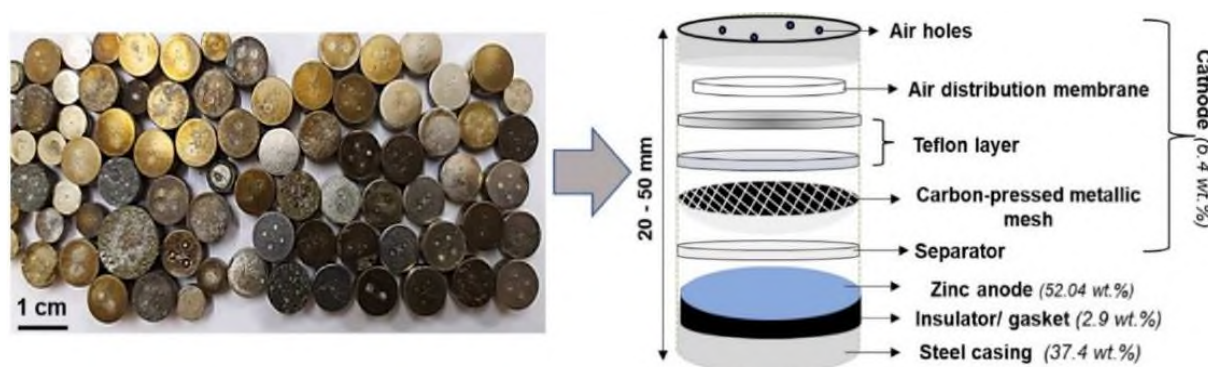
Figure 7.2 Photograph and internal structure of the discarded zinc-air battery used in hearing aids [574].

Batteries were manually dismantled into components: anode, cathode, and separator. The anode powder was scrapped off from the anode case and dried overnight. As observed in **Figure 7.2**, the cathode electrode is porous, providing air diffusion passage into the electrode. Further, the cathode consisted of a gas diffusion membrane, a catalyst layer, and a current collector, and the porous separator physically separated the anode and cathode electrodes [574].

7.5 Methods and observations

The separated anode was subjected to various characterization studies to delineate the metal values and association. X-ray diffraction (XRD, Rigaku) of anode powder was carried out at 2θ range of 20-90∘ with a scanning rate of 3∘/min to determine the underlying phases. The thermal response of the anode was studied using thermogravimetric analysis (TGA) in the temperature range of 25-1000 ∘C under air and argon atmosphere at 10 ∘C/min. Morphology and elemental analysis of the anode and catalyst layer were carried out using Scanning Electron Microscopy equipped with Energy Dispersive X-ray Spectroscopy (SEM-EDS) (FE-SEM, Zeiss EVO18). X-ray fluorescence technique was used to determine the elemental composition of the anode powder [574].

The batteries were left to discharge in the open air, and it was observed that they are prone to the formation of white powder on the outside surface, which tends to clog the air pores. EDS analysis revealed that the powder consists of C-12.0 %, O-48.2 %, K-34.6 %, and Ni-8.2 %, which is indicative of electrolyte flooding (K), carbonate precipitation (C and O), and corrosion of outer nickel casing which was primarily used for good electrical contact. The representative XRD analysis of anode powders in **Figure 7.3 (a)** reveals a variable degree of zinc oxidation on usage. It is observed that some discarded batteries showed both Zn (~ 41 %) and ZnO (~ 59 %) phases, indicating the

114

tendency to form passivating products. The XRF analysis of the representative sample revealed that the anode comprises Zn ~ 88.1 %, K ~ 10.3 %, and additives like Al (0.48 %) and In (0.36 %), which are used as passivating agents and surface modifiers, respectively [592, 593]. It was also observed that the anode consisted of zinc powder gelled with an alkaline electrode (KOH) [**Figure 7.3 (b)**], while in a discharged/used condition, either characteristic crystallites of zinc oxide [**Figure 7.3 (c)**] or flaky zinc particles [**Figure 7.3 (d)**] are observed.
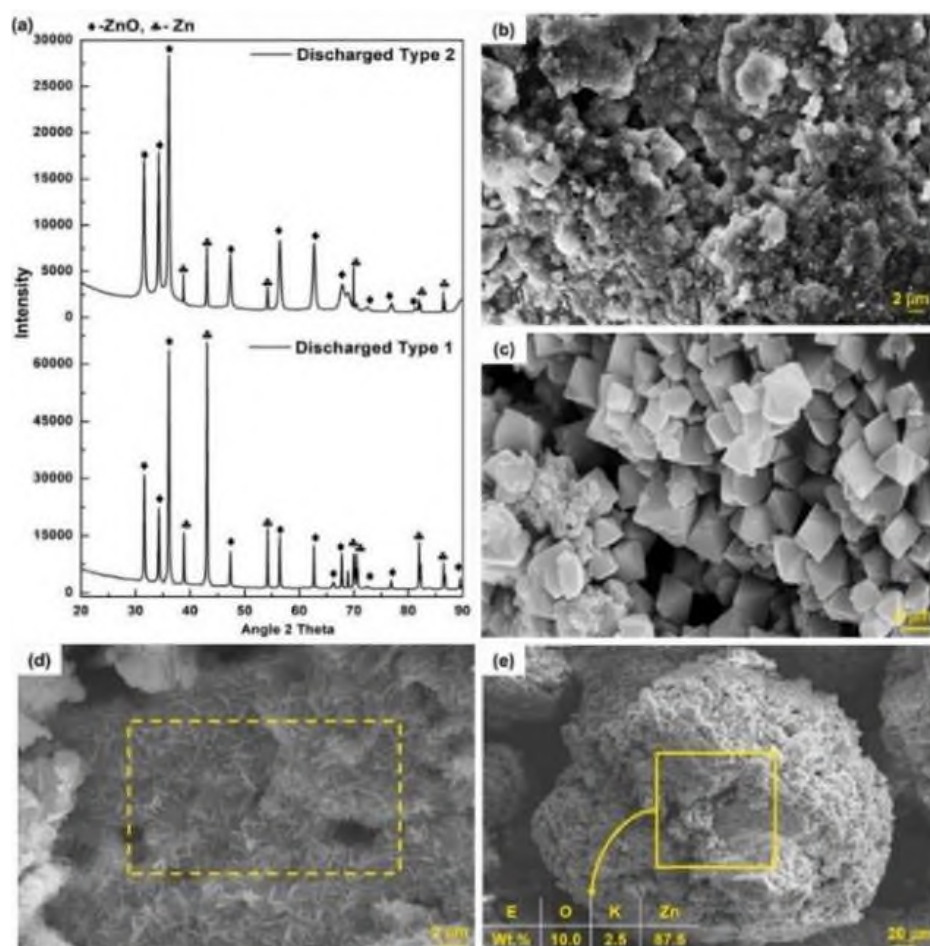
Figure 7.3 Variation of zinc anodes as observed by (a) XRD and (b-e) SEM/EDS analysis. Morphology of (b) unused and (c)-(e) end-of-life zinc anode [574].

These dendritic particles possibly indicate an incomplete chemical reaction in the cell caused by ZnO passivation [592]. **Figure 7.3 (e)** represents EDS analysis of the zinc anode particles indicating Zn, O, and K values. The catalyst layer and current collector consist of a carbon (38.9 %) layer pressed on a Ni (73.9 %) mesh [**Figure 7.4 (a)**]. Furthermore, Mn (oxide) is embedded in the C layer [594].

Thermogravimetric Analysis (TGA) [**Figure 7.4 (b)**] reveals a slight decrease in weight above 300 °C under both argon and air atmospheres. Above 650 °C, an increase in weight (~ 8.2 %) in the air atmosphere represents the oxidation of residual zinc. In an argon atmosphere, weight loss of ~ 35.1 % was observed above 650 °C due to zinc vaporization [595].
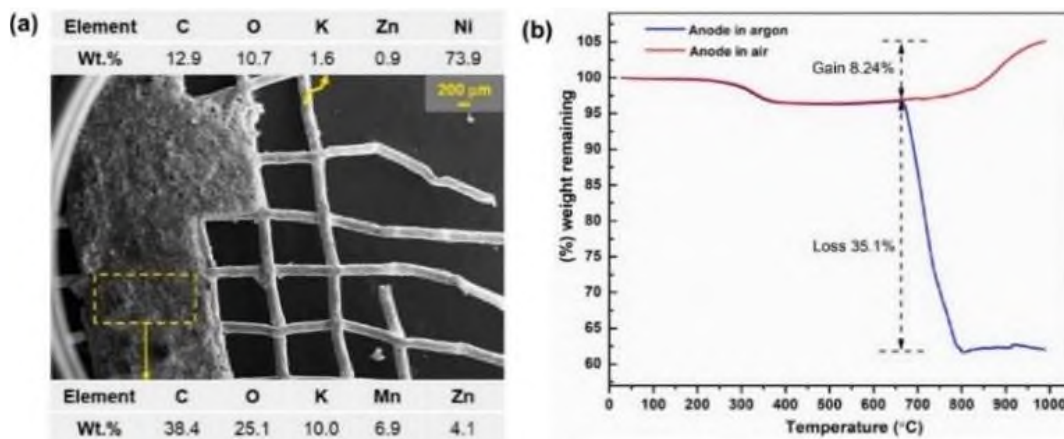
Figure 7.4 (a) Carbon pressed catalyst layer on a current collector, (b) Thermogravimetric analysis [574].

The activation energy (Ea) is determined using TG data by the Coats-Redfern (C-R) method, which can provide valuable guidelines for recycling the zinc anode during pyrometallurgical processes.

7.6 Recycling of ZABs: Outlook and recommendations

The measures for prolonging the life of batteries in favor of a circular economy involves the storage of batteries in original packaging before use, covering terminals, and embedding them in dry sand [596]. It is essential to study zinc flow analysis concerning zinc applications in batteries, their collection, separation, and recycling stages. The recommendations are broadly shown in **Figure 7.5**.

Recycling ZABs is recommended due to the risk of harmful disposal (children swallowing due to small cell size), presence of metal values, possible waste generation, and outsourcing of batteries from developed countries. Due to their smaller size, and heterogeneity in the batteries (size and type), the ZABs are unlikely to enter the recycling chain (formal/informal) unless a systematic collection system is enforced. As per EU battery regulations, higher collection targets of ~ 70 % by 2030 are enforced to cater to improper disposal of portable batteries [597].

In the EU, the battery waste management rules advocate the Extended Producer Responsibility (EPR) principle, wherein the producers are responsible for the product's overall lifecycle, from production through end-of-life. The responsibilities of the producers include (a) designing safe and durable products, (b) collection, (c) recycling of end-of-life products, and (d) re-using the recovered material in newer batteries as per the set targets [591]. EPR involves channelizing the e-waste to authorized dismantlers or recyclers through a take-back system or by the setting of a collection network. As a result, the financial burden of product disposal lies on the producer, which compels for eco-friendly designs, saving of natural resources, efficient

collection, and reduction of environmental impacts of the products [598]. EPR is an effective framework that enables the transition from a linear to a circular recycling model.
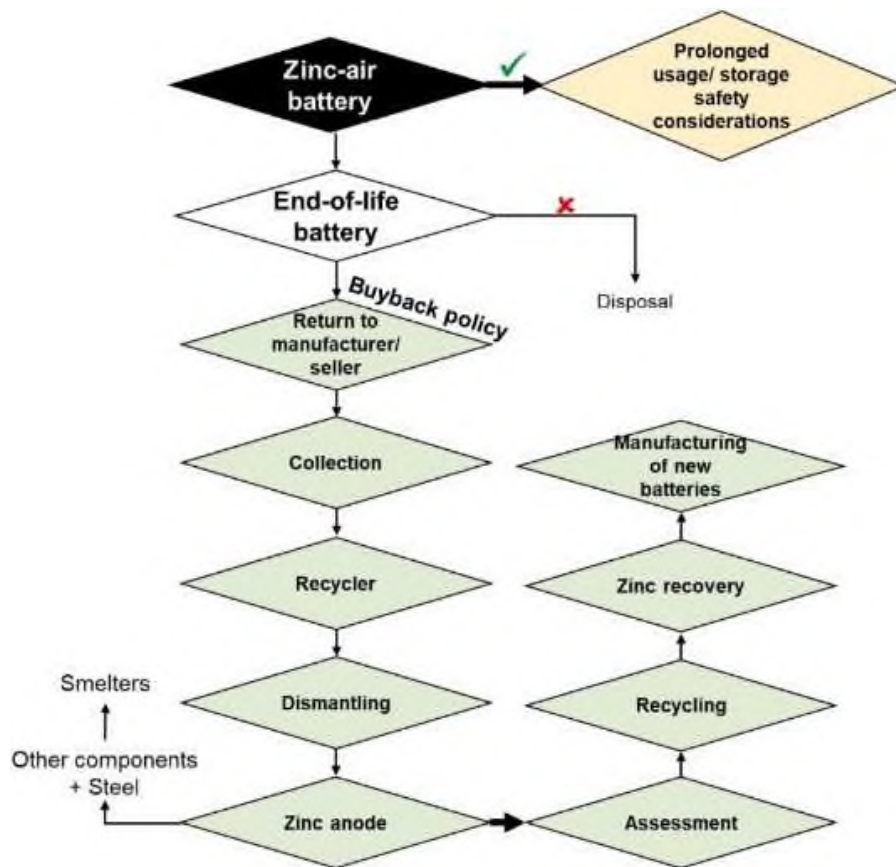
Figure 7.5 *Guidelines / recommendations for the recycling of end-of-life ZABs [574].*

Under EU regulations, labeling batteries or bearing a QR code that covers the details of the kind and type of battery may facilitate the identification and sorting of batteries for efficient recycling. Further, accurately identifying the type of batteries using deep learning (X-ray imaging) and their sorting before dismantling may ease the downstream processing routes [599]. The extended producer responsibility targets are specific to the kind of battery that needs to be streamlined for zinc-based batteries, particularly zinc-air batteries. It is recommended to make a policy of issuing new batteries at a lower price in exchange for discarded batteries to consumers or buyback to prevent disposal and maintain the recycling chain. The collected batteries can be sent to formal recyclers for value recovery [600]. However, the imbalance between resource recovery and collection cost (prevalent in battery recycling) needs detailed investigation. In general, the responsibility for collecting and recycling household batteries is not taken due to negative economic incentives [601]. Moreover, formal recycling is hampered by a lack of awareness, limited collection centers, and the non-implementation of rules and regulations.

The Zn/ZnO obtained from batteries can be used as feedstock in the zinc production process for metallic zinc. The recovered anode material can be re-processed for various

applications (such as ZnO) in electronics, optics, sensors, and UV detectors [602]. Like the concept of regeneration of zinc anodes from refuelable zinc-air batteries, ZnO product can be dissolved in a KOH solution to form zincate solution [$ZnO + 2KOH + H_2O \rightleftarrows K_2Zn(OH)_4$] followed by electrowinning to recover Zn. The recovered zinc can be re-processed for zinc anodes, provided good electrochemical characteristics are attained.

7.7 Zinc recycling: Various secondary sources and ZABs

The possible pathways for recycling ZABs could be identified from the available literature on various zinc sources, especially where zinc is present as ZnO. The identified zinc recycling sources are electric arc furnace (EAF) dust, primary production waste, and zinc-based e-waste (zinc-alkaline, zinc-carbon, and silver oxide batteries). A summarized literature on the recycling of zinc from various secondary sources is shown in **Table 7.2**.

Table 7.2 *Summarized literature on the recycling of zinc from various secondary sources [574, 603, 606, 607, 609-611, 626].*

Process and salient features		Product form; recovery (%)
EAF dust ($ZnFe_2O_4$, ZnO, ZnS, Zn_2SiO_4); (%) Zn: 15-34, (%) Fe: 18-38		
Thermal treatment (CaO, 900-1100 $^{\circ}$C, 3-6 h), magnetic separation (5 T) (ZnO non-magnetic). Unwanted residue generation.		ZnO; >95
Leaching	Two-stage (2 M HCl, 20 $^{\circ}$C, 30 min), refining (activated C/ metallic Zn), electrolysis (cationic exchange membrane, 300-2000 A/m^2). Acidic electrolysis is costly	Zn metal; >90
	($FeCl_3 \cdot 6H_2O$, 150 $^{\circ}$C, 8 h), Unwanted addition of ferric salts.	Zn (II); 100
	Thermal treatment (CaO, 1100 $^{\circ}$C, 5 h), alkaline (NaOH), or chloride (NH_4Cl) leaching (2 M, 70 $^{\circ}$C, 2 h). Generation of unwanted residue, high cost of alkaline reagents.	Zn (II); >95
	10 % aqua regia, 1.2 M HCl, 0.94 M citric acid, 1.5 M HNO_3, 1 M H_2SO_4, 25-80 $^{\circ}$C, 168 h. Long reaction time, high acid consumption with the possibility of co-dissolution.	Zn (II); >75
	Roasting (dust/NaOH-1.94, 450 $^{\circ}$C, 1 h), 0.94 M citric acid, 40 $^{\circ}$C, 120 min. High cost of alkaline reagents.	Zn (II); 100
	I- atmospheric (6 M NaOH, 70 $^{\circ}$C, 2 h), II- hydrothermal reduction (6 M NaOH, 260 $^{\circ}$C, 10 g/L starch). Unwanted addition of sodium salts.	Zn (II); >69
	Heat treatment (SO_2, 600 $^{\circ}$C, 30 min), Water (80 $^{\circ}$C, 20 min)	Zn (II); >93
Primary production		
Leaching	**(i) Jarosite** ($ZnSO_4$, $ZnFe_2O_4$); (%) Zn- 6; Fe-22 1.5 M H_2SO_4, 80 $^{\circ}$C, 7 h, reduction of Fe(III) to Fe(II) (50 $^{\circ}$C, 4 h), electrodeposition-500 A/m2	Fe-Zn alloy; 60
	(ii) Geothite sludge ($ZnFe_2O_4$, $ZnSiO_4$); **(iii) Zinc residue** (ZnS, $ZnSO_4$); (%) Zn-3-6, Fe-4-24 MW assisted (0.1-1 M HCl, 280-300 g/L NaCl, 200 $^{\circ}$C, 30-60 min)	Zn (II); 70-90
	(iii) Zinc ash (ZnO, Zn, $Zn_5(OH)_8Cl_2 \cdot H_2O$); (%) Zn-55-61, Cl-14-17 2 M HCl/ 20 wt% H_2SO_4, 20 $^{\circ}$C, 30 min- 3 h), precipitation of Fe (pH-4.5, CaO), electrowinning (1-5 A/dm^2)	Zn (II) or Zn metal; Zn-95-100
	(iv) Zn plating mud (ppm) Zn-440, Mn- 8.5, Cd- 1.7, Fe-240 0.01 M HCl + few drops of HNO_3, 60 $^{\circ}$C, SX (0.002 M Cyphos 104, 2 stages, A/O-1:1), stripping (1 M HNO_3)	Zn (II); 93
	(v) Zn oxide dust ZnO, ZnS (%) Zn- 46, Pb-8, Fe-8 choline chloride -urea-ethylene-glycol, (2:4:1, 80 $^{\circ}$C, 48 h), ligand (nitrilotriacetic acid, 0.05 to 0.11 mol/L), electrodeposition (2 V, 80 $^{\circ}$C)	Zn metal; 85-87
	MSWI- Fly ash (%) Zn- 2.5 (HCl, H_2SO_4, 60 $^{\circ}$C, 10 min), precipitation (NaOH, 60 min)	$Zn(OH)_2$; 70
	Zinc rich paint Zn, ZnO; (%) Zn- 46, Ca-8.4 NaOH- 250 g/L, airflow rate-0.6 L/min, 1.5 h, electrowinning 50 mg/L of gelatin, 200 A/m^2.	Zn; 98

118

The purpose is to understand possible recycling pathways and establish the importance of ZAB recycling given its uncomplicated structure, higher zinc concentration, and comparatively pristine zinc source.

7.7.1 Electric arc furnace (EAF) dust

The Waelz process (based on the carbothermal reduction) is employed to recycle the hazardous EAF dust ($ZnFe_2O_4$ and ZnO). ZABs consist of zinc values above the threshold limit of the Waelz process (> 18 %); however, it incurs the challenge of higher energy and carbon requirements, environmental regulations, and uneconomical processing [603, 604]. Gibbs's free energy plot using *HSC Chemistry, 10.1*, shown in **Figure 7.6 (a)**, reveals that above 1100 ∘C (Waelz process), higher energy is required for producing zinc from ZnO (-6.59 cal/mol) [**Figure 7.6 (a)**].
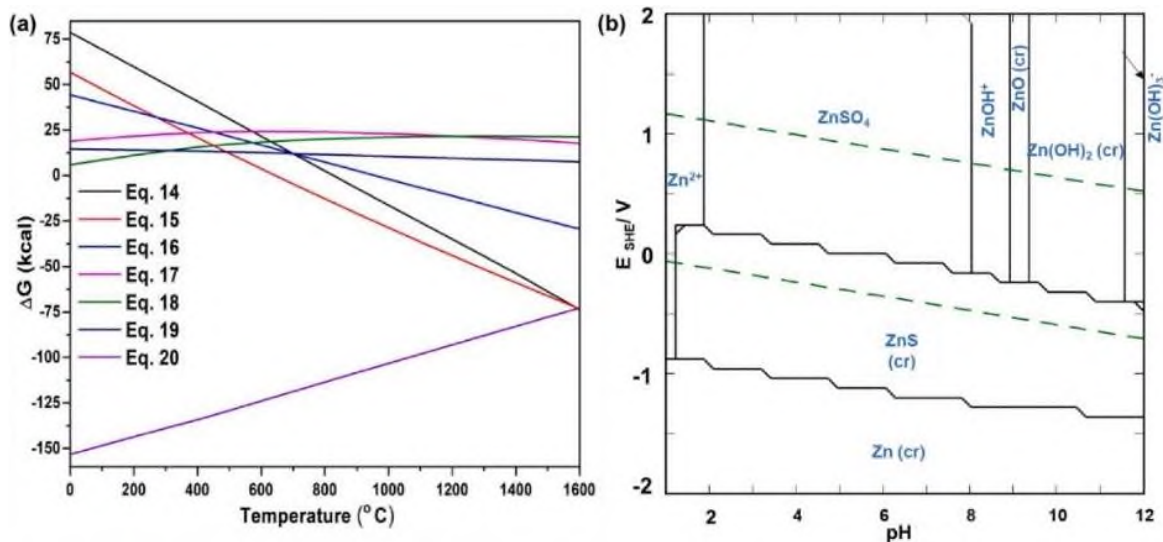
***Figure 7.6** (a) Free energy plot of various zinc phases observed in different secondary sources, (b) Pourbaix diagram for zinc leaching in sulfate media [574].*

Hydrometallurgy for recycling zinc is advantageous with comparatively lower energy requirements, environment friendliness, easy scalability, predictability, controllability, and high selectivity [605]. Also, ZnO can be dissolved in solution either by acidic (pH < 7) [$ZnO(s) + 2H^+ (aq) \rightleftarrows Zn^{2+} (aq) + H_2O$] or alkaline conditions [$ZnO(s) + H_2O \rightleftarrows ZnO_2^{2-} (aq) + 2H^+$]. In contrast to zinc-air batteries, most zinc in EAF dust exists in an un-leachable form ($ZnFe_2O_4$). Therefore, pre-treatments such as alkali treatment (CaO, NaOH) are necessary to convert it into leachable compounds making the overall process costly and complicated. ZABs are a preferable zinc source due to their higher zinc concentration, easily recoverable zinc (ZnO) form, and absence of impurities such as Fe, Pb, and halogens.

7.7.2 Zinc production waste

Primary zinc production waste is also explored for zinc extraction via leaching (direct and microwave-assisted) due to comparatively lower zinc content (3-6 %) [606-608]. However, the recovery suffers from drawbacks due to low zinc content (less than primary ore concentration) and complicated and multi-elemental chemical composition ($ZnFe_2O_4$, Fe_2SiO_4, Fe_3O_4 phase). The hydrometallurgical route for zinc recycling from zinc ash (Zn = 55-61 %) or zinc oxide dust (Zn = 46-80 %) involves leaching (HCl, H_2SO_4, choline chloride - urea - ethylene-glycol) followed by electrowinning, and it could be extended to zinc-air batteries due to the similar ZnO phase (~ 20 %) [609-611]. However, the cost of collection, process economics, solution contamination (Fe, Mn, Cl ions), the surface morphology of deposited zinc, and product yield need to be ascertained.

Dismantling and separation/scrapping off anode are the only process steps for zinc-air batteries due to the non-involvement of complex components. It is observed that a dominantly hydrometallurgical route is adopted for the recovery of zinc values from zinc batteries [612-616]. Sulfuric acid leaching is preferred due to better reaction kinetics with reducing agents (glucose, H_2O_2, others) mainly employed for leaching complex manganese phases. Purifying the leachate containing major elements such as Zn and Mn from multiple impurities (Fe, K, Ni, Cu, Co, Pb) is challenging (due to flux usage during remelting co-precipitation, interference in the electrowinning step). In the case of zinc-air batteries, as per the Eh-pH diagram in **Figure 7.6 (b)**, ZnO is easily converted to soluble zinc sulfate, and due to minimal impurities, reducing agent consumption and multiple purification steps are avoided. For the production of highly pure Zn/ZnO (95-99 %; 3-11 µm) from alkaline batteries, energy-intensive carbothermal reduction (1150-1200 ∘C, 1-2 h) process was adopted [617, 618] while it is available in pristine form in zinc-air anodes. However, the yield and quality of Zn/ZnO significantly impacts raw material, labor, and utility costs, which needs to be considered in detail.

The imperial smelting process (ISP) (Duisburg, Germany) recycles zinc-carbon and zinc-air batteries alongside zinc production [619]; however, complete details are not available in the public domain. On an industrial scale, hydro-based recycling (MMM Sedema, Batenus, Revabat, Recupyl) can recycle ZABs via mechanical process, leaching ($H_2SO_4 + H_2O_2$) and refining [620]. In the pyro process, sequential pyrolysis, reduction, and incineration are possible options (Recytec, Sumitomo, Batrec, Citron), wherein the zinc is recovered in vapour form and cast into ingots [621]. Recycling zinc-air with other batteries may dilute/compromise the purity of available zinc;

however, this route seems preferable due to the lack of specific recycling studies and robust collection systems.

The thermodynamic analysis in **Figure 7.6 (a)** reveals that reducing ZnO using carbon is unfavorable below 650 °C. However, as the Gibbs free energy decreases (negative) above 650 °C, ZnO can be reduced by C at the expense of CO/CO_2 formation (endothermic process). Using CO as a reductant for low-temperature reductions makes the reaction more favored. However, it is important to understand the kinetics of the reaction and the effect of mixture quality (Zn/ZnO) on the recovery economics in bulk discarded ZABs. In the case of mixed zinc alkaline and zinc-carbon batteries, pyrometallurgical process routes involving pyrolysis ($5\%H_{2(g)}$–$N_{2(g)}$ mixture, 950 °C) and oxidative roasting (700-1150 °C) are adopted to recover either zinc metal (due to vaporization and condensation) or ZnO respectively [622-623]. The energy required to produce per mole of Zn from ZnO and $ZnMn_2O_4$ using pyrolysis (H_2) [**Figure 7.6 (a)**] are almost similar; however, from alkaline batteries, the obtained ZnO contained high Cl and F impurities; which poses a serious challenge in electrowinning for zinc metal production. In contrast, the zinc-air battery is free from such impurities; however, feasibility and process economics needs further exploration. Hydrogen reduction depends on factors such as hydrogen partial pressure, the surface area of ZnO, and the presence of a third gas, such as N_2/zinc vapors [624].

7.7.3 Recycling zinc from spent zinc-based batteries

The most suitable battery recycling processes and selected representative companies in the EU for alkaline battery recycling are mostly based on pyrometallurgical treatment or possess a stage with thermal pre-treatment. These pyrometallurgical techniques consist mainly on the selective volatilization of metals at elevated temperature followed by condensation [792]. These methods are usually seen as less expensive routes, capable of high metal recovery with a rapid reaction rate without the requirement of complex pre-treatment process, as they permit the separation of materials in the form of molten metal or gases from other products that can be high value by-products. Nevertheless, because of the high temperatures needed, these techniques tend to be highly energy intensive and can emit dust and release dangerous gases, demanding expensive cleaning and dust collecting system to prevent air pollution [793].

These constraints explain the recent progress of further research on alternatives methods, specifically hydrometallurgical methods. These processes do not demand extremely high temperatures, as the pyrometallurgical ones. Hence, the energy consumption is reduced and dust production are minimized.

7.7.3.1 Hydrometallurgical recycling of spent batteries

After the collection of spent batteries and before their chemical treatment, some mechanical/physical pre-treatments are needed. These may involve shredding or cut-crashing, thermal procedures, separation of ferrous metal from inert compounds (plastic, paper, ferrous and non-ferrous scraps) by the use of magnets as well as powder sieving [792]. Afterwards, hydrometallurgical processes can be applied, often in small scale plants, which include leaching, separation and metal recovery steps. Because of the complex nature and several parameters that could impact the efficiency of leaching and the subsequent separation step(s), these processes still remain a significant research avenue.

➢ Leaching

The target of the leaching is to extract the metals from the solid matrix into the aqueous phase. Often, strongly acidic or alkali solutions, with or without the presence of reducing agents, are used. The leaching processes may be categorized into four simplified main types: neutral, acid (or acid-reductive), alkaline and complexation leaching. These processes depend on the type of chemicals applied and reactions may vary from simple dissolution to dissolution plus redox reactions.

➢ Neutral leaching

Neutral leaching corresponds to the use of deionized water to leach out the electrolyte and other soluble components of the spent batteries. In the case of alkaline batteries, this electrolyte is KOH while for zinc-carbon is NH_4Cl, as referenced above. In the case of a subsequent acid leaching implementation, neutral leaching is formerly used to leach these and other water soluble components of the spent batteries in order to prevent extreme use of acid as well as to prevent interferences with other later processes, like electrolysis [794]. During the neutral leaching, the KOH and NH_4Cl dissolve in the deionized water and can afterwards be recovered, ready for reuse as electrolytes for new batteries [795].

➢ Alkaline leaching

Alkaline leaching is mainly applied using a strong base (e.g. NaOH), which reacts according to the following equations [796]:

$$Zn(s) + 2NaOH(aq) + 2H_2O(aq) \rightarrow 2Na^+(aq) + Zn(OH)_4^{2-}(aq) + H_2(g) \tag{7.1}$$

$$ZnO(s) + 2NaOH(aq) + 2H_2O(l) \rightarrow 2Na^+(aq) + Zn(OH)_4^{2-}(aq) + H_2O(l) \tag{7.2}$$
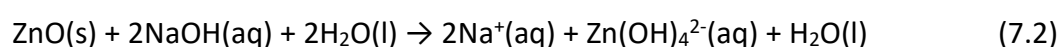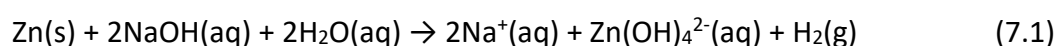
➢ Acid leaching

Acid leaching is mainly conducted using mineral acids, like hydrochloric acid (HCl), nitric acid (HNO_3) and especially sulphuric acid (H_2SO_4) because of its low cost. The reactions of the

main Zn forms that can be present in alkaline spent batteries after leaching with acid, like H_2SO_4, are represented below [794]:

$$ZnO(s) + H_2SO_4(aq) \rightarrow ZnSO_4(aq) + H_2O(l) \qquad (7.3)$$

$$Zn(s) + H_2SO_4(aq) \rightarrow ZnSO_4(aq) + H_2(g) \qquad (7.4)$$
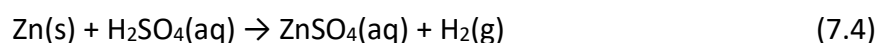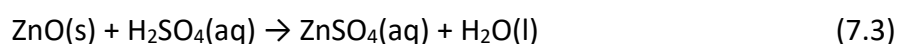
➢ Complexation-assisted leaching

Complexation-assisted leaching is a method that implies the use of complexing agents, like ammonium carbonate $[(NH_4)_2CO_3]$ or ammonium chloride (NH_4-Cl). The ability of these leaching agents originates from the formation of soluble complexes of Zn with the added ligands, which activate selective dissolution of Zn from the battery waste using less aggressive conditions (near neutral pH) than when alkaline leaching is used (pH > 13). The following equations represent the formation of the most dominant complexes formed between Zn with the complexing agents added [797]:

$$ZnO(s) + 2NH_4^+(aq) + 3Cl^-(aq) \rightarrow ZnCl_3NH_3^-(aq) + NH_3(aq) + H_2O(l) \qquad (7.5)$$

$$ZnO(s) + 2NH_4^+(aq) + 4Cl^-(aq) \rightarrow ZnCl_4^{2-}(aq) + 2NH_3(aq) + H_2O(l) \qquad (7.6)$$

$$ZnO(s) + 2NH_4^+(aq) + 3NH_3(aq) \rightarrow Zn(NH_3)_4^{2+}(aq) + H_2O(l) \qquad (7.7)$$
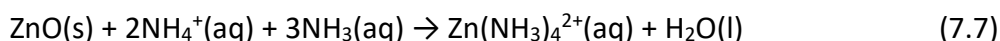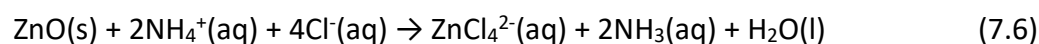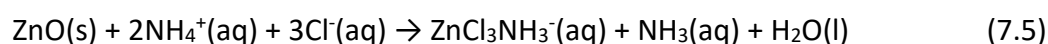
In **Table 7.3**, are listed the works in which alkaline complexation and acid leaching were used.

Table 7.3 Detailed performance of alkaline, complexation and acid leaching strategies tested on spent alkaline and/or zinc carbon batteries. Data were normalized in function of both the molar quantities of leachant per g of waste [795, 798-804, 814].

	S/L ratio (g/mL)	Leachant (M)	Mol leachant /g waste	Time (h)	Particle size (μm)	T (°C)	Zn (%)
Alkaline leaching	0.1	NaOH (4)	0.04	1	<2380	80	63.4
	0.1	NaOH (4)	0.04	0.5	<2380	80	82
	0.1	NaOH (4)	0.04	3	<1000	80	38
	0.1	NaOH (4)	0.04	0.05	<1000	*	82
	0.1	NaOH (4)	0.04	0.23	<1000	**	81
	0.1	NaOH (6)	0.06	2	<1250	80	>64
	0.1	NaOH (6.5)	0.065	3	-	80	52
Complexation leaching	0.1	$(NH_4)_2CO_3$ (2)	0.02	1	<2380	60	83
	0.1	NH_3 (2.5)	0.025	1.5	<2380	60	39
	0.05	NH_4Cl (5)	0.1	4	<3970	100	72
Acid leaching	0.1	H_2SO_4 (1)	0.01	1.5	<2380	30-32	98
	0.1	H_2SO_4 (1)	0.01	3	<1000	80	86
	0.1	H_2SO_4 (1)	0.01	8×10^{-3}	<1000	*	94
	0.1	H_2SO_4 (1)	0.01	3.3×10^{-2}	<1000	**	92
	0.1	H_2SO_4 (1.5)	0.015	3	<1000	80	99
	0.1	H_2SO_4 (2)	0.02	3	-	80	100
	0.1	H_2SO_4 (2)	0.02	1	<1250	60	96
	0.1	H_2SO_4 (2)	0.02	-	<2380	60	92
	0.1	HCl (5)	0.05	2	-	70	96.1

*Microwave-assisted / **Ultrasound-assisted

The main results using reductive acid leaching are demonstrated in **Table 7.4** by alphabetical order of the reductant.

Table 7.4 Detailed performance of reductive acid leaching tested on spent alkaline and/or zinc carbon batteries. Data were normalized in function of the molar quantities of leachant, expressed in mol of leachant per g of waste, as well as the quantity of reductant, expressed in mmol of reductant per g of waste [794, 796, 798, 802, 805-814].

S/L ratio (g/mL)	Leachant (M)	Mol leachant /g waste	Reductant	SP	mmol reductant /g waste	NTSR	Time (h)	Particle size (µm)	T (°C)	Zn (%)
0.05	H_2SO_4 (1)	0.02	Activated carbon	2	5.0	-	3	<88	80	84.08
0.05	H_2SO_4 (0.5)	0.01	Ascorbic acid	10	1.1	2.0	2	5-100	25	98
0.05	H_2SO_4 (2)	0.01	Ascorbic acid	10	1.5	2.5	3	<88	70	99.99
0.2	H_2SO_4 (1.8)	0.009	Citric acid	9	1.0	1.3	1	<2000	40	100
0.02	H_2SO_4 (2)	0.1	Glucose	12	0.6	1.2	1	<53	100	100
0.1	H_2SO_4 (2)	0.02	Glucose	12	0.1	0.2	1	<53	100	70
0.1	H_2SO_4 (1.5)	0.015	Glucose	12	1.1	2.6	0.017	<566	-	95
0.05	H_2SO_4 (2)	0.04	Guar meal	12	2.2	-	3	<88	70	100
0.1	H_2SO_4 (3)	0.03	H_2O_2	1	58	9.3	1	<2380	60	98
0.1	H_2SO_4 (2)	0.02	H_2O_2	1	58	11.1	1	-	25	98
0.1	H_2SO_4 (2)	0.02	H_2O_2	1	58	16.1	0.5	<2380	60	93.3
0.1	HCl (6)	0.06	H_2O_2	1	50	9.5	1	<1000	-	99.9
0.1	H_2SO_4 (4.5)	0.045	H_2O_2	1	50	9.5	3	<1000	-	99.9
0.1	H_2SO_4 (2)	0.02	Lactose	12	0.3	0.7	3	<1000	90	100
0.2	H_2SO_4 (1.8)	0.009	Oxalic acid	1	3.3	0.5	5	<500	80	100
0.1	H_2SO_4 (1)	0.01	SO_2	-	N.A.	-	1.5	<2380	30-40	98

In **Table 7.4**, SP is the Stoichiometric Proportion of reductant used, when applicable and NTSR is the Number of times that the reductant was used relatively to the stoichiometry required.

7.8 Proposed flowsheet for discarded ZABs

The proposed method is envisaged based on current zinc battery recycling practices, which can also be integrated for ZABs as shown in **Figure 7.7**.
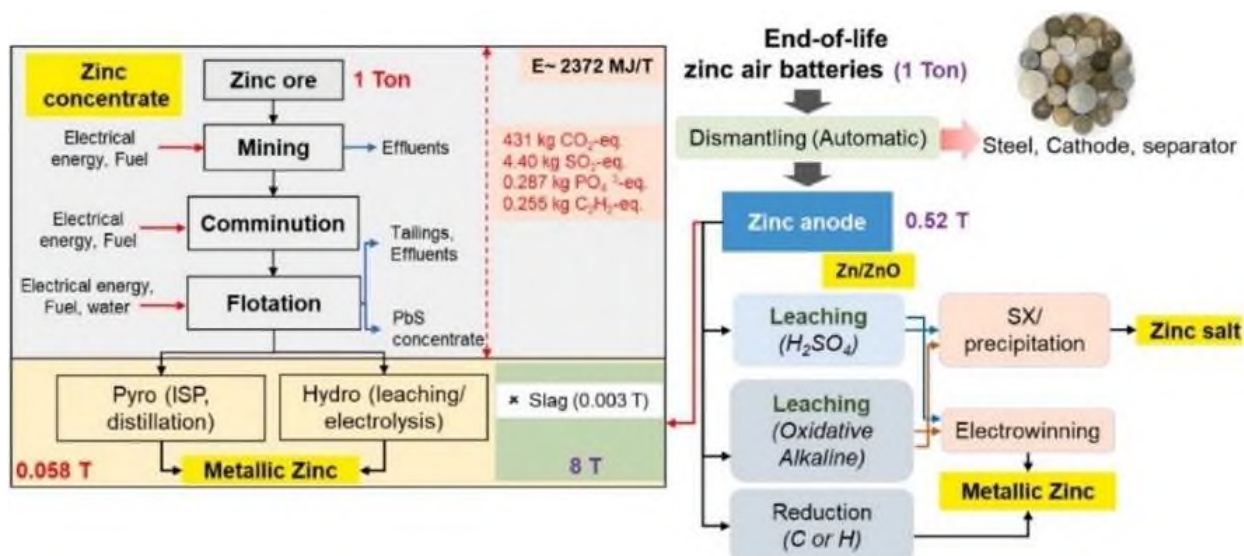
Figure 7.7 Proposed recycling flowsheet for recovering zinc values from discarded ZABs [574].

One-ton primary ore contains 0.058-ton metal zinc, while end-of-life ZABs contain zinc equivalent to 8 tons of primary ore. Several challenges related to recycling zinc from ZABs include collection/sorting, process integration, comparative life-cycle assessments with similar secondary zinc sources, and effluent treatment. Predominantly, the collection stage is a major challenge, which will affect more in the case of ZABs due to their much smaller size and lack of awareness. Identifying batteries and their chemical composition before any recycling step is crucial, which can be achieved by advanced tools such as X-Ray imaging, deep learning, and QR labeling. A comparatively low zinc concentration (less than ~ 35 %) in the waste source is considered uneconomical for recycling; therefore, a certain pre-processing method is required for upgradation (55-60 %). However, the zinc content is much higher in the case of ZABs without any harmful impurities and requires no pre-processing.

The ZABs should be dismantled, preferably via automation, to separate the anode powder (Zn/ZnO), followed by a suitable treatment to recover Zn. Possible methods are the hydrometallurgical treatment of leaching in acidic (H_2SO_4) or alkaline conditions and reduction by carbon or hydrogen. The acid leaching leads to intense hydrogen evolution due to a reaction with metallic zinc (apart from ZnO), which utilizes corrosive chemicals in large quantities, which is unfavorable for industrial applications. Moreover, hydrometallurgical treatment releases effluents generally neutralized using $CaCO_3$ and $Ca(OH)_2$. In sulphuric acid, CaO forms $CaSO_4$, which is undesirable, while Na_2CO_3 and NaOH perform comparatively better but are expensive [625].

On the other hand, oxidative alkaline leaching (NaOH) studied for the leaching of zinc (Zn/ZnO), followed by electrowinning, is a preferred route to obtain pure zinc metal [626]. The pyrometallurgical process suffers from the drawbacks of possible emissions, CO_2 release, high energy requirements, and investment costs. However, the emissions, residues, and recovered metal would be a function of the amount, composition, and recovery route followed, which needs further evaluation. Hydrometallurgical zinc production offers the lowest operational costs; however, in pyrometallurgical processes, the flexibility of feedstock and comparatively feasible recovery from by-products and residues are advantageous [627].

The recycling studies can be widened by utilizing solar energy for reduction/electrowinning. The thermodynamic efficiencies on comparison showed that the solar-carbothermal process functions better (19-36 %) than the solar-electrowinning process (2.4-11.4 %) at commercial scales [628]. However, process development and economic returns, particularly in the case of ZABs, need to be ascertained.

Recycling only ZABs by formal recyclers would be unprofitable, with other limiting factors such as high investment and higher labour costs (in developed countries). Moreover, formal recycling in developing countries faces challenges such as inconsistent supplies, high costs, inadequate infrastructure, and lack of financial incentives [629]. Adopting the recycling flowsheet solely for zinc-battery recycling will not be economically feasible. Therefore, it is recommended to integrate recycling with the primary processing route (as utilized for PCB recycling via copper smelting route) or with other zinc-based battery recycling methods. However, having a uniform feedstock at a plant site and preventing contamination, such as Cd, Hg, Mn, etc., from other zinc-based batteries is essential.

The recycled mass should be reutilized in the primary zinc production stream for sustainable cyclic metal flow for an efficient recycling approach. Generally, recycled metals in primary production have significant chances of degrading the quality of recovered metal (due to secondary impurities). Nevertheless, using zinc-anode from batteries may bypass such challenges. Additionally, the utilization of recovered anode in the primary processing stream may save energy ~ 2372 MJ/ton, reduce the emissions (431 kg CO_2-eq.) and slag production (3.8 kg/ton) [630, 631]. Hence, challenges, possibilities, energy consumption, and economics should be considered to sustain zinc through utilization in primary production.

CHAPTER 8

Materials Design for Rechargeable Metal-Air Batteries

8.1 Introduction

MABs are a family of electrochemical cells powered by metal oxidation and oxygen reduction, exhibiting a great advantage regarding theoretical energy density, which is about 3-30 times higher than commercial LIBs [632-635]. The two types of batteries that have attracted most attention are LABs and ZABs [636]. LABs (with Li_2O_2 as the discharge product) can deliver a superior theoretical performance of a large energy density of 11,429 Wh kg^{-1} (based on the mass of Li metal), a high specific capacity of 3,860 mAh g^{-1} (based on the mass of Li metal), and a cell voltage as high as 2.96 V [637]. For ZABs the theoretical energy density is 1,350 Wh kg^{-1} (based on the mass of Zn metal), still about 5-fold higher than LIBs [638]. In addition, ZABs also have the advantage of low cost compared with LIBs [638]. Except LABs and ZABs, other types of MABs also have their own superiorities. For instance, Al-air batteries exhibit the highest volumetric capacity (8,040 Ah L^{-1}) [639], and Na-air batteries show smaller charge overpotentials than LABs [640]. So, the MAB family has great potential to serve as next-generation electrochemical energy-storage devices.

MABs most of the times contain four major parts: an air electrode, metal electrode, electrolyte, and separator, as illustrated in **Figure 8.1 (A)**.
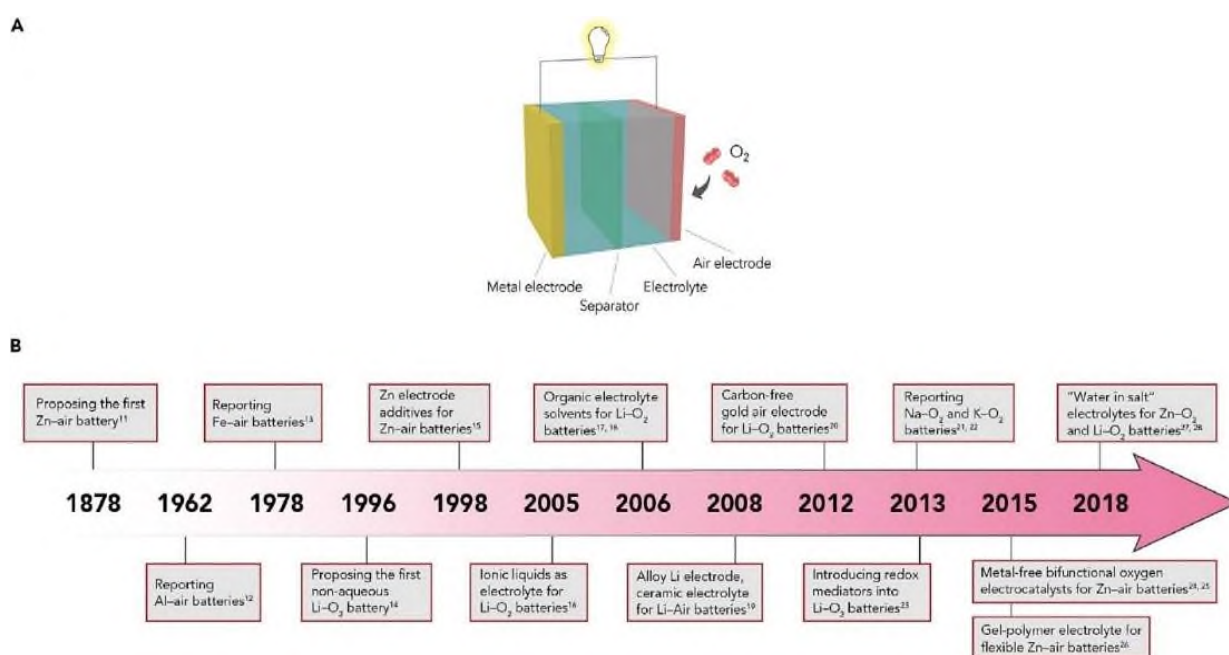
Figure 8.1 *Introduction of MABs: (A) Schematic illustration of a MAB. (B) A brief timeline of research progress in MABs [642-658, 791].*

For most MABs, the air electrode reactant O_2 is obtained from the ambient air rather than encapsulated in the cell. So, the air electrode several times consists of only an electrocatalyst layer to reduce the electrode overpotential and a gas-diffusion layer (GDL) to enhance the oxygen diffusion between the ambient air and the catalyst surface. The commonly investigated metals for the metal electrode include zinc, lithium, aluminum, magnesium, and sodium [641]. For highly active metals that are unstable in aqueous systems, such as Li, Na, and K, a non-aqueous aprotic electrolyte is usually required, while for relatively inactive metals such as Zn, Al, Mg, and Fe, alkaline aqueous electrolytes are widely employed [635]. The separator is an optional component in a MAB used to separate two different electrolytes, obstruct some mass transportation processes between the electrodes, and prevent the short-circuit caused by metal dendrites.

Much progress has been made in the research on MABs from the invention of the first primary ZAB in 1878 [**Figure 8.1 (B)**]. In general, ZABs are composed of zinc plate or zinc foil as anode, high-concentration alkaline solution and zinc ion salt as electrolyte, and oxygen reduction reaction (ORR) catalyst as cathode. Such primary ZABs have been widely commercialized. For rechargeable ZABs, the catalyst also needs to have the catalytic activity of oxygen evolution reaction (OER) which is thus called "bifunctional". Compared with traditional lithium-ion battery, ZABs have higher theoretical specific energy (1218 Wh kg^{-1}), lower price and intrinsic safety. In particular, the tolerance of flexible ZABs assembled with solid electrolyte in bending, torsion, tensile, compression and other flexibility tests is much better than that of flexible lithium-ion batteries, making it one of the most powerful competitors for commercially flexible energy devices [642-650].

Nevertheless, it does not mean that flexible ZABs can certainly become the energy source of the next-generation flexible and wearable electronics. In fact, there are still many problems to be solved in the process of industrialization. First, as the most important part of the whole device, catalytic activity, durability and cost of the oxygen catalyst still needs to be optimized. In addition, the solid electrolyte used by most flexible ZABs contains a certain amount of water, which makes it easy for the high-concentration alkaline electrolyte to seep from semi open devices during bending and compression, which is absolutely unacceptable in the field of flexible and wearable electronics. Furthermore, although most studies claim that the assembled ZABs are flexible and give demonstration as evidence, these flexibility tests are usually just simple bending and tensile under low strains. It is far from enough to expect that these simple tests can be applied in practically complex environments [651-658].

8.2 Evaluation Parameters and Current Issues of MABs

The discharge properties and the rechargeability are the two aspects that the performance evaluation of rechargeable MABs can be divided into. Unfortunately, by this time, most of the MABs under study still have only very limited practical application areas. It is still a huge challenge the improvement of the MABs' performance concerning both discharge properties and recharge ability. So, it is important for promoting the further development of the MABs to study the problems and challenges in these batteries from the perspective of materials science and look for solutions through the material design of air electrode, metal electrode, electrolyte, and separator materials. The discharge properties and the rechargeability of MABs, which are the main challenges, are mentioned here.

Information about how much the current density can be reached at a specific discharge voltage can be given from the polarization performance and also reflects the peak power density that a MAB can provide. The overpotential and the reaction rate of air electrode and metal electrode reactions are the factors that affect the polarization performance of MABs. The reduction of oxygen on the air electrode is sluggish in kinetic and is considered to be the rate-determining step. So, efficient electrocatalysts are required on the air electrode to reduce the oxygen reduction overpotential, thus achieving a high reaction rate [659, 660]. Apart from the reaction kinetics, the mass transport is also a serious factor in affecting the reaction rate [638]. Rational material designs are needed to minimize the mass transport resistance, including employing a GDL on the air electrode, regulating the pore structure of electrodes, and preventing the deposition of insulating products/by-products on the electrodes.

The theoretical capacity of a MAB is determined by the amount of metal encapsulated in the battery as the metal electrode, as the air electrode reactant O_2 is achieved from ambient air and is nearly infinite. Nevertheless, there are also some factors that limit the practical capacity of a MAB. For aqueous MABs, passivation of the metal electrode could occur as the metal electrode is being coated by an insulating metal oxide film during the discharge process, resulting in termination of the discharge process [641]. There is another cause for the degradation of capacity for non-aqueous MABs: the limited storage of metal peroxides or superoxides in the air electrode [636]. Modification of metal electrodes, the introduction of additives in the electrolytes, and the pore-structure design of air electrode electrocatalysts are some of the material design strategies that are under development, in order to minimize the capacity loss of MABs.

Round-trip efficiency, Coulombic efficiency, and cycle life are some of the typical parameters to describe the rechargeability of MABs. The round-trip efficiency is determined by the ratio of the energy released during discharge and the energy needed in the recharge process, representing the energy-utilizing efficiency of a MAB. It is often characterized by dividing the discharge voltage by the charge voltage obtained at a constant current density. The round-trip efficiency depends on the overpotential of both discharge and charge reactions. It requires the air electrode electrocatalyst to be bifunctional toward the conversions between oxygen and water/peroxides/superoxides. The mass transport during the charge and discharge process should also be taken into account. Note that in the charge process of non-aqueous MABs, the decomposition of peroxides and superoxides on the air electrode needs a solid-solid contact of the reactant and the electrocatalyst, when a charge process of non-aqueous MABs occurs. Material design methods such as regulating the air electrode structure and adding redox mediators in the electrolyte have been proposed in order to lower the overpotential induced by the insufficient solid-solid contact [659, 661].

The Coulombic efficiency is defined as the ratio of charge capacity and discharge capacity in a full discharge-recharge cycle, representing the capacity loss after a cycle. The Coulombic efficiency of a battery must be higher than 99.98 % in order to retain 80 % of the initial capacity after 1,000 cycles [662]. But, MABs most of the times suffer from irreversible consumption of metal electrodes and parasitic reactions, resulting in low Coulombic efficiency [637]. The low Coulombic efficiency of MABs that have been studied so far strongly limits their applications as truly rechargeable batteries in mobile electronics and electric vehicles. Optimizations of the electrode, electrolyte, and separator materials have been studied to minimize this problem [637, 641].

The cycle life of a MAB relies on the stability of all the parameters covered above and on high Coulombic efficiency. A long cycle life needs the stable structure and composition of all the components in the battery. Some common issues in MABs, such as the deactivation of electrocatalysts shape and the decomposition of electrolytes and the dendrites change of metal electrodes could cause shortening of the cycle life [637, 663].

In conclusion, the problems of MABs' performance mainly come from the materials side. Through rational material designs these problems can be minimized and the battery performance improved, as presented in **Figure 8.2**.
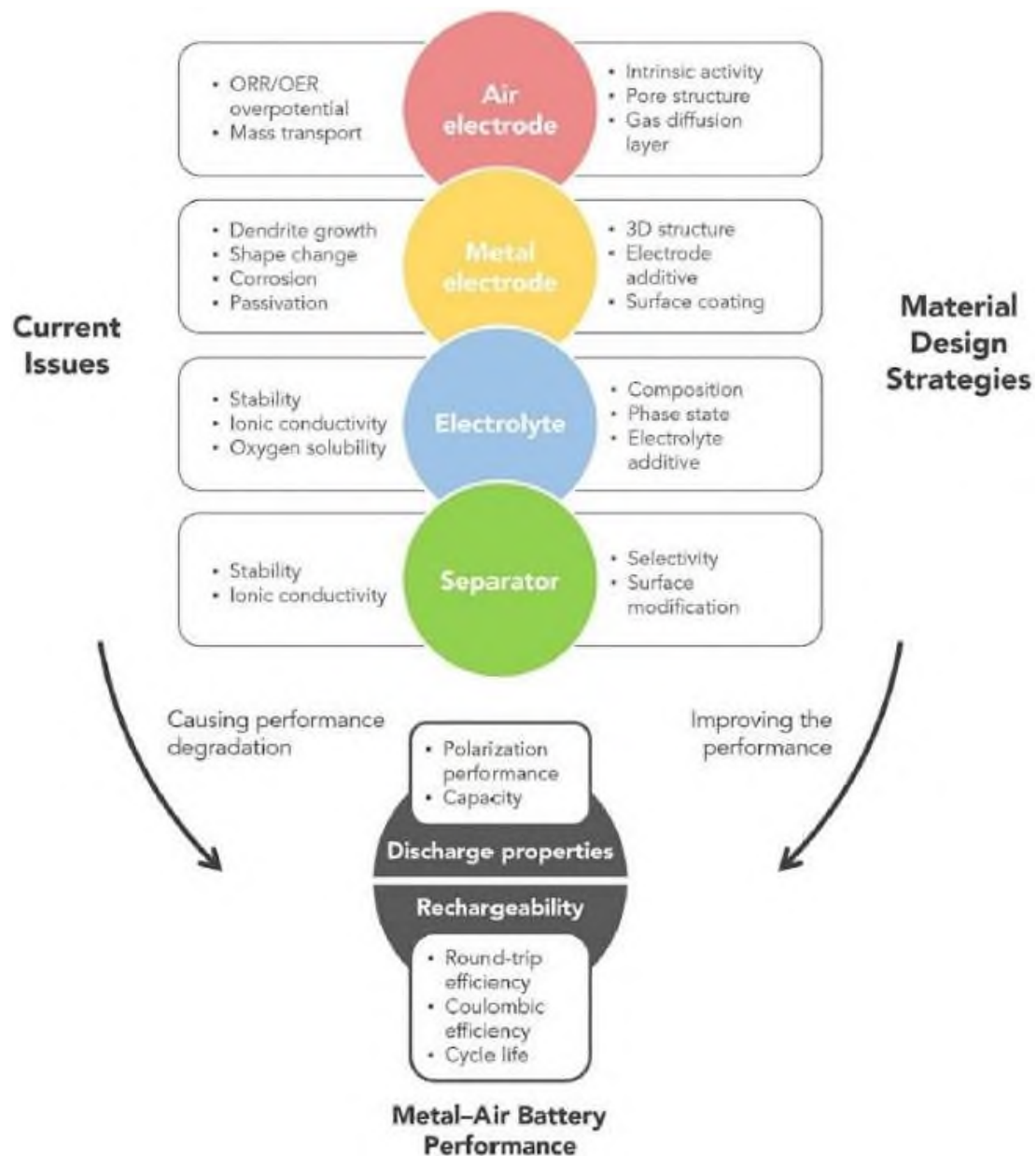
Figure 8.2 *Summarization of Evaluation Parameters, Material Challenges and Material Design Strategies for MABs [791].*

Taking under consideration that previous research on MABs mainly focused on Zn-air and Li-air batteries [636], these two systems will be chosen as representatives for non-aqueous and aqueous MABs in the present chapter.

8.3 Material Design of Air Electrodes

8.3.1 Electrocatalyst Layer

A key role in achieving high power density and high round-trip efficiency plays oxygen electrocatalysts on the air electrode of MABs. Aqueous and non-aqueous MABs have distinct air electrode reactions. For that reason, electrocatalysts for these two types of MABs will be analyzed separately [664, 665].

8.3.1.1 Electrocatalysts for Aqueous MABs

Aqueous MABs need efficient ORR/OER bifunctional electrocatalysts on the air electrode to lower the overpotential of both the discharge and charge process. The main difficulty in developing an ORR/OER bifunctional electrocatalyst is that ORR and OER have different requirements for electrocatalysts. ORR and OER are multi-step reactions, involving the adsorption of various kinds of oxygen-containing species on the surface of electrocatalysts. Analyses of the mechanism of ORR and OER revealed that the desired adsorption energies of the oxygen-containing species on electrocatalysts, are most of the times different, to achieve the best ORR or OER activity [666]. Most reported materials for ORR and OER bifunctional electrocatalysis can be classified into two categories: transition-metal-based materials and carbon-based materials [638, 654, 655, 667-669]. The common regulation strategies of these catalytic materials for achieving high intrinsic activity are presented in **Figure 8.3**.
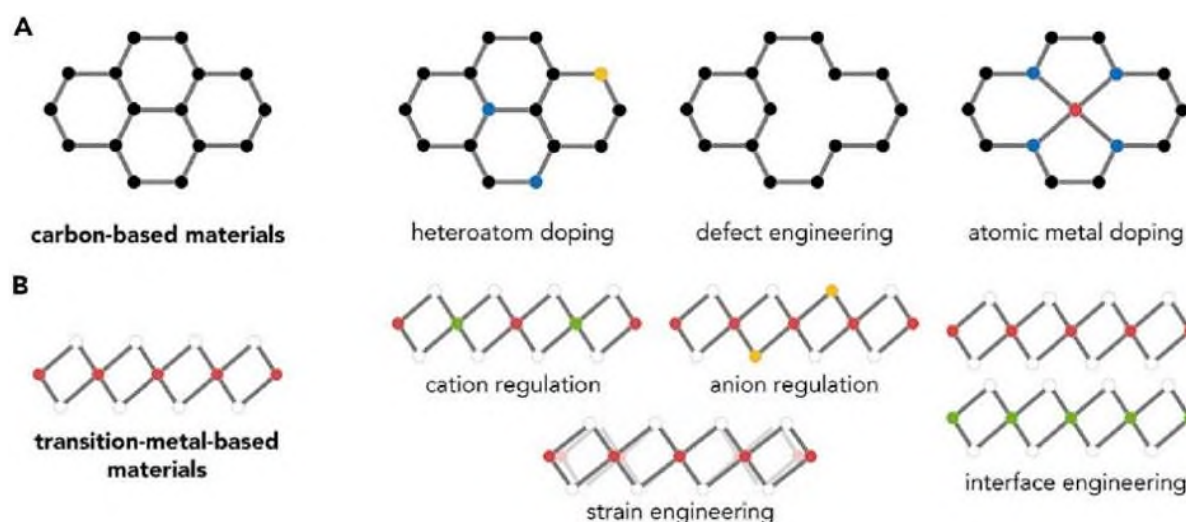
Figure 8.3 Material Design Strategies for Improving the Intrinsic Activity of ORR/OER Electrocatalysts in Aqueous MABs: (A) Material design strategies for carbon-based materials. (B) Material design strategies for transition-metal-based materials [791].

High apparent activity for electrocatalysts is also achieved with high intrinsic activity, fast gas, electrolyte, and electron transport. The electrocatalysts employed in MABs could lower the discharge and charge overpotentials, leading to high power density and round-trip efficiency, through the combination of high intrinsic activity and favorable microstructures. A short time ago, an approach on the material design of metal-organic framework (MOF)-derived air electrode electrocatalysts was proposed by Zou et al. [670] to obtain high power density in Zn-air batteries. Cobalt nanoparticle-embedded N-doped carbon nanotubes (CNTs) grown on carbon fibers (NCo@CNT-NF700) were obtained through the pyrolysis of single-crystal cobalt MOF-74 nanotubes and dicyandiamide (DCDA) as additional carbon and nitrogen source at 700 ^{o}C. A three-dimensional (3D) hierarchical structure was noticed by scanning electron

microscopy (SEM) and transmission electron microscopy (TEM) characterizations [**Figures 8.4** (A) and **8.4** (B)].
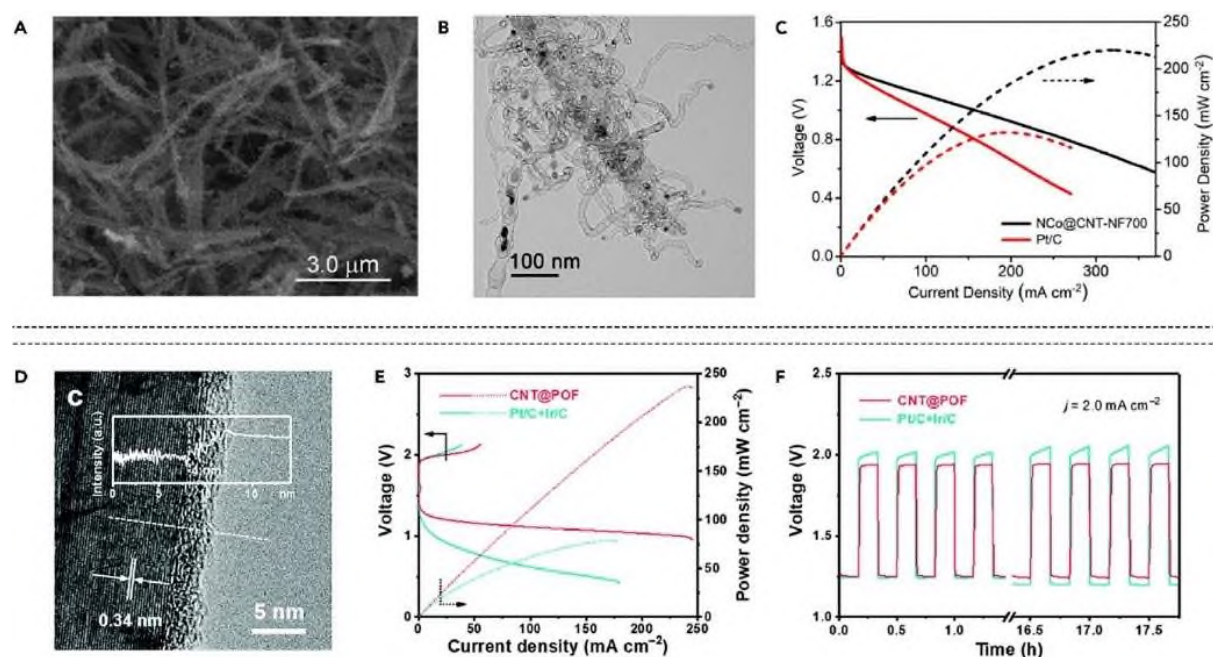
Figure 8.4 *Material Design of Electrocatalysts in Aqueous MABs: (A and B) SEM (A) and TEM (B) images of NCo@CNT-NF700. (C) Polarization curve and corresponding power density plot of the primary Zab using NCo@CNT-NF700 and Pt/C as the air electrode catalyst. (D) High-resolution TEM images of CNT@POF. Inset: the contrast profile along the white dashed line. (E) Polarization curve and corresponding power density plot of the rechargeable ZAB using CNT@POF and Pr/C+Ir/C as the air electrode catalyst. (F) Galvanostatic discharge-charge cycling curves at 2.0 mA cm^{-2} of CNT@POF and Pt/C+Ir/C [670, 671, 791].*

Co nanoparticles and N-doped carbon provide the electrocatalytic ORR activity, and the network constructed by carbon fibers and carbon nanotubes ensures the high electrical conductivity and porous structure of Co-MOF-74-NT700. As a result, Co-MOF-74-NT700 exhibited an outstanding electrocatalytic ORR performance with a half-wave potential of 0.87 V versus reversible hydrogen electrode, only 7 mV lower than a Pt/C electrocatalyst. When applied into a ZAB, a high peak power density of 220 mW cm^{-2} can be achieved, shown by the polarization curve [**Figure 8.4** (C)]. So, improvements on the MAB discharge performance were realized by the design of efficient air electrode ORR electrocatalysts.

Both discharge and charge processes of MABs, can be helped by the development of bifunctional ORR/OER electrocatalysts. For instance, Li et al. [671] reported a hybrid material of cobalt-coordinated porphyrin covalent organic framework (POF)-coated CNTs, named CNT@POF, as a bifunctional electrocatalyst for ZABs. Thin POF layers coaxially wrap the surface of the CNTs, facilitating fast electron transfer [**Figure 8.4** (D)]. The coating of POF also leads to a superb hydrophilic surface, which ensures the accessibility of electrolytes. Zn-air batteries with

CNT@POF as the air electrode electrocatalyst exhibited satisfactory discharge and charge performances, through the rational design of the CNT@POF electrocatalyst. For discharging, a peak power density of 237 mW cm^{-2} was revealed by the polarization curve [**Figure 8.4** (E)]. In respect of cycling properties, the galvanostatic discharge-charge cycling test at 2.0 mA cm^{-2} [**Figure 8.4** (F)] exhibited an initial discharge and charge voltage of 1.25 V and 1.96 V, respectively, with a voltage gap of 0.71 V and a round-trip efficiency as high as 63.8 %. In addition, no obvious performance degradation was observed after 200 cycles (over 66 h).

For other types of aqueous MABs such as Mg-air batteries and Al-air batteries, the air electrode reactions are the same as those of ZABs. So, these aqueous MABs share the same electrocatalyst design principles [672]. In a word, the design of air electrode electrocatalysts for aqueous MABs mostly emphasizes on the fast conversions between oxygen and water with low overpotential, thus improving the power density and energy efficiency.

8.3.1.2 Electrocatalysts for Non-Aqueous MABs

The air electrode reactions of non-aqueous MABs are different from those of aqueous MABs. Therefore, the material design of air electrode electrocatalysts for non-aqueous MABs demands different strategies to boost the air electrode reactions. Taking LABs for example, the two-electron reactions of the formation and decomposition of Li_2O_2 contain fewer steps than four-electron aqueous ORR and OER. However, the conversion between O_2 and Li_2O_2 is still sluggish because of the complicated intermediates and multiple side reactions [673]. Moreover, the insulating nature of Li_2O_2 and the limited storage of Li_2O_2 in the air electrode could also affect the capacity and recharge properties [674]. Mitigation of the problems of air electrode reactions can be achieved by the material regulations on air electrode electrocatalysts and electrolytes [637, 659, 675]. In this chapter, materials for non-aqueous MABs electrocatalysts are discussed from the aspect of active material selection and pore-structure design.

Carbon materials have been widely investigated as air electrode electrocatalysts and supports for Li-air batteries, for their high electrical conductivity, large specific surface area, porous structure and their high electrical conductivity, which are favorable for achieving rate capability and high discharge capacity [667, 676]. On the other hand, carbon materials suffer from their low activity on Li_2O_2 decomposition and poor stability at high charge potentials, leading to inferior round-trip efficiency and cycling stability [673, 676]. So, much attention has been paid to non-carbon LIB air electrode materials in recent years. Materials including precious metals [650, 677, 678] and transition metal oxides [679-682] have proved their activity on aprotic oxygen reduction and evolution reactions. Similar to aqueous MABs, structure and

composition regulation strategies can be applied on the electrocatalysts to enhance the performance of non-aqueous MABs.

A multifaceted design of Co_3O_4 electrocatalyst on surface, interface, and doping was recently mentioned by Gao et al. [683] $Co_3O_4@Co_3O_4$/Ag hybrids with a yolk-shell structure, as presented in **Figure 8.5 (A)**, were synthesized by a synchronous reduction method. On the porous Co_3O_4 shell, part of the Ag is doped into the crystal lattice and part of the Ag is on the surface of Co_3O_4 shell in the form of single atoms or clusters. The Ag-Co_3O_4 interface tunes the electronic structure to provide active sites with higher activity for ORR and OER. When applied as the air electrode electrocatalyst of a LAB, $Co_3O_4@Co_3O_4$/Ag exhibited a high initial capacity (12,000 mAh g^{-1}@200 mA g^{-1}, based on the mass of electrocatalyst) and rate capability (4,700 mAh g^{-1}@800 mA g^{-1}). In a charge-discharge cycling test with a limited capacity of 1,000 mAh g^{-1} at the current density of 200 mA g^{-1}, the LAB catalyzed by $Co_3O_4@Co_3O_4$/Ag could retain the initial capacity after 80 cycles. This great performance can be attributed to the highly active species, the electrical conductivity of Ag nanoparticles, the porous structure of Co_3O_4, and the modified structure of the discharge product Li_2O_2.
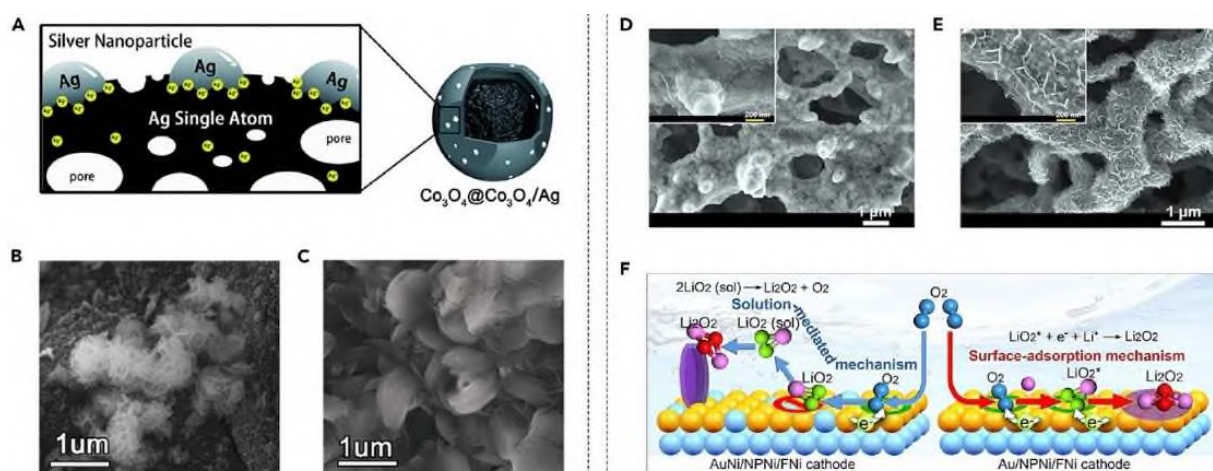
Figure 8.5 Design of Catalytic Materials in Non-aqueous MABs: (A) Schematic illustration of $Co_3O_4@Co_3O_4$/Ag yolk-shell structure. (B and C) SEM images of $Co_3O_4@Co_3O_4$/Ag-based (B) and Co_3O_4-based (C) air electrode after discharge. (D and E) Field-emission SEM images of Au/NPNi/FNi (D) and AuNi/NPNi/FNi (E) air electrode after discharge with a limited discharge capacity of 3,000 mAh g^{-1}. (F) A mechanism of Li_2O_2 electrochemical growth on AuNi/NPNi/FNi and Au/NPNi/FNi air electrode [683, 685, 791].

Air electrodes with $Co_3O_4@Co_3O_4$/Ag and Co_3O_4 as electrocatalysts exhibited different morphology after discharge [**Figures 8.5 (B) and 8.5 (C)**]. The flowerlike structure of Li_2O_2 on $Co_3O_4@Co_3O_4$/Ag possesses larger surface area, which is favorable for mass diffusion and Li_2O_2 decomposition. The change in Li_2O_2 morphology is benefited by the introduction of Ag, which provides nucleation sites for Li_2O_2 deposition [684].

Although a wide investigation has been held on non-carbon electrocatalysts, carbon materials are still utilized as conductive additives and as catalyst supports the air electrode of many LABs. So it is necessary to develop non-carbon air electrodes, which are free of carbon in the whole electrode. This requires free-standing and conductive features of electrocatalysts. Considering this, Xu et al. [685] proposed an all-metal air electrode architecture of nanoporous Ni (NPNi) with a nanoengineered AuNi alloy surface directly attached to Ni foam (FNi), denoted as AuNi/NPNi/FNi. The Ni foam ensures the mechanical stability and the electrical conductivity of the air electrode; the porous Ni facilitates mass transfer; and the AuNi alloy provides ORR and OER activity. Thus, the LAB with AuNi/ NPNi/FNi as the air electrode exhibited ultrahigh capacity of 22,551 mAh g^{-1}_{AuNi} and long cycling life (286 cycles) at a current density of 1.0 A g^{-1}_{AuNi} with a capacity limit of 3,000 mAh g^{-1}_{AuNi}. For the LAB with Au/NPNi/FNi as the air electrode, in which nanoporous Ni is coated by pure Au instead of AuNi alloy, the air electrode was covered by Li_2O_2 film after discharge [**Figure 8.5 (D)**], while for AuNi/ NPNi/FNi, Li_2O_2 showed a nanosheet-like structure [**Figure 8.5 (E)**], similar to that in **Figure 8.5 (B)**, which is favorable for achieving a high capacity. A possible mechanism is presented in **Figure 8.5 (F)**. The Ni atoms in AuNi alloy prevent the reduction of LiO_2 on the surface and promote their diffusion into the electrolyte. The dissolved LiO_2 then undergoes disproportionation to form Li_2O_2 nanosheets. However, for AuNi/NPNi/FNi, the ORR occurs on the Au air electrode surface, resulting in the formation of Li_2O_2 thin films. As can be seen from the above research, regulation of the active material of electrocatalysts can accelerate the reaction kinetics, as well as tuning the structures of discharge products of non-aqueous MABs.

For a certain active material, a well-designed pore structure can bring about further improvements in the mass transport and the deposition of the discharge products. For conventional air electrodes with electrocatalysts coated or grown on conductive porous substrates, the specific capacity is limited by the surface passivation and low mass loading of the discharge products [**Figures 8.6 (A) and 8.6 (B)**] [686]. Thus, Lyu et al. [686] designed a 3D-printed hierarchically porous air electrode for Li-O₂ batteries, the schematic diagram of which is presented in **Figure 8.6 (C)**. This hierarchical pore structure can provide sufficient space for Li_2O_2 storage, and the good contact between electrocatalysts and Li_2O_2 nanoparticles is favorable for Li_2O_2 decomposition.

The air electrode design was then realized by the carbonization of 3D-printed Co-MOF, with Co nanoparticles assembled in nitrogen-doped nanoporous carbon flakes as active material [690], denoted as 3DP-NC-Co [**Figure 8.6 (D)**]. Compared with NC-Co randomly packed on carbon

paper (RP-NC-Co) and NC-Co grown on carbon paper (CP-NC-Co), Li-air batteries with 3DP-NC-Co as the air electrode exhibit much superior performances for specific capacity [**Figure 8.6** (E)], overpotential [**Figure 8.6** (F)], and cycle stability [**Figure 8.6** (G)]. Therefore, electrocatalytic materials for non-aqueous MABs can be rationally designed from the aspects of active material and pore structure and give rise to the cell performances.
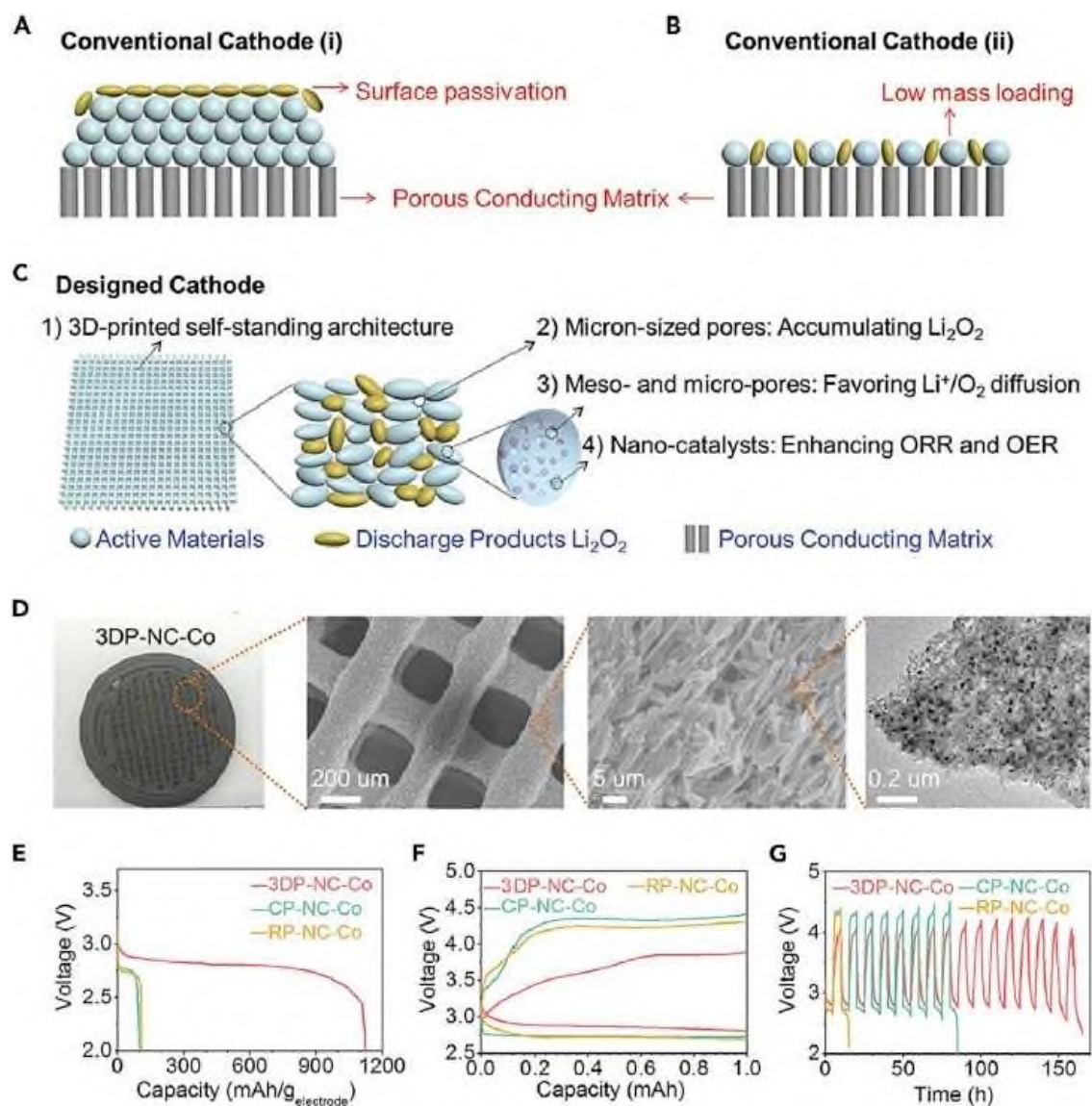
Figure 8.6 *Design of Air Electrode Structure in Non-aqueous MABs: (A and B) Schematic illustrations of Li_2O_2 growth on air electrodes with conventional structure. (C) Schematic illustration and advantages of 3D-printed self-standing and hierarchically porous catalyst framework as the air electrode. (D) Optical, SEM, and TEM images of 3DP-NC-Co. (E-G) First discharge curves at the current density of 0.05 mA cm^{-2}, (E) charge and discharge overpotentials at a limited capacity of 1 mAh, (F) and cycle abilities with the current density of 0.1 mA cm^{-2} (G) of 3DP-NC-Co and contrast samples in Li-O$_2$ batteries [686, 791].*

The air electrode reactions of Na-air and K-air batteries are not exactly identical to those of Li-air batteries for the different discharge products: Na_2O_2 and NaO_2 for Na-air batteries, and KO_2 for K-air batteries [635, 640, 687]. As Na$^+$ and K$^+$ could more effectively stabilize superoxide

ions than Li⁺, lower ORR overpotentials can be obtained on Na-air and K-air batteries [688]. Nevertheless, material designs of Na-air and K-air batteries are still required to regulate the growth and decomposition mechanism of discharge products, thus achieving better discharge capacity and Coulombic efficiency [689].

8.3.2 Gas-Diffusion Layer (GDL)

In the air electrode of MABs, the GDL is outside the electrocatalyst layer. Primary roles of the GDL include preventing electrolyte flooding and leakage, ensuring efficient gas diffusion between the electrolyte and ambient air and providing a conductive support for electrocatalysts and a mechanically stable. The gas-diffusion layer for fuel cells has been well studied, and commercial GDLs have been developed, which can be directly employed in MABs. The most commonly used materials for GDLs are woven carbon paper and non- woven carbon cloth, both composed of carbon fibers. GDLs are usually surface treated to reduce their affinity to the electrolyte and coated by a microporous layer of carbon powder on one side to strengthen the interaction with electrocatalysts. This type of commercial carbon fiber-based GDL has been widely utilized in MABs. Laboratory-made GDLs have also been reported. For instance, Yang et al. [691] fabricated a polydimethylsiloxane (PDMS)-based flexible and stretchable GDL for use in flexible Li-O₂ batteries. Liquid PDMS was poured on Ni foam and filled in the holes, and after the solidification of PDMS, the removal of Ni foam template, and drying in vacuum, the GDL was obtained. This new type of GDL exhibits excellent mechanical stability and flexible ability, which are essential features of the flexible LAB.

The degradation of the electrode may be caused by the corrosion of carbon-based GDLs, thus influencing the cycle life [692]. So, metal-based GDLs with higher electrochemical stability and electrical conductivity have also attracted much attention. Metal-based materials such as Ni foam [685, 693], stainless-steel mesh [692], and titanium mesh [694] have been investigated to serve as media for gas diffusion in both aqueous and non-aqueous MABs.

Until now, commercial carbon papers or carbon cloths have been used as GDLs in the majority of the reported MABs. For modifications on GDLs and developments of new types of GDLs in future research, the following issues need to be addressed. (1) Commercial GDLs are mainly designed for aqueous fuel cells. Surface treatments such as a coating of polyvinylidene difluoride or polytetrafluoroethylene are applied to improve their hydrophobicity. Nevertheless, such types of GDLs may not be suitable for organic electrolytes. For that reason, it is necessary to develop specialized GDLs according to the properties of electrolytes. (2) The electrocatalyst

layers are often combined with GDLs by drop casting or heat pressing. The weak interaction of electrocatalysts and GDLs may result in the immersion of electrocatalysts in the electrolyte, which blocks the contact between electrocatalysts and the oxygen. Therefore, the design of integrated air electrode structure is also worth investigating.

8.4 Material Design of Metal Electrodes

Metal electrodes of MABs face the challenges of electrode shape change, corrosion, side reactions, metal dendrites and surface passivation [641, 695]. For different types of metals, the key issues and the mitigation strategies can be different. In this section, the material design of the most investigated Zn and Li metal electrodes will be analyzed, and advances in other metal electrodes will also be shorty presented. It is worth mentioning that the solutions to the problems of the metal electrode can also be obtained from the research on the electrolyte and the separator.

8.4.1 Zn Electrode

Zinc-air batteries are usually filled with a high concentration of alkaline solution as the electrolyte. The reactions on the Zn electrode of alkaline Zn-air batteries are as follows:

$$Zn + 4OH^- \rightleftarrows Zn(OH)_4^{2-} + 2e^- \tag{8.1}$$

$$Zn(OH)_4^{2-} \rightleftarrows ZnO + H_2O + 2OH^- \tag{8.2}$$
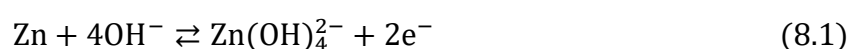
In the discharge process, the metallic Zn is oxidized to Zn^{2+} and then converted to zincate in the strong alkaline solution. After the zincate ions are saturated, the ZnO will precipitate as the final discharge product. The deposition of insulating ZnO on Zn electrode leads to the passivation of Zn, which is a key factor that determines the specific discharge capacity of Zn-air batteries [696]. In addition, the diffusion of zincate ions in the electrolyte makes the ZnO deposit not only on the Zn electrode but also on the air electrode and the inner side of the battery shell. Zinc oxides that are not deposited on the Zn electrode may cause the capacity loss and a low Coulombic efficiency. ZnO coated on the air electrode could also influence the performance of the oxygen electrocatalyst. Hence, the main target of the material design for the discharge process in Zn-air batteries is to regulate the ZnO deposition.

Factors that may cause Zn electrode failure in the charge process can be separated into two categories. The first one is the morphology change. The concentration of zincates is unevenly distributed in the electrolyte, as a function of the distance from the Zn electrode surface. That results to a preference to zincate ions to be deposited on protrusions of the Zn electrode surface during charge [641]. With continuous cycling, sharp needle-like Zn dendrites

would grow on the electrode surface, which can pierce the separator and even lead to short-circuit. Apart from dendrites, changes on the electrode thickness and surface area can also be observed during the cycling of Zn-based batteries [697]. The Zn electrode shape change can be attributed to the non-uniform distribution of the current and reaction zones on the electrode, bringing about densification of the electrode and a decrease in capacity [663]. The other issue is the hydrogen evolution on the Zn electrode. The hydrogen evolution reaction (HER) is the main side reaction on the Zn electrode of aqueous Zn-air batteries. The energy provided for charging would be partly consumed by hydrogen generation, resulting in low Coulombic efficiency. Additionally, the corrosion of Zn electrode could take place under non-operating status, due to the coupling of hydrogen evolution and zinc oxidation. This self-discharge process is also an important reason for the decay in capacity.

The main target for improving Zn electrode performance is to retain its original status after long discharge-charge cycles. Efforts made on the modification of Zn electrodes to improve their reversibility were focused on designing the electrode structure and introducing electrode additive [641, 645, 663]. Issues such as dendrites, ZnO deposition, and electrode corrosion are widespread problems for batteries with Zn as the metal electrode. Hence, some design strategies for Zn electrode in other types of Zn-based batteries can also be applicable in ZABs.

An optimized structure of Zn electrode can control the dissolution/precipitation process of Zn and ZnO and minimize the shape change of Zn electrode under long-time cycling [698]. Parker et al. proposed a 3D-structured Zn sponge with interconnected pores and long-range electrical conductivity and have utilized it as the Zn electrode in various types of Zn-based aqueous batteries [698-700].

Figure 8.7 (A) presents the application of 3D Zn sponge electrode in alkaline Ni-3D Zn batteries, in which the reactions on the Zn electrode are the same as those in Zn-air batteries [700]. In contrary to the serious dendrite problem on commercial Zn powder electrode, the 3D Zn sponge electrode exhibited minimal shape change with no dendrites observed. The high surface area and the monolithic structure of the 3D Zn sponge electrode also contributes to a high utilization efficiency of Zn. The battery achieved over 90 % of the theoretical capacity based on the mass of Zn, and more than 95 % of the capacity can be recovered in the charge process. The superior performance of the 3D Zn electrode can be attributed to the well-distributed current and electrolyte [698]. Nevertheless, the reduced resistance of HER due to the high electrical conductivity and high surface area of the 3D-structured Zn electrode should be examined [663].

Introducing surface coatings additives or surface coatings into Zn electrodes can regulate their interface structures and their chemical properties. Electrode additives are expected to improve the Zn electrode performance from the following aspects: (1) regulating the surface structure, electrical conductivity, and current distribution to inhibit the growth of dendrites; (2) limiting the migration of $Zn(OH)_4^{2-}$ to minimize electrode shape change and irreversible consumption; and (3) stabilizing the Zn electrode and preventing electrode corrosion.
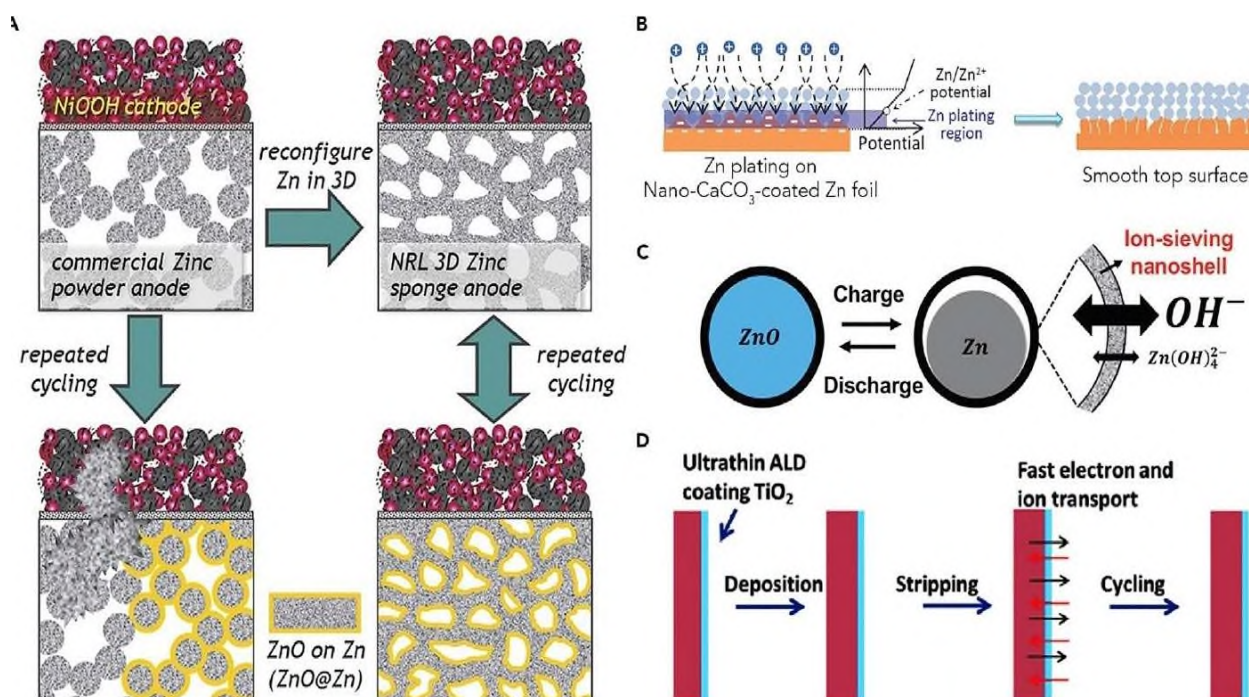
Figure 8.7 Regulation of the Structure and Composition of Zn Electrodes for Zn-Air Batteries: (A) Effect of the 3D sponge structure on the reversibility of Zn electrode. (B) Schematic illustrations of morphology evolution for nano-CaCO₃-coated Zn foils during Zn stripping/plating cycling. (C) The role of ion-sieving nanoshell on a ZnO nanoparticle on limiting zincate mitigation. (D) Schematic illustration of a thin TiO₂ to protect the Zn electrode [700-703, 791].

Carbon materials [704, 705], metals [706-708], and metal compounds [701, 709] have been investigated as additives for Zn electrodes to prevent dendrite formation. Kang et al. [701] coated nanoporous CaCO₃ on Zn foil to realize uniform Zn dissolution and precipitation. **Figure 8.7** (B) presents the mechanism for maintaining a smooth electrode surface by nano-CaCO₃ coating. On one hand, the high porosity of CaCO₃ layer induces uniform electrolyte flux and zinc dissolution/precipitation rate over the electrode surface. On the opposite, the insulating feature of CaCO₃ enlarges the potential gradient across the CaCO₃ layer. Thus, only the area near the electrode surface can provide negative enough potentials for Zn formation in the charge process, thus preventing the accumulation of Zn on the protrusions. When applied in rechargeable aqueous batteries, Zn electrode with nano-CaCO₃ coating afforded 42.7 % higher discharge capacity and over 15-fold longer cycle life than bare Zn foil.

The migration of $Zn(OH)_4^{2-}$ can be limited by ion-sieve coatings or additives with high affinity to $Zn(OH)_4^{2-}$. Carbon materials have been studied as Zn electrode coatings to limit zincate diffusion [702, 710]. Wu et al. [702] synthesized carbon shell coated ZnO nanoparticles as the metal electrode of Zn-based aqueous batteries. As presented in **Figure 8.7 (C)**, the carbon shell slows down the migration of zincate, and thus confines the anode shape change in a small space. At the same time, the carbon shell is permeable to smaller OH^- ions. When applied as metal electrode material in Ni-Zn batteries, the carbon shell coated ZnO exhibited about 1.6- and 6-fold longer cycle life than bare ZnO powder and Zn foil electrodes. Besides carbon materials, polymer coatings have also been used to control the zincate migration and the Zn electrode shape change [711]. For additives with high zincate affinity, Ca-based materials were greatly investigated because they can form solid compound $Ca(OH)_2 \bullet 2Zn(OH)_2 \bullet H_2O$ with zincate. Carbon materials with oxygen-containing groups have also been reported to form a hydrogen bond with zincates [710].

The stabilization of Zn electrode can be achieved by adding metals [712, 713], metal compounds [703, 714], and polymers [715] in the electrode. Lately, ultrathin TiO_2 coating on Zn plate was reported by Zhao et al. to mitigate hydrogen evolution and Zn corrosion in alkaline Zn-MnO_2 batteries [703]. The ultrathin TiO_2 of ≈ 5 nm was coated via an atomic layer deposition process. As illustrated by **Figure 8.7 (D)**, the ultrathin TiO_2 layer avoids the direct contact of the Zn electrode and the electrolyte while allowing fast electron and ion transport. The Zn-MnO_2 battery with the TiO_2-coated Zn plate as the metal electrode can maintain 85 % of the first capacity after 1,000 cycles, exhibiting much higher stability than pristine Zn plate with a cycle life of about 400 cycles.

According to the above, regulations on the composition and structure of Zn electrodes can mitigate the problems of corrosion, shape change, passivation, and dendrites, leading to a better reversibility of Zn electrodes. Similar strategies have also been applied on Mg and Al electrodes in aqueous batteries with similar challenges [716, 717].

8.4.2 Li Electrode

Li metal electrode is considered the ''Holy Grail'' in energy-storage systems due to its high theoretical specific capacity (3,860 mAh g^{-1}), low density (0.59 g cm^{-3}), the lowest negative redox potential (-3.04 versus standard hydrogen electrode) [719]. Lithium metal batteries (LMBs), including Li-S and Li-air batteries, have been mostly examined as next-generation energy-storage devices [719, 720]. In the research on LMBs, the inhibition of Li dendrites has attracted most attention [721]. Similar to Zn dendrites as discussed above, Li dendrites can lead to degradations in

specific capacity, Coulombic efficiency, stability, and so forth. More seriously, as Li is much more active than Zn, the piercing of the separator and the circuit shortcut can cause severe safety issues [722]. In addition to the dendrite problem, which is common for all types of LMBs, the Li electrode in Li-air batteries also suffers from the O_2 crossover effect [723]. The diffusion of O_2 from the air electrode induces the electrolyte decomposition and the formation of LiOH and carbonates on the Li electrode [724]. At the same time, the influence of H_2O, CO_2, and N_2 on the Li electrode stability when LABs are operated in ambient air should not be ignored [725]. To solve these problems, material design methods for Li electrode, electrolyte, and separator have been announced [637]. In this section, modification strategies for Li metal electrode are outlined.

The performance of Li metal electrodes can be improved by applying a 3D Li host [726-729], tuning the electrode composition [649, 730-732] and surface coating [730, 733-736]. One important target of applying these regulation methods is to control the current distribution and ion flow, so changing the nucleation and deposition behavior of Li and inhibiting the Li dendrite growth [728, 737]. Lately, Guo et al. [738] applied this strategy to stabilize Li metal anodes for Li-air batteries by using lithiophilic Co/Co_4N nanoparticles to regulate lithium nucleation and deposition. The anode was fabricated by depositing Li on MOF-derived hollow N-doped carbon-based cubes with uniformly embedded Co/Co_4N nanoparticles (Co/Co_4N-NC), as presented in **Figure 8.8 (A)**.

Lithiophilic functional groups such as N heteroatoms in carbon and Co_4N promote the homogeneous nucleation of Li deposits, and the porous carbon structure provides high Li-storage capacity. Thus, the lithiated Co/Co_4N-NC electrode exhibits a smooth and dendrite-free morphology [**Figure 8.8 (B)**]. When serving as the metal electrode of a Li-air battery, the lithiated Co/Co_4N-NC electrode remained reproducible after 70 cycles at a current density of 200 mA g^{-1} and a limited specific capacity of 500 mA g^{-1} [**Figure 8.8 (C)**].

On the contrary, pure Li electrode failed after only 34 cycles in the same testing condition. The solid electrolyte interface (SEI) formed on the surface of Li electrode in Li metal batteries is considered to be favorable for enhancing the cycling ability of the Li electrode as a protective layer [730, 739]. Hence, approaches have been developed to improve the stability and uniformity of SEI or build an artificial SEI to stabilize Li electrode [719, 733-736]. The protective layer for the Li electrode in LABs is required to afford properties such as high mechanical strength to suppress the Li dendrite growth, low O_2 and H_2O permeability to protect the Li electrode, good electronic insulation to avoid electrolyte decomposition, high ionic conductivity to ensure fast Li-ion diffusion, and high stability. Given these requirements, Liao et al. [734] created a Ge-based artificial SEI layer on the Li surface to allow stable cycling of Li-O_2

batteries. The protective layer was generated by immersing Li foil in GeCl$_4$-tetrahydrofuran steam. The as-synthesized film is about 1.5 mm thick with micrometer-scale spheres containing amorphous germanium (Ge and GeO$_x$) and lithium compounds (Li$_2$CO$_3$, LiOH, Li$_2$O, and LiCl). This protective layer is robust enough to suppress the Li dendrite growth and keep the Li surface smooth after Li plating/stripping cycling and is also able to protect the Li electrode against H$_2$O attack, as presented in **Figure 8.8 (D)**. As a result, the LAB with Ge-based artificial SEI layer on Li electrode can be stably discharged and charged over 150 cycles in humid O$_2$ with 45 % relative humidity.
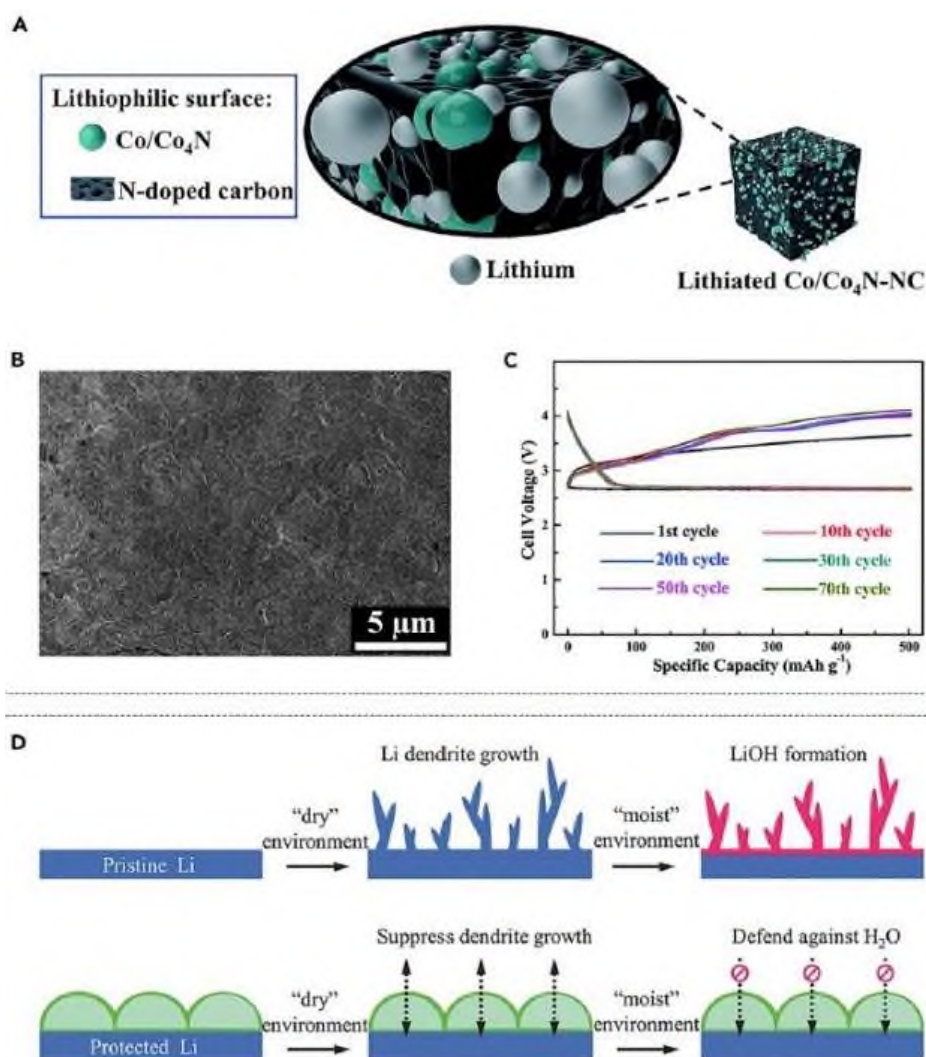
Figure 8.8 Design of Lithium-Containing Electrodes and Lithium Surface Coatings for Li-Air Batteries: (A) Schematic illustration of lithiated Co/Co$_4$N-NC nanoparticles. (B) SEM image of Co/Co$_4$N-NC electrode after Li deposition with a limited capacity of 2.0 mAh cm^{-2}. (C) Discharge/ charge profiles of the LAB using the lithiated Co/Co$_4$N-NC electrode at a current density of 200 mA g^{-1} with a limited capacity of 500 mAh g^{-1}. (D) Schematic illustration of Li plating/ stripping on pristine lithium electrode and protected lithium electrode [734, 738, 791].

Na and K electrodes face challenges similar to those of the Li electrode, including O$_2$ crossover and dendrite growth. Similar strategies have also been developed to improve the performances of Na and K electrodes [740, 741].

The development of stable and reversible metal electrodes for metal batteries has attracted much attention recently, and most of the battery performances are tested in a closed system [721, 742]. For the open system of MABs, the side reactions on the metal electrode can be more complicated [743]. So, specific requirements for MABs need to be under consideration when adopting the metal electrode design methods for other metal-based batteries.

8.5 Material Design of Electrolytes

8.5.1 Aqueous Electrolytes

MABs with water-stable metal electrodes, such as Al-air batteries and Zn-air batteries and Al-air, usually use aqueous alkaline electrolytes [636, 639]. Compared with acidic and neutral electrolytes, MABs with alkaline electrolytes can reach better oxygen electrocatalysis activity and higher metal corrosion resistance [663]. Among the commonly used alkaline electrolytes including NaOH, KOH and LiOH, concentrated KOH solutions, with the highest ionic conductivity and the lowest viscosity, are most frequently employed in MABs [663].

Alkaline electrolytes are sensitive to the CO_2, resulting in the formation of carbonates and decrease in electrolyte concentration. The adsorption of CO_2 has been confirmed to have negative effects on the capacity and cycle life of ZABs [636]. In addition, strong alkaline electrolytes are also environmentally unfriendly. Thus, proper neutral electrolytes for MABs have been examined [744, 745]. For the future development of neutral electrolytes, electrocatalysts with high OER and ORR activity in neutral conditions are highly desirable.

As above discussed, metal electrodes in aqueous MABs suffer from issues such as dendrite growth, passivation, hydrogen evolution and dendrite growth. Some of these issues can be mitigated by the material design of the electrolyte [706, 746]. In addition, aqueous electrolytes have also been used in the air electrode side of LABs to enhance the tolerance to ambient air and the electrolyte stability [747]. In this case, solid-state glass ceramic electrolytes are commonly used to protect the Li electrode [636, 659].

8.5.1.1 Aqueous Electrolytes for Improving Metal Electrode Performance

Much research on ZABs used 6 M KOH solution with 0.2 M zinc chloride or zinc acetate as the electrolyte [638, 660]. The additional zinc ions convert to zincate ions in strong alkaline solution, which can improve the reversibility of the metal electrode and the rechargeability of the battery [748]. Zincate ions generated on the Zn electrode rapidly precipitate as ZnO in a concentrated zincate solution and thus the migration of zincate ions is limited, leading to a minimized shape change.

Modifications on the KOH electrolyte such as reducing the KOH concentration and adding potassium salts have been investigated to reduce the zincate solubility, thus minimizing the Zn electrode shape change [663], mostly applied on Ni-Zn batteries [749].

The reversibility of Zn electrodes can also be enhanced by changing the existing form of zinc species in the electrolyte. Wang et al. [658] studied a highly concentrated Zn-ion electrolyte (HCZE) to realize dendrite-free Zn plating/stripping at nearly 100 % Coulombic efficiency. In this 1 mol kg^{-1} Zn(TFSI)$_2$ + 20 mol kg^{-1} LiTFSI electrolyte (TFSI, bis(trifluoro-methanesulfonyl)imide), zinc ions are surrounded by TFSI ions instead of water. The Zn^{2+}-solvation sheath occupied by TFSI suppressed the hydrogen evolution on the Zn surface, leading to a reversible and dendrite-free Zn plating/stripping. In a Pt/Zn coin cell with HCZE, the Zn plating and stripping at a constant current density exhibited ≈99.5 % Coulombic efficiency after the first three cycles [**Figure 8.9 (A)**].
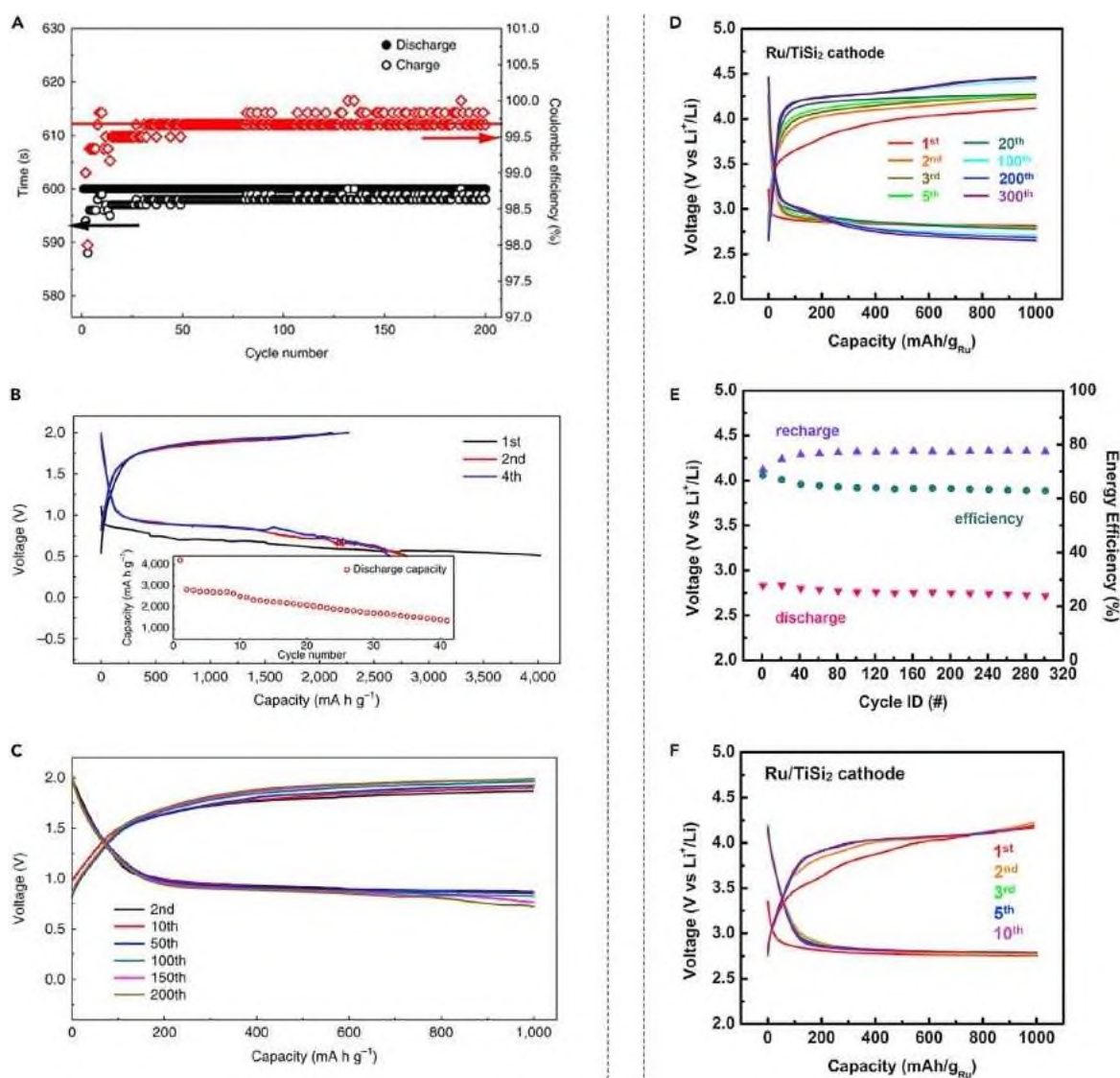
Figure 8.9 Modifications of Aqueous Electrolytes to Improve Metal Electrode Performance to Be Employed in LABs: (A) Zn plating/stripping time (left) and Coulombic efficiency at the current density of 1 mA cm^{-2} on Pt electrode in HCZE. (B) Full-range voltage profile of the ZAB in HCZE with 70 wt % super P as the air electrode at a constant current of 50 mA g^{-1} (based on the air

electrode). (C) Cycling performance of the ZAB in HCZE at a constant current of 50 mA g^{-1} and a limited capacity of 1,000 mAh g^{-1}. (D) Cycling performance of the LAB in WiS electrolyte with LFP as pseudo-metal electrode and Ru/TiSi$_2$ as air electrode. (E) Average voltage and round-trip energy efficiencies as a function of cycling numbers calculated from the data in (D). (F) Cycling performance of the LAB in WiS electrolyte with protected Li metal electrode and Ru/TiSi$_2$ air electrode [657, 658, 791].

When applying HCZE in a Zn-air cell with carbon paper as air electrode, the cell delivered a capacity of ≈3,000 mAh g^{-1} and discharge/charge voltages of around 0.9/1.9 V at 50 mA g^{-1} [**Figure 8.9 (B)**]. The Zn-air battery also showed good stability after 200 cycles at a limited capacity of 1,000 mAh g^{-1} and a current density of 50 mAh g^{-1} [**Figure 8.9 (C)**]. Lee et al. [750] used alkoxide and acetate ions as additives in a KOH electrolyte to replace hydroxide ions in zincate. The formation of ZnO was suppressed by this method, resulting in enhanced reversibility of the Zn electrode. Electrolyte additives have also been utilized to enhance the performance of metal electrodes beyond zinc. Aluminum is highly active in alkaline solutions, and electrolyte additives, named as corrosion inhibitors in aluminum electrode research, have been studied to prevent Al self-corrosion in Al-air batteries [639, 751-753].

8.5.1.2 Aqueous Electrolytes for Li-Air Batteries

The use of aqueous lithium salt solutions as electrolytes for LABs can avoid the side reactions and electrolyte decomposition problems caused by organic solvents. Nevertheless, the application of aqueous electrolytes for Li-based batteries is limited by their narrow potential window [754]. The high-voltage operation of aqueous electrolytes can be achieved by eliminating free water molecules in the electrolyte, for instance by using high concentration water-in-salt (WiS) electrolytes [755] or hydrate-melt electrolytes [756]. Lately, Dong et al. [657] designed a water-in-salt system with superconcentrated 21 mol kg^{-1} LiTFSI to serve as the electrolyte for LABs. The LAB with WiS electrolyte, Ru/TiSi$_2$ as air electrode, and LiFePO$_4$ (LFP) as pseudo-metal electrode exhibited stable cycling performance for 300 cycles at a discharge depth of 1,000 mAh g^{-1} Ru [**Figure 8.9 (D)**], and the energy efficiency remained higher than 62 % [**Figure 8.9 (E)**].

When using as metal electrode, glass ceramic-protected Li, the LAB delivered good polarization performance but poor stability [10 cycles, **Figure 8.9 (F)**]. For that reason, the engineering of the electrolyte and the electrode should be considered together in the full cell design of MABs.

8.5.2 Organic Electrolytes

Aprotic organic electrolytes are widely employed in MABs with metal electrodes that are unstable in water, such as Na and Li. Optimizations of this type of electrolyte have been studied with respect to metal salt solutes, electrolyte additives and organic solvents. The material designs are mostly aimed at enhancing the air/metal electrode performance and improving the stability of the electrolytes.

8.5.2.1 Electrolyte Stability

In MABs, the superoxide species generated on the air electrode can cause the decomposition of organic solvents, forming CO_2, H_2O, and metal carbonates [33, 45]. Thus, unceasing efforts have been made in searching for stable organic solvents that meet the standards for MABs, including wide potential window, high oxygen solubility, low volatility in air, and high solvation of superoxides/peroxides and good metal ion conductivity [675]. Carbonate-based solvents were firstly investigated but were then under the attack of superoxide species found to be unstable [662, 674]. Ether-based solvents were then studied and confirmed to be more insusceptible to reduced oxygen species than carbonate-based solvents [757]. Nevertheless, research on LABs has revealed that the O_2 crossover could induce the decomposition of ether-based electrolytes on the Li electrode [724]. Other types of organic solvents including sulfoxide-based and amide-based solvents have also been employed in MABs [687]. A protective layer on the metal electrode is usually needed for better electrolyte stability [675, 687].

Metal salt solutes are another essential part of organic electrolytes. Highly soluble metal salts with stable anions are recommended for metal-air batteries. Taking LABs as an example, lithium salts including $LiPF_6$, $LiClO_4$, LiBr, $LiNO_3$, LiTFSI, and $LiCF_3SO_3$ have been studied [758]. The discharge product Li_2O_2 and other oxygen species are the major cause of the decomposition of lithium salts, especially for that with F-containing anions [637]. The stability of metal salts also varies with the type of electrolyte solvents and the concentration [759, 760]. Therefore, the optimization of metal salts and organic solvents should be considered together for better electrolyte stability.

8.5.2.2 Organic Electrolytes for Improving Air Electrode Performance

Regulation of the electrolyte in non-aqueous MABs can improve the air electrode performance by increasing the superoxide/peroxide storage during the discharge process and facilitating the superoxide/peroxide decomposition during charge process. Influences of

electrolyte solvents, metal salts, and additives on the Li_2O_2 generation and decomposition have been intensively studied in LABs [675, 761].

On the air electrode of LABs, oxygen is first reduced to O_2^-. The solubility of superoxide intermediates depends on the donor number (DN) of the electrolyte solvent, which represents the solvent basicity according to the HSAB theory [675]. Solvents with high DN can afford higher stability for the (Li^+-[solvent]$_n$-O_2^-) complex [659, 674] and induce a solution growth mechanism for Li_2O_2 formation, whereby soluble LiO_2 disproportionates into Li_2O_2 and O_2 in solution. On the contrary, the oxygen reduction in low-DN solvents obeys the surface mechanism. LiO_2 is adsorbed on the electrode surface and then electrochemically reduced to an insulating film of Li_2O_2 on the Li surface [761]. Thus, electrolytes with high-DN solvents are beneficial for achieving high capacity in MABs. Moreover, the lithium salts and water content in the electrolyte also affect the Li_2O_2 growth mechanism, as presented in **Figure 8.10 (A)** [762].
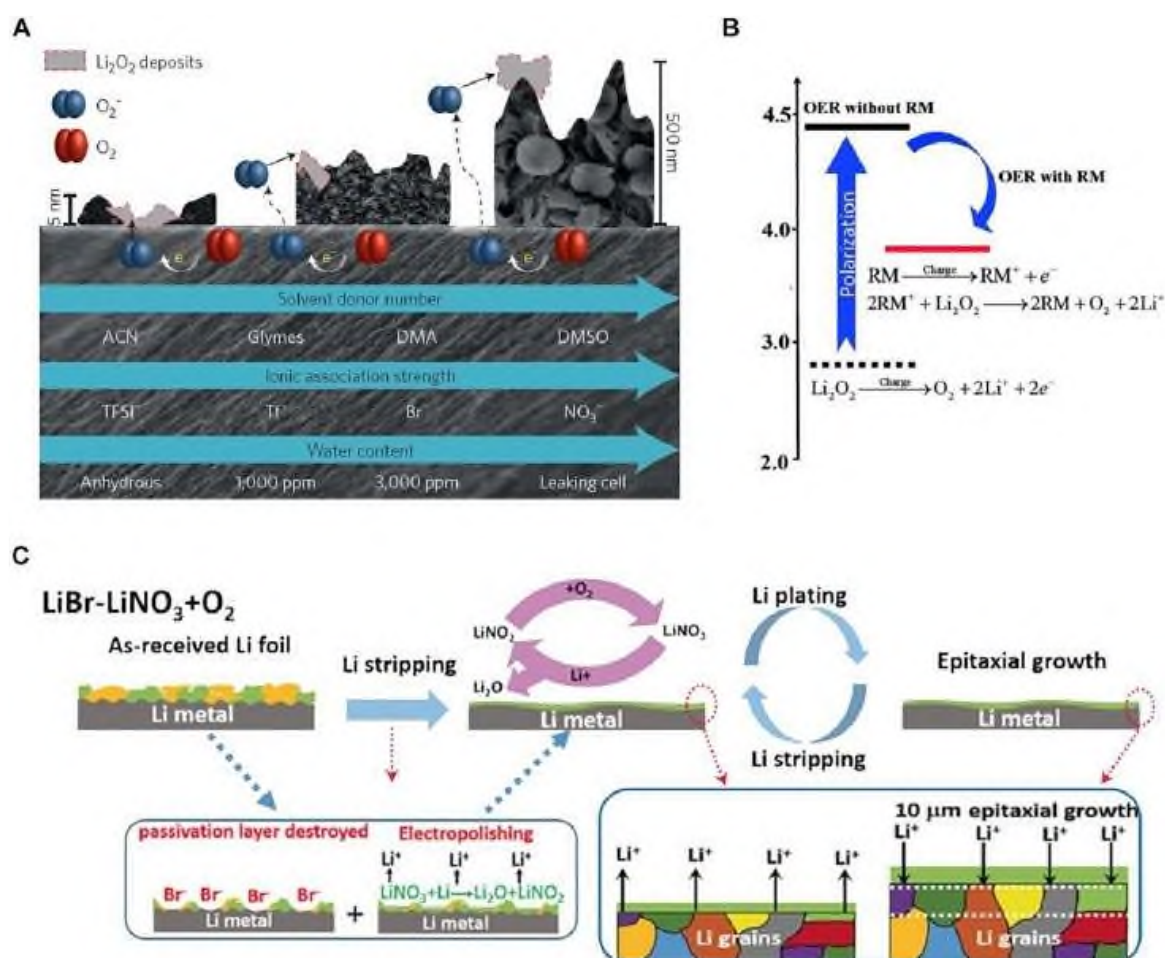
Figure 8.10 Material Designs of Non-aqueous Electrolytes with Organic Solvents and Their Effects on the Performance of Air Electrode and Metal Electrode of MABs: (A) Effects of solvents, lithium salts, and water content on the Li_2O_2 growth mechanism on air electrodes. can, acetonitrile; glymes, polyethers $(CH_3O(CH_2CH_2O)_nCH_3)$; DMA, dimethylacetamide; DMSO, dimethyl sulfoxide; Tf$^-$, trifluoromethanesulfonate. (B) Diagram of the mechanism and the suitable redox potential region of redox mediators. (C) Schematic illustration of dendrite-free epitaxial growth of Li in LiBr-LiNO$_3$ electrolyte under O_2 atmosphere. [762-764, 791].

This indicates that a trace amount of water in the electrolyte can be favorable for the air electrode performance, while the parasitic reactions induced by water should also not be ignored.

In the charge process of LABs, the oxidation of Li_2O_2 primarily occurs at the contacting part of the Li_2O_2 and the solid electrocatalyst, resulting in insufficient charging and low Coulombic efficiency. Hence, a specific type of electrolyte additive, called redox mediators (RMs), has been employed in LABs to promote the Li_2O_2 decomposition by catalyzing the reaction in the solution [653]. At the same time of charging, RMs are first oxidized on the air electrode, after which the oxidized RMs react with Li_2O_2 to form Li^+ and O_2. A suitable RM for this process needs to be soluble and stable in the electrolyte, and its redox potential should be in an appropriate range to reduce the charge overpotential, as presented in **Figure 8.10** (B) [763]. Since now various materials including organic, organometallic, and halide materials have been investigated as RMs in LABs [661]. RMs for the ORR process have also been developed to improve the discharge capacity and to regulate the Li_2O_2 formation [765].

8.5.2.3 Organic Electrolytes for Improving Metal Electrode Performance

One strategy in the material design of the metal electrode is to build a protective layer on the metal electrode to suppress the dendrite growth and avoid side reactions [730]. The protective layer can be coated on the metal electrode before the fabrication of a MAB and can also be generated in the metal-air battery with the assistance of the electrolyte [764, 766, 767]. The formation of an ultrathin and homogeneous SEI layer on the Li electrode in a Li-air battery with LiBr-LiNO$_3$ dual-anion electrolyte was reported by Xin et al. [764]. **Figure 8.10** (C) schematically presents Li stripping and plating in the LiBr-LiNO$_3$ electrolyte. In the discharge process, Br$^-$ ions promote the corrosion of the original irregularly shaped SEI layer, and NO$_3^-$ ions immediately passivate the Li surface to form a thin Li_2O-rich SEI layer. This thin and homogeneous SEI layer contributes to a dendrite-free epitaxial growth of Li in the charge process. This leads to, a stable cycle performance of more than 900 h at the current density of 0.5 mA cm^{-2}.

8.5.3 Ionic Liquid Electrolytes

Room-temperature ionic liquids are a type of salts whose melting point is below 100 ºC and composed of large organic cations and organic/inorganic anions. Ionic liquids are promising alternatives for the electrolyte solvents in both aqueous and non-aqueous electrolytes due to their low volatility, high ionic conductivity, nonflammability and wide potential window

[637, 646, 663]. Ionic liquids can benefit metal-air battery performance from various aspects. Shiga et al. [768] employed ionic liquid electrolyte in a Ca-air battery to enhance the reversibility of Ca stripping/plating. Thomas et al. [769] designed a Li-air battery with [Li(G4)][TFSA] electrolyte (G4 = tetra-glyme, TFSA = bis(trifluoromethanesulfonyl)amide). Benefited by the hydrophobic nature of ionic liquids, the LAB exhibited high moisture resistance. Ionic liquids were also studied as electrolyte additives. A tetramethylpiperidinyloxyl (TEMPO)-grafted ionic liquid (IL-TEMPO) was synthesized by Zhang et al. [770] and employed as an electrolyte additive in LABs. The TEMPO group functions as the redox mediator and oxygen shuttle, and the imidazolium moiety facilitates the formation of a stable SEI layer. The IL-TEMPO can also serve as the electrolyte solvent to enable the operation in atmospheric air. Asadi et al. [771] introduced a LAB with a mixed electrolyte of 25 % ionic liquid 1-ethyl-3-methylimidazolium tetrafluoroborate (EMIM-BF4) and 75 % dimethyl sulfoxide (DMSO). This electrolyte is stable in the Li-air system and affords high LiO_2 solubility to ensure the solution growth mechanism of Li_2O_2. The strong binding of H_2O and CO_2 in the ionic liquid also prevents side reactions on Li_2O_2.

8.5.4 Solid-State Electrolytes

In comparison with liquid electrolytes, solid-state electrolytes can avoid the problems of electrolyte leakage, gas crossover and electrolyte evaporation [637]. Additionally, the application of solid-state electrolytes is favorable for improving the energy density of MABs, and at the same time enables the fabrication of flexible and wearable devices [772]. For the development of solid-state electrolytes for MABs, suitable materials with high ionic conductivity, wide potential window, and chemical stability are required [773].

8.5.4.1 Gel-Polymer Electrolytes

Gel-polymer electrolytes consist of a 3D polymer skeleton with a liquid electrolyte expanded throughout its whole volume to afford fast ion transport similar to liquid electrolytes, as well as high flexibility. Recently gel-polymer electrolytes have been widely investigated in both aqueous and non-aqueous flexible MABs [656, 774, 775].

MABs with gel-polymer electrolytes suffer from the quick loss of electrolyte solvents and the limited stability of polymer frameworks, resulting in short cycle life. Thus, stable, solvent-retaining gel-polymer electrolytes are highly desired for extending the battery lifetime. Taking into account this, Huang et al. [776] studied a sodium polyacrylate hydrogel (PANa) for flexible ZABs. ZAB with PANa electrolyte exhibited stable cycling performance at 2 mA cm^{-2} for 160 h

[**Figure 8.11** (A)], significantly superior to traditional polyvinyl alcohol (PVA) electrolyte, which showed a rapid drop of round-trip efficiency from 60.4 % to 29.3 % after only 16 h.

In addition, the electrostatic interactions between acrylate ions in PANa and Zn ions induce the formation of a quasi-SEI layer to avoid Zn dendrite growth [**Figure 8.11** (B)]. For flexible LABs, gel-polymer electrolytes have been reported to ensure the flexibility and protect the Li electrode from corrosion in ambient air [777, 778].
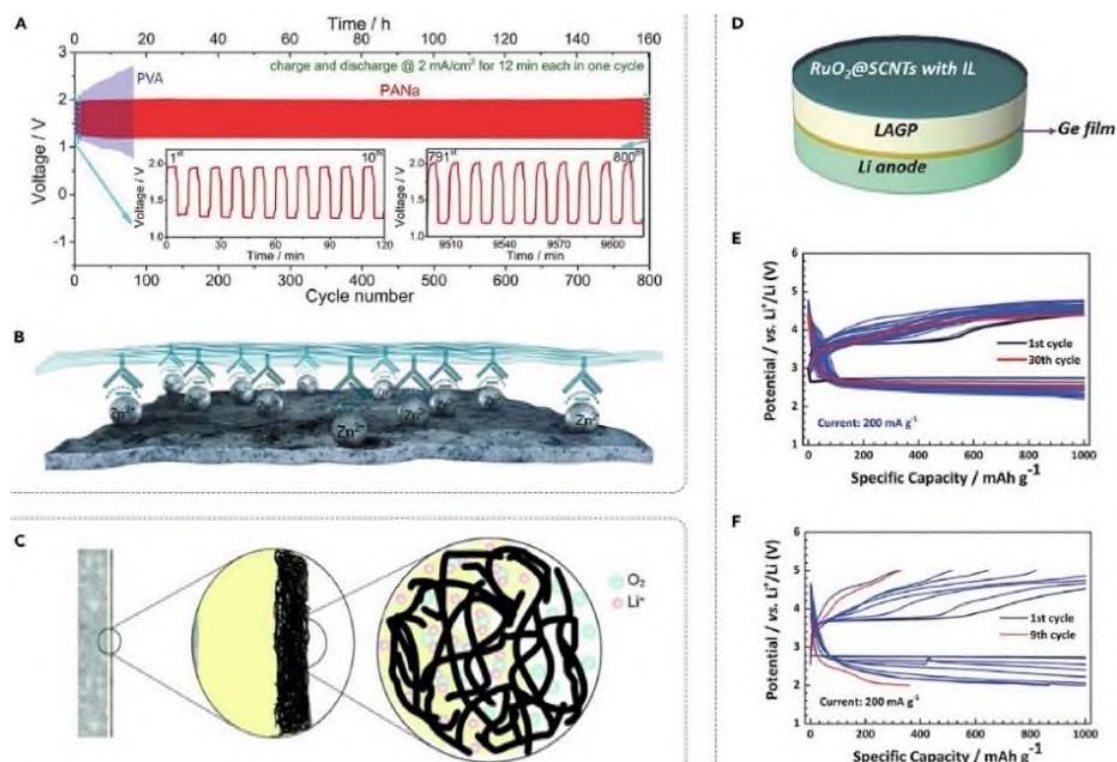
Figure 8.11 Applications and Optimization Methods of Solid-State Electrolytes for MABs: (A) Galvanostatic discharge-charge cycling curves at 2 mA cm^{-2} of ZABs with PANa and PVA gel polymer electrolytes. (B) Schematic illustration of the formation of quasi-SEI to prevent Zn dendrite growth. (C) Schematic illustration of a LAB with a solid polymer electrolyte. (D) Schematic diagram of a LAB with Ge film-coated LAGP solid-state electrolyte. (E and F) Cycling performance of LABs with Ge film-coated LAGP (E) and uncoated LAGP (F) at a constant current of 2,000 mA g^{-1} and a limited capacity of 1,000 mAh g^{-1}. [776, 779, 791].

8.5.4.2 Solid Polymer Electrolytes

Similar to gel-polymer electrolyte, a solid polymer electrolyte is composed of an ion-conducting polymer matrix, but not swollen with liquid solvents. Due to the absence of liquid solvents, the ionic conductivity in solid polymer electrolytes is limited [781]. Commonly investigated polymer materials for solid polymer electrolytes include polyacrylonitrile (PAN), poly(carbonate-ether), and poly(ethylene oxide) (PEO) [637]. **Figure 8.11** (C) schematically illustrates a LAB with PEO-based electrolyte proposed by Balaish et al. [779]. But, this LAB was operated at 80 °C, above the melting point of the poly(ethylene oxide)-lithium triflate

electrolyte, to obtain acceptable ionic conductivity. Theoretical studies on the ion-conduction mechanisms revealed that polymers with lower glass transition temperature (T_g) and more amorphous structure could provide higher ionic conductivity [781].

8.5.4.3 Ceramic Electrolytes

Inorganic ceramic electrolytes, including LISICON (Li^+ superionic conductor), NASICON (Na^+ superionic conductor), perovskite, garnet, and sulfides, have demonstrated their applications in solid-state Li and Na metal batteries [773]. The high mechanical strength of ceramic electrolytes is favorable for mitigating the dendrite growth on the metal electrode [781]. For better performance of MABs with ceramic electrolytes, the material design on ceramic electrolytes mostly focuses on the following points: the stability with Li/Na metal, the electrolyte-electrode interfacial contact and the ionic conductivity [772, 773, 780, 782].

Liu et al. [780] reported a protective film between the Li electrode and a NASICON type solid-state electrolyte to protect the electrolyte and enhance its contact with the Li electrode. The NASICON type solid electrolyte LAGP ($Li_{1.5}Al_{0.5}Ge_{0.5}P_3O_{12}$) exhibits high lithium ionic conductivity and good mechanism strength, but Ge^{4+} ions are feasible to be reduced to Ge^0 and Ge^{2+} on the Li electrode, leading to a decrease on the Li-ion conductivity. To alleviate this problem, an amorphous Ge thin film is introduced between LAGP and the Li electrode, as presented in **Figure 8.11 (D)**. This Ge film can suppress the reduction of Ge^{4+} and also form a Li ionic interlayer to ensure intimate contact between Li metal and the solid electrolyte. Thus, the solid-state LAB with Ge/LAGP electrolyte exhibited stable cycling performance at 200 mA g^{-1} for 30 cycles [**Figure 8.11 (E)**], while the LAGP electrolyte without Ge coating showed much inferior stability [**Figure 8.11 (F)**]. Nevertheless, the cycling stability of 30 cycles is still far from satisfactory, and further investigations of solid-state MABs with performances acceptable for practical use are required.

8.6 Material Design of Separators

A separator is a membrane placed in the electrolyte between the electrodes to avoid direct contact of the electrodes while permitting the ionic flow. An ideal separator should be electronic insulating, inert to chemical reactions, and with no resistance for ionic transport, while separators in reality could only be close to the ideal status, with acceptable electronic/ionic resistivity and chemical stability [783]. Materials for battery separators include polymer films, solid ion conductors and woven fibers [783]. Apart from the basic functions, a separator can also

improve the MAB' performance by limiting the migration of some specific ions or molecules [784-790].

In ZABs, the migration of zincate ions to the air cathode is responsible for the loss of Coulombic efficiency and also influences the activity of oxygen electrocatalysts. Hence, separators that suppress zincate crossover have been studied to solve this problem [786, 787]. Kim et al. [787] introduced a polymer blend electrolyte (PBE) membrane composed of ion-conducting PVA/PAA (PAA = polyacrylic acid) and ion-repelling Nafion as the separator of ZABs. The Nafion phase can limit the diffusion of zincate ions by the Donnan exclusion effect, thus minimizing the formation of ZnO on the air electrode, as presented in **Figure 8.12** (A).

The ZAB with the PBE separator showed electrochemical rechargeability over 2,500 min at 20 mA cm^{-2}. On the other hand, the ZAB with commercial Celgard3501 separator reached the cutoff voltage after only 900 min. For LABs, to prevent the decomposition of redox mediators on the Li electrode, one solution is to apply an RM-sieving separator to restrain the shuttling [788, 789]. Lee et al. [789] modified a commercial glass fiber (GF/C) separator with a polymer mixture of PEDOT: PSS (poly(3,4-ethylenedioxythiophene) polystyrene sulfonate) to suppress the migration of the redox mediator DMPZ (5,10-dihydro-5,10-dimethylphenazine) in LABs.
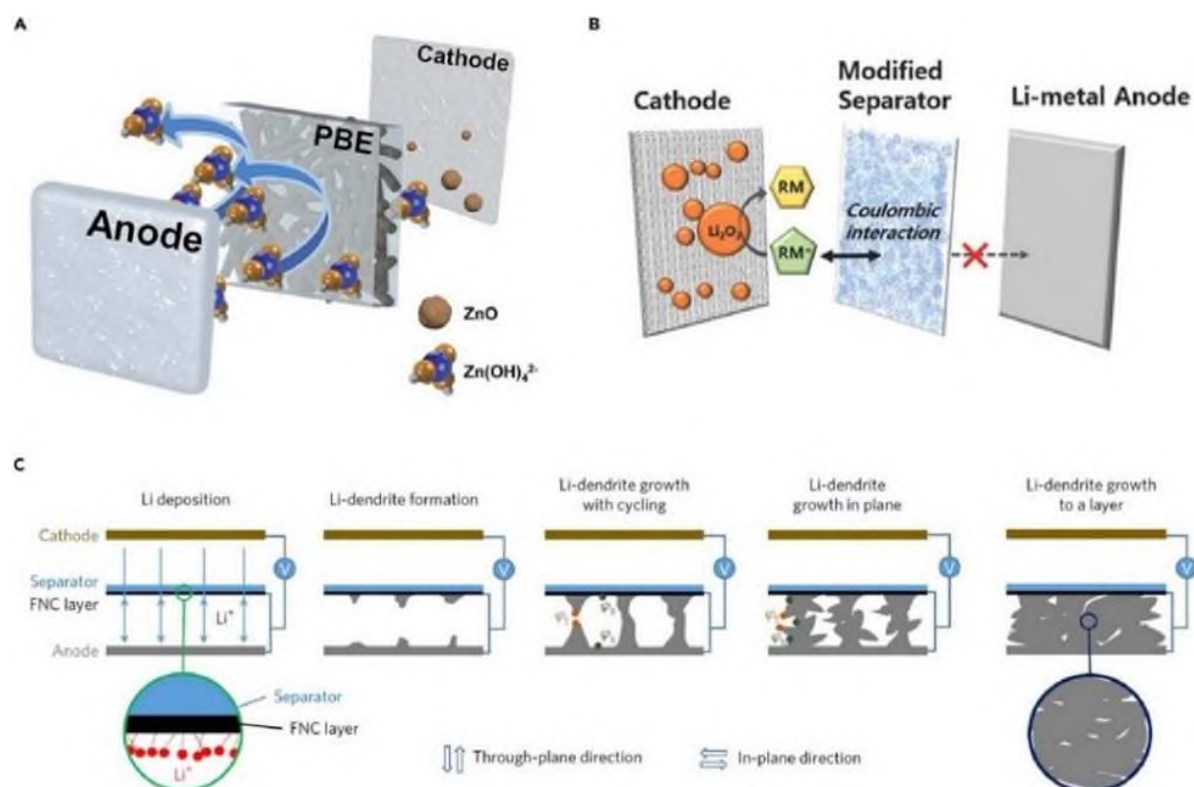
Figure 8.12 *Material Design of Separators to Improve the Performance of MABs: (A) Conceptual illustration of the role of PBE separator on mitigating zincate crossover in ZABs. (B) Schematic illustration of a modified separator to suppress the migration of redox mediators in LABs. (C) Li dendrite growth in a cell with FNC-coated separator. φ_s and φ_t represent the potentials at the base and the tip of the dendrite, respectively. The potential difference of φ_t and φ_s is the driving force for the dendrite growth. [787, 789-791].*

The role of this modified separator is presented in **Figure 8.12 (B)**. The negatively charged groups in the separator interact with DMPZ$^+$ by Coulombic interactions, thus preventing DMPZ$^+$ from diffusing to the Li electrode. As a result, the LAB with this modified separator and high concentration of DMPZ exhibited stable cycling performance of 90 % round-trip efficiency for more than 20 cycles. The modification on the separator was also reported to control the dendrite growth of metal electrodes. Liu et al. [790] presented a unique method of coating functionalized nano-carbon (FNC) on the commercial Celgard separator of Li metal batteries to prevent the short-circuit caused by dendrites. Battery configuration is illustrated in **Figure 8.12 (C)**. The FNC layer is immobilized with Li$^+$ ions and electrically connected to Li electrode. When charging, Li dendrites grow from both the Li electrode and the FNC layer, in the through-plane direction. With cycling, the dendrites from the opposite directions contact with each other and then grow in the in-plane-direction instead of piercing through the separator. Finally, a dense Li metal layer is formed between the Li anode and the separator. In Li/Li symmetric cells with various types of electrodes, the cells with FNC-coated separators exhibited improved cycle life and Coulombic efficiency compared with the blank cells with clean Celgard separators.

8.7 Key materials of flexible ZABs

Flexible cathode, solid electrolyte and flexible zinc anode are the three main components and also the decisive factors affecting the performance of flexible ZABs. This section will comprehensively introduce the current research status and development trend of these three key materials.

8.7.1 Flexible cathode

The flexible cathode is composed of a current collector and an ORR/ OER bifunctional catalyst supported thereon. According to the different combination modes of current collector and catalyst, it can be divided into bifunctional catalyst containing binder and self-supporting bifunctional catalyst. The development process will be introduced from these two aspects below.

8.7.1.1 Bifunctional catalyst containing binder

The kinetically sluggish ORR/OER processes severely limit the catalytic effectiveness of the air electrode, which therefore has an impact on the performance of ZABs [815]. As a result, it is critical to fabricate cathode catalysts with high catalytic activity. In fact, under both acidic and alkaline conditions, the most practicable ORR catalysts are platinum [816-819]. Platinum has

gotten a lot of interest since Balantin researched the binding energy of the catalyst and developed the volcano map in 1969. Platinum is the element with the most moderate binding energy.

Nevertheless, due to the disadvantages of limited raw resources and high cost, researchers have been focusing on non-noble metal catalysts to replace noble metal catalysts. Among these researches, carbon-based catalysts are the most active ones. It can be divided into transition metal doped carbon based catalysts and non metal doped carbon based catalysts [820]. Non metal doped carbon based catalysts refer to ORR catalysts synthesized with carbon materials as matrix and N [821, 822], O [823, 824], B [825, 826], P [827, 828], S [829, 830] and F [831, 832] as doped elements, especially N-C materials. Although the cost of non-metal-doped carbon-based materials is extremely low, it is difficult to become a strong competitor of noble metal catalysts due to poor catalytic activity. In comparison, the catalytic activity of transition metal doped carbon based catalysts has reached or even exceeded that of noble metal catalysts. Transition metal doped carbon based catalysts are noble metal like catalysts with Fe [833, 834], Co [835, 836], Mn [837, 838] and Ni [839, 840] as active sites. Because of its wide source of raw materials, high catalytic activity and good stability, it is the mainstream research direction of non-noble metal catalysts [841-843].

OER catalysts, like ORR catalysts, are nowadays commonly used noble metal catalysts such as RuO_2 and IrO_2. Researchers are also exploring for high-performance non-noble metal based OER catalysts to replace RuO_2 and IrO_2, with transition metal hydroxyl oxides serving as an example [844, 845]. FeOOH [846-848], NiOOH [849-851] and CoOOH [852-854] hydroxyl oxides have OER performance that is comparable to or even better than noble metal based catalysts. In addition, the modification of transition metal hydroxy oxides is also a method to further enhance their oxygen electrocatalytic activity. For example, Deng et al. obtained oxygen electrocatalysts with high catalytic activity and cyclic stability through simple spontaneous vulcanization [855]. Most of the high-performance bifunctional catalysts synthesized at present are powders, so it is necessary to use binders to cover them on flexible current collectors as cathodes [856-859].

Due to the low cost, high activity and multifunctional design, heteroatom-doped carbon materials have received a lot of attention among all bifunctional catalysts comprising binder. The addition of trace transition metals can greatly boost their catalytic activity [863]. The adsorption energy of intermediates in the ORR/OER reaction process is greatly lowered due to the change in local electronic structure generated by coordination between metals and heteroatoms in the

carbon matrix, resulting in good activity equivalent to noble metal catalysts [864]. For instance, Tang et al. used defect engineering to create atomically distributed Co-N$_x$-C active sites in nano carbon, exhibiting good performance for flexible ZABs [**Figure 8.13** (a)] [860]. The carbon matrix is made up of multilayer graphene sheets, and there are no apparent cobalt nanoparticles according to TEM images. The cobalt atoms that survived from pickling are believed to be the bright dots in the dark field high-resolution TEM image [**Figure 8.13** (b)].
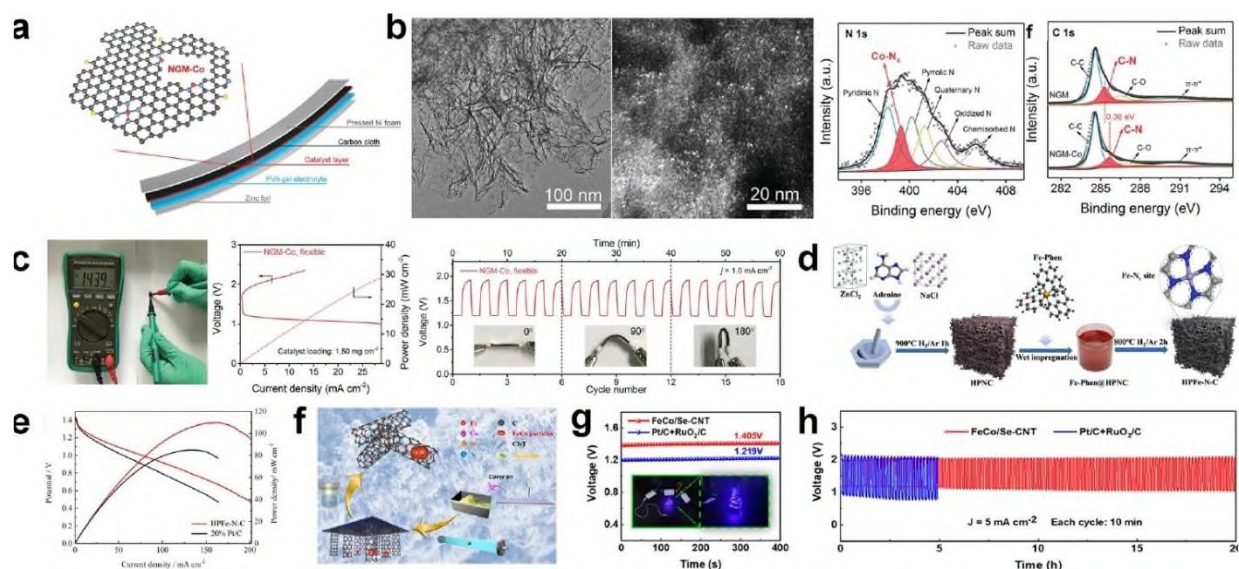
Figure 8.13 *(a) Schematic illustration of the hierarchical Co/N/O tri-doped graphene catalyst (NGM-Co). The grey atom represents for carbon, blue for nitrogen, yellow for oxygen and red for cobalt. (b) Morphology and composition characterization of NGM-Co catalyst. (c) Application of NGM-Co in flexible ZAB. (d) The preparation flow chart for hierarchically porous nitrogen-doped carbon (HPNC) and hierarchically porous iron/nitrogen co-doped carbon (HPFe-N-C). (e) Potential-current density curves and corresponding power density. (f) Schematic illustration of the synthesis of FeCo/Se-CNT catalyst. (g) Open-circuit plots of ZAB with FeCo/Se-CNT vs. Pt/C+RuO$_2$/C (inset shows LED bulbs lit by three flexible ZABs). (h) Cycling stability of the solid flexible Zn-air battery at 5 mA cm^{-2}. [860-862, 924].*

The presence of pyridine nitrogen coupled with Co as well as a carbon matrix doped with N and O, is revealed by XPS fine spectrum analysis. The former is known to be a good ORR catalytic site, whilst the latter improves the reaction kinetics by lowering the electron density of nearby carbon atoms and increasing the adsorption of ORR and OER intermediates.

The flexible ZABs had an air cathode made of Co/N/O tri-doped graphene catalyst (NGM-Co) coated carbon cloth, an anode made of flexible zinc foil, and an electrolyte made of alkaline polyvinyl alcohol (PVA) gel. The flexible battery, as illustrated in **Figure 8.13** (c), can deliver a high open circuit voltage of up to 1.439 V and a power density of about 30 mW cm^{-2}. The good flexibility is demonstrated by the stable charge/ discharge voltage platform under various bending angles.

Moreover, the research on-single atom iron-doped carbon material as an ORR/OER bifunctional catalyst is significant, because calculations suggest that Fe-N has somewhat higher catalytic activity than Co- N. Using a simple double molten salts mediated template process, Xu et al. created a novel Fe-N-C porous carbon material [861]. As presented in **Figure 8.13 (d)**, the authors used $ZnCl_2$ and NaCl as pore forming agents, adenine as a carbon and nitrogen source and high-temperature pyrolysis to obtain porous carbon skeleton, which was then pyrolyzed again after mixing with Fe phen to obtain a dual functional catalyst. The authors employed an alkaline polyvinyl alcohol (PVA) gel electrolyte to fabricate a flexible ZAB being similar to the above. The open circuit voltage of this battery can reach 1.431 V. As presented in **Figure 8.13 (e)**, the flexible ZABs can reach a peak power density of 109 mW cm^{-2}.

Even though monatomic catalysts having advantages of excellent chemical selectivity and atomic economy, they have challenges in becoming a large-scale alternative to noble metal catalysts due to low productivity and poor stability [865-868]. Zhang et al. used chemical vapor deposition to create a very stable FeCo bifunctional oxygen electrocatalyst on Se-doped CNT [**Figure 8.13 (f)**] [862]. The FeCo/Se-CNT catalyst exhibits good ORR and OER performance ($E_{1/2}$ =0.9 V vs. RHE, E_{10} = 1.57 V vs. RHE) as well as the excellent stability over 30,000 cycles. Similarly, a flexible ZAB with the catalyst as the cathode can achieve a high open circuit voltage of 1.405 V, and three solid-state batteries can power a string of blue LED bulbs [**Figure 8.13 (g)**]. The flexible ZABs based on FeCo/Se-CNT has better charge/discharge cycle stability than Pt/C + RuO$_2$ catalyst. After 20 h (120 cycles), the performance loss is almost negligible [**Figure 8.13 (h)**].

8.7.1.2 Self-supporting bifunctional catalyst

The bifunctional catalyst containing binder has advantages of simple synthesis. Nevertheless, the addition of binder hinders the contact between active sites and electrolyte, leading to the decline of ORR/OER performance of air electrode. Additionally, the binder also destroys the microstructure of the bifunctional catalyst, which further weakens the catalytic activity and increases the resistance of the catalyst. Researchers devised self-supporting air electrodes with bifunctional catalytic activity in order to address these problems. Generally, a flexible conductive matrix such as stainless steel mesh [869], nickel foam [870, 871] and carbon cloth [872-874] are used as the substrate, on which a high-performance catalytically active unit is built using electrodeposition or chemical deposition. The resulted self-supporting air electrode unites the catalyst and the current collector, considerably lowering the transfer resistance and

increasing the durability. These advantages determine that the self-supporting air electrode might be more promising for the commercialization of flexible ZABs.

Many self-supporting bifunctional catalysts, including powdered bifunctional oxygen electrocatalysts, are still carbon materials. For example, Li created a porphyrin covalent organic skeleton (POF) and employed it as the cathode catalyst in a flexible zinc-air battery [875]. Cobalt ions are first coordinated in porphyrin units, then coated on CNTs with high hydrophobicity, as presented in **Figure 8.14** (a).
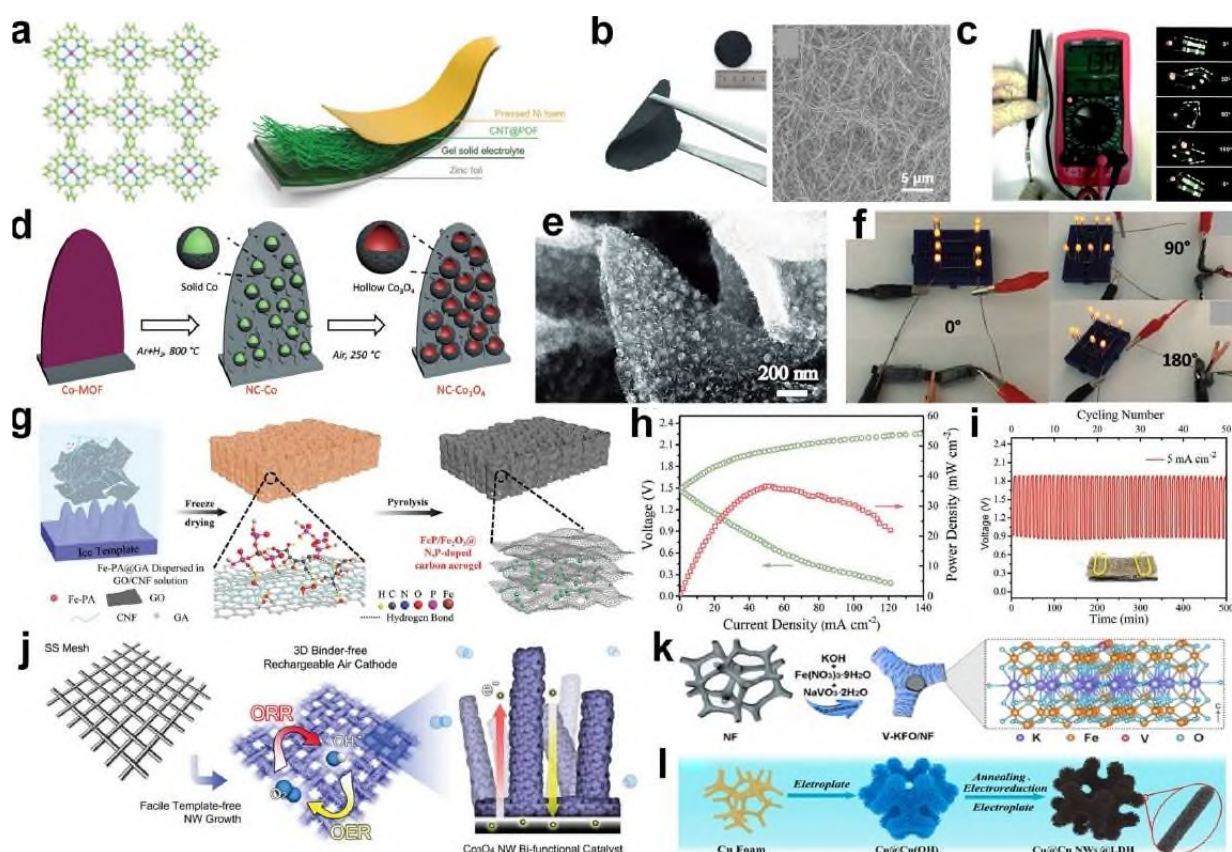
Figure 8.14 (a) Schematics of a flexible ZAB assembled by the CNT@POF cathode and chemical structure of the single-layer POF. (b) Photograph of the free-standing CNT@POF film in the bent and extended (inset) states, and SEM image of CNT@POF. (c) Open-circuit voltage and polarization curves of the flexible ZAB with the CNT@POF cathode, galvanostatic discharge-charge cycling curves at 1.0 mA cm^{-2} under bending at 0∘, 90∘ and 180∘, respectively, and photographs of a commercial red LED lit by two flexible ZABs connected in series when bent to various angles. (d) Schematic illustration of the fabrication process for hierarchical NC-Co$_3$O$_4$ arrays on flexible carbon cloth. (e) SEM images of NC-Co$_3$O$_4$ nanoarrays on carbon cloth. Charge/discharge curves and the corresponding power density plot. (f) Digital image of eight orange LEDs powered by two ZABs connected in series with different bending angles of 0∘, 90∘ and 180∘. (g) Schematic illustration of the synthesis of FeP/Fe$_2$O$_3$ @NPCA. (h) Charge/discharge curves and the corresponding power density plot. (i) Cyclic galvanostatic charge-discharge plots at 5 mA cm^{-2}. (j) Schematic illustration of the growth of 3D rechargeable Co$_3$O$_4$ nanowires (NMs) air cathode for bifunctional catalysis of ORR and OER. (k) Schematics of the synthetic route and the corresponding structural unit of V-K$_2$Fe$_4$O$_7$/Nickel foam. (l) Schematic illustration of the four-step synthesis process for 3D core-shell Cu@Cu NWs@LDH electrocatalysts. [875-880, 924].

After a further dehydration procedure, a POF coating with a thickness of roughly 4 nm is created. The film has good flexibility, as shown in physical **Figure 8.14 (b)**, and there is no damage or cracking while bending. It is worth noting that since the bonding mode between the catalyst and the current collector is Van der Waals force rather than the adhesion of the binder, the catalyst can be classified as a self-supporting cathode catalyst. The film is intertwined with CNT as the skeleton, as evidenced by SEM pictures. The film is directly employed as an air cathode in the construction of a flexible all-solid-state zinc air battery, with an open circuit voltage of 1.39 V. The entire solid-state battery is a promising energy-efficient conversion device, with a peak power density of 22.3 mW cm^{-2} and a robust charge/discharge process in bending state. Two all-solid-state zinc-air batteries connected in series can power a red LED bulb, demonstrating its wearable potential. Carbon cloth (CC) [**Figure 8.14 (c)**], which is commonly employed as a fluid collector in flexible energy storage devices, can also be used as a conductive substrate in addition to CNT.

By embedding hollow Co_3O_4 on the flexible carbon fabric, Guan and colleagues created a self-supporting air electrode with good cycle stability and mechanical flexibility [876]. Cobalt ions were turned into uniform and plentiful Co_3O_4 nanoparticles in the oxidation process due to the nitrogen doped carbon coating's ability to govern cobalt ion diffusion [**Figure 8.14 (d-e)**]. Its remarkable catalytic activity arises from the greatly concentrated Co_3O_4 active sites. The two flexible ZABs are connected in series and light up eight orange LED bulbs at varied bending angles because one ZAB can yield an open circuit voltage of roughly 1.44 V [**Figure 8.14 (f)**].

There are also self-supporting bifunctional catalysts made from pyrolyzed carbon-containing precursors [881-884]. Using directional freeze casting and pyrolysis, Wu et al. created a carbon aerogel [877]. The as-fabricated self-supporting air electrode has a 3D honeycomb form, and in-situ grown FeP/Fe_2O_3 nanoparticles are dispersed between carbon nanosheets, as presented in **Figure 8.14 (g)**. The catalyst achieved a high peak power density and stability thanks to its extensive pore structure and nanoparticle active sites [**Figure 8.14 (h)**]. As illustrated in **Figure 8.14 (i)**, the battery exhibits stable charge and discharge voltages at the current density of 5 mA cm^{-2}. During 50 cycles for 500 min, slight voltage change can be discerned on both the charge and discharge segments with a high energy efficiency.

In addition to carbon based self-supporting electrode, metal based self-supporting electrode is also a kind of bifunctional self-supporting air electrode that has been widely studied. As presented in **Figure 8.14 (j)**, Chen et al. used a simple template free method to directly grow mesoporous Co_3O_4 nanowires (NW) arrays on stainless steel mesh [878]. Thanks to the self-supporting property of the NM array, the specific surface area of the electrode is larger, so the

160

reactants can diffuse better in the active site and electrolyte. In addition to stainless steel mesh, such as foam nickel and foam copper have become hot materials in the field of self-supporting electrodes due to their high specific surface area and certain oxygen electrocatalytic ability. Chang et al. in-situ synthesized V-$K_2Fe_4O_7$ on the surface of foam nickel through a one-step hydrothermal reaction. Since the active site is generated on the surface of the collector rather than bonding with adhesive, the electrode shows excellent cycle stability for up to 550 h [**Figure 8.14** (k)] [879]. In addition, Wu's research team epitaxially grew copper nanowires on foam copper substrate, and then in situ grew NiFe-LDH [**Figure 8.14** (l)] [880]. The electrode synthesized by this method has a higher binding strength between the matrix and the active site, and the copper nanowires also provide sufficient nucleation sites for the growth of the active site. However, compared with carbon matrix, metal matrix will inevitably appear metal fatigue phenomenon in the process of a large number of bending of flexible energy storage devices, resulting in reduced mechanical flexibility or even fracture. At the same time, since the construction of active sites on the self-supporting electrode is often accompanied by high temperature heating, solution corrosion, phosphorus/sulfide and other processes, the mechanical strength of the metal collector will be greatly reduced. Thus, the current mainstream research on self-supporting electrodes is still mainly carbon based collectors.

To sum up, the method for preparing flexible cathodes by coating powder catalysts and binders has the advantages of simple and diverse synthesis as well as high catalytic activity. Nevertheless, because of the influence of the process and the properties of the adhesive, the catalyst is likely to fall off and crack during the bending and stretching process. Fortunately, the flexible electrodes obtained by the commercially used slit extrusion coating method can well alleviate the problems of interfacial cracking and peeling of active materials. In contrast, the self-supported catalyst grows the active sites on the conductive substrate in situ, which not only reduces the diffusion path and interface resistance of the reaction, but also prevents the active substances from falling off and cracking during bending and stretching, greatly improving the mechanical stability of flexible ZABs. **Figure 8.15** presents the performance comparison of some representative flexible ZAB cathode catalysts, in which five catalysts near the left side are bifunctional catalyst containing binder and five catalysts near the right side are self-supporting bifunctional catalyst.
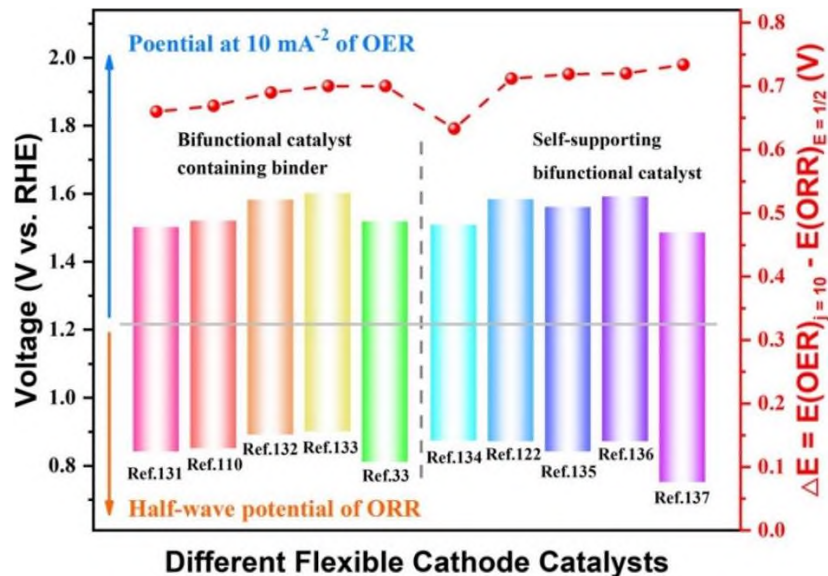
Figure 8.15 *Comparisons of potential difference between the half-wave potential of ORR and overpotential at 10 mA cm^{-2} of OER for typical bifunctional flexible air cathodes reported [864, 876, 885-891, 924].*

8.7.2 Solid electrolyte

Solid electrolyte is the most significant difference between flexible ZABs and liquid ZABs. In flexible ZABs devices, solid electrolyte plays an important role in mass transfer and moisture preservation. Therefore, it is very necessary to understand its development process and trend comprehensively and systematically.

8.7.2.1 Gel electrolyte

Gel electrolyte is a type of hydrogel that contains a significant number of hydrophilic groups and can absorb a large amount of alkaline solutions, giving it a high ionic conductivity [892]. Simultaneously, the three-dimensional matrix structure gives it good mechanical properties like flexibility, extensibility, and compressibility [893]. Furthermore, its synthesis technique is very mature, low-cost, and convenient for large-scale manufacturing after years of research [894]. All of these demonstrates enormous promise in the realm of flexible ZABs.

Zhi and his colleagues created a sodium polyacrylate hydrogel (PANa) by neutralizing acrylic acid with NaOH and then polymerizing it. This novel PANa hydrogel has a number of advantages including high water absorption (i.e., high ionic conductivity) and strong water retention ability, giving the as-built flexible ZAB a large capacity and ultra-long cycle life. Chen et al. increased electrostatic attraction in hydrogel by alkalinizing the carboxyl group in polyacrylic acid (PAA) to an alkaline state (A-PAA) [887]. The interaction between water molecules and certain polar end groups can help the hydrogel retain more water and have better mechanical properties. The hydrogel synthesized by this approach has a rich porosity structure, as presented

in **Figure 8.16 (a)**, which implies that it can absorb more alkaline solution. This electrolyte gives a peak power density of up to 160 mW cm^{-2} in a flexible ZAB, which is higher than many liquid-electrolyte ZABs [**Figure 8.16 (b)**]. As previously stated, the hydrogel endows the ZAB stable charge and discharge platforms at any mechanical deformation state [**Figure 8.16 (c)**].

The hydroxyl group, like the carboxyl group, is well known for its outstanding hydrophilicity. Polyvinyl alcohol (PVA) hydrogel, as an example of hydroxy-containing hydrogels, has emerged as an alternative for electrolyte of flexible ZABs due to its excellent chemical stability, low toxicity and ease of manufacture [897]. But it has some flaws including limited ionic conductivity, poor mechanical characteristics and water retention. As a result, researchers made some modifications to address these issues [898]. Lee and colleagues electrospun PVA/PAA nanofiber felt and immersed it in a solution containing Nafion to create a continuous anion exclusion phase. The resultant electrolyte efficiently improved ion transport efficiency and suppressed the formation of zinc dendrites, resulting in flexible ZABs with high cycle stability. Song et al. also developed an alkaline hydrogel by crosslinking PVA, PAA and graphene oxide [**Figure 8.16 (d)**]. Mechanical characteristics, ionic conductivity, and water retention capability have all been improved in this modified hydrogel [895]. When ZABs with this hydrogel electrolyte are bent to different angles or entirely folded, they can still provide a nearly lossless voltage platform. Additionally, ZABs are placed inside textile as a wristband to power smart watches and flexible electroluminescent devices, demonstrating their application potential in the wearable industry [**Figure 8.16 (e)**]. In addition to hydrogels mentioned above, polyacrylamide (PAM) is a well-known gel electrolyte [899]. The amide group in PAM possesses strong hydrophilicity, just like PAA and PVA. It can be quickly hydrolyzed under alkaline circumstances, resulting in poor water retention, ionic conductivity, alkaline tolerance and mechanical characteristics [900].
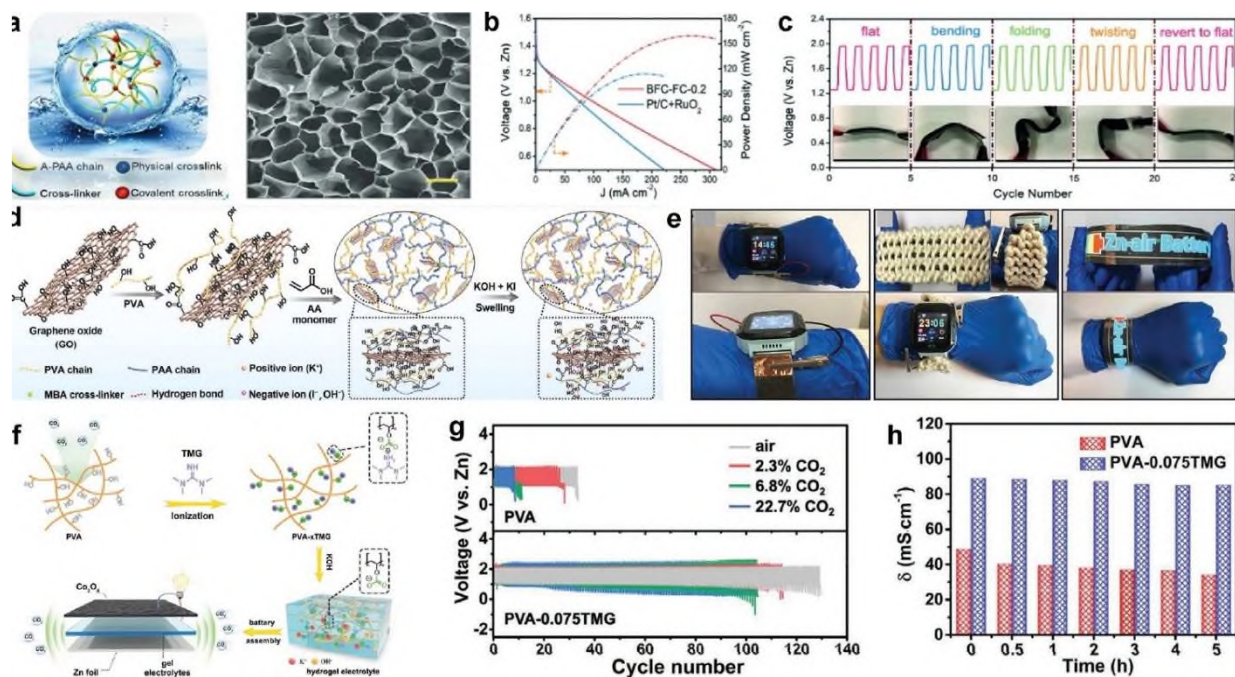
Figure 8.16 *(a) Schematic of the structure of A-PAA hydrogel and SEM image of the freeze-dried A-PAA hydrogel (scale bar: 10 mm). (b) Discharging and power density plots of flexible ZABs. (c) Cycling profiles of flexible ZABs at the current density of 2 mA cm^{-2} upon various mechanical deformations. (d) Schematic of the fabrication process for the basic GPE co crosslinked by PVA, PAA and graphene oxide (GO) containing KI additive (KI–PVAA–GO GPE), highlighting the microstructure of the PVAA–GO polymer network. (e) Photographs of three sandwich- and cable-type ZABs connected in series to power a commercial smart watch, and a flexible display hand strap powered by four integrated sandwich-type ZABs in series. (f) Schematic illustration of the synthetic procedure of the PVA-Tetramethylguanidine hydrogel and its application as electrolyte for CO$_2$ tolerant ZABs. (g) Galvanostatic discharge-charge cycling curves of flexible ZABs at 5 mA cm^{-2} in the atmosphere with various CO$_2$ concentrations. (h) Changes in the conductivity of PVA and PVA-0.075TMG gels exposed in pure CO$_2$ atmosphere for different time. [887,895,896,924].*

It has to be noticed that environmental conditions, particularly CO$_2$, alter the electrochemical and mechanical properties of the hydrogel electrolyte. Because ZABs frequently require high-concentration alkaline solutions, OH$^-$ in these alkaline solutions transform to carbonate and bicarbonate ions when in contact with CO$_2$ from the air for an extended period of time, resulting in inevitable decrease of ionic conductivity (so-called CO$_2$ poisoning). To overcome this problem, Yan's team created a novel electrolyte. Excellent CO$_2$ tolerance can be accomplished by pre-immobilizing CO$_2$ in PVA hydrogel to produce the -OCO$_2$ group, as presented in **Figure 8.16 (f)** [896]. The hydrogel can also minimize the development of zinc dendrites and achieve greater ionic conductivity thanks to the strong contact between the -OCO$_2$ group and Zn^{2+}. **Figure 8.16 (g)** shows that the cycle life of a flexible ZAB in the atmosphere with a CO$_2$ volume fraction of 22.7 % is 12 times that of the original PVA. Besides the much higher ionic conductivity of the CO$_2$-fixed hydrogel, it also demonstrated much more stable ionic conductivity in pure CO$_2$ when compared to the pure PVA counterpart [**Figure 8.16 (h)**].

In addition to modifying the solid electrolyte to enhance its resistance to CO_2 toxicity, Dekel et al. showed that under high current density, the concentrations of HCO_3^- and CO_3^{2-} in the electrolyte would be significantly reduced, which is the so-called "self-purification mechanism" of carbonate [901]. The principle is that a large amount of OH^- will be generated in the electrolyte under high current density. When the generation rate of OH^- is greater than the consumption rate of its reaction with CO^2, the concentration of carbonate in the electrolyte will be reduced. In this simple way, the research team increased the conductivity by 2-10 times. Since the poisoning effect of CO_2 is caused by its reaction with alkaline electrolyte to generate carbonate, Sun uses weakly acidic zinc acetate aqueous solution as the electrolyte of the zinc-air battery, which greatly reduces the poisoning effect of CO_2 [902]. Benefiting from its novel reaction mechanism based on basic zinc acetate hydrate, the battery can operate stably for more than 600 h in air.

8.7.2.2 Alkaline anion exchange membrane (AAEM)

Alkaline anion exchange membrane (AAEM) is a type of polymer membrane in which basic functional groups are impregnated into the main chain of the polymer to give it a selective permeability of hydroxyl ions [903]. Compared to hydrogel electrolyte, the selective permeability of AAEM prevents Zn^{2+} from migrating to the air electrode via the electrolyte, which improves the longevity of air electrode. Furthermore, because AAEM is always thinner than hydrogel electrolyte, its application potential in small devices is significantly greater [904, 905]. However, AAEM is weak in water absorption and retention, which causes its ionic conductivity to rapidly diminish when utilized in air, resulting in performance impairment of ZABs. In response to these issues, Fu's research group created an AAEM with high water retention [906]. Cellulose fiber rich in hydroxyl served as the matrix to form an AAEM with outstanding mechanical strength and OH selective permeability by quaternizing, cross-linking and alkalizing, as illustrated in **Figure 8.17 (a)**. A flexible ZAB in the shape of a band aid was fabricated and wrapped around the finger to illuminate a red LED bulb [**Figure 8.17 (b)**].
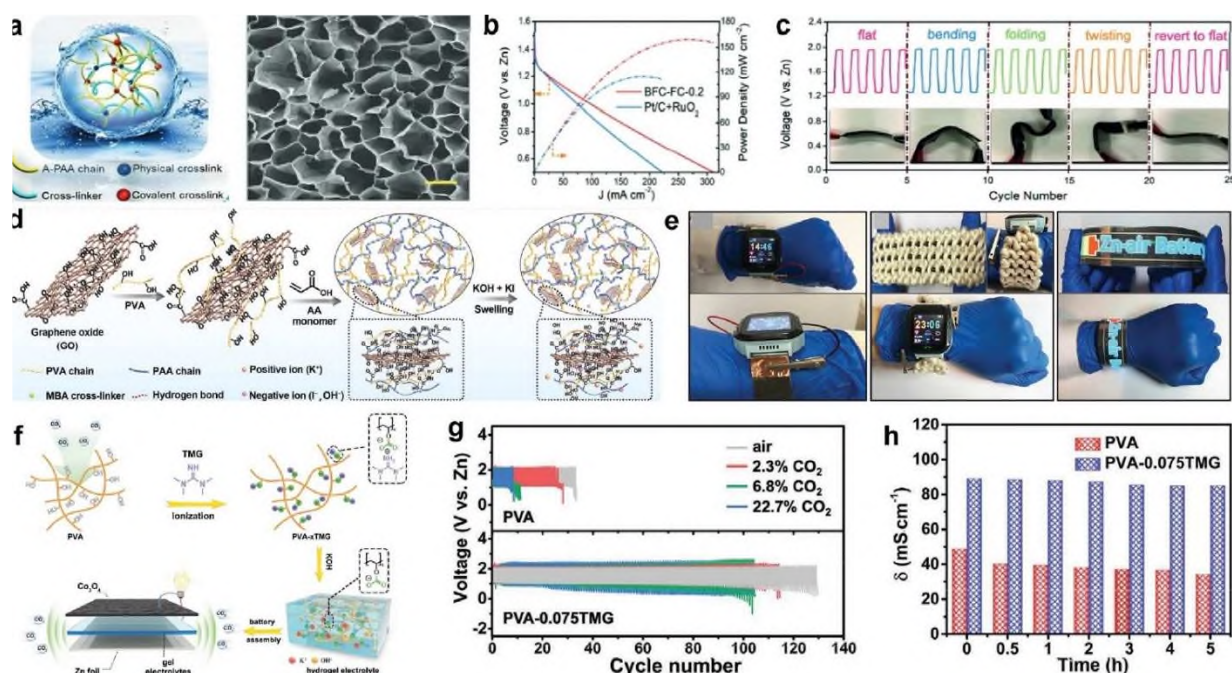
Figure 8.17 *(a) The chemical structure evolution of the cellulose nanofibre surface after functionalization, crosslinking and hydroxyl exchange. (b) Schematic diagram of a flexible ZAB integrated with a band aid, and a demonstration of the device wrapped around an index finger to power a red LED under bending condition. (c) Schematic illustration of the substrate-free flexible ZAB, cross-sectional SEM image (left) and the elementary mapping (right) of the battery. (d) Digital images of the prepared ZAB (left) and two sides of the battery (right). (e) Comparison of the design of traditional and our new flexible ZAB. (f) Polarization and power density curves. [906, 907, 924].*

As mentioned above, AAEM as the electrolyte of ZABs has the advantage of being light and thin. Chen et al. brought this advantage to the extreme. They used heat pressing to apply zinc powder and cathode catalyst directly on the surface of AAEM, resulting in a highly compact ZAB [**Figure 8.17 (c)**] [907]. It is extremely light, weighing only 0.0495 g [**Figure 8.17 (d)**]. The AAEM functions as both an electrolyte and a separator. As a result, it has strong ionic conductivity, chemical stability, and mechanical strength [**Figure 8.17 (e)**]. The ZAB delivered a peak power density of 250 mW cm^{-2} as shown in **Figure 8.17 (f)**. The flexible battery discharged at a current density of 8.3 mA cm^{-3}, showing a stable voltage platform. After the zinc layer is depleted, it shows a high specific capacity of 150.4 mAh cm^{-3} [**Figure 8.17 (g)**].

For electrolyte of flexible ZABs, ionic conductivity and mechanical properties (such as bending resistance and stretchability) are the two most important indicators. Although the ionic conductivity of alkaline hydrogel electrolyte (10^{-1} S cm^{-1}) is far better than that of AEEM (10^{-3} S cm^{-1}), there is still a big gap compared with liquid electrolyte. Improving the water absorption and retention capacity of solid electrolyte is an effective means to improve the ionic conductivity of electrolyte. For example, Chen et al. introduced hollow polymer microcapsules into the hydrogel polymer network, which greatly enhanced the water absorption and retention properties of the electrolyte. Its water absorption rate was up to 107 g g^{-1}, and it had an ultra-

high ionic conductivity (0.215 S cm^{-1}) [908]. In addition, the ionic conductivity of the electrolyte can be increased by introducing hydrophilic groups or manufacturing porous structures. For solid electrolytes, increasing the mechanical strength often means that the resistance of ion migration becomes greater, which leads to the reduction of ion conductivity. Therefore, balancing the mechanical properties and ionic conductivity of solid electrolytes has always been a research focus of solid electrolytes for ZABs. In general, solid electrolytes with satisfactory mechanical strength and ionic conductivity can be obtained by means of chemical crosslinking of small molecules, construction of cross polymer networks and addition of support materials [898, 909, 910]. For example, Xia et al. used the double network structure formed by intertwining with Zn^{2+} cross-linked sodium alginate and covalently cross-linked PAM network to improve the ionic conductivity and meanwhile obtain excellent water retention ability and mechanical flexibility [911].

8.7.3 Flexible zinc anode

In comparison to the extensive study on cathode and electrolyte, the anode of flexible ZABs has received comparatively fewer attentions because zinc foils utilized in the vast majority of ZABs are intrinsically flexible to some extent [912-914]. However, the direct use of untreated zinc foil has many disadvantages. First of all, the zinc foil will produce uncontrolled dendritic growth and side reactions during the deposition/dissolution of zinc, which will lead to the poor cyclic stability of the zinc-air battery, or even failure [915]. Second, zinc foil is rigid in nature, which leads to poor mechanical flexibility [916]. At the same time, interface cracking and even fracture may occur under the condition of a large number of bending or tensile flexibility tests. Therefore, the modification of zinc foil or the use of other zinc anodes can not only improve its mechanical properties but also electrochemical performance. Even though there are few reports on the modification of flexible ZAB anode, fortunately, the anodic reaction of ZAB is similar to that of zinc ion battery. Hence, the study on the flexibility strategy of zinc ion battery anode can provide reference for improving the flexibility of ZAB anode.

Lu's research group reported a highly flexible fiber-shape zinc-ion battery [917]. **Figure 8.18** (a) depicts the electrode preparation procedure.
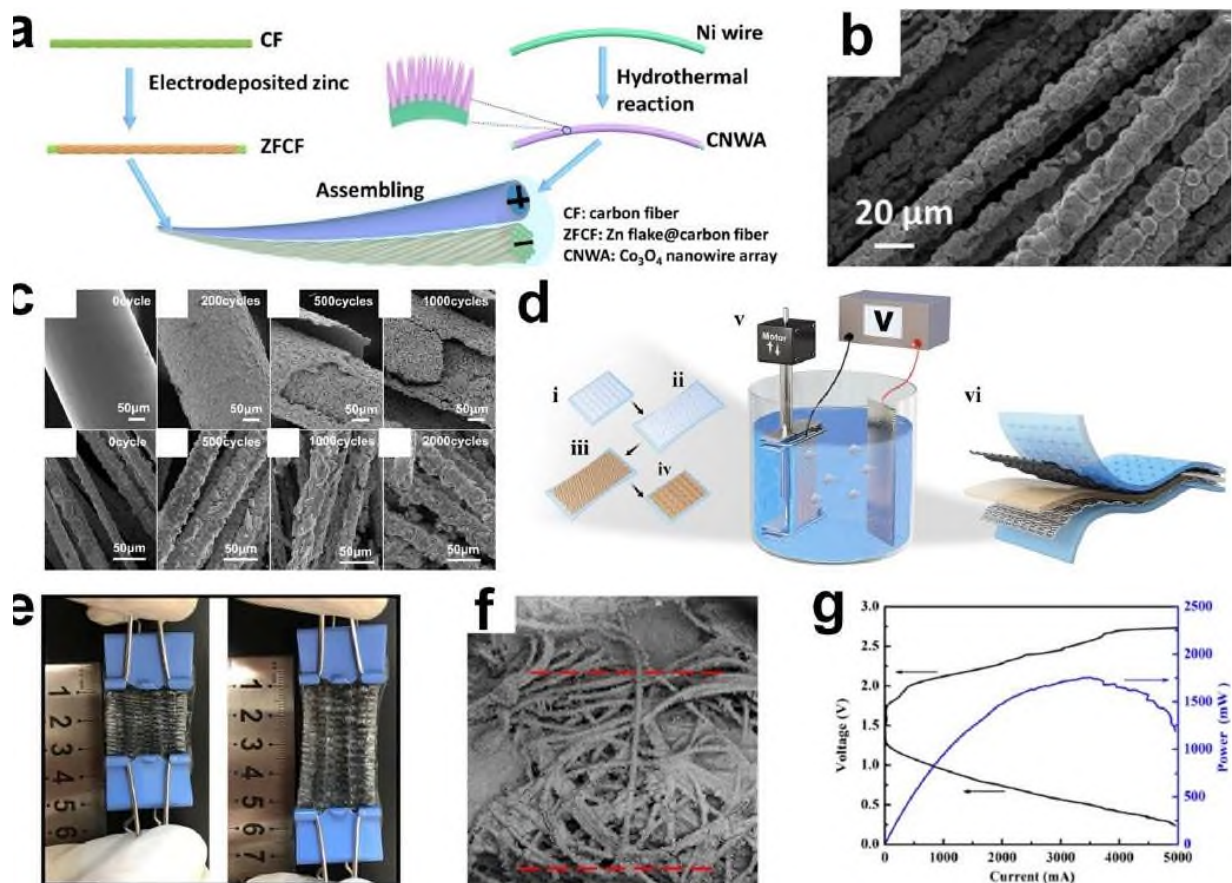
Figure 8.18 *(a) Schematic illustration of fabrication of aqueous fiber-shaped Zn//Co₃O₄ battery. (b) SEM image of the Zn flake deposited on the carbon fiber (ZFCF). (c) SEM images of zinc electrode at the current density of 1 A cm^{-3} during different cycles: top is the commercial zinc wire anode; bottom is the ZFCF anode. (d) Schematic procedure of (steps i-v) an electroless Cu-layer plating on spandex textile using a prestrain-load-recovery method, dynamic stretching-electroplating of a Zn (or Ni) layer on Cu-coated textile, and (Step vi) ZABs assembly based on Zn- and Ni-coated textile electrodes and in situ crosslinked hydrogel electrolyte. (e) Photographs of the Zn-coated textile before and after stretching by 100 %. (f) In- situ SEM image of the Zn-coated textile under 100 % tensile strain. (g) Discharge polarization curve of the large-area ZAB textile. [917, 918, 924].*

A carbon fiber surface was first submerged in heated concentrated nitric acid to decorate N and O functional groups and then electrodeposited a layer of zinc on the surface. **Figure 8.18 (b)** shows a SEM picture of the deposited fiber. Zinc flakes were uniformly electrodeposited on the carbon fiber and layered in a neat manner along its surface. The electrode did not generate evident zinc dendrites after 2000 cycles in the long-term charge/discharge test and the structure did not collapse appreciably compared to the carbon fiber without nitric acid treatment, demonstrating outstanding reversibility [**Figure 8.18 (c)**].

In addition to the strategy of directly referring from zinc-ion batteries, there are still solutions for the anode flexibility of ZABs documented. Hu's research group conducted a representative work. Through dynamic stretch plating on wavy spandex fabric, they obtained a zinc anode with 100 % high elongation and stable conductivity [**Figure 8.18 (d)**] [918]. Thanks to the high elasticity caused by the wrinkle and multi-space network structure of spandex fabric, a

pre-strain can be applied and then copper and zinc can be plated on the pre-strained surface, resulting in a galvanized fabric with 100 % elongation [**Figure 8.18 (e)**]. **Figure 8.18 (f)** depicts morphology of the stretchy electrode. This approach has created a structure that adapts to tensile deformation throughout the galvanizing process, allowing the textile to maintain stable tensile capability following electrodeposition. This ZAB fabric with an area of 14×6.5 cm^2 delivered a maximum output power of 1757 mW [**Figure 8.18 (g)**].

In short, because zinc anode will inevitably be affected by zinc dendrite, hydrogen evolution reaction and passivation in the actual charging and discharging process, the development of zinc anode with high performance and lasting stability has always been a challenging subject. It should be noted that these three main problems are not independent, and they will interact with each other during the actual charging and discharging process. For example, the hydrogen evolution reaction will lead to an increase in the local OH$^-$ concentration, and then the passivation of the anode surface will become more obvious. The increase of passivation products will also reduce the active sites of zinc, which will make the electric field distribution more uneven, and then appear more serious dendrite phenomenon. Therefore, zinc anode protection strategies should focus more on overall optimization rather than just individual issues.

It has to be noticed that even though most studies claim good cycling stability of the assembled ZABs, the charge/discharge currents used in these studies tend to be small (less than 10 mA cm^{-1}), which is unacceptable for the consumer market pursuing fast charging. There are three main reasons for the poor rate capability of ZABs: the aggravation of anode dendrites and side reactions, the low diffusion rate of ions in the electrolyte, and the slow oxygen electrocatalytic reaction kinetics. The first is that as the charge/discharge current increases, the zinc anode develops dendrites that are enough to damage the battery. Through morphological analysis of the zinc coating under neutral/mild electrolyte conditions, Zhi et al. found that with the increase of current density from 1 mA cm^{-1} to 10 mA cm^{-1}, the morphology of zinc deposited on the electrode surface changed from uniform distribution to zinc flakes growing perpendicular to the electrode, and finally became hexagonal zinc nano-flakes with sharp tips [919]. These hexagonal zinc nanosheets produced by non-uniform deposition at high current densities pierce the separator during prolonged operation, resulting in an internal short circuit. In addition, the work of Tan et al. showed that a large number of micron-sized bubbles adhered to the surface of the air electrode would appear at high current densities, and the generation of bubbles would hinder the contact between the electrolyte and the active site and consume the electrolyte, eventually leading to battery failure [920]. The second is because the low diffusivity of cations

169

and anions in the electrolyte leads to concentration gradients at high current densities, which affect the diffusion rate and ultimately exhibit a limited diffusion current density [921]. Finally, the slow kinetics of oxygen electrocatalytic reaction leads to its poor rate. There have been many excellent works in optimizing oxygen electrocatalytic reactions. For example, Lei et al. synthesized a highly interconnected graphene network with a hierarchical porous structure, which is conducive to fast charge transport and thus still maintain a strong cycle stability under large current densities [922]. In addition, Wu et al. synthesized cobalt nanoclusters confined to specific nanopores. Due to the existence of high active sites and the effect of nanopores, the catalyst could form an abundant and stable gas-solid-liquid three-phase reaction interface, enhancing the charge transfer ability of the catalyst. Electrochemical data show that the catalyst can still operate stably for more than 90 h at a high current density of 100 mA cm^{-1} [923].

CHAPTER 9

Conclusions

Currently, much concern has been given to global warming resulting from fossil fuels. Renewable energy sources are the most promising choice, as they are sustainable and have no or low environmental implications. Nevertheless, the remarkable growth in renewable energy demands a suitable energy storage system. With the increasing dominance of renewable energy production sources such as solar and wind energy, the electricity grid will require the assistance of a large-scale electrical energy storage system. The energy produced from renewable sources is periodic and variable in nature, demanding continuous attention. Therefore, storing energy during unexpected energy production periods is important to maintain the quality of the electricity generated and satisfy the growing electricity demand. Electrochemical energy storage systems could be more cost-effective than other systems. Normally, electrochemical energy storage refers to electrochemical capacitors and rechargeable batteries, which can be used in conjunction with other systems in a hybrid configuration.

The airflow maintains the reaction of the air electrode in the MABs, which minimizes the requirement for tanks to store the reactant. Moreover, for the use of large-scale energy storage, the air electrode should be bifunctional for both OER and ORR during charge and discharge, in order to be effective. Since MABs are cost-effective, ultralightweight, and have a high energy density, they are an exceptional alternative to gasoline. On the contrary, its energy efficiency is weak, and its charge/discharge life cycle is short. Although MABs have a good energy density, the technology is still in the development stage in terms of efficiency and availability. Yet, it has evolved into an excellent energy storage technology for ecologically friendly and high-performance electric cars, among other applications. Rather than this, MABs' large-scale use is restricted by their weak energy efficiency and power density, caused by a higher overpotential and slow oxygen reactions at the air cathode.

Iron-air batteries (IABs) are a potential option for large-scale energy storage because of their environmental friendliness, low cost, long-term viability, and a variety of raw materials, among other specifications. Nevertheless, in order to be a viable option, IABs' efficiency and cycle life must be improved. In addition, aluminum-air batteries (AABs) have the lowest cost and the second greatest specific capacity theoretically, making them a powerful prospect for large-scale energy applications in the future among MABs, especially in renewable energy. As a result,

AABs are very attractive as a sustainable and efficient technology for energy storage and conversion, with the capability of providing power for large electronic devices and automobiles. Both high energy density and the unique design of structural components of MABs and redox flow batteries (RFBs), have shown significant promise for large-scale electrical energy storage as efficient electrochemical systems. Metal-air flow technologies, due to their inherent advantages and the high degree of design freedom they provide, have enormous potential for large-scale energy storage and transmutation in the next-generation power grid. It is essential to improve the efficiency and energy density of vanadium-air flow batteries (VAFBs) and also to lower the stack cost used on large scales in commercial applications.

The following conclusions are driven:

1. A variety of metals can be used as an anode of MABs. Each metal has its own advantages and disadvantages. Al is one of the promising electrodes because of its low weight and cost, high energy density, good recyclability, environmental friendliness.

2. Despite the high ionic conductivity of the aqueous electrolytes, the leakage, stability, and thermodynamic limitations are failures of MABs' applications. Electrolyte additives or non-aqueous electrolytes can mitigate or solve these problems and hence increase the durability and energy density of MABs.

3. A mechanically and thermally porous cathode electrode that can perform OER and ORR effectively is important for commercial MABs.

4. Both AABs and IABs are good candidates for the large-scale production of MABs.

5. Flow MABs are safe and have a long operational life due to the flow of anolyte/electrolyte, which reduces side reactions. Flow MABs can be used both for large-scale energy storage and stationary power plants.

For the future research on MABs, some perspectives are being highlighted for reference:

1. *More integrated studies*. Research on oxygen electrocatalysts makes up the majority of the research on MABs. Often MABs are just an evaluation method for the oxygen electrocatalysts. Nevertheless, due to the development of MAB technology, the whole cell system must be considered together.

2. *Rechargeability*. The low rechargeability of existing MABs mostly manifest in the round-trip and Coulombic efficiency. A low round-trip efficiency makes MABs exceptionally uneconomical and energy - consuming. A low Coulombic efficiency leads to fast capacity loss in MABs. These considerably hinder the practical use of rechargeable MABs. Studies

on the material design of MABs should ideally address the issue of rechargeability by improving metal electrode reversibility and suppressing side reactions.

3. *Fundamental understanding*. Effective material design strategies of MABs depend on the fundamental comprehension of the electrode reactions, side reactions and dendrite growth. Hence, progress in advanced experimental technologies and theoretical researches can benefit the design of suitable materials for MABs.

4. *Finding proper applications*. MABs have remarkable advantages regarding energy density, but also carry certain disadvantages regarding rechargeability. Besides developing material design methods to improve the battery performance, finding proper applications, highly desirable for high-capacity energy storage, is also critical for realizing the practical development of MABs.

In situ spectroelectrochemical techniques have been priceless in the designation of the underpinning reactions involving dioxygen in the metal-air cell, of which *in situ* Surface-Enhanced Raman Spectroscopy (SERS) has performed a great role. From these SERS researches outstanding progress has been made recently in the understanding of the influence of organic solvent and water on reaction pathways.

The appearance of the Shell-Isolated Nanoparticle-Enhanced Raman Spectroscopy (SHINERS) technique to monitor a variety of electrode interfaces with significant Raman enhancement will undoubtably be an important tool in comprehension of oxygen chemistry on a wide range of electrode substrates. Great progress has also been made in complementary *in situ* Infrared Spectroscopy (IR) techniques and may also become a beneficial experimental technique within this field, while UV/Vis (Visible) and Electron Paramagnetic Resonance (EPR) have been shown to be crucial techniques in addressing specific mechanistic processes.

Zinc-air batteries (ZABs) are always used for hearing aid applications because of their high energy density and low power output. The greatest conclusions are as follows:

1. ZABs consist majorly of the anode (~ 52 wt %) comprising zinc (~ 88 %), which is much higher than the natural ores (~ 5.8 %). It is estimated that nearly 8566-21415 tons of ore are demanded globally to produce zinc for ZABs per year. Thus, ZABs are highly recommended to be studied for recycling.

2. Although other zinc-based batteries are commonly considered for recycling, ZABs are often neglected due to their lower price, lack of technical diligence. It is evaluated that the contribution of zinc towards the total market value in ZABs is nearly 60.9 %, higher than alkaline (40.7 %) and zinc-carbon batteries (29.6 %).

3. A comparison of ZABs with other secondary sources of zinc (electronic waste, EAF dust, primary production waste etc.) showed that it consists of simpler and easy-to-process zinc phases (Zn/ZnO) without other impurities such as Fe (as in EAF dust), Mn, Cl, F (as in alkaline batteries). The zinc anode recovered from ZABs can be treated with the concentrate received in primary ore processing.

Developing efficient MABs requires the rational design of materials of the metal and air electrode, separator and electrolyte. Comprehensive understanding of materials of each part of MABs demands the integration of interdisciplinary knowledge of electrochemistry, organic and inorganic chemistry, material science, catalysis and engineering. Hence, collaborations among researchers with different backgrounds are expected to overcome crucial scientific and technical failures of MABs and furthermore promote their practical applications.

174

REFERENCES

[1]	Xin-bo, Zhang; Zhiwen, Chang. Introduction to Metal-Air Batteries: Theory and Basic Principles. Li-Air Batteries: Discharge Products. *Metal-Air Batteries*. Wiley-VCH Verlag GmbH & Co. India, p.1,41, **2018**.
[2]	Abdelrahman, Azzuni; Christian, Breyer. Energy security and energy storage technologies. 12th International Renewable Energy Storage Conference, IRES 2018. *Energy Procedia*. Finland, 155, 237-258, **2018**. 10.1016/j.egypro.2018.11.053.
[3]	Abdul, Ghani, Olabi; Enas, Taha, Sayed; Tabbi, Wilberforce; Aisha, Jamal; Abdul, Hai, Alami; Khaled, Elsaid; Shek, Mohammod, Atiqure, Rahman; Sheikh, Khaleduzzaman, Shah; Mohammad, Ali, Abdelkareem. Metal-Air Batteries – A Review. Special Issue: Advances in Solar Thermal Energy Storage Technologies. Energies 2021, 14(21), 7373. Edited by Dr. Sheikh Khaleduzzaman Shah. (Accessed 20/3/2023). Available online: https://doi.org/10.3390/ en14217373, **2021**.
[4]	Cheng, F. and Chen, J. Metal-air batteries: from oxygen reduction electrochemistry to cathode catalysts. Chem. Soc. Rev. 41 (6): 2172-2192, **2011**.
[5]	Chang, Z.W., Xu, J.-J., Liu, Q.-C. et al. Recent progress on stability enhancement for cathode in rechargeable non-aqueous lithium-oxygen battery. Adv. Energy Mater. 1500633, **2015**.
[6]	Ersha, Fan; "Li Li", Zhenpo, Wang; Jiao, Lin; Yongxin, Huang; Ying, Yao; Renjie, Chen; Feng, Wu. Sustainable Recycling Technology for Li-Ion Batteries and Beyond: Challenges and Future Prospects. *Chemical Reviews*. American Chemical Society, 120, 7020-7063, **2020**.
[7]	Ibrahim, Dincer. Environmental impacts of energy. Energy policy (Volume 27, Issue 14). Pages 845-854, **1999**. Available online: https://www.sciencedirect.com/science/article/abs/pii/S03 01421599000683. (Accessed 20/3/2023).
[8]	Daniel, Davi-Arderius; Tim, Schittekatte. Environmental impacts of redispatching in decarbonizing electricity systems. Working Paper 01-2023. Department of Economics, Copenhagen Business School, Denmark, **2023**. Available online: https://papers.ssrn.com/ sol3/papers.cfm?abstractid=4339705. (Accessed 20/3/2023).
[9]	Apergis. N.; Bhattacharya. M.; Hadhri. W. Health care expenditure and environmental pollution: a cross-country comparison across different income groups. Environ Sci Pollut Res: 1-15, **2020**.
[10]	Md. Aslam, Ansari. Environmental impacts of non-renewable energy sources. Jagannath Jain College. Jhumritelaiya Koderma, Jharkhand, India, **2017**. Available online: https://ijcrt.org/papers/IJCRT1133009.pdf. (Accessed 20/3/2023).
[11]	Mahesh, Kumar. Social, Economic, and Environmental Impacts of Renewable Energy Resources. Department of Electrical Engineering, Mehran University of Engineering and Technology. Jamshoro, Sindh, Pakistan, **2020**. Available online: https://www.intechopen.com/chapters/ 70874. (Accessed 20/3/2023).
[12]	Union of Concerned Scientists. Environmental Impacts of Renewable Energy Technologies. **2013**. Available online: https://www.ucsusa.org/resources/environmental-impacts-renewable-energy-technologies. (Accessed 20/3/2023).
[13]	J. Deng, C. Bae, A. Denlinger, T. Miller, Electric vehicles batteries: requirements and challenges, Joule 4, 511e515, **2020**. https://doi.org/10.1016/j.joule.2020.01.013.
[14]	J. Wen, Y. Yu, C. Chen, A review on lithium-ion batteries safety issues: existing problems and possible solutions, Mater. Express. 2, 197e212, **2012**. https://doi.org/10.1166/mex.2012.1075.

[15]	S. Ferrari, M. Falco, A.B. Munoz-García, M. Bonomo, S. Brutti, M. Pavone, C. Gerbaldi, Solid-state post Li metal ion batteries: a sustainable forthcoming reality? Adv. Energy Mater. 11, 2100785, **2021**. https://doi.org/10.1002/aenm.202100785.
[16]	M. Garside, Global Projection of Total Lithium Demand 2016-2030, **2022**. Avalaible at: https://www.Statista.Com/Statistics/452025/Projected-Total-Demandfor-Lithium-Globally/.
[17]	I. Ore, I.O. Pigments, P. Rock, Q. Crystal, R. Earths, S. Ash, Mineral Commodity Summaries. **2020**. Available online: https://pubs.usgs.gov/periodicals/mcs2020/ mcs2020.pdf.
[18]	M.M. Titirici, Sustainable Batteries - Quo Vadis? Adv. Energy Mater. 2003700, **2021**. https://doi.org/10.1002/aenm.202003700, n/a.
[19]	J. Piatek, S. Afyon, T.M. Budnyak, S. Budnyk, M.H. Sipponen, A. Slabon. Sustainable Li-ion Batteries: Chemistry and Recycling. Advanced Energy Materials. 2003456, **2020**. https://doi.org/ 10.1002/aenm.202003456, n/a.
[20]	Y. Li, Y. Liu, S. Chen, P. Wang, S. Yuan, X. Li, H. Song, C. Chen, Self-templating synthesis nitrogen and sulfur co-doped hierarchical porous carbons derived from crab shells as a high-performance metal-free oxygen electroreduction catalyst, Mater. Today Energy 10, 388e395, **2018**. https://doi.org/10.1016/ j.mtener.2018.09.012.
[21]	The spiralling environmental cost of our lithium battery addiction, n.d., **2010**. https://www.wired. co.uk/article/lithium-batteries-environment-impact.
[22]	G. Harper, R. Sommerville, E. Kendrick, L. Driscoll, P. Slater, R. Stolkin, A. Walton, P. Christensen, O. Heidrich, S. Lambert, A. Abbott, K. Ryder, L. Gaines, P. Anderson, Recycling lithium-ion batteries from electric vehicles, Nature 575, 75e86, **2019**. https://doi.org/10. 1038/s41586-019-1682-5.
[23]	P. Nuss, M.J. Eckelman, Life cycle assessment of metals: a scientific synthesis, PLoS One 9, e101298, **2014**. https://doi.org/10.1371/journal.pone.0101298.
[24]	A.R. Dehghani-Sanij, E. Tharumalingam, M.B. Dusseault, R. Fraser, Study of energy storage systems and environmental challenges of batteries, Renew. Sustain. Energy Rev. 104, 192e208, **2019**. https://doi.org/10.1016/ j.rser.2019.01.023.
[25]	Chengjian Xu, Bernhard Steubing, Mingming Hu, Carina Harpprecht, Marc van der Meide, Arnold Tukker. Future greenhouse gas emissions of automotive lithium-ion battery cell production. *Resources, Conservation & Recycling*. The Netherlands, Stuttgart, Germany, 187, 106606, **2022**. https://doi.org/10.1016/j.resconrec.2022.106606.
[26]	T.M. Kousemaker, G.H. Jonker, A.I. Vakis, LCA practices of plastics and their recycling: a critical review, Appl. Sci. 11, 3305, **2021**. https://doi.org/ 10.3390/app11083305.
[27]	A. Serra, X. Domenech, E. Brillas. J. Peral, Life cycle assessment of solar photo-Fenton and solar photoelectro-Fenton processes used for the degradation of aqueous a-methylphenylglycine, J. Environ. Monit. 13, 167e174, **2011**. https://doi.org/10.1039/c0em00552e.
[28]	Manuel, Salado; Erlantz, Lizundia. Advances, challenges, and environmental impacts in metal-air battery electrolytes. Materials Today Energy 28, 101064. Available online: https://addi.ehu.es/bitstream/handle/10810/57918/1-s2.0-S2468606922001228main.pdf?sequence=1. Spain, **2022**. (Accessed 20/3/2023).
[29]	M. Iturrondobeitia, O. Akizu-Gardoki, O. Amondarain, R. Minguez, E. Lizundia, Environmental impacts of aqueous zinc ion batteries based on life cycle assessment, Adv. Sustainable Syst. **2022**. https://doi.org/10.1002/adsu.202100308.

[30]	F. Santos, A. Urbina, J. Abad, R. Lopez, C. Toledo, A.J. Fern andez Romero, Environmental and economical assessment for a sustainable Zn/air battery, Chemosphere 250, 126273, **2020**. https://doi.org/10.1016/j.chemosphere.2020.126273.
[31]	E. Zhao, P.D. Walker, N.C. Surawski, N.S. Bennett, Assessing the life cycle cumulative energy demand and greenhouse gas emissions of lithium-ion batteries, J. Energy Storage 43, 103193, **2021**. https://doi.org/10.1016/ j.est.2021.103193.
[32]	M. Zackrisson, K. Fransson, J. Hildenbrand, G. Lampic, C. O'Dwyer, Life cycle assessment of lithium-air battery cells, J. Clean. Prod., **2016**. https://doi.org/10.1016/j.jclepro.2016.06.104.
[33]	F. Wang, Y. Deng, C. Yuan, Life cycle assessment of lithium oxygen battery for electric vehicles, J. Clean. Prod. 264, 121339, **2020**. https://doi.org/10.1016/j.jclepro.2020.121339.
[34]	A. Mayyas, M. Omar, M. Hayajneh, A.R. Mayyas, Vehicle's lightweight design vs. electrification from life cycle assessment perspective, J. Clean. Prod., **2017**. https://doi.org/10.1016/j. jclepro.2017.08.145.
[35]	M. Iturrondobeitia, O. Akizu-Gardoki, R. Minguez, E. Lizundia, Environmental impact analysis of aprotic $LieO_2$ batteries based on life cycle assessment, ACS Sustain. Chem. Eng. 9, 7139e7153, **2021**. https://doi.org/10.1021/acssuschemeng.1c01554.
[36]	Badwal, Sukhvinder P. S., Sarbjit S. Giddey, Christopher Munnings, A.I.B. and A.F.H. Emerging electrochemical energy conversion and storage technologies. *Frontiers in Chemistry*. **2014**.
[37]	Bhatt, M.D. et al. Key Scientific Challenges in Current Rechargeable Nonaqueous. $Li-O_2$ Batteries: Experiment and Theory. *Physical Chemistry Chemical Physics*, (16), pp.12093-12130 **2014**.
[38]	Notter, D. et al. Contribution of Li-Ion Batteries to the Environmental Impact of Electric Vehicles. *Environmental Science &Technology*. **2010**.
[39]	Zackrisson, M., Fransson, K., Hildenbrand, J., Lampic, G., O'Dwyer, C. Life cycle assessment of lithium-air battery cells. *Journal of Cleaner Production*, 135, 299-311. **2016**.
[40]	Kushnir, D. & Sandén, B.A. The time dimension and lithium resource constraints for electric vehicles. *Resources Policy*, 37(1), pp.93-103, **2012**.
[41]	Hauschild, M.Z., Jolliet, O. & Huijbregts, M.A.J. A bright future for addressing chemical emissions in life cycle assessment. *International Journal of Life Cycle Assessment*, 16(8), pp.697-700, **2011**.
[42]	Kang, D.H.P., Chen, M. & Ogunseitan, O.A. Potential environmental and human health impacts of rechargeable lithium batteries in electronic waste. *Environmental science & technology*, 47(10), pp.5495-503, **2013**.
[43]	Luntz, A.C. & McCloskey, B.D. Nonaqueous Li–Air Batteries: A Status Report. *Chemical Reviews*, 114(23), pp.11721-11750, **2014**.
[44]	Wang, X., Gaustad, G., Babbitt, C.W., et al. Economic and environmental characterization of an evolving Li-ion battery waste stream. *Journal of environmental management*, 135, pp.126-34, **2014**.
[45]	Wang, X., Gaustad, G., Babbitt, C.W., et al. Economies of scale for future lithium-ion battery recycling infrastructure. *Resources, Conservation and Recycling*, 83, pp.5-62, **2014**.
[46]	Shabbir, I.; Mirzaeian, M. Feasibility analysis of different cogeneration systems for a paper mill to improve its energy efficiency. Int. J. Hydrogen Energy. 41, 16535-16548, **2016**.
[47]	Kutscher, C.F. Principles of Sustainable Energy Systems, 3rd ed.; Informa UK Limited: Colchester, UK, **2018**.
[48]	Dehghani-Sanij, A.; Dehghani, S.; Naterer, G.; Muzychka, Y. Marine. Icing phenomena on vessels and offshore structures: Prediction and analysis. Ocean Eng. 143, 1-23, **2017**.

[49]	Khajuria, A.; Ravindranath, N. Climate Change Vulnerability Assessment: Approaches DPSIR Framework and Vulnerability Index. J. Earth Sci. Clim. Chang., **2012**.
[50]	Guney, M.S.; Tepe, Y. Classification and assessment of energy storage systems. Renew. Sustain. Energy Rev. 75, 1187-1197, **2017**.
[51]	Bird, L.; Lew, D.; Milligan, M.; Carlini, E.M.; Estanqueiro, A.; Flynn, D.; Gomez-Lazaro, E.; Holttinen, H.; Menemenlis, N.; Orths, A.; et al. Wind and solar energy curtailment: A review of international experience. Renew. Sustain. Energy Rev. 65, 577-586, **2016**.
[52]	Lu, L.; Han, X.; Li, J.; Hua, J.; Ouyang, M. A review on the key issues for lithium-ion battery management in electric vehicles. J. Power Sour. 226, 272-288, **2013**.
[53]	Mernagh, T.P. A Review of Australian Salt Lakes and Assessment of Their Potential for Strategic Resources. Geosci. Aust. Record 2013/39; Geoscience Australia: Canberra, Australia. p.8, **2013**.
[54]	Wanger, T.C. The Lithium future-resources, recycling, and the environment. Conserv. Lett. 4, 202-206, **2011**.
[55]	Dawouda, H.D.; Altahtamounia, T.M.; Zaghoa, M.M.; Bensalahb, N. A brief overview of flexible CNT/PANI super capacitors. Mater. Sci. Nanotechnol. 1, 23-36, **2017**.
[56]	Watanabe, M.; Tryk, D.A. Fuel Cells: An Overview with Emphasis on Polymer Electrolyte Fuel Cells. In Electrochemical Science for a Sustainable Society; Springer Science and Business Media LLC: Berlin/Heidelberg, Germany, pp. 51-94, **2017**.
[57]	Qaisar, Abbas; Mojtaba, Mirzaeian; Michael, R.C., Hunt; Peter, Hall; Rizwan, Raza. Current State and Future Prospects for Electrochemical Energy Storage and Conversion Systems. Special Issue: High Energy Electrochemical Capacitors. *Energies.* 13, 5847, **2020**. doi: 10.3390/en13215847.
[58]	Brett, M.A., Christopher; Brett, Ana, Maria, Oliveira. The scope of electrochemistry. The nature of electrode reactions. *Electrochemistry: Principles, Methods, and Applications*. Oxford University Press. Published in the United States by Oxford University Press Inc., New York. Printed in Great Britain by Bookcraft (Bath) Ltd, Avon, pp.1-2, **1994**.
[59]	Ferreira, H.L.; Garde, R.; Fulli, G.; Kling, W.; Lopes, J.P. Characterisation of electrical energy storage technologies. Energy. 53, 288-298, **2013**.
[60]	Mirzaeian, M.; Abbas, Q.; Ogwu, A.; Hall, P.; Goldin, M.; Mirzaeian, M.; Jirandehi, H.F. Electrode and electrolyte materials for electrochemical capacitors. Int. J. Hydrogen Energy. 42, 25565-25587, **2017**.
[61]	Kötz, R.; Carlen, M. Principles and applications of electrochemical capacitors. Electrochim. Acta. 45, 2483-2498, **2000**.
[62]	Conway, B.E. Transition from "Supercapacitor" to "Battery" Behavior in Electrochemical Energy Storage. J. Electrochem. Soc. 138, 1539-1548, **1991**.
[63]	Conway, B.; Birss, V.; Wojtowicz, J. The role and utilization of pseudocapacitance for energy storage by supercapacitors. J. Power Sour. 66, 1-14, **1997**.
[64]	Gogotsi, Y.; Penner, R.M. Energy Storage in Nanomaterials - Capacitive, Pseudocapacitive, or Battery-like? ACS Nano. 12, 2081-2083, **2018**.
[65]	Xu, B.; Feng, W.; Chen, S.; Zhou, Z.; Cao, G.; Yang, Y. High-capacitance carbon electrode prepared by PVDC carbonization for aqueous EDLCs. Electrochim. Acta. 54, 2185-2189, **2009**.
[66]	Augustyn, V.; Simon, P.; Dunn, B. Pseudocapacitive oxide materials for high-rate electrochemical energy storage. Energy Environ. Sci. 7, 1597-1614, **2014**.

[67]	Senthilkumar, B.; Khan, Z.; Park, S.; Kim, K.; Ko, H.; Kim, Y. Highly porous graphitic carbon and $Ni_2P_2O_7$ for a high performance aqueous hybrid supercapacitor. J. Mater. Chem. A. 3, 21553-21561, **2015**.
[68]	Wei, J.-S.; Wan, S.; Zhang, P.; Ding, H.; Chen, X.-B.; Xiong, H.-M.; Gao, S.; Wei, X. Preparation of porous carbon electrodes from semen cassiae for high-performance electric double-layer capacitors. New J. Chem. 42, 6763-6769, **2018**.
[69]	Wang, G.; Oswald, S.; Löffler, M.; Müllen, K.; Feng, X. Beyond Activated Carbon: Graphite-Cathode-Derived Li-Ion Pseudocapacitors with High Energy and High Power Densities. Adv. Mater. 31, e1807712, **2019**.
[70]	Ahn,W.; Lee, D.U.; Li, G.; Feng, K.;Wang, X.; Yu, A.; Lui, G.; Chen, Z. Highly Oriented Graphene Sponge Electrode for Ultra High Energy Density Lithium Ion Hybrid Capacitors. ACS Appl. Mater. Interfaces. 8, 25297-25305, **2016**.
[71]	Mostazo-López, M.J.; Ruiz-Rosas, R.; Castro-Muñiz, A.; Nishihara, H.; Kyotani, T.; Morallón, E.; Cazorla-Amorós, D. Ultraporous nitrogen-doped zeolite-templated carbon for high power density aqueous-based supercapacitors. Carbon. 129, 510-519, **2018**.
[72]	Gao, H.; Li, J.; Miller, J.R.; Outlaw, R.A.; Butler, S.; Lian, K. Solid-state electric double layer capacitors for ac line-filtering. Energy Storage Mater. 4, 66-70, **2016**.
[73]	Liu, Q.; Ji, S.; Yang, J.; Wang, H.; Pollet, B.G.; Wang, R. Enhanced Cycleability of Amorphous MnO_2 by Covering on α-MnO_2 Needles in an Electrochemical Capacitor. Materials. 10, 988, **2017**.
[74]	Attias, R.; Hana, O.; Sharon, D.; Malka, D.; Hirshberg, D.; Luski, S.; Aurbach, D. Solid state synthesis of Li0.33MnO$_2$ as positive electrode material for highly stable 2V aqueous hybrid supercapacitors. Electrochim. Acta. 254, 155-164, **2017**.
[75]	Wang, D.; Geng, Z.; Li, B.; Zhang, C. High performance electrode materials for electric double-layer capacitors based on biomass-derived activated carbons. Electrochim. Acta. 173, 377-384, **2015**.
[76]	Senthilkumar, S.T.; Selvan, R.K.; Ponpandian, N.; Melo, J.S.; Lee, Y.S. Improved performance of electric double layer capacitor using redox additive (VO2+/VO2+) aqueous electrolyte. J. Mater. Chem. A. 1, 7913-7919, **2013**.
[77]	Yang, H.-Z.; Zou, J.-P. Controllable preparation of hierarchical NiO hollow microspheres with high pseudo-capacitance. Trans. Nonferrous Met. Soc. China. 28, 1808-1818, **2018**.
[78]	Cheng, Z.; Tan, G.; Qiu, Y.; Guo, B.; Cheng, F.; Fan, H. High performance electrochemical capacitors based on MnO2/activated-carbon-paper. J. Mater. Chem C. 3, 6166-6171, **2015**.
[79]	Wang, P.; Wang, R.; Lang, J.; Zhang, X.; Chen, Z.; Yan, X. Porous niobium nitride as a capacitive anode material for advanced Li-ion hybrid capacitors with superior cycling stability. J. Mater. Chem. A. 4, 9760-9766, **2016**.
[80]	Zeng, Z.;Wang, D.; Zhu, J.; Xiao, F.; Li, Y. NiCo2S4 nanoparticles//activated balsam pear pulp for asymmetric hybrid capacitors. *CrystEngComm*. 18, 2363-2374, **2016**.
[81]	Linden, D. Handbook of Batteries and Fuel Cells; McGraw-Hill Book Co.: New York, NY, USA. p.1075, **1984**.
[82]	Ponrouch, A.; Bitenc, J.; Dominko, R.; Lindahl, N.; Johansson, P.; Palacin, M. Multivalent rechargeable batteries. Energy Storage Mater. 20, 253-262, **2019**.
[83]	Bradbury, K. Energy Storage Technology Review; Duke University: Durham, NC, USA. pp. 1-34, **2010**.

[84]	Dunlop, J.P. Batteries and Charge Control in Stand-Alone Photovoltaic Systems: Fundamentals and Application; FSEC-CR-1292-01; Florida Solar Energy Center/University of Central Florida: Cocoa, FL, USA, **1997**.
[85]	Chen, H.; Cong, T.N.; Yang,W.; Tan, C.; Li, Y.; Ding, Y. Progress in electrical energy storage system: A critical review. Prog. Nat. Sci. 19, 291-312, **2009**.
[86]	Díaz-González, F.; Sumper, A.; Gomis-Bellmunt, O.; Villafáfila-Robles, R. A review of energy storage technologies for wind power applications. Renew. Sustain. Energy Rev. 16, 2154-2171, **2012**.
[87]	Liang, Y.; Zhao, C.; Yuan, H.; Chen, Y.; Zhang, W.; Huang, J.; Yu, D.; Liu, Y.; Titirici, M.; Chueh, Y.; et al. A review of rechargeable batteries for portable electronic devices. InfoMat. 1, 6-32, **2019**.
[88]	Chen, R.; Li, L.; Fan, E.; Xue, Q.; Bian, Y.;Wu, F.; Chen, R. Toward sustainable and systematic recycling of spent rechargeable batteries. Chem. Soc. Rev. 47, 7239-7302, **2018**.
[89]	Gauthier, M.; Nguyen, M.H.; Blondeau, L.; Foy, E.; Wong, A. Operando NMR characterization of a metal-air battery using a double-compartment cell design. *Solid State Nucl. Magn. Reson. 113*, 101731, **2021**.
[90]	Bo, W.; Ahmad, Z.; Alanzi, A.R.A.; Al-Omari, A.I.; Hafez, E.H.; Abdelwahab, S.F. The Current COVID-19 Pandemic in China: An Overview and Corona Data Analysis. *Alex. Eng. J.*, **2021**.
[91]	Liu, Q.; Pan, Z.; Wang, E.; An, L.; Sun, G. Aqueous metal-air batteries: Fundamentals and applications. *Energy Storage Mater. 27*, 478-505, **2020**.
[92]	Nagy, T.; Nagy, L.; Erdélyi, Z.; Baradács, E.; Deák, G.; Zsuga, M.; Kéki, S. Environmentally friendly Zn-air rechargeable battery with heavy metal free charcoal based air cathode. *Electrochim. Acta. 368*, 137592, **2021**.
[93]	Marini, E.; Jörissen, L.; Brimaud, S. Rational design of a low-cost, durable and efficient bifunctional oxygen electrode for rechargeable metal-air batteries. *J. Power Sources. 482*, 228900, **2021**.
[94]	Yuan, T.; Tan, Z.; Ma, C.; Yang, J.; Ma, Z.; Zheng, S. Challenges of Spinel $Li_4Ti_5O_{12}$ for Lithium-Ion Battery Industrial Applications. Adv. Energy Mater. 7, 1601625, **2017**.
[95]	Ren,W.-F.; Zhou, Y.; Li, J.-T.; Huang, L.; Sun, S.-G. Si anode for next-generation lithium-ion battery. Curr. Opin. Electrochem. 18, 46-54, **2019**.
[96]	Pistoia, G. Lithium-Ion Batteries: Advances and Applications; Elsevier: Amsterdam, The Netherlands. p.664, **2013**.
[97]	Wu, Y.-P.; Rahm, E.; Holze, R. Carbon anode materials for lithium-ion batteries. J. Power Sour. 114, 228-236, **2003**.
[98]	Shen, X.; Tian, Z.; Fan, R.; Shao, L.; Zhang, D.; Cao, G.; Kou, L.; Bai, Y. Research progress on silicon/carbon composite anode materials for lithium-ion battery. J. Energy Chem. 27, 1067-1090, 2018.
[99]	Mahmood, N.; Tang, T.; Hou, Y. Nanostructured Anode Materials for Lithium-Ion Batteries: Progress, Challenge and Perspective. Adv. Energy Mater. 6, 1600374, **2016**.
[100]	Zuo, D.; Tian, G.; Li, X.; Chen, D.; Shu, K. Recent progress in surface coating of cathode materials for lithium ion secondary batteries. J. Alloys Compd. 706, 24-40, **2017**.
[101]	Schipper, F.; Nayak, P.K.; Erickson, E.M.; Amalraj, S.F.; Srur-Lavi, O.; Penki, T.R.; Talianker, M.; Grinblat, J.; Sclar, H.; Breuer, O.; et al. Study of Cathode Materials for Lithium-Ion Batteries: Recent Progress and New Challenges. Inorganics. 5, 32, **2017**.

[102]	Montanino, M.; Moreno, M.; Carewska, M.; Maresca, G.; Simonetti, E.; Presti, R.L.; Alessandrini, F.; Appetecchi, G. Mixed organic compound-ionic liquid electrolytes for lithium battery electrolyte systems. J. Power Sour. 269, 608-615, **2014**.
[103]	Eshetu, G.G.; Judez, X.; Li, C.; Martinez-Ibañez, M.; Sánchez-Diez, E.; Rodriguez-Martinez, L.M.; Zhang, H.; Armand, M. CHAPTER 4. Solid Electrolytes for Lithium Metal and Future Lithium-ion Batteries. In Future Lithium-ion Batteries; Royal Society of Chemistry (RSC): London, UK. pp. 72-101, **2019**.
[104]	Arya, A.; Sharma, A.L. Polymer electrolytes for lithium-ion batteries: A critical study. Ionics. 23, 497-540, **2017**.
[105]	Sullivan, J.; Gaines, L. Status of life cycle inventories for batteries. Energy Convers. Manag. 58, 134-148, **2012**.
[106]	Pavlov, D. Lead-Acid Batteries: Science and Technology; Elsevier BV: Amsterdam, The Netherlands. **2011**.
[107]	Ballantyne, A.D.; Hallett, J.P.; Riley, D.J.; Shah, N.; Payne, D.J. Lead acid battery recycling for the twenty-first century. R. Soc. Open Sci. 5, 171368, **2018**.
[108]	May, G.J.; Davidson, A.J.; Monahov, B. Lead batteries for utility energy storage: A review. J. Energy Storage. 15, 145-157, **2018**.
[109]	Rand, D.; Holden, L.; May, G.; Newnham, R.; Peters, K. Valve-regulated lead/acid batteries. J. Power Sour. 59, 191-197, **1996**.
[110]	Gaines, L.; Sullivan, J.; Burnham, A.; Belharouak, I. Life-cycle analysis for lithium-ion battery production and recycling. In Proceedings of the Transportation Research Board 90th Annual Meeting, Washington, DC, USA, 23-27 January **2011**; Available online: https://www.researchgate.net/profile/Linda_Gaines/publication/265158823_ Paper_No._11-3891_LifeCycle_Analysis_for_LithiumIon_Battery_Production_and Recycling/links/547336180cf216f8cfaeb58a.pdf. (Accessed 20/3/2023).
[111]	Sullivan, J.; Gaines, L. A Review of Battery Life-Cycle Analysis: State of Knowledge and Critical Needs; Argonne National Lab. (ANL): Argonne, IL, USA, **2010**. Available online: https://publications.anl.gov/anlpubs/2010/11/68455.pdf. (Accessed 20/3/2023).
[112]	Otto, J. Lead Acid Type Storage Battery. Google Patents US3257237A, **1966**.
[113]	Mcclelland, D.H.; Devitt, J.L. Maintenance-Free Type Lead Acid. Google Patents US4166155A, **1979**.
[114]	Beaudin, M.; Zareipour, H.; Schellenberglabe, A.; Rosehart, W. Energy storage for mitigating the variability of renewable electricity sources: An updated review. Energy Sustain. Dev. 14, 302-314, **2010**.
[115]	Hadjipaschalis, I.; Poullikkas, A.; Efthimiou, V. Overview of current and future energy storage technologies for electric power applications. Renew. Sustain. Energy Rev. 13, 1513-1522, **2009**.
[116]	Kondoh, J.; Ishii, I.; Yamaguchi, H.; Murata, A.; Otani, K.; Sakuta, K.; Higuchi, N.; Sekine, S.; Kamimoto, M. Electrical energy storage systems for energy networks. Energy Convers. Manag. 41, 1863-1874, **2000**.
[117]	Linden, D.; Reddy, T.B. Handbook of Batteries, 3rd ed.; McGraw-Hill: New York, NY, USA, **2002**.
[118]	McKeon, B.B.; Furukawa, J.; Fenstermacher, S. Advanced Lead-Acid Batteries and the Development of Grid-Scale Energy Storage Systems. Proc. IEEE. 102, 951-963, **2014**.
[119]	Farret, F.A.; Simoes, M.G. Integration of Alternative Sources of Energy; John Wiley & Sons: Hoboken, NJ, USA, **2006**.

[120]	Rastler, D. Electricity Energy Storage Technology Options: A White Paper Primer on Applications, Costs, and Options; Electric Power Research Institute (EPRI): Palo Alto, CA, USA, **2010**. Available online: http://large.stanford.edu/courses/2012/ph240/doshay1/docs/EPRI.pdf. (Accessed 20/3/2023).
[121]	Hage, D.S. Reference Module in Chemistry, Molecular Sciences and Chemical Engineering; Elsevier Inc.: Amsterdam, The Netherlands, **2013**.
[122]	Zelinsky, M.; Fetcenko, M.; Kusay, J.; Koch, J. Storage-integrated PV systems using advanced NiMH battery technology. In Proceedings of the Fifth International Renewable Energy Storage Conference (IRES 2010), Berlin, Germany, **2010**.
[123]	Poullikkas, A. A comparative overview of large-scale battery systems for electricity storage. Renew. Sustain. Energy Rev. 27, 778-788, **2013**.
[124]	Rydh, C.J.; Karlström, M. Life cycle inventory of recycling portable nickel-cadmium batteries. Resour. Conserv. Recycl. 34, 289-309, **2002**.
[125]	Bruce, P.G. Energy storage beyond the horizon: Rechargeable lithium batteries. Solid State Ion. 179, 752-760, **2008**.
[126]	Wakihara, M. Recent developments in lithium ion batteries. Mater. Sci. Eng. R Rep. 33, 109-134, **2001**.
[127]	Avril, S.; Arnaud, G.; Florentin, A.; Vinard, M.Multi-objective optimization of batteries and hydrogen storage technologies for remote photovoltaic systems. Energy. 35, 5300-5308, **2010**.
[128]	Hung, Y.-Y.; Yin, L.-T.;Wang, J.-W.;Wang, C.-T.; Tsai, C.-H.; Kuo, Y.-M. Recycling of spent nickel-cadmium battery using a thermal separation process. Env. Prog. Sustain. Energy. 37, 645-654, **2017**.
[129]	Zelinsky, M.A.; Koch, J.; Young, K.-H. Performance Comparison of Rechargeable Batteries for Stationary Applications (Ni/MH vs. Ni-Cd and VRLA). Batteries. 4, 1, **2017**.
[130]	Moeller, K.-C. Overview of battery systems. In Lithium-Ion Batteries: Basics and Applications; Springer Science and Business Media LLC: Berlin/Heidelberg, Germany. pp. 3-10, **2018**.
[131]	Williams, J.B. Portable Power: Batteries. In The Electric Century; Springer Science and Business Media LLC: New York, NY, USA. pp. 84-92, **2017**.
[132]	Yazami, R.; Deschamps, M. The 13th International Seminar on Primary and Secondary Battery Technology and Application; Florida Educational Seminars: Boca Raton, FL, USA. p. 19960304, **1996**.
[133]	Dhar, S.; Ovshínsky, S.; Gifford, P.; Corrigan, D.; Fetcenko, M.; Venkatesan, S. Nickel/metal hydride technology for consumer and electric vehicle batteries-A review and up-date. J. Power Sour. 65, 1-7, **1997**.
[134]	Rantik, M. Life Cycle Assessment of Five Batteries for Electric Vehicles under Different Charging Regimes, Technical Report for, Life Cycle Assessment of Five Batteries for Electric Vehicles under Different Charging Regimes; U.S. Department of Energy: Washington, DC, USA, ISSN 1401-1271. TRN: SE0007008, **1999**.
[135]	Fetcenko, M.; Ovshinsky, S.; Reichman, B.; Young, K.; Fierro, C.; Koch, J.; Zallen, A.; Mays, W.; Ouchi, T. Recent advances in NiMH battery technology. J. Power Sour. 165, 544-551, **2007**.
[136]	Notten, P.H. Nickel-metal hydride batteries: From concept to characteristics. Hem. Ind. 54, 102-115, **2000**.

[137]	Qiao, S.; Hu, M.; Fu, C.; Qin, D.; Zhou, A.; Wang, P.; Lin, F. Experimental Study on Storage and Maintenancem Method of Ni-MH Battery Modules for Hybrid Electric Vehicles. Appl. Sci. 9, 1742, **2019**.
[138]	Noga, M.; Juda, Z. The application of nimh batteries in a light-duty electric vehicle. Czas. Tech. 1, 197-222, **2019**.
[139]	Budde-Meiwes, H.; Drillkens, J.; Lunz, B.; Muennix, J.; Rothgang, S.; Kowal, J.; Sauer, D.U. A review of current automotive battery technology and future prospects. Proc. Inst. Mech. Eng. Part. D J. Automob. Eng. 227, 761-776, **2013**.
[140]	El Kharbachi, A.; Zavorotynska, O.; Latroche, M.; Cuevas, F.; Yartys, V.; Fichtner, M. Exploits, advances and challenges benefiting beyond Li-ion battery technologies. J. Alloys Compd. 817, 153261, **2020**.
[141]	Landi, B.J.; Ganter, M.J.; Cress, C.D.; Dileo, R.A.; Raffaelle, R.P. Carbon nanotubes for lithium ion batteries. Energy Environ. Sci. 2, 638-654, **2009**.
[142]	Zubi, G.; Dufo-López, R.; Carvalho, M.; Pasaoglu, G. The lithium-ion battery: State of the art and future perspectives. Renew. Sustain. Energy Rev. 89, 292-308, **2018**.
[143]	Wang, W.; Luo, Q.; Li, B.; Wei, X.; Li, L.; Yang, Z. Recent Progress in Redox Flow Battery Research and Development. Adv. Funct. Mater. 23, 970-986, **2013**.
[144]	Li, L.; Kim, S.;Wang,W.; Vijayakumar, M.; Nie, Z.; Chen, B.; Zhang, J.; Xia, G.; Hu, J.; Graff, G.L.; et al. Astable Vanadium Redox-Flow Battery with High Energy Density for Large-Scale Energy Storage. Adv. Energy Mater. 1, 394-400, **2011**.
[145]	Gandomi, Y.A.; Aaron, D.S.; Houser, J.R.; Daugherty, M.C.; Clement, J.T.; Pezeshki, A.M.; Ertugrul, T.Y.; Moseley, D.P.; Mench, M.M. Critical Review - Experimental Diagnostics and Material Characterization Techniques Used on Redox Flow Batteries. J. Electrochem. Soc. 165, A970-A1010, **2018**.
[146]	Ye, R.; Henkensmeier, D.; Yoon, S.J.; Huang, Z.; Kim, D.K.; Chang, Z.; Kim, S.; Chen, R. Redox Flow Batteries for Energy Storage: A Technology Review. J. Electrochem. Energy Convers. Storage. 15, 010801, **2017**.
[147]	Xu, Q.; Ji, Y.; Qin, L.; Leung, P.; Qiao, F.; Li, Y.; Su, H. Evaluation of redox flow batteries goes beyond round-trip efficiency: A technical review. J. Energy Storage. 16, 108-115, **2018**.
[148]	McCrabb, H.; Snyder, S.; Taylor, E.J. An Electrochemical Etching Process for Flow Battery Structures to Improve Performance and Reduce Manufacturing Cost. ECS Meet. Abstr. **2014**.
[149]	Nguyen, T.; Savinell, R.F. Flow batteries. Elec. Soc. Interf. 19, 54, **2010**.
[150]	Perry, M.L.; Fuller, T.F. A Historical Perspective of Fuel Cell Technology in the 20th Century. J. Electrochem. Soc. 149, S59-S67, **2002**.
[151]	Sharaf, O.Z.; Orhan, M.F. An overview of fuel cell technology: Fundamentals and applications. Renew. Sustain. Energy Rev. 32, 810-853, **2014**.
[152]	Hoed, R.V.D.; Vergragt, P.J. Institutional change in the automotive industry. In The Business of Sustainable Mobility; Informa UK Limited: Colchester, UK, pp. 61-79, **2017**.
[153]	Raza, R.; Akram, N.; Javed, M.S.; Rafique, A.; Ullah, K.; Ali, A.; Saleem, M.; Ahmed, R. Fuel cell technology for sustainable development in Pakistan - An over-view. Renew. Sustain. Energy Rev. 53, 450-461, **2016**.
[154]	Alaswad, A.; Baroutaji, A.; Achour, H.; Carton, J.; Al Makky, A.; Olabi, A. Developments in fuel cell technologies in the transport sector. Int. J. Hydrogen Energy. 41, 16499-16508, **2016**.

[155]	Xu, Q.; Zhang, F.; Xu, L.; Leung, P.; Yang, C.; Li, H. The applications and prospect of fuel cells in medical field: A review. Renew. Sustain. Energy Rev. 67, 574-580, **2017**.
[156]	A. Brouzgou, A. Demin, P.Tsiakaras. Interconnects for solid oxide fuel cells. Interconnects for Solid Oxide Fuel Cells. In: Boaro, M., Salvatore, A. (eds) Advances in Medium and High Temperature Solid Oxide Fuell Cell Technology. *CISM International Centre for Mechanical Sciences*, vol 574. Springer, Cham., **2017**.
[157]	Mekhilef, S.; Saidur, R.; Safari, A. Comparative study of different fuel cell technologies. Renew. Sustain. Energy Rev. 16, 981-989, **2012**.
[158]	Dong, X.; Tian, L.; Li, J.; Zhao, Y.; Tian, Y.; Li, Y. Single layer fuel cell based on a composite of $Ce_{0.8}Sm_{0.2}O_2$-δ-Na_2CO_3 and a mixed ionic and electronic conductor $Sr_2Fe_{1.5}Mo_{0.5}O_6$ -δ. J. Power Sour. 249, 270-276, **2014**.
[159]	Nymand, M.; Andersen, M.A.E.Anew approach to high efficiency in isolated boost converters for high-power low-voltage fuel cell applications. In Proceedings of the 2008 13th International Power Electronics and Motion Control Conference, Poznan, Poland. Institute of Electrical and Electronics Engineers (IEEE): Piscataway Township, NJ, USA. pp. 127-131, **2008**.
[160]	P. Tsiakaras, C.G. Vayenas. Oxidative coupling of CH_4 on Ag catalyst-electrodes deposited on ZrO_2 (8 mol% Y_2O_3). *Journal of Catalysis 144 (1)*, 333-347, **1993**.
[161]	Song, X.; Dong, X.; Li, M.;Wang, H. Effects of adding alumina to the nickel-zirconia anode materials for solid oxide fuel cells and a two-step sintering method for half-cells. J. Power Sour. 308, 58-64, **2016**.
[162]	Da Silva, F.S.; De Souza, T.M. Novel materials for solid oxide fuel cell technologies: A literature review. Int. J. Hydrogen Energy. 42, 26020-26036, **2017**.
[163]	Alnegren, P.; Sattari, M.; Froitzheim, J.; Svensson, J.-E. Degradation of ferritic stainless steels under conditions used for solid oxide fuel cells and electrolyzers at varying oxygen pressures. Corros. Sci. 110, 200-212, **2016**.
[164]	Fan, L.; Zhu, B.; Su, P.-C.; He, C. Nanomaterials and technologies for low temperature solid oxide fuel cells: Recent advances, challenges and opportunities. Nano Energy. 45, 148-176, **2018**.
[165]	P. Tsiakaras, C. Athanasiou, G. Marnellos, M. Stoukides, J.E. ten Elshof. Methane activation on a $La_{0.6}Sr_{0.4}Co_{0.8}Fe_{0.2}O3$ perovskite: Catalytic and electrocatalytic results. *Applied catalysis A: General 169 (2)*, 249-261, **1998**.
[166]	Irvine, J.; Tao, S. Fuel Electrodes for Solid Oxide Fuel Cells. Lubr. Addit. 8, 739-765, **2005**.
[167]	Bae, K.; Jang, D.Y.; Choi, H.J.; Kim, D.; Hong, J.; Kim, B.-K.; Lee, J.-H.; Son, J.-W.; Shim, J.H. Demonstrating the potential of yttrium-doped barium zirconate electrolyte for high-performance fuel cells. Nat. Commun. 8, 14553, **2017**.
[168]	Goor, M.; Menkin, S.; Peled, E. High power direct methanol fuel cell for mobility and portable applications. Int. J. Hydrogen Energy. 44, 3138-3143, **2019**.
[169]	Das, S.; Dutta, K.; Nessim, G.D.; Kader, M.A. Direct Methanol Fuel Cell Technology. In Direct Methanol Fuel Cell Technology; Elsevier BV: Amsterdam, The Netherlands. pp. 1-12, **2020**.
[170]	Xia, Z.; Zhang, X.; Sun, H.; Wang, S.; Sun, G. Recent advances in multi-scale design and construction of materials for direct methanol fuel cells. Nano Energy. 65, 104048, **2019**.
[171]	Z. Chen, J. Liu, B. Yang, M. Lin, C. Molochas, P. Tsiakaras, P. Shen. Two-stage confinement derived small-sized highly ordered L_{10}-PtCoZn for effective oxygen reduction catalysis in PEM fuel cells. *Journal of Colloid and Interface Science 652*, 388-404, **2023**.

[172]	Behret, H. Karl Kordesch und Günter Simader: Fuel Cells and Their Applications, VCH, Weinheim, 1996. ISBN 3-527-28579-2, DM 248,-. Ber. Der Bunsenges. Für Phys. Chem. 100, 1922, **1996**.
[173]	Jung, G.-B.; Tu, C.-H.; Chi, P.-H.; Su, A.; Weng, F.-B.; Lin, Y.-T.; Chiang, Y.-C.; Lee, C.-Y.; Yan, W.-M. Investigations of flow field designs in direct methanol fuel cell. J. Solid State Electrochem. 13, 1455-1465, **2008**.
[174]	Kakati, B.K.; Mohan, V. Development of Low-Cost Advanced Composite Bipolar Plate for Proton Exchange Membrane Fuel Cell? Fuel Cells. 8, 45-51, **2008**.
[175]	Authayanun, S.; Im-Orb, K.; Arpornwichanop, A. A review of the development of high temperature proton exchange membrane fuel cells. Chin. J. Catal. 36, 473-483, **2015**.
[176]	Zhu, B.; Raza, R.; Abbas, G.; Singh, M. An Electrolyte-Free Fuel Cell Constructed from One Homogenous Layer with Mixed Conductivity. Adv. Funct. Mater. 21, 2465-2469, **2011**.
[177]	Zhu, B.; Raza, R.; Qin, H.; Fan, L. Single-component and three-component fuel cells. J. Power Sour. 196, 6362-6365, **2011**.
[178]	Mahato, N.; Banerjee, A.; Gupta, A.; Omar, S.; Balani, K. Progress in material selection for solid oxide fuel cell technology: A review. Prog. Mater. Sci. 72, 141-337, **2015**.
[179]	Tiwari, J.N.; Tiwari, R.N.; Singh, G.; Kim, K.S. Recent progress in the development of anode and cathode catalysts for direct methanol fuel cells. Nano Energy. 2, 553-578, **2013**.
[180]	Ursua, A., Gandia, L. M., Sanchis, P. "Hydrogen production from water electrolysis: current status and future trends" in Proceedings of the IEEE (New York, NY: Electronics and Electrical Engineers, Inc.), 410-426, **2012**.
[181]	Badwal, S. P. S., Giddey, S., and Munnings, C. Hydrogen production via solid electrolyte routes. *WIREs Energy Environ*. 2, 473-487, **2013**. doi:10.1002/wene.50.
[182]	Badwall, P.S. Sukhvinder; Giddey, S. Sarbjit; Munnings, Christopher; Bhatt; I. Anand; Hollenkamp, F. Anthony. Emerging electrochemical energy conversion and storage technologies. *Frontiers in Chemistry*. 2, 79 5847. Edited by Lapkin Alexei. Reviewed by Gu Shuang, **2014**. doi: 10.3389/fchem.2014.00079.
[183]	Edwards, J. H., Badwal, S. P. S., Duffy, G., Lasich, J., and Ganakas, G. The application of solid state ionics technology for novel methods of energy generation and supply. *Solid State Ionics* 152-153, 843-852, **2002**. doi:10.1016/S0167-2738(02)00384-3.
[184]	Brisse, A., Schefold, J., and Zahid, M. High temperature water electrolysis in solid oxide cells. *Int. J. Hydrogen Energy* 33, 5375-5382, **2008**. doi: 10.1016/j.ijhydene.2008.07.120.
[185]	Laguna-Bercero, M. A. Recent advances in high temperature electrolysis using solid oxide fuel cells: a review. *J. PowerSources* 203, 4-16, **2012**. doi: 10.1016/j.jpowsour. 2011.12.019.
[186]	Fujiwara, S., Kasai, S., Yamauchi, H., Yamada, K., Makino, S., Matsunaga, K., et al. Hydrogen production by high temperature electrolysis with nuclear reactor. *Prog. Nuclear Energy*. 50, 422-426, **2008**. doi: 10.1016/j.pnucene.2007.11.025.
[187]	Coughlin, R. W., and Farooque, M. Thermodynamic, kinetic, and mass balance aspects of coal-depolarized water electrolysis. *Ind. Eng. Chem. Process Des. Dev*. 21, 559-564, **1982**. doi: 10.1021/i200019a004.
[188]	Seehra, M. S., and Bollineni, S. Nanocarbon boosts energy-efficient hydrogen production in carbon-assisted water electrolysis. *Int. J. Hydrogen Energy* 34, 6078-6084, **2009**. doi: 10.1016/j.ijhydene.2009.06.023.
[189]	Ewan, B.C.R., and Adeniyi, O.D. A demonstration of carbon-assisted water electrolysis. *Energies* 6, 1657-1668, **2013**. doi: 10.3390/en6031657.

185

[190]	Girishkumar, G., McCloskey, B., Luntz, A. C., Swanson, S., and Wilcke, W. Lithium-air battery: promise and challenges. *J. Phys. Chem. Lett*. 1, 2193-2203, **2010**. doi: 10.1021/jz1005384.
[191]	Bruce, P. G., Hardwick, L. J., and Abraham, K. M. Lithium-air and lithium-sulfur batteries. *MRS Bull*. 36, 506-511, **2011**. doi: 10.1557/mrs.2011.157.
[192]	Kraytsberg, A., and Ein-Eli, Y. Review on Li-air batteries - opportunities, limitations and perspective. *J. PowerSources* 196, 886-893, **2011**. doi: 10.1016/j.jpowsour.2010.09.031.
[193]	Imanishi, N., and Yamamoto, O. Rechargeable lithium-air batteries: characteristics and prospects. *Mater. Today* 17, 24-30, **2014**. doi: 10.1016/j.mattod.2013.12.004.
[194]	Ellis, B. L., and Nazar, L. F. Sodium and sodium-ion energy storage batteries. *Curr. Opin. Solid State Mater. Sci*. 16, 168-177, **2012**. doi: 10.1016/j.cossms.2012.04.002.
[195]	Hartmann, P., Bender, C. L., Sann, J., Dürr, A. K., Jansen, M., Janek, J., et al. A comprehensive study on the cell chemistry of the sodium superoxide (NaO_2) battery. *Phys. Chem. Chem. Phys*. 15, 11661-72, **2013**. doi: 10.1039/c3cp50930c.
[196]	Bruce, P. G., Freunberger, S. A., Hardwick, L. J., and Tarascon, J.-M. Li-O_2 and Li-S batteries with high energy storage. *Nat. Mater*. 11, 19-29, **2012**. doi: 10.1038/nmat3191.
[197]	Manthiram, Y. F., and Su, Y.-S. Challenges and prospects of lithium-sulfur batteries. *Acc. Chem. Res*. 46, 1125-1134, **2013**. doi: 10.1021/ar300179v.
[198]	Song, M.-K., Cairns, E. J., and Zhang, Y. Lithium/Sulfur batteries with high specific energy: old challenges and new opportunities. *Nanoscale* 5, 2186-2204, **2013**. doi: 10.1039/C2NR33044J.
[199]	Jitaru, M. Electrochemical carbon dioxide reduction-fundamental and applied topics (Review). *J. Univ. Chem. Technol. Metal.* 42, 333-344, **2007**.
[200]	Hori, Y. "Electrochemical CO_2 reduction on metal electrodes," in *Modern Aspects of Electrochemistry*, eds C. G. Vayenas, R. E. White, and M. E. Gamboa-Aldeco (New York, NY: Springer), 89-189, **2008**. doi: 10.1007/978-0-387-49489-0_3.
[201]	Lee, J., Kwon, Y., Machunda, R. L., and Lee, H. J. Electrocatalytic recycling of CO_2 and small organic molecules. *Chem. Asian J*. 4, 1516-1523, **2009**. doi: 10.1002/asia. 200900055.
[202]	Beck, J., Johnson, R., and Naya, T. *Electrochemical Conversion of Carbon Dioxide to Hydrocarbon Fuels*. EME 580 Spring, 1-42, **2010**. Available online at: http://www.ems.psu.edu/ ~elsworth/courses/egee580/2010/Final%20Reports/co2_electrochem.pdf. (Accessed 20/3/2023).
[203]	Li, W. "Electrocatalytic reduction of CO_2 to small organic molecule fuels on metal catalysts," in *Advances in CO_2 Conversion and Utilization*, ed Y. Hu (Washington, DC: ACS Symposium Series, American Chemical Society), 55-76, **2010**.
[204]	Whipple, D. T., and Kenis, P. J. A. Prospects of CO_2 utilization via direct heterogeneous electrochemical reduction. *J. Phys. Chem. Lett*. 1,3451-3458, **2010**. doi: 10.1021/jz1012627.
[205]	Hu, B., Guild, C., and Suib, S. L. Thermal, electrochemical and photochemical conversion of CO_2 to fuels and value-added products. *J. CO_2 Util*. 1, 18-27, **2013**. doi: 10.1016/j.jcou.2013.03.004.
[206]	Jhong, H. R. M., Ma, S., and Kenis, P. J. A. Electrochemical conversion of CO_2 to useful chemicals: current status, remaining challenges, and future opportunities. *Curr. Opin. Chem. Eng*. 2, 191-199, **2013**. doi: 10.1016/j.coche.2013.03.005.
[207]	Qiao, J., Liu, Y., Hong, F., and Zhang, J. A review of catalysts for the electroreduction of carbon dioxide to produce low-carbon fuels. *Chem. Soc. Rev*. 43, 631-675, **2014**. doi: 10.1039/c3cs60323g.

[208]	Cook, R. L., MacDuff, R. C., and Sammells, A. F. High rate gas phase CO_2 reduction to ethylene and methane using gas diffusion electrodes. *J. Electrochem. Soc.* 137, 607-608, **1990**. doi: 10.1149/1.2086515.
[209]	Hara, K., Kudo, A., and Sakata, T. High efficiency electrochemical reduction of carbon dioxide under high pressure on a gas diffusion electrode containing Pt catalysts. *J. Electrochem. Soc.* 142, L57-L59, **1995**. doi: 10.1149/1.2044182.
[210]	Hara, K., and Sakata, T. Electrocatalytic formation of CH_4 from CO_2 on a Pt gas diffusion electrode. *J. Electrochem. Soc.* 144, 539-545, **1997**. doi: 10.1149/1.1837445.
[211]	Ogura, K. Electrochemical reduction of carbon dioxide to ethylene: mechanistic approach. *J. CO2 Util*. 1, 43-49, **2013**. doi: 10.1016/j.jcou.2013.03.003.
[212]	Delacourt, C., Ridgway, P. L., Kerr, J. B., and Newman, J. Design of an electrochemical cell making syngas ($CO+H_2$) from CO_2 and H_2O reduction at room temperature. *J. Electrochem. Soc*. 155, B42-B49, **2008**. doi: 10.1149/1.2801871.
[213]	Aeshala, L. M. Effect of cationic and anionic solid polymer electrolyte on direct electrochemical reduction of gaseous CO_2 to fuel. *J. CO2 Util.* 3-4, 49-55, **2013**. doi: 10.1016/j. jcou.2013.09.004.
[214]	Licht, S., Wang, B., Ghosh, S., Ayub, H., Jiang, D., and Ganley, J. A new solar carbon capture process: solar thermal electrochemical photo (STEP) carbon capture. *J. Phys. Chem. Lett*. *1*, 2363-2368, **2010**. doi: 10.1021/jz100829s.
[215]	Stoots, C. M. "High-temperature co-Electrolysis of H_2O and CO_2 for syngas production," in *Fuel Cell Seminar, Preprint, INL/CON-06-11719* (Honolulu, HI), **2006**.
[216]	Stoots, C. Production of synthesis gas by high-temperature electrolysis of H_2O and CO_2 (coelectrolysis), in *Sustainable Fuels from CO2, H2O, and Carbon-Free Energy* (New York, NY: Columbia University), **2010**. Available online: http://energy.columbia.edu/files/2012/11/Coelectrolysis-Rev-2.pdf (Accessed 20/3/2023).
[217]	Bidrawn, F., Kim, G., Corre, G., Irvine, J. T. S., Vohs, J. M., and Gorte, R. J. Efficient reduction of CO_2 in a solid oxide electrolyser. *Electrochem. Solid State Lett.* 11, B167-B170, **2008**. doi: 10.1149/1.2943664.
[218]	Hartvigsen, J., Elangovan, S., Frost, L., Nickens, A., Stoots, C., O'Brien, J., et al. Carbon dioxide recycling by high temperature co-electrolysis and hydrocarbon synthesis. *ECS Trans.* 12, 625-637, **2008**. doi: 10.1149/1.2921588.
[219]	Ebbesen, S. D., and Mogensen, M. Electrolysis of carbon dioxide in solid oxide electrolysis cells. *J. Power Sources* 193, 349-358, **2009**. doi: 10.1016/j.jpowsour.2009.02.093.
[220]	Zhan, Z., Kobsiriphat, J., Wilson ,R., Pillai, M., Kim, I., and Barnett, S. A. Syngas production by coelectrolysis of CO_2/H_2O: the basis for a renewable energy cycle. *Energy Fuels* 23, 3089-3096, **2009**. doi: 10.1021/ef900111f.
[221]	Fu, Q., Dailly, J., Brisse, A., and Zahid, M. High-temperature CO_2 and H_2O electrolysis with an electrolyte-supported solid oxide cell. *ECS Trans.* 35, 2949-2956, **2011**. doi: 10.1149/ 1.3570294.
[222]	Graves, C., Ebbesen, S. D., and Mogensen, M. Co-electrolysis of CO_2 and H_2O in solid oxide cells: performance and durability. *Solid State Ionics* 192, 398-403, **2011**. doi: 10.1016/ j.ssi.2010.06.014.
[223]	Narasimhaiah, G. and Janardhanan, V. M. Modeling CO_2 electrolysis in solid oxide electrolysis cell. *J Solid State Electrochem*. 17, 2361-2370, **2013**. doi: 10.1007/s10008-013-2081-8.
[224]	Wang, H., and Ren, Z. J. A comprehensive review of microbial electrochemical systems as a platform technology. *Biotechnol. Adv*. 31, 1796-1807, **2013**. doi: 10.1016/j.biotechadv.2013.10.001.

187

[225]	Hulanicki, A.; Glab, S.; Ingman, F. Chemical sensors: Definitions and classification. *Pure Appl. Chem. 63*, 1247-1250, **1991**.
[226]	Miri, P.S.; Khosroshahi, N.; Darabi Goudarzi, M.; Safarifard, V. MOF-biomolecule nanocomposites for electrosensing. *Nanochem. Res. 6*, 213-222, **2021**.
[227]	Shetti, N.P.; Nayak, D.S.; Reddy, K.R.; Aminabhvi, T.M. Graphene-Clay-Based Hybrid Nanostructures for Electrochemical Sensors and Biosensors. In *Graphene-Based Electrochemical Sensors for Biomolecules*; Elsevier: Amsterdam, The Netherlands. pp. 235-274, **2019**.
[228]	Meti, M.D.; Abbar, J.C.; Lin, J.; Han, Q.; Zheng, Y.; Wang, Y.; Huang, J.; Xu, X.; Hu, Z.; Xu, H. Nanostructured Au-graphene modified electrode for electrosensing of chlorzoxazone and its biomedical applications. *Mater. Chem. Phys.* 266, **2021**.
[229]	Neiva, E.G.C.; Bergamini, M.F.; Oliveira, M.M.; Marcolino, L.H.; Zarbin, A.J.G. PVP-capped nickel nanoparticles: Synthesis, characterization and utilization as a glycerol electrosensor. *Sens. Actuators B Chem. 196*, 574-581, **2014**.
[230]	Baranwal, Jaya; Barse, Brajesh; Gatto, Gianluca; Broncova, Gabriela; Kumar, Amit. Electrochemical Sensors and Their Applications: A Review. *Chemosensors*. Special Issue: Electrochemical Detection: Analytical and Biological Challenges. 10, 363, **2022**. Edited by Dr. Broncova Gabriela. Academic Editor: Moscone Danila. https://doi.org/10.3390/chemosensors 10090363.
[231]	A. Volkov, E. Gorbova, A. Vylkov, D. Medvedev, A. Demin, P. Tsiakaras. Design and applications of potentiometric sensors based on proton-conducting ceramic materials. A brief review. Sensors and Actuators B: Chemical 244, 1004-1015, **2017**.
[232]	G. Fadeyev, A. Kalyakin, E. Gorbova, A. Brouzgou, A. Demin, A. Volkov, P. Tsiakaras. A simple and low-cost amperometric sensor for measuring H_2, CO, and CH_4. Sensors and Actuators B: Chemical 221, 879-883, **2015**.
[233]	Y. Liu, X. Zhang, Z. Chen, X. Zhang, P. Tsiakaras, P.K. Shen. Electrocatalytic reduction of nitrogen on FeAg/Si for ammonia synthesis: A simple strategy for continuous regulation of faradaic efficiency by controlling H^+ ions transfer rate. Applied Catalysis B: Environmental 283, 119606, **2021**.
[234]	T. Najam, S.S.A. Shah, L. Peng, M.S. Javed, M. Imran, M.Q. Zhao, P. Tsiakaras. Synthesis and nano-engineering of MXenes for energy conversion and storage applications: Recent advances and perspectives. Coordination Chemistry Reviews 454, 214339, **2022**.
[235]	G. Zhang, Y. Shi, H. Wang, L. Jiang, X. Yu, S. Jing, S. Xing, P. Tsiakaras. A facile route to achieve ultrafine Fe_2O_3 nanorods anchored on graphene oxide for application in lithium-ion battery. *Journal of Power Sources 416*, 118-124, **2019**.
[236]	H. Liang, L. Jia, F. Chen, S. Jing, P. Tsiakaras. A novel efficient electrocatalyst for oxygen reduction and oxygen evolution reaction in $Li-O_2$ batteries: Co/CoSe embedded N, Se co-doped carbon. Applied Catalysis B: Environmental 317, 121698, **2022**.
[237]	S. Shah S.A., T. Najam, A. Brouzgou, P. Tsiakaras. Alkaline Oxygen Electrocatalysis for Fuel Cells and Metal-Air Batteries. Encyclopedia of Electrochemistry; Wiley-VCH Verlag GmbH & Co; 9, 1-28, **2017**.
[238]	H. Liang, X. Gong, L. Jia, F. Chen, Z. Rao, S. Jing, P. Tsiakaras. Highly efficient $Li-O_2$ batteries based on self-standing NiFeP@ NC/BC cathode derived from biochar supported Prussian blue analogues. Journal of Electroanalytical Chemistry 867, 114124, **2020**.

[239]	S. Jing, Y. Zhang, F. Chen, H. Liang, S. Yin, P. Tsiakaras. Novel and highly efficient cathodes for Li-O_2 batteries: 3D self-standing NiFe@ NC-functionalized N-doped carbon nanonet derived from Prussian blue analogues/biomass composites. Applied Catalysis B: Environmental 245, 721-732, **2019**.
[240]	H. Liang, Z. Gai, F. Chen, S. Jing, W. Kan, B. Zhao, S. Yin, P. Tsiakaras. Fe_3C decorated wood-derived integral N-doped C cathode for rechargeable Li-O_2 batteries. Applied Catalysis B: Environmental 324, 122203, **2023**.
[241]	S.S.A. Shah, T. Najam, A. Brouzgou, P. Tsiakaras. Alkaline Oxygen Electrocatalysis for Fuel Cells and Metal-Air Batteries. Encyclopedia of Electrochemistry: Online, 1-28, **2021**.
[242]	S. Jing, Z. Gai, M. Li, S. Tang, S. Ji, H. Liang, F. Chen, S. Yin, P. Tsiakaras. Enhanced electrochemical performance of a Li-O_2 battery using Co and N co-doped biochar cathode prepared in molten salt medium. Electrochimica Acta 410, 140002, **2022**.
[243]	H. Liang, F. Chen, M. Zhang, S. Jing, B. Shen, S. Yin, P. Tsiakaras. Highly performing free standing cathodic electrocatalysts for Li-O_2 batteries: $CoNiO_2$ nanoneedle arrays supported on N-doped carbon nanonet. Applied Catalysis A: General 574, 114-121, **2019**.
[244]	H. Liang, Y. Zhang, F. Chen, S. Jing, S. Yin, P. Tsiakaras. A novel NiFe@ NC-functionalized N-doped carbon microtubule network derived from biomass as a highly efficient 3D free-standing cathode for Li-CO_2 batteries. Applied Catalysis B: Environmental 244, 559-567, **2019**.
[245]	Gu, P., Xu, Y.X., Zhao, Y.F., et al.: Electrocatalysis of rechargeable non-lithium metal-air batteries. Adv. Mater. Interfaces 4, 1700589, **2017**. https://doi.org/10.1002/admi.201700589.
[246]	Wenjie, Shao; Rui, Yan; Mi, Zhou; Lang, Ma; Christina, Roth; Tian, Ma; Sujiao, Cao; Chong, Cheng; Bo, Yin; Shuang, Li. Carbon-Based Electrodes for Advanced Zinc-Air Batteries: Oxygen-Catalytic Site Regulation and Nanostructure Design. Electrochemical Energy Reviews 6:11, **2023**.
[247]	Tan, P., Chen, B., Xu, H.R., et al.: Flexible Zn- and Li-air batteries: recent advances, challenges, and future perspectives. Energy Environ. Sci. 10, 2056-2080, **2017**. https://doi.org/10.1039/c7ee0 1913k.
[248]	T. Najam, S.S.A. Shah, S. Ibraheem, X. Cai, E. Hussain, S. Suleman, P. Tsiakaras. Single-atom catalysis for zinc-air/O_2 batteries, water electrolyzers and fuel cells applications. Energy Storage Materials 45, 504-540, **2022**.
[249]	D. Lyu, S. Yao, A. Ali, Z.Q. Tian, P. Tsiakaras, P.K. Shen. N, S Codoped Carbon Matrix-Encapsulated Co_9S_8 Nanoparticles as a Highly Efficient and Durable Bifunctional Oxygen Redox Electrocatalyst for Rechargeable Zn-Air Batteries. Advanced Energy Materials, 2101249, **2021**.
[250]	Y. Li, S.H. Talib, D. Liu, K. Zong, A. Saad, Z. Song, J. Zhao, W. Liu, F. Liu, Q. Ji, P. Tsiakaras. Improved oxygen evolution reaction performance in $Co0.4Mn0_{0,6}O_2$ nanosheets through Triple-doping (Cu, P, N) strategy and its application to Zn-air battery. Applied Catalysis B: Environmental 320, 122023, **2023**.
[251]	Chaturvedi, A., Chen, B., Zhang, K.K., et al.: A universal method for rapid and large-scale growth of layered crystals. SmartMat 1, e1011, **2020**. https://doi.org/10.1002/smm2.1011.
[252]	Fu, J., Cano, Z.P., Park, M.G., et al.: Electrically rechargeable zinc-air batteries: progress, challenges, and perspectives. Adv. Mater. 29, 1604685, **2017**. https://doi.org/10.1002/adma.201604685.
[253]	Zhou, J.W., Cheng, J.L., Wang, B., et al.: Flexible metal–gas batteries: a potential option for next-generation power accessories for wearable electronics. Energy Environ. Sci. 13, 1933-1970, **2020**. https://doi.org/10.1039/d0ee00039f.

[254]	A. Saad, Y. Gao, A. Ramiere, T. Chu, G. Yasin, Y. Wu, S. Ibraheem, M. Wang, P. Tsiakaras. Understanding the Surface Reconstruction on Ternary WxCoBx for Water Oxidation and Zinc-Air Battery Applications. Small 18 (17), 2201067, **2022**.
[255]	Zhou, T.P., Zhang, N., Wu, C.Z., et al.: Surface/interface nanoengineering for rechargeable Zn-air batteries. Energy Environ. Sci. 13, 1132-1153, **2020**. https://doi.org/10.1039/c9ee0 3634b.
[256]	S. Jing, P. Ding, Y. Zhang, H. Liang, S. Yin, P. Tsiakaras. Lithium-sulfur battery cathodes made of porous biochar support CoFe@ NC metal nanoparticles derived from Prussian blue analogues. Ionics 25 (11), 5297-5304, **2019**.
[257]	S.S.A. Shah, T. Najam, M.S. Javed, M.M. Rahman, P. Tsiakaras. Novel Mn-/Co-N x Moieties Captured in N-Doped Carbon Nanotubes for Enhanced Oxygen Reduction Activity and Stability in Acidic and Alkaline Media. ACS Applied Materials & Interfaces 13 (19), 23191-23200, **2021**.
[258]	C.G. Vayenas, S. Bebelis, I.V. Yentekakis, P. Tsiakaras, H. Karasali. Non-faradaic electrochemical modification of catalytic activity reversible promotion of platinum metals catalysts. *Platinum Metals Rev 34 (3)*, 122, **1990**.
[259]	H. Feng, Y. Luo, B. Yan, H. Guo, L. He, Z.Q. Tian, P. Tsiakaras, P.K. Shen. Highly stable cathodes for proton exchange membrane fuel cells: Novel carbon supported Au@PtNiAu concave octahedral core-shell nanocatalyst. Journal of Colloid and Interface Science 626, 1040-1050, **2022**.
[260]	D. Medvedev, V. Maragou, E. Pikalova, A. Demin, P. Tsiakaras. Novel composite solid state electrolytes on the base of $BaCeO_3$ and CeO_2 for intermediate temperature electrochemical devices. Journal of Power Sources 221, 217-227, **2013**.
[261]	S.S.A. Shah, T. Najam, C. Molochas, M.A. Nazir, A. Brouzgou, M.S. Javed, P. Tsiakaras. Nanostructure engineering of metal–organic derived frameworks: Cobalt phosphide embedded in carbon nanotubes as an efficient ORR catalyst. Molecules 26 (21), 6672, **2021**.
[262]	E. Gorbova, V. Maragou, D. Medvedev, A. Demin, P. Tsiakaras. Influence of sintering additives of transition metals on the properties of gadolinium-doped barium cerate Solid State Ionics 179 (21-26), 887-890, **2008**.
[263]	Y. Luo, W. Lou, H. Feng, Z. Liu, Q. Chen, G. Liao, X. Huang, P. Tsiakaras. Ultra-Small Nanoparticles of Pd-Pt-Ni Alloy Octahedra with High Lattice Strain for Efficient Oxygen Reduction Reaction. Catalysts 13 (1), 97, **2023**.
[264]	Z. Chen, C. Hao, B. Yan, Q. Chen, H. Feng, X. Mao, J. Cen, Z.Q. Tian, P. Tsiakaras, P.K. Shen. ZIF-$Mg(OH)_2$ Dual Template Assisted Self-Confinement of Small PtCo NPs as Promising Oxygen Reduction Reaction in PEM Fuel Cell. Advanced Energy Materials 12 (32), 2201600, **2022**.
[265]	Q. Chen, Z. Chen, A. Ali, Y. Luo, H. Feng, Y. Luo, P. Tsiakaras, P.K. Shen. Shell-thickness-dependent Pd@PtNi core-shell nanosheets for efficient oxygen reduction reaction. Chemical Engineering Journal 427, 131565, **2022**.
[266]	A. Tan, Y. Wang, Z. Fu, P. Tsiakaras, Z. Liang. Highly effective oxygen reduction reaction electrocatalysis: Nitrogen-doped hierarchically mesoporous carbon derived from interpenetrated nonporous metal-organic frameworks. Applied Catalysis B: Environmental 218, 260-266, **2017**.
[267]	R. Wu, P. Tsiakaras, P.K. Shen. Facile synthesis of bimetallic Pt-Pd symmetry-broken concave nanocubes and their enhanced activity toward oxygen reduction reaction. Applied Catalysis B: Environmental 251, 49-56, **2019**.

[268]	Q. Chen, Z. Chen, A. Ali, Y. Luo, H. Feng, Y. Luo, P. Tsiakaras, P.K. Shen. Shell-thickness-dependent Pd@PtNi core-shell nanosheets for efficient oxygen reduction reaction. Chemical Engineering Journal 427, 131565, **2022**.
[269]	X. Zhu, L. Huang, M. Wei, P. Tsiakaras, P.K. Shen. Highly stable Pt-Co nanodendrite in nanoframe with Pt skin structured catalyst for oxygen reduction electrocatalysis. Applied Catalysis B: Environmental 281, 119460, **2021**.
[270]	X. Zhu, L. Huang, M. Wei, P. Tsiakaras, P.K. Shen. Highly stable Pt-Co nanodendrite in nanoframe with Pt skin structured catalyst for oxygen reduction electrocatalysis. Applied Catalysis B: Environmental 281, 119460, **2021**.
[271]	F. Coutelieris, S. Douvartzides, P. Tsiakaras. The importance of the fuel choice on the efficiency of a solid oxide fuel cell system. Journal of Power Sources 123 (2), 200-205, **2003**.
[272]	Y. Wang, C. He, A. Brouzgou, Y. Liang, R. Fu, D. Wu, P. Tsiakaras, S. Song. A facile soft-template synthesis of ordered mesoporous carbon/tungsten carbide composites with high surface area for methanol electrooxidation. Journal of Power Sources 200, 8-13, **2012**.
[273]	K. Wang, Y. Wang, Z. Liang, Y. Liang, D. Wu, S. Song, P. Tsiakaras. Ordered mesoporous tungsten carbide/carbon composites promoted Pt catalyst with high activity and stability for methanol electrooxidation. Applied Catalysis B: Environmental 147, 518-525, **2014**.
[274]	GM Andreadis, AKM Podias, PE Tsiakaras. The effect of the parasitic current on the direct ethanol PEM fuel cell operation. Journal of Power Sources 181 (2), 214-227, **2008**.
[275]	X. Li, Y. Liu, J. Zhu, P. Tsiakaras, P.K. Shen. Enhanced oxygen reduction and methanol oxidation reaction over self-assembled Pt-M (M=Co, Ni) nanoflowers. Journal of Colloid and Interface Science 607, 1411-1423, **2022**.
[276]	J. Liu, J. Wang, Y. Fo, B. Zhang, C. Molochas, J. Gao, W. Li, X. Cui, X. Zhou, P. Tsiakaras. Engineering of unique Ni-Ru nano-twins for highly active and robust bifunctional hydrogen oxidation and hydrogen evolution electrocatalysis. Chemical Engineering Journal 454, 139959, **2023**.
[277]	S. Li, Z.Q. Tian, Y. Liu, Z. Jang, S.W. Hasan, X. Chen, P. Tsiakaras, P.K. Shen. Hierarchically skeletal multi-layered Pt-Ni nanocrystals for highly efficient oxygen reduction and methanol oxidation reactions. Chinese Journal of Catalysis 42 (4), 648-657, **2021**.
[278]	A. Brouzgou, A. Seretis, S. Song, P.K. Shen, P. Tsiakaras. CO tolerance and durability study of PtMe (Me=Ir or Pd) electrocatalysts for H_2-PEMFC application. *International Journal of Hydrogen Energy 46 (26)*, 13865-13877, **2021**.
[279]	C. Molochas, P. Tsiakaras. Carbon Monoxide Tolerant Pt-Based Electrocatalysts for H_2-PEMFC Applications: Current Progress and Challenges, Catalysts 11 (9), 1127, **2021**.
[280]	K. Wang, H. Chen, X. Zhang, Y. Tong, S. Song, P. Tsiakaras, Y. Wang. Iron oxide@ graphitic carbon core-shell nanoparticles embedded in ordered mesoporous N-doped carbon matrix as an efficient cathode catalyst for PEMFC. *Applied Catalysis B: Environmental 264*, 118468, **2020**.
[281]	M.A. Goula, S.K. Kontou, P.E. Tsiakaras. Hydrogen production by ethanol steam reforming over a commercial Pd/γ-Al_2O_3 catalyst. Applied Catalysis B: Environmental 49 (2), 135-144, **2004**.
[282]	C. Yu, J. Lu, L. Luo, F. Xu, P.K. Shen, P. Tsiakaras, S. Yin. Bifunctional catalysts for overall water splitting: CoNi oxyhydroxide nanosheets electrodeposited on titanium sheets. Electrochimica Acta 301, 449-45, **2019**.
[283]	L. Zhang, J. Lu, S. Yin, L. Luo, S. Jing, A. Brouzgou, J. Chen, P.K. Shen, P. Tsiakaras. One-pot synthesized boron-doped RhFe alloy with enhanced catalytic performance for hydrogen evolution reaction. Applied Catalysis B: Environmental 230, 58-64, **2018**.

[284]	C. Yu, F. Xu, L. Luo, H.S. Abbo, S.J.J. Titinchi, P.K. Shen, P. Tsiakaras, S. Yin. Bimetallic Ni–Co phosphide nanosheets self-supported on nickel foam as high-performance electrocatalyst for hydrogen evolution reaction. Electrochimica Acta 317, 191-198, **2019**.
[285]	B. Long, H. Yang, M. Li, M.S. Balogun, W. Mai, G. Ouyang, Y. Tong, P. Tsiakaras, S. Song. Interface charges redistribution enhanced monolithic etched copper foam-based Cu_2O layer/TiO_2 nanodots heterojunction with high hydrogen evolution electrocatalytic activity. Applied Catalysis B: Environmental 243, 365-372, **2019**.
[286]	J. Lu, Z. Tang, L. Luo, S. Yin, P.K. Shen, P. Tsiakaras. Worm-like S-doped RhNi alloys as highly efficient electrocatalysts for hydrogen evolution reaction. Applied Catalysis B: Environmental 255, 117737, **2019**.
[287]	J. Cen, E. Jiang, Y. Zhu, Z. Chen, P. Tsiakaras, P.K. Shen. Enhanced electrocatalytic overall water splitting over novel one-pot synthesized $Ru-MoO_3$-x and Fe_3O_4-NiFe layered double hydroxides on Ni foam. Renewable Energy 177, 1346-13, **2021**.
[288]	P. Xu, L. Qiu, L. Wei, Y. Liu, D. Yuan, Y. Wang, P. Tsiakaras. Efficient overall water splitting over Mn doped Ni_2P microflowers grown on nickel foam. Catalysis Today 355, 815-821, **2020**.
[289]	L. Yan, B. Zhang, J. Zhu, Y. Li, P. Tsiakaras, P.K. Shen. Electronic modulation of cobalt phosphide nanosheet arrays via copper doping for highly efficient neutral-pH overall water splitting. Applied Catalysis B: Environmental 265, 118555, **2020**.
[290]	B. Zhang, J. Shan, W. Wang, P. Tsiakaras, Y. Li. Oxygen Vacancy and Core–Shell Heterojunction Engineering of Anemone-Like CoP@ CoOOH Bifunctional Electrocatalyst for Efficient Overall Water Splitting. Small 18 (12), 2106012, **2022**.
[291]	J. Cen, E. Jiang, Y. Zhu, Z. Chen, P. Tsiakaras, P.K. Shen. Enhanced electrocatalytic overall water splitting over novel one-pot synthesized $Ru-MoO_3$-x and Fe_3O_4-NiFe layered double hydroxides on Ni foam. Renewable Energy 177, 1346-13, **2021**.
[292]	G. Long, K. Wan, M. Liu, Z. Liang, J. Piao, P. Tsiakaras. Active sites and mechanism on nitrogen-doped carbon catalyst for hydrogen evolution reaction. Journal of Catalysis 348, 151-159, **2017**.
[293]	A. Saad, Y. Gao, K.A. Owusu, W. Liu, Y. Wu, A. Ramiere, H. Guo, P. Tsiakaras. Ternary Mo_2NiB_2 as a Superior Bifunctional Electrocatalyst for Overall Water Splitting. Small 18 (6), 2104303, **2022**.
[294]	Z. Xie, Z. Song, J. Zhao, Y. Li, X. Cai, D. Liu, J. Shen, P. Tsiakaras. CuZr Metal Glass Powder as Electrocatalysts for Hydrogen and Oxygen Evolution Reactions Catalysts 12 (11), 1378, **2022**.
[295]	W. Xie, J. Huang, L. Huang, S. Geng, S. Song, P. Tsiakaras, Y. Wang. Novel fluorine-doped cobalt molybdate nanosheets with enriched oxygen-vacancies for improved oxygen evolution reaction activity. Applied Catalysis B: Environmental 303, 120871, **2022**.
[296]	D. Liu, Z. Song, S. Cheng, Y. Wang, A. Saad, S. Deng, J. Shen, X. Huang, P. Tsiakaras. Mesoporous IrNiTa metal glass ribbon as a superior self-standing bifunctional catalyst for water electrolysis. Chemical Engineering Journal 431, 134210, **2022**.
[297]	A. Saad, D. Liu, Y. Wu, Z. Song, Y. Li, N. Tayyaba, K. Zong, P. Tsiakaras, X. Cai. Ag nanoparticles modified crumpled borophene supported Co_3O_4 catalyst showing superior oxygen evolution reaction (OER) performance. Applied Catalysis B: Environmental, 120529, **2021**.
[298]	S. Jing, D. Wang, S. Yin, J. Lu, P.K. Shen, P. Tsiakaras. P-doped CNTs encapsulated nickel hybrids with flower-like structure as efficient catalysts for hydrogen evolution reaction. Electrochimica acta 298, 142-149, **2019**.
[299]	S.S.A. Shah, N.A. Khan, M. Imran, M. Rashid, M.K. Tufail, A. Rehman, P. Tsiakaras. Recent Advances in Transition Metal Tellurides (TMTs) and Phosphides (TMPs) for Hydrogen Evolution Electrocatalysis. *Membranes 13 (1)*, 113, **2023**.

[300]	S. Song, V. Maragou, P. Tsiakaras. How far are direct alcohol fuel cells from our energy future? J. Fuel Cell Sci. Technol. 4(2): 203-209, **2007**.
[301]	Q. Chen, P. Tsiakaras, P. Shen. Electrochemical Reduction of Carbon Dioxide: Recent Advances on Au-Based Nanocatalysts. Catalysts 12 (11), 1348, **2022**.
[302]	S.S.A. Shah, M.S. Javed, T. Najam, C. Molochas, N.A. Khan, M.A. Nazir, M. Xu, P.E. Tsiakaras. Metal oxides for the electrocatalytic reduction of carbon dioxide: Mechanism of active sites, composites, interface and defect engineering strategies. Coordination Chemistry Reviews 471, 214716, **2022**.
[303]	A. Wang, H. Liang, F. Chen, X. Tian, S. Yin, S. Jing, P. Tsiakaras. Facile synthesis of C_3N_4/$NiIn_2S_4$ heterostructure with novel solar steam evaporation efficiency and photocatalytic H_2O_2 production performance. Applied Catalysis B: Environmental 310, 121336, **2022**.
[304]	Q.S. Chen, P.L. Cui, J. Yang, D. Chen, H. Liu, H. Feng, P. Tsiakaras, P.K. Shen. Efficient carbon dioxide electroreduction over rationally designed heterogeneous Ag_2S-Au nanocomposites. Journal of Colloid and Interface Science 623, 1172-1180, **2022**.
[305]	Son, H.; Uthirakumar, P.; Chung, T.H.; Polyakov, A.Y.; Lee, I.H. Influence of Ga-halogen bond formation at the interface of nanoporous GaN photoelectrodes for enhanced photo-electrochemical water splitting efficiency. Appl Surf Sci 547:149105, **2021**. https://doi.org/10.1016/j.apsusc.2021.149105.
[306]	Fujishima, A.; Honda, K. Electrochemical photolysis of water at a semiconductor Electrode. Nature 37:238, **1972**. https://doi.org/10.1038/238037a0.
[307]	Reddy, N.L.; Rao, V.N.; Kumari, M.M.; Kakarla, R.R.; Ravi, P.; Sathish, M.; Venkatakrishnan, S.M. Nanostructured semiconducting materials for efficient hydrogen generation. Environ Chem Lett 16:765−796, **2018**. https://doi.org/10.1007/s10311-018-0722-y.
[308]	Lin, J.; Yu, Y.; Xu, Z.; Gao, F.; Zhang, Z.; Zeng, F.; Li, G. Electronic engineering of transition metal Zn-doped InGaN nanorods arrays for photoelectrochemical water splitting. J Power Sources 450:227578, **2020**. https://doi.org/10.1016/j.jpowsour.2019.227578.
[309]	Hassan, N.S.; Jalil, A.A.; Khusnun, N.F.; Ahmad, T.A.T.; Kasmani, R.M.; Norazahar, N.; Kamaroddin, M.F.A.; Vo, D.V.N. Photoelectrochemical water splitting using post-transition metal oxides for hydrogen production: a review. *Environmental Chemistry Letters*. 20:311-333, **2022**. https://doi.org/10.1007/s10311-021-01357-x.
[310]	Liu, Y.; Li, J.; Zhou, B.; Bai, J.; Zheng, Q.; Zhang, J.; Cai, W. Comparison of photo-electrochemical properties of TiO_2-nanotube-array photoanode prepared by anodization in different electro-lyte. Environ Chem Lett 7(4):363-368, **2009**. https://doi.org/10.1007/s10311-008-0180-z.
[311]	Reddy, C.V.; Reddy, K.R.; Shetti, N.P.; Shim, J.; Aminabhavi, T.M.; Dionysiou, D.D. Hetero-nanostructured metal oxide-based hybrid photocatalysts for enhanced photo-electrochemical water splitting - a review. Int J Hydrog Energy 45:18331-18347, **2020**. https://doi.org/10.1016/j.ijhydene.2019.02.109.
[312]	Mohamed, N.A.; Safaei, J.; Ismail, A.F.; Khalid, M.N.; Jailani, M.F.A.M.; Noh, M.F.M.; Teridi, M.A.M. Boosting photocatalytic activities of $BiVO_4$ by creation of g-C_3N_4/ZnO@ $BiVO_4$ Heterojunction. Mater Res Bull 125:110779, **2020**. https://doi.org/10.1016/j.materresbull.2020.110779.
[313]	S. Zhang, F. Zhao, G. Yasin, Y.Y. Dong, J. Zhao, Y. Guo, P. Tsiakaras, J. Zhao. Efficient photocatalytic hydrogen evolution: Linkage units engineering in triazine-based conjugated porous polymers. Journal of Colloid and Interface Science, 637, 41-54, **2023**.

[314]	Suarez, C.M.; Hernandez, S.; Russo, N. $BiVO_4$ as photocatalyst for solar fuels production through water splitting: a short review. Appl Catal A Gen 504:158-170, **2015**. https://doi.org/10.1016/j.apcata.2014.11.044.
[315]	T. Mi, F. Zhao, Y.Y. Dong, J. Zhao, J. Zhao, X. Zhong, N. Zhang, P. Tsiakaras. Enhanced photocatalytic hydrogen evolution activity of co-catalyst free S-scheme polymer heterojunctions via ultrasonic assisted reorganization in solvent. Journal of Colloid and Interface Science, 636, 230-244, **2023**.
[316]	Zhang, J.; Wang, H.; Yuan, X.; Zeng, G.; Tu, W.; Wang, S. Tailored indium sulfide-based materials for solar-energy conversion and utilization. J Photochem Photobiol 38:1-26, **2019**. https://doi.org/10.1016/j.jphotochemrev.2018.11.001.
[317]	Y. Qin, Z. Jiang, Y. Guo, M.A. Mushtaq, Z. Shen, W. Du, C. Ni, G. Luo, Y. Ji, P. Tsiakaras. Benzotriazole-based structure in porous organic polymer enhancing O_2 activation for high-efficient degradation of tetracycline under visible light. Chemical Engineering Journal, 141810, **2023**.
[318]	Arifin, K.; Yunus, R.M.; Minggu, L.J.; Kassim, M.B. Improvement of TiO_2 nanotubes for photoelectrochemical water splitting. Int J Hydrog Energy 46:4998-5024, **2021**. https://doi.org/10.1016/j.ijhydene.2020.11.063.
[319]	G. Balkourani, T. Damartzis, A. Brouzgou, P. Tsiakaras. Cost effective synthesis of graphene nanomaterials for non-enzymatic electrochemical sensors for glucose: a comprehensive review. Sensors 22 (1), 355, **2022**.
[320]	G. Balkourani, A. Brouzgou, M. Archonti, N. Papandrianos, S. Song, P. Tsiakaras. Emerging materials for the electrochemical detection of COVID-19. Journal of Electroanalytical Chemistry 893, 115289, **2021**.
[321]	A. Brouzgou, E. Gorbova, Y. Wang, S. Jing, A. Seretis, Z. Liang, P. Tsiakaras. Nitrogen-doped 3D hierarchical ordered mesoporous carbon supported palladium electrocatalyst for the simultaneous detection of ascorbic acid, dopamine, and glucose. Ionics 25 (12), 6061-6070, **2019**.
[322]	A. Brouzgou, S. Song, P. Tsiakaras. Carbon-supported PdSn and Pd_3Sn_2 anodes for glucose electrooxidation in alkaline media. Applied Catalysis B: Environmental 158, 209-216, **2014**.
[323]	G. Balkourani, T. Damartzis, A. Brouzgou, P. Tsiakaras. Cost effective synthesis of graphene nanomaterials for non-enzymatic electrochemical sensors for glucose: a comprehensive review. Sensors 22 (1), 355, **2022**.
[324]	G. Balkourani, A. Brouzgou, M. Archonti, N. Papandrianos, S. Song, P. Tsiakaras. Emerging materials for the electrochemical detection of COVID-19. Journal of Electroanalytical Chemistry 893, 115289, **2021**.
[325]	X. Yuan, D. Yuan, F. Zeng, W. Zou, F. Tzorbatzoglou, P. Tsiakaras, Y. Wang. Preparation of graphitic mesoporous carbon for the simultaneous detection of hydroquinone and catechol. Applied Catalysis B: Environmental 129, 367-374, **2013**.
[326]	G. Balkourani, K. Molochas, A. Brouzgou, P. Tsiakaras. Me-NC (Me=Fe, Co) Electrocatalysts with EDTA-Derived N for Dopamine Electrochemical Detection. ECS Meeting Abstracts, 2079, **2021**.
[327]	E. Gorbova, G. Balkourani, C. Molochas, D. Sidiropoulos, A. Brouzgou, A.K. Demin, P.E. Tsiakaras. Brief Review on High-Temperature Electrochemical Hydrogen Sensors. Catalysts 12 (12), 1647, **2022**.

[328]	A. Kalyakin, A.K. Demin, E. Gorbova, A. Volkov, P.E. Tsiakaras. Sensor Based on a Solid Oxide Electrolyte for Measuring the Water-Vapor and Hydrogen Content in Air. Catalysts 12 (12), 1558, **2022**.
[329]	G. Balkourani, A. Brouzgou, C.L. Vecchio, A.S. Aricò, V. Baglio, P. Tsiakaras. Selective electro-oxidation of dopamine on Co or Fe supported onto N-doped ketjenblack. Electrochimica Acta 409, 139943, **2022**.
[330]	L.A. Dunyushkina, A.A. Pankratov, V.P. Gorelov, A. Brouzgou, P. Tsiakaras. Deposition and Characterization of Y-doped $CaZrO_3$ Electrolyte Film on a Porous $SrTi_{0,8}Fe_{0,2}O_3$-δ Substrate. Electrochimica Acta, 202, 39-46, **2016**.
[331]	G. Fadeyev, A. Kalyakin, A. Demin, A. Volkov, A. Brouzgou, P. Tsiakaras. Electrodes for solid electrolyte sensors for the measurement of CO and H_2 content in air. *International Journal of Hydrogen Energy, 38 (30)*, 13484-13490, **2013**.
[332]	E. Gorbova, F. Tzorbatzoglou, C. Molochas, D. Chloros, A. Demin, P. Tsiakaras. Fundamentals and Principles of Solid-State Electrochemical Sensors for High Temperature Gas Detection. Catalysts 12 (1), 1, **2022**.
[333]	A. Demin, E. Gorbova, A. Brouzgou, A. Volkov, P. Tsiakaras. Sensors based on solid oxide electrolytes. Solid Oxide-Based Electrochemical Devices, 167-215, **2020**.
[334]	G. Fadeyev, A. Kalyakin, A. Demin, A. Volkov, A. Brouzgou, P. Tsiakaras. Electrodes for solid electrolyte sensors for the measurement of CO and H_2 content in air. International journal of hydrogen energy 38 (30), 13484-13490, **2013**.
[335]	E. Gorbova, F. Tzorbatzoglou, C. Molochas, D. Chloros, A. Demin, P. Tsiakaras. Fundamentals and principles of solid-state electrochemical sensors for high temperature gas detection. Catalysts 12 (1), 1, **2022**.
[336]	A. Kalyakin, A. Demin, E. Gorbova, A. Volkov, P. Tsiakaras. Combined amperometric-potentiometric oxygen sensor. Sensors and Actuators B: Chemical 313, 127999, **2020**.
[337]	A. Kalyakin, A. Volkov, J. Lyagaeva, D. Medvedev, A. Demin, P. Tsiakaras. Combined amperometric and potentiometric hydrogen sensors based on $BaCe_{0,7}Zr_{0,1}Y_{0,2}O_3$–$\delta$ proton-conducting ceramic. Sensors and Actuators B: Chemical 231, 175-182, **2016**.
[338]	A. Kalyakin, G. Fadeyev, A. Demin, E. Gorbova, A. Brouzgou, A. Volkov, P. Tsiakaras. Application of Solid oxide proton-conducting electrolytes for amperometric analysis of hydrogen in H_2+N_2+H_2O gas mixtures. Electrochimica Acta 141, 120-125, **2014**.
[339]	A. Kalyakin, A. Volkov, A. Demin, E. Gorbova, P. Tsiakaras. Determination of nitrous oxide concentration using a solid-electrolyte amperometric sensor. Sensors and Actuators B: Chemical 297, 126750, **2019**.
[340]	A. Kalyakin, J. Lyagaeva, D. Medvedev, A. Volkov, A. Demin, P. Tsiakaras. Characterization of proton-conducting electrolyte based on $La_{0,9}Sr_{0,1}YO_3$-δ and its application in a hydrogen amperometric sensor. Sensors and Actuators B: Chemical 225, 446-452, **2016**.
[341]	Cheng, F. and Chen, J. Metal-air batteries: from oxygen reduction electrochemistry to cathode catalysts. *Chem. Soc. Rev.* 41 (6): 2172-2192, **2011**.
[342]	Chang, Z.W.; Xu, J.-J.; Liu, Q.-C. et al. Recent progress on stability enhancement for cathode in rechargeable non-aqueous lithium-oxygen battery. *Adv. Energy Mater.* 1500633, **2015**.
[343]	Chunlian, Wang; Yongchao, Yu; Jiajia, Niu; Yaxuan, Liu; Denzel, Bridges; Xianqiang, Liu; Joshi, Pooran; Yuefei, Zhang; Anming, Hu. Recent Progress of Metal-Air Batteries - A Mini Review. *Applied Sciences*. 9, 2787, **2019**. doi: 10.3390/app9142787. www.mdpi.com/journal/applsci.

[344]	Zhang, X.; Wang, X.G.; Xie, Z.; Zhou, Z. Recent progress in rechargeable alkali metal-air batteries. *Green Energy Environ*. 1, 4-17, **2016**.
[345]	Abdul, Ghani, Olabi; Enas, Taha, Sayed; Tabbi, Wilberforce; Aisha, Jamal; Abdul, Hai, Alami; Khaled, Elsaid; Shek, Mohammod, Atiqure, Rahman; Sheikh, Khaleduzzaman, Shah; Mohammad, Ali, Abdelkareem. Metal-Air Batteries – A Review. *Energies*. 14, 7373, **2021**. https://doi.org/10.3390/en14217373.
[346]	Wang, C.; Yu, Y.; Niu, J.; Liu, Y.; Bridges, D.; Liu, X.; Pooran, J.; Zhang, Y.; Hu, A. Recent progress of metal-air batteries - A mini review. *Appl. Sci. 9*, 2787, **2019**.
[347]	Gröger, O.; Gasteiger, H.A.; Suchsland, J.-P. Erratum: Review - Electromobility: Batteries or Fuel Cells? [J. Electrochem. Soc., 162, A2605 (2015)]. *J. Electrochem. Soc. 163*, X3, **2016**.
[348]	Rahman, M.A.; Wang, X.; Wen, C. High energy density metal-air batteries: A review. *J. Electrochem. Soc. 160*, A1759, **2013**.
[349]	Zhang, T.; Tao, Z.; Chen, J. Magnesium-air batteries: From principle to application. *Mater. Horiz. 1*, 196-206, **2014**.
[350]	Li, Y.; Zhang, X.; Li, H.-B.; Yoo, H.D.; Chi, X.; An, Q.; Liu, J.; Yu, M.; Wang, W.; Yao, Y. Mixed-phase mullite electrocatalyst for pH-neutral oxygen reduction in magnesium-air batteries. *Nano Energy. 27*, 8-16, **2016**.
[351]	Li, C.S.; Sun, Y.; Gebert, F.; Chou, S.L. Current progress on rechargeable magnesium-air battery. *Adv. Energy Mater. 7*, 1700869, **2017**.
[352]	Zhang, Z.; Zuo, C.; Liu, Z.; Yu, Y.; Zuo, Y.; Song, Y. All-solid-state Al-air batteries with polymer alkaline gel electrolyte. *J. Power Sources. 251*, 470-475, **2014**.
[353]	Liu, X.; Zhang, P.; Xue, J.; Zhu, C.; Li, X.; Wang, Z. High energy efficiency of Al-based anodes for Al-air battery by simultaneous addition of Mn and Sb. *Chem. Eng. J. 417*, 128006, **2021**.
[354]	Mokhtar, M.; Talib, M.Z.M.; Majlan, E.H.; Tasirin, S.M.; Ramli, W.M.F.W.; Daud, W.R.W.; Sahari, J. Recent developments in materials for aluminum-air batteries: A review. *J. Ind. Eng. Chem. 32*, 1-20, **2015**.
[355]	Bi, X.; Wang, R.; Yuan, Y.; Zhang, D.; Zhang, T.; Ma, L.; Lu, J. From sodium-oxygen to sodium-air battery: Enabled by sodium peroxide dihydrate. *Nano Lett. 20*, 4681-4686, **2020**.
[356]	Sahgong, S.H.; Senthilkumar, S.T.; Kim, K.; Hwang, S.M.; Kim, Y. Rechargeable aqueous Na-air batteries: Highly improved voltage efficiency by use of catalysts. *Electrochem. Commun. 61*, 53-56, **2015**.
[357]	Adelhelm, P.; Hartmann, P.; Bender, C.L.; Busche, M.; Eufinger, C.; Janek, J. From lithium to sodium: Cell chemistry of room temperature sodium-air and sodium-sulfur batteries. *Beilstein J. Nanotechnol. 6*, 1016-1055, **2015**.
[358]	Bansal, R.; Menon, P.; Sharma, R.C. Silicon-air batteries: Progress, applications and challenges. *SN Appl. Sci. 2*, 1-17, **2020**.
[359]	Leong, K.W.; Wang, Y.; Ni, M.; Pan, W.; Luo, S.; Leung, D.Y. Rechargeable Zn-air batteries: Recent trends and future perspectives. *Renew. Sustain. Energy Rev. 154*, 111771, **2022**.
[360]	Girishkumar, G.; McCloskey, B.; Luntz, A.C.; Swanson, S.; Wilcke, W. Lithium-air battery: Promise and challenges. *J. Phys. Chem. Lett. 1*, 2193-2203, **2010**.
[361]	Blurton, K.F.; Sammells, A.F. Metal/air batteries: Their status and potential - A review. *J. Power Sources. 4*, 263-279, **1979**.
[362]	Abraham, K.; Jiang, Z. A polymer electrolyte-based rechargeable lithium/oxygen battery. *J. Electrochem. Soc. 143*, 1, **1996**.

[363]	McCloskey, B.; Speidel, A.; Scheffler, R.; Miller, D.; Viswanathan, V.; Hummelshøj, J.; Nørskov, J.; Luntz, A. Twin problems of interfacial carbonate formation in nonaqueous Li-O$_2$ batteries. *J. Phys. Chem. Lett. 3*, 997-1001, **2012**.
[364]	Monroe, C.W. Does oxygen transport affect the cell voltages of metal/air batteries? *J. Electrochem. Soc. 164*, E3547, **2017**.
[365]	Horstmann, B.; Danner, T.; Bessler, W.G. Precipitation in aqueous lithium-oxygen batteries: A model-based analysis. *Energy Environ. Sci. 6*, 1299-1314, **2013**.
[366]	Danner, T.; Horstmann, B.; Wittmaier, D.; Wagner, N.; Bessler, W.G. Reaction and transport in Ag/Ag$_2$O gas diffusion electrodes of aqueous Li-O$_2$ batteries: Experiments and modeling. *J. Power Sources. 264*, 320-332, **2014**.
[367]	Vegge, T.; Garcia-Lastra, J.M.; Siegel, D.J. Lithium-oxygen batteries: At a crossroads? *Curr. Opin. Electrochem. 6*, 100-107, **2017**.
[368]	Pei, P.; Wang, K.; Ma, Z. Technologies for extending zinc-air battery's cyclelife: A review. *Appl. Energy. 128*, 315-324, **2014**.
[369]	Sumboja, A.; Ge, X.; Zheng, G.; Goh, F.T.; Hor, T.A.; Zong, Y.; Liu, Z. Durable rechargeable zinc-air batteries with neutral electrolyte and manganese oxide catalyst. *J. Power Sources. 332*, 330-336, **2016**.
[370]	Friesen, C.A.; Krishnan, R.; Friesen, G. Rechargeable Electrochemical Cell System with a Charging Electrode Charge/Discharge Mode Switching in the Cells. U.S. Patent Application No. 12/885,268, 24 March **2011**.
[371]	Liu, Q.; Chang, Z.; Li, Z.; Zhang, X. Flexible metal-air batteries: Progress, challenges, and perspectives. *Small Methods. 2*, 1700231, **2018**.
[372]	Zhang, X.-b. *Metal-Air Batteries: Fundamentals and Applications*; John Wiley & Sons: Hoboken, NJ, USA, **2018**.
[373]	Durmus, Y.E.; Zhang, H.; Baakes, F.; Desmaizieres, G.; Hayun, H.; Yang, L.; Kolek, M.; Küpers, V.; Janek, J.; Mandler, D.; et al. Side by Side Battery Technologies with Lithium-Ion Based Batteries. *Adv. Energy Mater. 10*, 2000089, **2020**.
[374]	McKerracher, R.; de Ponce Leon, C.; Wills, R.; Shah, A.; Walsh, F.C. A review of the iron-air secondary battery for energy storage. *ChemPlusChem. 80*, 323-335, **2015**.
[375]	Li, Y.; Dai, H. Recent advances in zinc-air batteries. *Chem. Soc. Rev. 43*, 5257-5275, **2014**.
[376]	Gür, T.M. Review of electrical energy storage technologies, materials and systems: Challenges and prospects for large-scale grid storage. *Energy Environ. Sci. 11*, 2696-2767, **2018**.
[377]	Komilis, D.; Evangelou, A.; Giannakis, G.; Lymperis, C. Revisiting the elemental composition and the calorific value of the organic fraction of municipal solid wastes. *Waste Manag. 32*, 372-381, **2012**.
[378]	Gesser, H. Electrochemistry, Batteries and Fuel Cells. In *Applied Chemistry*; Springer: Berlin/Heidelberg, Germany. pp. 159-190, **2002**.
[379]	Yoshio, M.; Brodd, R.J.; Kozawa, A. *Lithium-Ion Batteries*; Springer: New York, NY, USA. Volume 1, pp. 2-3, **2009**.
[380]	Kang, J.; Yan, F.; Zhang, P.; Du, C. A novel way to calculate energy efficiency for rechargeable batteries. *J. Power Sources. 206*, 310-314, **2012**.
[381]	Weinrich, H.; Durmus, Y.E.; Tempel, H.; Kungl, H.; Eichel, R.-A. Silicon and iron as resource-efficient anode materials for ambient-temperature metal-air batteries: A review. *Materials. 12*, 2134, **2019**.

[382]	Khan, Z.; Parveen, N.; Ansari, S.A.; Senthilkumar, S.; Park, S.; Kim, Y.; Cho, M.H.; Ko, H. Three-dimensional SnS_2 nanopetals for hybrid sodium-air batteries. *Electrochim. Acta. 257*, 328-334, **2017**.
[383]	Liu, Y.; Sun, Q.; Yang, X.; Liang, J.; Wang, B.; Koo, A.; Li, R.; Li, J.; Sun, X. High-performance and recyclable Al-air coin cells based on eco-friendly chitosan hydrogel membranes. *ACS Appl. Mater. Interfaces. 10*, 19730-19738, **2018**.
[384]	Zhao, Y.; Huang, G.; Zhang, C.; Peng, C.; Pan, F. Effect of phosphate and vanadate as electrolyte additives on the performance of Mg-air batteries. *Mater. Chem. Phys. 218*, 256-261, **2018**.
[385]	Chen, G.; Zhang, J.; Wang, F.; Wang, L.; Liao, Z.; Zschech, E.; Müllen, K.; Feng, X. Cobalt-Based Metal-Organic Framework Nanoarrays as Bifunctional Oxygen Electrocatalysts for Rechargeable Zn-Air Batteries. *Chem. A Eur. J. 24*, 18413-18418, **2018**.
[386]	Lai, C.; Wang, J.; Lei, W.; Xuan, C.; Xiao, W.; Zhao, T.; Huang, T.; Chen, L.; Zhu, Y.; Wang, D. Restricting growth of Ni_3Fe nanoparticles on heteroatom-doped carbon nanotube/graphene nanosheets as air-electrode electrocatalyst for Zn-air battery. *ACS Appl. Mater. Interfaces. 10*, 38093-38100, **2018**.
[387]	Figueredo-Rodríguez, H.; McKerracher, R.; Insausti, M.; Luis, A.G.; de León, C.P.; Alegre, C.; Baglio, V.; Aricò, A.;Walsh, F. A rechargeable, aqueous iron air battery with nanostructured electrodes capable of high energy density operation. *J. Electrochem. Soc. 164*, A1148, **2017**.
[388]	Sumathi, S.; Sethuprakash, V.; Basirun, W.; Zainol, I.; Sookhakian, M. Polyacrylamide-methanesulfonic acid gel polymer electrolytes for tin-air battery. *J. Sol-Gel Sci. Technol. 69*, 480-487, **2014**.
[389]	Najam, T.; Shah, S.S.A.; Ding, W.; Deng, J.; Wei, Z. Enhancing by nano-engineering: Hierarchical architectures as oxygen reduction/evolution reactions for zinc-air batteries. *J. Power Sources. 438*, 226919, **2019**.
[390]	Egan, D.R.; Ponce de León, C.; Wood, R.J.K.; Jones, R.L.; Stokes, K.R.; Walsh, F.C. Developments in electrode materials and electrolytes for aluminium-air batteries. *J. Power Sources. 236*, 293-310, **2013**.
[391]	Mutlu, R.N.; Ate¸s, S.; Yazıcı, B. Al-6013-T6 and Al-7075-T7351 alloy anodes for aluminium-air battery. *Int. J. Hydrogen Energy. 42*, 23315-23325, **2017**.
[392]	Chawla, N. Recent advances in air-battery chemistries. *Mater. Today Chem. 12*, 324-331, **2019**.
[393]	Melhem, Z. *Electricity Transmission, Distribution and Storage Systems*; Woodhead Publishing Series in Energy: Number 38; Woodhead Publishing: Shaxton, UK, **2013**.
[394]	Imanishi, N.; Yamamoto, O. Perspectives and challenges of rechargeable lithium–air batteries. *Mater. Today Adv. 4*, 100031, **2019**.
[395]	Rahman, M.A.; Wang, X.; Wen, C. A review of high energy density lithium-air battery technology. *J. Appl. Electrochem. 44*, 5-22, **2014**.
[396]	Lin, H.; Chen, Z.; Wang, D.; Wang, M.; Peng, Z.; Liu, Z.; He, H.; Wang, M.; Li, H. High-performance Li-air battery after limiting inter-electrode crosstalk. *Energy Storage Mater. 39*, 225-231, **2021**.
[397]	Otaegui, L.; Rodriguez-Martinez, L.M.; Wang, L.; Laresgoiti, A.; Tsukamoto, H.; Han, M.H.; Tsai, C.L.; Laresgoiti, I.; López, C.M.; Rojo, T. Performance and stability of a liquid anode high-temperature metal-air battery. *J. Power Sources. 247*, 749-755, **2014**.
[398]	Wang, H.-F.; Xu, Q. Materials design for rechargeable metal-air batteries. *Matter. 1*, 565-595, **2019**.

[399]	Jung, K.-N.; Kim, J.; Yamauchi, Y.; Park, M.-S.; Lee, J.-W.; Kim, J.H. Rechargeable lithium-air batteries: A perspective on the development of oxygen electrodes. *J. Mater. Chem. A. 4*, 14050-14068, **2016**.
[400]	Christensen, J.; Albertus, P.; Sanchez-Carrera, R.S.; Lohmann, T.; Kozinsky, B.; Liedtke, R.; Ahmed, J.; Kojic, A. A critical review of Li/air batteries. *J. Electrochem. Soc. 159*, R1, **2011**.
[401]	Gelman, D.; Shvartsev, B.; Ein-Eli, Y. Aluminum-air battery based on an ionic liquid electrolyte. *J. Mater. Chem. A. 2*, 20237-20242, **2014**.
[402]	Cohn, G.; Ein-Eli, Y. Study and development of non-aqueous silicon-air battery. *J. Power Sources. 195*, 4963-4970, **2010**.
[403]	Durmus, Y.E.; Aslanbas, Ö.; Kayser, S.; Tempel, H.; Hausen, F.; De Haart, L.; Granwehr, J.; Ein-Eli, Y.; Eichel, R.-A.; Kungl, H. Long run discharge, performance and efficiency of primary Silicon-air cells with alkaline electrolyte. *Electrochim. Acta. 225*, 215-224, **2017**.
[404]	Reinsberg, P.; Bondue, C.J.; Baltruschat, H. Calcium–Oxygen Batteries as a Promising Alternative to Sodium-Oxygen Batteries. *J. Phys. Chem. C. 120*, 22179-22185, **2016**.
[405]	Shiga, T.; Hase, Y.; Kato, Y.; Inoue, M.; Takechi, K. A rechargeable non-aqueous Mg-O_2 battery. *Chem. Commun. 49*, 9152-9154, **2013**.
[406]	Das, S.K.; Lau, S.; Archer, L.A. Sodium-oxygen batteries: A new class of metal-air batteries. *J. Mater. Chem. A. 2*, 12623-12629, **2014**.
[407]	Narayanan, S.R.; Prakash, G.K.S.; Manohar, A.; Yang, B.; Malkhandi, S.; Kindler, A. Materials challenges and technical approaches for realizing inexpensive and robust iron-air batteries for large-scale energy storage. *Solid State Ion. 216*, 105-109, **2012**.
[408]	Ren, X.; Wu, Y. A low-overpotential potassium-oxygen battery based on potassium superoxide. *J. Am. Chem. Soc. 135*, 2923-2926, **2013**.
[409]	Dincer, I. *Comprehensive Energy Systems*; Elsevier: Amsterdam, The Netherlands, **2018**.
[410]	Wei, W.; Xu, Y.; Huang, J.; Zhu, J. Review of the application of metal-air battery principle in water treatment. In Proceedings of the 2019 International Conference on Building Energy Conservation, Thermal Safety and Environmental Pollution Control, Hefei, China, p. 06035, 1-3 November **2019**.
[411]	Han, X.; Qu, Y.; Li, D.; Dong, Y.; Chen, D.; Yu, Y.; Ren, N.; Feng, Y. Combined microbial electrolysis cell-iron-air battery system for hydrogen production and swine wastewater treatment. *Process Biochem. 101*, 104-110, **2021**.
[412]	Han, X.; Qu, Y.; Dong, Y.; Zhao, J.; Jia, L.; Yu, Y.; Zhang, P.; Li, D.; Ren, N.; Feng, Y. Microbial electrolysis cell powered by an aluminum-air battery for hydrogen generation, in-situ coagulant production and wastewater treatment. *Int. J. Hydrog. Energy. 43*, 7764-7772, **2018**.
[413]	Demir-Cakan, R.; Palacin, M.R.; Croguennec, L. Rechargeable aqueous electrolyte batteries: From univalent to multivalent cation chemistry. *J. Mater. Chem. A. 7*, 20519-20539, **2019**.
[414]	Mori, R. Recent developments for aluminum-air batteries. *Electrochem. Energy Rev. 3*, 344-369, **2020**.
[415]	Kar, M.; Simons, T.J.; Forsyth, M.; MacFarlane, D.R. Ionic liquid electrolytes as a platform for rechargeable metal-air batteries: A perspective. *Phys. Chem. Chem. Phys. 16*, 18658-18674, **2014**.
[416]	Khan, Z.; Vagin, M.; Crispin, X. Can hybrid Na-air batteries outperform nonaqueous Na-O_2 batteries? *Adv. Sci. 7*, 1902866, **2020**.

[417]	Yu, X.; Manthiram, A. A voltage-enhanced, low-cost aqueous iron-air battery enabled with a mediator-ion solid electrolyte. *ACS Energy Lett. 2*, 1050-1055, **2017**.
[418]	No More Trial-and Error When Choosing an Electrolyte for Metal-Air Batteries. **2019**. Available online: https://phys.org/news/2019-07-trial-and-error-electrolyte-metal-air-batteries.html (Accessed 20/3/2023).
[419]	Sankarasubramanian, S.; Kahky, J.; Ramani, V. Tuning anion solvation energetics enhances potassium-oxygen battery performance. *Proc. Natl. Acad. Sci. USA. 116*, 14899-14904, **2019**.
[420]	Mainar, A.R.; Iruin, E.; Colmenares, L.C.; Kvasha, A.; De Meatza, I.; Bengoechea, M.; Leonet, O.; Boyano, I.; Zhang, Z.; Blazquez, J.A. An overview of progress in electrolytes for secondary zinc-air batteries and other storage systems based on zinc. *J. Energy Storage. 15*, 304-328, **2018**.
[421]	Zha, Z.; Shen, C.;Wang, D.; Han, W. Review on air cathode in Li-air batteries. *J. Technol. Innov. Renew. Energy. 2*, 293-305, **2013**.
[422]	Martin, J.; Neburchilov, V.; Wang, H.; Qu, W. Air Cathodes for Metal-air Batteries and Fuel Cells. In Proceedings of the 2009 IEEE Electrical Power & Energy Conference (EPEC), Montreal, QC, Canada, 22-23 October 2009; IEEE: Piscataway, NJ, USA, pp. 1-6, **2009**.
[423]	Cai, X.; Lai, L.; Lin, J.; Shen, Z. Recent advances in air electrodes for Zn-air batteries: Electrocatalysis and structural design. *Mater. Horiz. 4*, 945-976, **2017**.
[424]	Lee, C.H.; Lee, S.U. Theoretical basis of electrocatalysis. In *Electrocatalysts for Fuel Cells and Hydrogen Evolution-Theory to Design*; IntechOpen: London, UK, p. 13, **2018**.
[425]	Wang, Z.-L.; Xu, D.; Xu, J.-J.; Zhang, X.-B. Oxygen electrocatalysts in metal-air batteries: From aqueous to nonaqueous electrolytes. *Chem. Soc. Rev. 43*, 7746-7786, **2014**.
[426]	Abdelkareem, M.A.; Sayed, E.T.; Mohamed, H.O.; Obaid, M.; Rezk, H.; Chae, K.-J. Nonprecious anodic catalysts for lowmolecular-hydrocarbon fuel cells: Theoretical consideration and current progress. *Prog. Energy Combust. Sci. 77*, 100805, **2020**.
[427]	Al-Dhaifallah, M.; Abdelkareem, M.A.; Rezk, H.; Alhumade, H.; Nassef, A.M.; Olabi, A.G. Co-decorated reduced graphene/titanium nitride composite as an active oxygen reduction reaction catalyst with superior stability. *Int. J. Energy Res. 45*, 1587-1598, **2021**.
[428]	Wang, M.; Fang, Z.; Zhang, K.; Fang, J.; Qin, F.; Zhang, Z.; Li, J.; Liu, Y.; Lai, Y. Synergistically enhanced activity of graphene quantum dots/graphene hydrogel composites: A novel all-carbon hybrid electrocatalyst for metal/air batteries. *Nanoscale. 8*, 11398-11402, **2016**.
[429]	Jung, K.-N.; Hwang, S.M.; Park, M.-S.; Kim, K.J.; Kim, J.-G.; Dou, S.X.; Kim, J.H.; Lee, J.-W. One-dimensional manganese-cobalt oxide nanofibres as bi-functional cathode catalysts for rechargeable metal-air batteries. *Sci. Rep. 5*, 7665, **2015**.
[430]	Wang, M.; Lai, Y.; Fang, J.; Qin, F.; Zhang, Z.; Li, J.; Zhang, K. Hydrangea-like $NiCo_2S_4$ hollow microspheres as an advanced bifunctional electrocatalyst for aqueous metal/air batteries. *Catal. Sci. Technol. 6*, 434-437, **2016**.
[431]	Zhao, C.; Yan, X.; Wang, G.; Jin, Y.; Du, X.; Du, W.; Sun, L.; Ji, C. PdCo bimetallic nano-electrocatalyst as effective air-cathode for aqueous metal-air batteries. *Int. J. Hydrogen Energy. 43*, 5001-5011, **2018**.
[432]	Zhang, L.; Huang, Q.A.; Yan, W.; Shao, Q.; Zhang, J. Design and fabrication of non-noble metal catalyst-based air-cathodes for metal-air battery. *Can. J. Chem. Eng. 97*, 2984-2993, **2019**.
[433]	Tan, P.; Shyy, W.; Zhao, T.S.; Wei, Z.H.; An, L. Discharge product morphology versus operating temperature in non-aqueous lithium-air batteries. *J. Power Sources. 278*, 133-140, **2015**.

[434]	Gilligan, G.; Qu, D. Zinc-air and other types of metal-air batteries. In *Advances in Batteries for Medium and Large-Scale Energy Storage*; Elsevier: Amsterdam, The Netherlands, pp. 441-461, **2015**.
[435]	Han, X.; Li, X.; White, J.; Zhong, C.; Deng, Y.; Hu, W.; Ma, T. Metal-air batteries: From static to flow system. *Adv. Energy Mater. 8*, 1801396, **2018**.
[436]	Liu, W.; Zhang, J.; Bai, Z.; Jiang, G.; Li, M.; Feng, K.; Yang, L.; Ding, Y.; Yu, T.; Chen, Z. Controllable urchin-like $NiCo_2S_4$ microsphere synergized with sulfur-doped graphene as bifunctional catalyst for superior rechargeable Zn-air battery. *Adv. Funct. Mater. 28*, 1706675, **2018**.
[437]	Tran, T.N.T.; Chung, H.-J.; Ivey, D.G. A study of alkaline gel polymer electrolytes for rechargeable zinc-air batteries. *Electrochim. Acta. 327*, 135021, **2019**.
[438]	Jacas Biendicho, J.; Noréus, D.; Offer, C.; Svensson, G.; Smith, R.I.; Hull, S. New opportunities for air cathode batteries; in-situ neutron diffraction measurements. *Front. Energy Res. 6*, 69, **2018**.
[439]	Pan, J.; Xu, Y.Y.; Yang, H.; Dong, Z.; Liu, H.; Xia, B.Y. Advanced architectures and relatives of air electrodes in Zn-air batteries. *Adv. Sci. 5*, 1700691, **2018**.
[440]	Ye, L.; Hong, Y.; Liao, M.; Wang, B.; Wei, D.; Peng, H.; Ye, L.; Hong, Y.; Liao, M.; Wang, B.; et al. Recent advances in flexible fiber-shaped metal-air batteries. *Energy Storage Mater. 28*, 364-374, **2020**.
[441]	Xie, Z.; Wu, Z.; An, X.; Yue, X.; Xiaokaiti, P.; Yoshida, A.; Abudula, A.; Guan, G. A sandwich-type composite polymer electrolyte for all-solid-state lithium metal batteries with high areal capacity and cycling stability. *J. Membr. Sci. 596*, 117739, **2020**.
[442]	Qu, S.; Song, Z.; Liu, J.; Li, Y.; Kou, Y.; Ma, C.; Han, X.; Deng, Y.; Zhao, N.; Hu, W.; et al. Electrochemical approach to prepare integrated air electrodes for highly stretchable zinc-air battery array with tunable output voltage and current for wearable electronics. *Nano Energy. 39*, 101-110, **2017**.
[443]	Teabnamang, P.; Kao-ian, W.; Nguyen, M.T.; Yonezawa, T.; Cheacharoen, R.; Kheawhom, S. High-Capacity Dual-Electrolyte Aluminum-Air Battery with Circulating Methanol Anolyte. *Energies. 13*, 2275, **2020**.
[444]	Cheng, Y.; Li, D.; Shi, L.; Xiang, Z. Efficient unitary oxygen electrode for air-based flow batteries. *Nano Energy. 47*, 361-367, **2018**.
[445]	Sun, C.; Negro, E.; Nale, A.; Pagot, G.; Vezzù, K.; Zawodzinski, T.A.; Meda, L.; Gambaro, C.; Di Noto, V. An efficient barrier toward vanadium crossover in redox flow batteries: The bilayer [Nafion/(WO3)x] hybrid inorganic-organic membrane. *Electrochim. Acta. 378*, 138133, **2021**.
[446]	Pichler, B.; Berner, B.S.; Rauch, N.; Zelger, C.; Pauling, H.-J.; Gollas, B.; Hacker, V. The impact of operating conditions on component and electrode development for zinc-air flow batteries. *J. Appl. Electrochem. 48*, 1043-1056, **2018**.
[447]	Zhang, H.; Tan, Y.; Luo, X.D.; Sun, C.Y.; Chen, N. Polarization Effects of a Rayon and Polyacrylonitrile Based Graphite Felt for Iron-Chromium Redox Flow Batteries. *Chem. Electr. Chem. 6*, 3175-3188, **2019**.
[448]	Grosse Austing, J.; Nunes Kirchner, C.; Hammer, E.-M.; Komsiyska, L.; Wittstock, G. Study of an unitised bidirectional vanadium/air redox flow battery comprising a two-layered cathode. *J. Power Sources. 273*, 1163-1170, **2015**.
[449]	Clark, S.; Latz, A.; Horstmann, B. A review of model-based design tools for metal-air batteries. *Batteries. 4*, 5, **2018**.

[450]	Lubna, Yaqoob; Tayyaba, Noor; Nassem, Iqbal. An overview of metal-air batteries, current progress, and future perspectives. *Journal of Energy Storage 56*, 106075, **2022**. https://doi.org/10.1016/j.est.2022.106075.
[451]	Y. Li, H. Dai. Recent advances in zinc-air batteries. *Chem. Soc. Rev. 43*, 5257-5275, **2014**.
[452]	X.G. Zhang. Fibrous zinc anodes for high power batteries. *J. Power Sources 163*, 591-597, **2006**.
[453]	J.-F. Drillet, M. Adam, S. Barg, A. Herter, D. Koch, V. Schmidt, et al. Development of a novel zinc/air fuel cell with a zn foam anode, a PVA/KOH membrane and a MnO_2/SiOC-based air cathode. *ECS Trans. 28,* 13, **2010**.
[454]	L. Baugh, F. Tye, N. White. Corrosion and polarization characteristics of zinc in battery electrolyte analogues and the effect of amalgamation. *J. Appl. Electrochem. 13*, 623-635, **1983**.
[455]	Y.-D. Cho, G.T.-K. Fey. Surface treatment of zinc anodes to improve discharge capacity and suppress hydrogen gas evolution. *J. Power Sources 184,* 610-616, **2008**.
[456]	J. Vatsalarani, D. Trivedi, K. Ragavendran, P. Warrier. Effect of polyaniline coating on "shape change" phenomenon of porous zinc electrode. *J. Electrochem. Soc. 152*, A1974, **2005**.
[457]	J. Pan, Y.Y. Xu, H. Yang, Z. Dong, H. Liu, B.Y. Xia. Advanced architectures and relatives of air electrodes in Zn-air batteries. *Adv. Sci. 5* 1700691, **2018**.
[458]	D. Stock, S. Dongmo, D. Schroder, J.r. Janek. Benchmarking anode concepts: the future of electrically rechargeable zinc-air batteries. *ACS Energy Letters 4*, 1287-1300, **2019**.
[459]	X. Cai, L. Lai, J. Lin, Z. Shen. Recent advances in air electrodes for Zn-air batteries: electrocatalysis and structural design. *Mater. Horiz. 4*, 945-976, **2017**.
[460]	A.L. Zhu, D.P. Wilkinson, X. Zhang, Y. Xing, A.G. Rozhin, S.A. Kulinich. Zinc regeneration in rechargeable zinc-air fuel cells - a review. *J. Energy Storage 8*, 35-50, **2016**.
[461]	C. Han, W. Li, H.-K. Liu, S. Dou, J. Wang. Design strategies for developing non-precious metal based bi-functional catalysts for alkaline electrolyte based zinc-air batteries. *Mater. Horiz. 6*, 1812-1827, **2019**.
[462]	H.F. Wang, C. Tang, Q. Zhang. A review of precious-metal-free bifunctional oxygen electrocatalysts: rational design and applications in Zn-air batteries. *Adv. Funct. Mater. 28*, 1803329, **2018**.
[463]	G.M. Tomboc, P. Yu, T. Kwon, K. Lee, J. Li. Ideal design of air electrode - a step closer toward robust rechargeable Zn-air battery. *APL Mater. 8*, 050905, **2020**.
[464]	E. Davari, D. Ivey. Bifunctional electrocatalysts for Zn-air batteries. *Sustain. Energy Fuels 2*, 39-67, **2018**.
[465]	Z. Ma, P. Pei, K. Wang, X. Wang, H. Xu, Y. Liu. Degradation characteristics of air cathode in zinc-air fuel cells. *J. Power Sources 274*, 56-64, **2015**.
[466]	G. Wu, S. Lin, J. You, C. Yang. Study of high-anionic conducting sulfonated microporous membranes for zinc-air electrochemical cells. *Mater. Chem. Phys. 112*, 798-804, **2008**.
[467]	H. Saputra, R. Othman, A. Sutjipto, R. Muhida. MCM-41 as a new separator material for electrochemical cell: application in zinc-air system. *J. Membr. Sci. 367*, 152-157, **2011**.
[468]	E.L. Dewi, K. Oyaizu, H. Nishide, E. Tsuchida. Cationic polysulfonium membrane as separator in zinc-air cell. *J. Power Sources 115*, 149-152, **2003**.
[469]	G.S. Park, J.-S. Lee, S.T. Kim, S. Park, J. Cho. Porous nitrogen doped carbon fiber with churros morphology derived from electrospun bicomponent polymer as highly efficient electrocatalyst for Zn-air batteries. *J. Power Sources 243*, 267-273, **2013**.

[470]	Z. Chen, A. Yu, R. Ahmed, H. Wang, H. Li, Z. Chen. Manganese dioxide nanotube and nitrogen-doped carbon nanotube based composite bifunctional catalyst for rechargeable zinc-air battery. *Electrochim. Acta 69*, 295-300, **2012**.
[471]	Q. Liu, Y. Wang, L. Dai, J. Yao. Scalable fabrication of nanoporous carbon fiber films as bifunctional catalytic electrodes for flexible zn-air batteries. *Adv. Mater. 28*, 3000-3006, **2016**.
[472]	X. Cai, L. Lai, L. Zhou, Z. Shen. Durable freestanding hierarchical porous electrode for rechargeable zinc-air batteries. *ACS Appl. Energy Mater. 2*, 1505-1516, **2019**.
[473]	Y. Xu, Y. Zhang, Z. Guo, J. Ren, Y. Wang, H. Peng. Flexible, stretchable, and rechargeable fiber-shaped zinc-air battery based on cross-stacked carbon nanotube sheets. *Angew. Chem. 127*, 15610-15614, **2015**.
[474]	L. Hadidi, E. Davari, M. Iqbal, T.K. Purkait, D.G. Ivey, J.G. Veinot. Spherical nitrogen-doped hollow mesoporous carbon as an efficient bifunctional electrocatalyst for Zn-air batteries. *Nanoscale 7*, 20547-20556, **2015**.
[475]	K. Tang, C. Yuan, Y. Xiong, H. Hu, M. Wu. Inverse-opal-structured hybrids of N, S-codoped-carbon-confined Co_9S_8 nanoparticles as bifunctional oxygen electrocatalyst for on-chip all-solid-state rechargeable Zn-air batteries. *Appl. Catal. B Environ. 260*, 118209, **2020**.
[476]	Y. Wang, N. Xu, R. He, L. Peng, D. Cai, J. Qiao. Large-scale defect-engineering tailored tri-doped graphene as a metal-free bifunctional catalyst for superior electrocatalytic oxygen reaction in rechargeable Zn-air battery. *Appl. Catal. B Environ. 285*, 119811, **2021**.
[477]	J. Wang, H. Wu, D. Gao, S. Miao, G. Wang, X. Bao. High-density iron nanoparticles encapsulated within nitrogen-doped carbon nanoshell as efficient oxygen electrocatalyst for zinc-air battery. *Nano Energy 13*, 387-396, **2015**.
[478]	A. Sumboja, X. Ge, F.T. Goh, B. Li, D. Geng, T.A. Hor, et al. Manganese oxide catalyst grown on carbon paper as an air cathode for high-performance rechargeable zinc-air batteries. *ChemPlusChem 80*, 1341-1346, **2015**.
[479]	L. Grande, E. Paillard, J. Hassoun, J.B. Park, Y.J. Lee, Y.K. Sun, et al. The lithium/air battery: still an emerging system or a practical reality? *Adv. Mater. 27*, 784-800, **2015**.
[480]	R.S. Assary, J. Lu, P. Du, X. Luo, X. Zhang, Y. Ren, et al. The effect of oxygen crossover on the anode of a $Li-O_2$ battery using an ether-based solvent: insights from experimental and computational studies. *ChemSusChem 6*, 51-55, **2013**.
[481]	R. Xu, X.Q. Zhang, X.B. Cheng, H.J. Peng, C.Z. Zhao, C. Yan, et al. Artificial soft-rigid protective layer for dendrite-free lithium metal anode. *Adv. Funct. Mater. 28*, 1705838, **2018**.
[482]	X. Zhang, Q. Zhang, X.G. Wang, C. Wang, Y.N. Chen, Z. Xie, et al. An extremely simple method for protecting lithium anodes in $li-O_2$ batteries. *Angew. Chem. 130*, 12996-13000, **2018**.
[483]	M. Eswaran, N. Munichandraiah, L. Scanlon. High capacity $Li-O_2$ cell and electrochemical impedance spectroscopy study. *Electrochem. Solid-State Lett. 13*, A121, **2010**.
[484]	D. Zhang, Z. Fu, Z. Wei, T. Huang, A. Yu. Polarization of oxygen electrode in rechargeable lithium oxygen batteries. *J. Electrochem. Soc. 157*, A362, **2010**.
[485]	M. Mirzaeian, P.J. Hall. Characterizing capacity loss of lithium oxygen batteries by impedance spectroscopy. *J. Power Sources 195*, 6817-6824, **2010**.
[486]	G. Zhang, J. Zheng, R. Liang, C. Zhang, B. Wang, M. Hendrickson, et al. Lithium-air batteries using SWNT/CNF buckypapers as air electrodes. *J. Electrochem. Soc. 157*, A953, **2010**.
[487]	X.-H. Yang, Y.-Y. Xia. The effect of oxygen pressures on the electrochemical profile of lithium/oxygen battery. *J. Solid State Electrochem. 14*, 109-114, **2010**.

[488]	S.J. Visco, V.Y. Nimon, A. Petrov, K. Pridatko, N. Goncharenko, E. Nimon, et al. Aqueous and nonaqueous lithium-air batteries enabled by water-stable lithium metal electrodes. *J. Solid State Electrochem. 18*, 1443-1456, **2014**.
[489]	Y. Takeda, O. Yamamoto, N. Imanishi. Lithium dendrite formation on a lithium metal anode from liquid, polymer and solid electrolytes. *Electrochemistry 84*, 210-218, **2016**.
[490]	M. Xie, Z. Huang, X. Lin, Y. Li, Z. Huang, L. Yuan, et al. Oxygen selective membrane based on perfluoropolyether for Li-air battery with long cycle life. *Energy Storage Mater. 20*, 307-314, **2019**.
[491]	A. Suryatna, I. Raya, L. Thangavelu, F.R. Alhachami, M.M. Kadhim, U.S. Altimari, et al. A review of high-energy density lithium-air battery technology: investigating the effect of oxides and nanocatalysts. *J. Chem. 2022*, **2022**.
[492]	Y.-C. Lu, Z. Xu, H.A. Gasteiger, S. Chen, K. Hamad-Schifferli, Y. Shao-Horn, Platinum-gold nanoparticles: a highly active bifunctional electrocatalyst for rechargeable lithium-air batteries. *J. Am. Chem. Soc. 132*, 12170-12171, **2010**.
[493]	W. Xu, J. Xiao, D. Wang, J. Zhang, J.-G. Zhang. Effects of nonaqueous electrolytes on the performance of lithium/air batteries. *J. Electrochem. Soc. 157*, A219, **2009**.
[494]	M.J. Song, M.W. Shin. Fabrication and characterization of carbon nanofiber@ mesoporous carbon core-shell composite for the li-air battery. *Appl. Surf. Sci. 320*, 435-440, **2014**.
[495]	C.K. Lee, Y.J. Park. Polyimide-wrapped carbon nanotube electrodes for long cycle Li-air batteries. *Chem. Commun. 51*, 1210-1213, **2015**.
[496]	R. Yu, W. Fan, X. Guo, S. Dong. Highly ordered and ultra-long carbon nanotube arrays as air cathodes for high-energy-efficiency li-oxygen batteries. *J. Power Sources 306*, 402-407, **2016**.
[497]	W.-J. Kwak, T.-G. Kang, Y.-K. Sun, Y.J. Lee. Iron-cobalt bimetal decorated carbon nanotubes as cost-effective cathode catalysts for Li-O$_2$ batteries. *J. Mater. Chem. A 4*, 7020-7026, **2016**.
[498]	Z.D. Yang, X.Y. Yang, T. Liu, Z.W. Chang, Y.B. Yin, X.B. Zhang, et al. In situ CVD derived Co-N-C composite as highly efficient cathode for flexible Li-O$_2$ batteries. *Small 14*, 1800590, **2018**.
[499]	L. Li, A. Manthiram. O-and N-doped carbon nanowebs as metal-free catalysts for hybrid li-air batteries. *Adv. Energy Mater. 4*, 1301795, **2014**.
[500]	B. Sun, B. Wang, D. Su, L. Xiao, H. Ahn, G. Wang. Graphene nanosheets as cathode catalysts for lithium-air batteries with an enhanced electrochemical performance. *Carbon 50*, 727-733, **2012**.
[501]	L. Fan, H. Lu, J. Leng, Z. Sun, C. Chen. The effect of crystal orientation on the aluminum anodes of the aluminum-air batteries in alkaline electrolytes. *J. Power Sources 299*, 66-69, **2015**.
[502]	Y. Yu, M. Chen, S. Wang, C. Hill, P. Joshi, A. Hu. Laser sintering of Al nanoparticles for Al-air batteries. *J. Laser Appl. 30*, 032605, **2018**.
[503]	L. Fan, H. Lu. The effect of grain size on aluminum anodes for Al-air batteries in alkaline electrolytes. *J. Power Sources 284*, 409-415, **2015**.
[504]	M. Pino, J. Chacon, E. Fatas, P. Ocon. Performance of commercial aluminium alloys as anodes in gelled electrolyte aluminium-air batteries. *J. Power Sources 299*, 195-201, **2015**.
[505]	K.-N. Jung, J. Kim, Y. Yamauchi, M.-S. Park, J.-W. Lee, J.H. Kim. Rechargeable lithium-air batteries: a perspective on the development of oxygen electrodes. *J. Mater. Chem. A 4*, 14050-14068, **2016**.
[506]	M. Srinivas, S.K. Adapaka, L. Neelakantan. Solubility effects of sn and ga on the microstructure and corrosion behavior of Al-Mg-Sn-Ga alloy anodes. *J. Alloys Compd. 683*, 647-653, **2016**.

[507]	L. Fan, H. Lu, J. Leng. Performance of fine structured aluminum anodes in neutral and alkaline electrolytes for Al-air batteries. *Electrochim. Acta 165*, 22-28, **2015**.
[508]	C. Zhu, H. Yang, A. Wu, D. Zhang, L. Gao, T. Lin. Modified alkaline electrolyte with 8-hydroxyquinoline and ZnO complex additives to improve Al-air battery. *J. Power Sources 432*, 55-64, **2019**.
[509]	M. Deyab. 1-Allyl-3-methylimidazolium bis (trifluoromethylsulfonyl) imide as an effective organic additive in aluminum-air battery. *Electrochim. Acta 244*, 178-183, **2017**.
[510]	J. Liu, D. Wang, D. Zhang, L. Gao, T. Lin. Synergistic effects of carboxymethyl cellulose and ZnO as alkaline electrolyte additives for aluminium anodes with a view towards Al-air batteries. *J. Power Sources 335*, 1-11, **2016**.
[511]	D. Wang, D. Zhang, K. Lee, L. Gao. Performance of AA5052 alloy anode in alkaline ethylene glycol electrolyte with dicarboxylic acids additives for aluminium-air batteries. *J. Power Sources 297*, 464-471, **2015**.
[512]	D. Wang, H. Li, J. Liu, D. Zhang, L. Gao, L. Tong. Evaluation of AA5052 alloy anode in alkaline electrolyte with organic rare-earth complex additives for aluminium-air batteries. *J. Power Sources 293*, 484-491, **2015**.
[513]	Y. Lai, Q. Wang, M. Wang, J. Li, J. Fang, Z. Zhang. Facile synthesis of mesoporous fe-NC electrocatalyst for high performance alkaline aluminum-air battery. *J. Electroanal. Chem. 801*, 72-76, **2017**.
[514]	K. Hu, T. Yu, Y. Zhang, X. Lin, Y. Zhao, G. Xie, et al. Inhibiting surface diffusion to synthesize 3D bicontinuous nanoporous N-doped carbon for boosting oxygen reduction reaction in flexible all-solid-state Al-air batteries. *Adv. Funct. Mater. 31*, 2103632, **2021**.
[515]	M. Guo, X. Zhang, T. Yang, Q. Dang, X. Li, Y. Wang, et al. Binary FeCo-N-doped carbon/carbon nanotube composites for efficient oxygen reduction and high-performance aluminum-air battery. *J. Power Sources 456*, 227933, **2020**.
[516]	Z. Wang, H. Zhou, J. Xue, X. Liu, S. Liu, X. Li, et al. Ultrasonic-assisted hydrothermal synthesis of cobalt oxide/nitrogen-doped graphene oxide hybrid as oxygen reduction reaction catalyst for Al-air battery. *Ultrason. Sonochem. 72*, 105457, **2021**.
[517]	G. Li, D. Yu, J. Song, F. Hu, L. Li, S. Peng. FeNi nanoparticles encapsulated in nitrogen-doped carbon frame for efficient and stable Al-air batteries. *Mater. Lett. 296*, 129890, **2021**.
[518]	J. Wang, H. Lu, Q. Hong, Y. Cao, X. Li, J. Bai. Porous N, S-codoped carbon architectures with bimetallic sulphide nanoparticles encapsulated in graphitic layers: highly active and robust electrocatalysts for the oxygen reduction reaction in Al-air batteries. *Chem. Eng. J. 330*, 1342-1350, **2017**.
[519]	M. Wang, Y. Li, J. Fang, C.J. Villa, Y. Xu, S. Hao, et al. Superior oxygen reduction reaction on phosphorus-doped carbon Dot/Graphene aerogel for all-solid-state flexible Al-air batteries. *Adv. Energy Mater. 10*, 1902736, **2020**.
[520]	L. Zhang, Q. Shao, J. Zhang. An overview of non-noble metal electrocatalysts and their associated air cathodes for mg-air batteries. *Mater. Rep. Energy 1*, 100002, **2021**.
[521]	F. Tong, S. Wei, X. Chen, W. Gao. Magnesium alloys as anodes for neutral aqueous magnesium-air batteries. *Journal of Magnesium and Alloys 9 (6)*, 1861-1883, **2021**.
[522]	N. Wang, R. Wang, Y. Feng, W. Xiong, J. Zhang, M. Deng. Discharge and corrosion behaviour of Mg-Li-Al-Ce-Y-Zn alloy as the anode for mg-air battery. *Corros. Sci. 112*, 13-24, **2016**.
[523]	M. Deng, D. Hoche, S.V. Lamaka, D. Snihirova, M.L. Zheludkevich. Mg-ca binary alloys as anodes for primary Mg-air batteries. *J. Power Sources 396*, 109-118, **2018**.

[524]	M. Deng, L. Wang, D. Hoche, S.V. Lamaka, P. Jiang, D. Snihirova, et al. Ca/In micro alloying as a novel strategy to simultaneously enhance power and energy density of primary Mg-air batteries from anode aspect. *J. Power Sources 472*, 228528, **2020**.
[525]	N. Shrestha, K. Raja, V. Utgikar. Mg-RE alloy anode materials for mg-air battery application. *J. Electrochem. Soc. 166*, A3139, **2019**.
[526]	N. Shrestha, J. Zillinger, V. Utgikar, K.S. Raja. Design strategies for anode of Mg-air batteries and hydrogen evolution reactions on Mg-RE alloys. *ECS Trans. 85*, 95, **2018**.
[527]	F.W. Richey, B.D. McCloskey, A.C. Luntz. Mg anode corrosion in aqueous electrolytes and implications for mg-air batteries. *J. Electrochem. Soc. 163*, A958, **2016**.
[528]	M. Deyab. Decyl glucoside as a corrosion inhibitor for magnesium-air battery. *J. Power Sources 325*, 98-103, **2016**.
[529]	T. Khoo, P.C. Howlett, M. Tsagouria, D.R. MacFarlane, M. Forsyth. The potential for ionic liquid electrolytes to stabilise the magnesium interface for magnesium/air batteries. *Electrochim. Acta 58*, 583-588, **2011**.
[530]	M. Jiang, H. He, C. Huang, B. Liu, W.-J. Yi, Z.-S. Chao. α-MnO_2 nanowires/ graphene composites with high electrocatalytic activity for mg-air fuel cell. *Electrochim. Acta 219*, 492-501, **2016**.
[531]	Z. Zhang, Z. Li, C. Sun, T. Zhang, S. Wang. Preparation and properties of an amorphous MnO_2/CNTs-OH catalyst with high dispersion and durability for magnesium-air fuel cells. *Catal. Today 298*, 241-249, **2017**.
[532]	Y. Zhang, X. Wu, Y. Fu, W. Shen, X. Zeng, W. Ding. Carbon aerogel supported Pt-Zn catalyst and its oxygen reduction catalytic performance in magnesium-air batteries. *J. Mater. Res. 29*, 2863-2870, **2014**.
[533]	B.T. Hang, D.H. Thang, N.T. Nga, P.T. Le Minh, E. Kobayashi. Nanoparticle Fe_2O_3-loaded carbon nanofibers as iron-air battery anodes. *J. Electrochem. Soc. 160*, A1442, **2013**.
[534]	A. Ito, L. Zhao, S. Okada, J.-I. Yamaki. Synthesis of nano-Fe_3O_4-loaded tubular carbon nanofibers and their application as negative electrodes for Fe/air batteries. *J. Power Sources 196*, 8154-8159, **2011**.
[535]	G. Balkourani, A. Brouzgou, P. Tsiakaras. A review on recent advancements in electrochemical detection of dopamine using carbonaceous nanomaterials. *Carbon*, 118281, **2023**.
[536]	K.L. Hawthorne, T.J. Petek, M.A. Miller, J.S. Wainright, R.F. Savinell. An investigation into factors affecting the iron plating reaction for an all-iron flow battery. *J. Electrochem. Soc. 162*, A108, **2014**.
[537]	B. Tian, J. Swiatowska, V. Maurice, S. Zanna, A. Seyeux, P. Marcus. The effect of Na_2S additive in alkaline electrolyte on improved performances of Fe-based air batteries. *Electrochim. Acta 259*, 196-203, **2018**.
[538]	P. Jakes, G. Cohn, Y. Ein-Eli, F. Scheiba, H. Ehrenberg, R.A. Eichel. Limitation of discharge capacity and mechanisms of air-electrode deactivation in silicon-air batteries. *ChemSusChem 5*, 2278-2285, **2012**.
[539]	G. Cohn, R.A. Eichel, Y. Ein-Eli. New insight into the discharge mechanism of silicon-air batteries using electrochemical impedance spectroscopy. *Phys. Chem. Chem. Phys. 15*, 3256-3263, **2013**.
[540]	Y.E. Durmus, S. Jakobi, T. Beuse, O. Aslanbas, H. Tempel, F. Hausen, et al. Influence of dopant type and orientation of silicon anodes on performance, efficiency and corrosion of silicon-air cells with EMIm (HF) 2.3 F electrolyte. *J. Electrochem. Soc. 164*, A2310, **2017**.

[541]	R. Bansal, P. Menon, R. Sharma. Silicon-air batteries: progress, applications and challenges. *SN Appl. Sci. 2*, 1-17, **2020**.
[542]	Iain, M., Aldous; Laurence, J., Hardwick; Richard, J., Nichols; J., Padmanabhan, Vivek. Metal-Air Battery: In Situ Spectroelectrochemical Techniques. *Metal-Air Batteries. Fundamentals and Applications*. Edited by Xin-bo Zhang. Wiley-VCH Verlag GmbH & Co. India, p.233-264, **2018**.
[543]	Arnolds, H. Vibrational dynamics of adsorbates - Quo vadis? *Prog. Surf. Sci.* 86: 1-40, **2011**.
[544]	Le, Ru, E.C.; Etchegoin, P.G. Principles of Surface-Enhanced Raman Spectroscopy and Related Plasmonic Effects. Elsevier, **2009**.
[545]	Schlucker, S. Surface-Enhanced Raman Spectroscopy: Concepts and Chemical Applications. *Angew. Chem. Int. Ed.* 53: 4756-4795, **2014**.
[546]	Fleischmann, M.; Hendra, P.J.; McQuillan, A.J. Raman spectra of pyridine adsorbed at a silver electrode. *Chem. Phys. Lett.* 26: 163-166, **1974**.
[547]	Albrecht, M.G.; Creighton, J.A. Anomalously intense Raman spectra of pyridine at a silver electrode. *J. Am. Chem. Soc.* 99: 5215-5217, **1977**.
[548]	Powell, J.A.; Venkatakrishnan, K.; Tan, B. A primary SERS-active interconnected Si-nanocore network for biomolecule detection with plasmonic nanosatellites as a secondary boosting mechanism. *Royal Society of Chemistry 7*: 33688-33700, **2017**.
[549]	Gomez, M.; Lazzari, M. Reliable and cheap SERS active substrates. *Mater. Today* 17: 358-359, **2014**.
[550]	Lee, Johnson; Chunmei, Li; Zheng, Liu; Yuhui, Chen; Stefan, A., Freunberger; Praveen, C., Ashok; Bavishna, B., Praveen; Kishan, Dholakia; Jean-Marie, Tarascon; Peter, G., Bruce. *Nat. Chem.* 6: 1091-1099, **2014**.
[551]	Aldous, I.M.; Hardwick, L.J. Solvent-Mediated Control of the Electrochemical Discharge Products of Non-Aqueous Sodium-Oxygen Electrochemistry. *Angew. Chem. Int. Ed.* 55: 8254-8257, **2016**.
[552]	Aldous, I.M.; Hardwick, L.J. Influence of Tetraalkylammonium Cation Chain Length on Gold and Glassy Carbon Electrode Interfaces for Alkali Metal - Oxygen Batteries. *J. Phys. Chem. Lett.* 5: 3924-3930, **2014**.
[553]	Stefan, A., Freunberger; Yuhui, Chen; Zhangquan, Peng; John, M., Griffin; Laurence, J., Hardwick; Fanny, Barde; Petr, Novak; Peter, G., Bruce. *J. Am. Chem. Soc.* 133: 8040-8047, **2011**.
[554]	Zhangquan, Peng; Stefan, A., Freunberger; Laurence, J., Hardwick; Yuhui, Chen; Vincent, Giordani; Fanny, Bardé; Petr, Novák; Duncan, Graham; Jean-Marie, Tarascon; Peter, G., Bruce. *Angew. Chem. Int. Ed.* 50: 6351-6355, **2011**.
[555]	Peng, Z.; Chen, Y.; Bruce, P.G.; Xu, Y. Direct Detection of the Superoxide Anion as a Stable Intermediate in the Electroreduction of Oxygen in a Non-Aqueous Electrolyte Containing Phenol as a Proton Source. *Angew. Chem. Int. Ed.* 54: 8165-8168, **2015**.
[556]	Wang, J.; Zhang, Y.; Guo, L.; Wang, E.; Peng, Z. Identifying Reactive Sites and Transport Limitations of Oxygen Reactions in Aprotic Lithium-O_2 Batteries at the Stage of Sudden Death. *Angew. Chem. Int. Ed.* 55: 5201-5205, **2016**.
[557]	Yu, Qiao; Ye, Shen. In Situ Study of Oxygen Reduction in Dimethyl Sulfoxide (DMSO) Solution: A Fundamental Study for Development of the Lithium-Oxygen Battery. *J. Phys. Chem. C* 119: 12236-12250, **2015**.
[558]	Qiao, Yu; Ye, Shen. Spectroscopic Investigation for Oxygen Reduction and Evolution Reactions with TTF as a Redox Mediator in Li-O Battery *J. Phys. Chem. C* 120: 15830-15845, **2016**.

[559]	Jakub, Staszak-Jirkovský; Ram, Subbaraman; Dusan, Strmcnik; Katharine, L., Harrison; Charles, E., Diesendruck; Rajeev, Assary; Otakar, Frank; Lukáš, Kobr; Gustav, K.H., Wiberg; Bostjan, Genorio; Justin, G., Connell; Pietro, P., Lopes; Vojislav, R., Stamenkovic; Larry, Curtiss; Jeffrey, S., Moore; Kevin, R., Zavadil; Nenad; M; Markovic. *ACS Catal.* 5: 6600-6607, **2015**.
[560]	Frith, J.T.; Russell, A.E.; Garcia-Araez, N.; Owen, J.R. An in-situ Raman study of the oxygen reduction reaction in ionic liquids. *Electrochem. Commun.* 46: 33-35, **2014**.
[561]	Galloway, T.A.; Hardwick, L.J. Utilizing in situ Electrochemical SHINERS for Oxygen Reduction Reaction Studies in Aprotic Electrolytes. *J. Phys. Chem. Lett.* 7: 2119-2124, **2016**.
[562]	Otto, A. Excitation of Nonradiative Surface Plasma Waves in Silver by Method of Frustrated Total Reflection. *Z. Phys.* 216: 398-410, **1968**.
[563]	Kretschmann, E. Die Bestimmung optischer Konstanten von Metallen durch Anregung von Oberflächenplasmaschwingungen. *Z. Phys.* 241: 313-324, **1971**.
[564]	Hartstein, A.; Kirtley, J.R.; Tsang, J.C. Enhancement of the Infrared Absorption from Molecular Monolayers with Thin Metal Overlayers. Phys. Rev. Lett. 45: 201-204, **1980**.
[565]	Osawa, M.; Kuramitsu, M.; Hatta, A.; Suetaka, W.; Seki, H. Electromagnetic effect in enhanced infrared absorption of adsorbed molecules on thin metal films. *Surf. Sci.* 175: L787-L793, **1986**.
[566]	Masatoshi, Osawa; Ken-Ichi, Ataka; Katsumasa, Yoshii; Yuji, Nishikawa. Surface-Enhanced Infrared Spectroscopy: The Origin of the Absorption Enhancement and Band Selection Rule in the Infrared Spectra of Molecules Adsorbed on Fine Metal Particles. *Appl. Spectrosc.* 47: 1497-1502, **1993**.
[567]	Miyake, Hiroto; Ye, Shen; Osawa, Masatoshi. Electroless deposition of gold thin films on silicon for surface-enhanced infrared spectroelectrochemistry. *Electrochem. Commun.* 4: 973-977, **2002**.
[568]	Hof, Martin. Basics of Optical Spectroscopy. *Handbook of Spectroscopy*, Wiley-VCH, 37-47, **2005**.
[569]	Shin, D.S.; Doddapaneni, N.; Park, S.M. In situ spectroelectrochemical studies of oxygen reduction in dimethyl sulfoxide and pyridine. *Inorg. Chem.* 31: 4060-4064, **1992**.
[570]	Wen-Wen, Yin; Zulipiya, Shadike; Yin, Yang; Fei, Ding; Lin, Sang; Hong, Li; Zheng-Wen, Fu. A long-life Na-air battery based on a soluble NaI catalyst. *Chem. Commun.* 51: 2324-2327, **2015**.
[571]	Lamy, C.; Crouigneau, P. In situ electron spin resonance spectroscopy studies of electrode processes. *J. Electroanal. Chem.* 150: 545-552, **1983**.
[572]	Wandt, J.; Jakes, P.; Granwehr, J.; Gasteiger, H.A.; Eichel, R.-A. Singlet Oxygen Formation during the Charging Process of an Aprotic Lithium-Oxygen Battery. *Angew. Chem. Int. Ed.* 55: 6892-6895, **2016**.
[573]	Wandt, J.; Marino, C.; Gasteiger, H.A.; Jakes, P.; Eichel, R.-A.; Granwehr, J. Operando electron paramagnetic resonance spectroscopy - formation of mossy lithium on lithium anodes during charge-discharge cycling. *Energy Environ. Sci.* 8: 1358-1367, **2015**.
[574]	Shaila, Mir; Sunali, Vij; Nikhil, Dhawan. Evaluation of end-of-life zinc-air hearing aid batteries for zinc recovery. *Minerals Engineering 198*, 108082, **2023**. https://doi.org/10.1016/j.mineng.2023.108082.
[575]	Cai, X.; Lai, L.; Lin, J.; Shen, Z. Recent advances in air electrodes for Zn-air batteries: Electrocatalysis and structural design. *Mater. Horizons 4, 945-976, 2017*. https://doi.org/10.1039/c7mh00358g.

[576]	Gabal, M.A.; Al-luhaibi, R.S.; Al Angari, Y.M. Recycling spent zinc-carbon batteries through synthesizing nano-crystalline Mn-Zn ferrites. *Powder Technol. 258*, 32-37, 2014. https://doi.org/10.1016/J.POWTEC.2014.03.003.
[577]	Harting, K.; Kunz, U.; Turek, T.; Zinc-air batteries: Prospects and challenges for future improvement. *Zeitschrift fur Phys. Chemie 226*, 151-166, **2012**. https://doi.org/ 10.1524/zpch.2012.0152.
[578]	MIT Technology review. Available online: https://www.technologyreview.com/2001/ 09/01/235591/zinc-air-batteries/ (Accessed 28/8/2023).
[579]	Fu, J.; Cano, Z.P.; Park, M.G.; Yu, A.; Fowler, M.; Chen, Z. Electrically Rechargeable Zinc-Air Batteries: Progress, Challenges, and Perspectives. *Adv. Mater. 29*, 1604685, **2017**. https://doi.org/10.1002/adma.201604685.
[580]	Clark, S.; Latz, A.; Horstmann, B. A Review of Model-Based Design Tools for Metal-Air Batteries. *Batteries 4*, 5, **2018**. https://doi.org/10.3390/batteries4010005.
[581]	Toussaint, G.; Stevens, P.; Akrour, L.; Rouget, R.; Fourgeot, F.. Development of a Rechargeable Zinc-Air Battery. *ECS Trans. 28*, 25-34, **2010**. https://doi.org/10.1149/ 1.3507924.
[582]	Wang, G.C. Nonferrous metal extraction and nonferrous slags. *Util. Slag Civ. Infrastruct. Constr.* 35-61, **2016**. https://doi.org/10.1016/b978-0-08-100381-7.00003-3.
[583]	Dhawan, N.; Safarzadeh, M.S.; Birinci, M. Kinetics of hydrochloric acid leaching of smithsonite. *Russ. J. Non-ferrous Metals 52*, 209, **2011**. https://doi.org/10.3103/ S1067821211030059.
[584]	Raghvan. Extractive Metallurgy of Non-ferrous Metals. *First ed. Vijay Nicole Imprints, Chennai*, **2016**.
[585]	USGS. **2021**. Available online: https://pubs.usgs.gov/periodicals/mcs2021/mcs2021.pdf (Accessed 28/8/2023).
[586]	USGS. **2022**. Available online: https://www.usgs.gov/news/national-news-release/us - geological-survey-releases-2022-list-critical-minerals (Accessed 28/8/2023).
[587]	CRM. **2020**. Available online: https://rmis.jrc.ec.europa.eu/?page=crm-list-2020-e294f6 (Accessed 28/8/2023).
[588]	Drake, A. Canadian Reserves of Selected Major Metals and Recent Production Decisions. **2018**. Available online: https://natural-resources.canada.ca/mining-materia ls/exploration/8294. (Accessed 28/8/2023).
[589]	Huston, D. Australian Resource Reviews: Zinc, Lead and Silver 2019. Geoscience Australia, Canberra, **2020**. Available online: https://doi.org/10.3133/70202434 (Accessed 28/8/2023).
[590]	Dobrowolski, Z.; Sulkowski, L.; Danielak, W. Management of waste batteries and accumulators: Quest of European Union goals. *Energies. 14*, 6273, **2021**. https://doi.org/10.3390/en 14196273.
[591]	EU legislations. **2022**. Available online: https://www.europarl.europa.eu/RegData/etudes/ BRIE/2021/689337/EPRS_BRI(2021)689337_EN.pdf. (Accessed 28/8/2023).
[592]	Caramia, V.; Bozzini, B. Materials science aspects of zinc-air batteries: A review. Mater. Renew. Sustain. Energy 3, 28, **2014**. https://doi.org/10.1007/s40243-014-0028-3.
[593]	Pei, P.; Wang, K.; Ma, Z. Technologies for extending zinc-air battery's cyclelife: A review. *Appl. Energy 128*, 315-324, **2014**. https://doi.org/10.1016/J. APENERGY.2014.04.095.
[594]	Tomboc, G.M.; Yu, P.; Kwon, T.; Lee, K.; Li, J. Ideal design of air electrode - A step closer toward robust rechargeable Zn-air battery 8, 50905, **2020**. https://doi.org/10.1063/5.0005137.

[595]	Vanithakumari, S.C.; Nanda, K.K.; Krupanidhi, S.B. Synthesis of one-dimensional ZnO nanostructures from Zn powder/granule. *J. Nanosci. Nanotechnol. 9*, 2061-2065, **2009**. https://doi.org/10.1166/jnn.2009.404.
[596]	Varta. Safety Data sheet. VARTA Microbattery GmbH VARTA-Platz 1 73479 Ellwangen Germany. Version: 13. Edition: 28.09.2020, **2022**. Available online: https://products.varta-microbattery.com/applications/mb_data/documents/material_safety_data_sheets/MSDS_22_ Primary_Silver_Button_ Series_V_MF_en.pdf (Accessed 28/8/2023).
[597]	Halleux, V. New EU regulatory framework for batteries. 6, **2022**. Available online: https://www.europarl.europa.eu/RegData/etudes/ATAG/2022/729285/EPRS_ATA(2022) 729285_EN.pdf. (Accessed 28/8/2023).
[598]	Dawson, L.; Ahuja, J.; Lee, R. Steering extended producer responsibility for electric vehicle batteries. *Environ. Law Rev. 23*, 128-143, **2021**. https://doi.org/10.1177/ 14614529211006069.
[599]	Sterkens, W.; Diaz-Romero, D.; Goedeme, T.; Dewulf, W.; Peeters, J.R. Detection and recognition of batteries on X-Ray images of waste electrical and electronic equipment using deep learning. *Resour. Conserv. Recycl. 168*, 105246, **2021**. https://doi.org/10.1016/j. resconrec.2020.105246.
[600]	Sengupta, D.; Ilankoon, I.M.; Kang, K.D.; Chong, M.N. Circular economy and household e-waste management in India: Integration of formal and informal sectors. *Miner. Eng. 184*, 107661, **2022**. https://doi.org/10.1016/j.mineng.2022.107661.
[601]	Sun, Y.; Shen, X.Y.; Zhai, Y.C. Thermodynamics and kinetics of extracting zinc from zinc oxide ore by the ammonium sulfate roasting method. *Int. J. Miner. Metall. Mater. 22*, 467-475, **2015**. https://doi.org/10.1007/s12613-015-1095-x.
[602]	Farzana, R.; Rajarao, R.; Hassan, K.; Behera, P.R.; Sahajwalla, V. Thermal nanosizing: Novel route to synthesize manganese oxide and zinc oxide nanoparticles simultaneously from spent Zn-C battery. *J. Clean. Prod. 196*, 478-488, **2018**. https://doi.org/10.1016/J.JCLEPRO.2018. 06.055.
[603]	Miki, T.; Chairaksa-Fujimoto, R.; Maruyama, K.; Nagasaka, T. Hydrometallurgical extraction of zinc from CaO treated EAF dust in ammonium chloride solution. *J. Hazard. Mater. 302*, 90-96, **2016**. https://doi.org/10.1016/J.JHAZMAT.2015.09.020.
[604]	Antrekowitsch, J.; Steinlechner, S.; Unger, A.; Rosler, G.; Pichler, C.; Rumpold, R. Zinc and Residue Recycling. *Handb. Recycl. State-of-the-art Pract. Anal. Sci*. 113-124, **2014**. https://doi.org/10.1016/B978-0-12-396459-5.00009-X.
[605]	Kaya, M.; Hussaini, S.; Kursunoglu, S. Critical review on secondary zinc resources and their recycling technologies. *Hydrometallurgy 195*, 105362, **2020**. https://doi.org/10.1016/J. HYDROMET.2020.105362.
[606]	Ahamed, A.M.; Pons, M.N.; Ricoux, Q.; Issa, S.; Goettmann, F.; Lapicque, F. New pathway for utilization of jarosite, an industrial waste of zinc hydrometallurgy. *Miner. Eng. 170*, 107030, **2021**. https://doi.org/10.1016/j.mineng.2021.107030.
[607]	Atia, A.T.; Wouters, W.; Monforte, G.; Spooren, J. Microwave chloride leaching of valuable elements from spent automotive catalysts: Understanding the role of hydrogen peroxide. *Resour. Conserv. Recycl. 166*, 105349, **2021**. https://doi.org/10.1016/ j.resconrec.2020.105349.
[608]	Zhang, B.; Guo, X.; Wang, Q.; Tian, Q. Thermodynamic analysis and process optimization of zinc and lead recovery from copper smelting slag with chlorination roasting. *Trans. Nonferrous Met. Soc. China 31*, 3905-3917, **2021**. https://doi.org/10.1016/S1003-6326(21)65773-4.
[609]	Trpcevska, J.; Rudnik, E.; Holkova, B.; Laubertova, M. Leaching of zinc ash with hydrochloric acid solutions. *Polish J. Environ. Stud. 27*, 1765-1771, **2018**. https://doi.org/10.15244/pjoes/ 78039.

[610]	Rudnik, E. Recovery of zinc from zinc ash by leaching in sulphuric acid and electrowinning. *Hydrometallurgy 188*, 256-263, **2019**. https://doi.org/10.1016/j.hydromet.2019.07.006.
[611]	Zhu, X.; Xu, C.; Tang, J.; Hua, Y.; Zhang, Q.; Liu, H.; Wang, X.; Huang, M. Selective recovery of zinc from zinc oxide dust using choline chloride based deep eutectic solvents. *Trans. Nonferrous Met. Soc. China 29*, 2222-2228, **2019**. https://doi.org/10.1016/S1003-6326(19) 65128-9.
[612]	Andak, B.; Ozduğan, E.; Türdü, S.; Bulutcu, A.N. Recovery of zinc and manganese from spent zinc-carbon and alkaline battery mixtures via selective leaching and crystallization processes. *J. Environ. Chem. Eng. 7*, 103372, **2019**. https://doi.org/ 10.1016/J.JECE.2019.103372.
[613]	Biswas, R.K.; Karmakar, A.K.; Kumar, S.L.; Hossain, M.N. Recovery of manganese and zinc from waste Zn-C cell powder: Characterization and leaching. *Waste Manag. 46*, 529-535, **2015**. https://doi.org/10.1016/J.WASMAN.2015.09.008.
[614]	Biswas, R.K.; Karmakar, A.K.; Kumar, S.L. Recovery of manganese and zinc from spent Zn-C cell powder: Experimental design of leaching by sulfuric acid solution containing glucose. *Waste Manag. 51*, 174-181, **2016**. https://doi.org/10.1016/J.WASMAN.2015.11.002.
[615]	Mahandra, H.; Singh, R.; Gupta, B. Recycling of Zn-C and Ni-Cd spent batteries using Cyphos IL 104 via hydrometallurgical route. *J. Clean. Prod. 172*, 133-142, **2018**. https://doi.org/10.1016/ J.JCLEPRO.2017.10.129.
[616]	Sadeghi, S.; Vanpeteghem, G.; Neto, I.F.F.; Soares, H.M.V.M. Selective leaching of Zn from spent alkaline batteries using environmentally friendly approaches. *Waste Manag. 60*, 696-705, **2017**. https://doi.org/10.1016/J.WASMAN.2016.12.002.
[617]	Mukhlis, R.; Mackenzie, A.; Rhamdhani, M.A. Small scale recycling process for spent alkaline batteries: Technoeconomic analysis and potential use of solar energy. *Resour. Conserv. Recycl. 166*, 105367, **2021**. https://doi.org/10.1016/J. RESCONREC.2020.105367.
[618]	Yesiltepe, S.; Bugdaycı, M.; Yücel, O.; Sesen, M.K. Recycling of Alkaline Batteries via a Carbothermal Reduction Process. *Batteries 5*, **2019**. https://doi.org/10.3390/batteries501 0035.
[619]	Bernardes, A.M.; Espinosa, D.C.; Tenorio, J.S. Recycling of batteries: a review of current processes and technologies. *J. of Power Sources. 130*, 291, **2004**. https://doi.org/10.1016/j. jpowsour.2003.12.026.
[620]	Sadeghi, S.M.; Jesus, J.; Soares, H.M. A critical updated review of the hydrometallurgical routes for recycling zinc and manganese from spent zinc-based batteries. *Waste Manag. 113*, 342-350, **2020**. https://doi.org/10.1016/j.wasman.2020.05.049.
[621]	Espinosa, D.C.; Bernardes, A.M.; Tenorio, J.A. An overview on the current processes for the recycling of batteries. *J. of Power Sources. 135*, 311, **2004**. https://doi. org/10.1016/j.jpowsour. 2004.03.083.
[622]	Ebin, B.; Petranikova, M.; Ekberg, C. Physical separation, mechanical enrichment and recycling-oriented characterization of spent NiMH batteries. *J. Mater. Cycles Waste Manag. 20*, 2018-2027, **2018**. https://doi.org/10.1007/s10163-018-0751-4.
[623]	Hu, X.; Robles, A.; Vikstrom, T.; Vaananen, P., Zackrisson, M., Ye, G. A novel process on the recovery of zinc and manganese from spent alkaline and zinc-carbon batteries. *J. Hazard. Mater. 411*, 124928, **2021**. https://doi.org/10.1016/j. jhazmat.2020.124928.
[624]	Rukini, A.; Rhamdhani, M.A.; Brooks, G.A.; Van den Bulck, A. Metals Production and Metal Oxides Reduction Using Hydrogen: A Review. *J. Sustain. Metall*. **2022**. https://doi.org/10. 1007/s40831-021-00486-5.

[625]	Yang, Z.; Uhrynowski, W.; Jakusz, G.; Retka, J.; Karczewska-Golec, J.; Debiec- Andrzejewska, K.; Rogulski, Z.; Drewniak, L. Biochemical treatment of leachates from hydrometallurgical recycling of spent alkaline batteries. *Hydrometallurgy. 191*, 105223, **2020**. https://doi.org/10.1016/ j.hydromet.2019.105223.
[626]	Xing, P.; Ma, B.; Wang, C.; Wang, L.; Chen, Y. A simple and effective process for recycling zinc-rich paint residue. *Waste Manag. 76*, 234-241, **2018**. https://doi.org/10.1016/J.WASMAN. 2018.03.018.
[627]	Verhoef, E.V.; Dijkema, G.P.J.; Reuter, M.A. Process Knowledge, System Dynamics, and Metal Ecology. *J. Ind. Ecol. 8*, 23-43, **2004**. https://doi.org/10.1162/1088198041269382.
[628]	Yadav, D.; Banerjee, R. Thermodynamic and economic analysis of the solar carbothermal and hydrometallurgy routes for zinc production. *Energy*. 123242, **2022**. https://doi.org/10.1016/ J.ENERGY.2022.123242.
[629]	Bakhiyi, B.; Gravel, S.; Ceballos, D.; Flynn, M.A.; Zayed, J. Has the question of e-waste opened a Pandora's box? An overview of unpredictable issues and challenges. *Environment international. 110*, 173, **2018**. https://doi.org/10.1016/j.envint.2017.10.021.
[630]	Alex, T.C.; Kalinkin, A.M.; Nath, S.K.; Gurevich, B.I.; Kalinkina, E.V.; Tyukavkina, V.V.; Kumar, S. Utilization of zinc slag through geopolymerization: Influence of milling atmosphere. *Int. J. Miner. Process. 123*, 102-107, **2013**. https://doi.org/10.1016/J.MINPRO.2013.06.001.
[631]	Genderen, E.V.; Wildnauer, M.; Santero, N.; Sidi, N. A global life cycle assessment for primary zinc production. *Int. J. Life Cycle Assess. 21*, 1580-1593, **2016**. https://doi. org/10.1007/s11367-016-1131-8.
[632]	Chu, S.; Cui, Y.; Liu, N. The path towards sustainable energy. *Nat. Mater. 16*, 16-22, **2017**.
[633]	Yang, Z.G.; Zhang, J.L.; Kintner-Meyer, M.C.W.; Lu, X.C.; Choi, D.W.; Lemmon, J.P.; Liu, J. Electrochemical energy storage for green grid. *Chem. Rev. 111*, 3577-3613, **2011**.
[634]	Li, H.; Wang, Z.X.; Chen, L.Q.; Huang, X.J. Research on advanced materials for Li-ion batteries. *Adv. Mater. 21*, 4593-4607, **2009**.
[635]	Li, Y.G.; Lu, J. Metal air batteries: will they be the future electrochemical energy storage device of choice? *ACS Energy Lett. 2*, 1370-1377, **2017**.
[636]	Lee, J.S.; Kim, S.T.; Cao, R.; Choi, N.S.; Liu, M.; Lee, K.T.; Cho, J. Metal-air batteries with high energy density: Li-air versus Zn-air. *Adv. Energy Mater. 1*, 34-50, **2011**.
[637]	Zhang, P.; Zhao, Y.; Zhang, X.B. Functional and stability orientation synthesis of materials and structures in aprotic Li-O$_2$ batteries. *Chem. Soc. Rev. 47*, 2921-3004, **2018**.
[638]	Wang, H.F.; Tang, C.; Zhang, Q. A review of precious-metal-free bifunctional oxygen electrocatalysts: rational design and applications in Zn-air batteries. *Adv. Funct. Mater. 28*, 1803329, **2018**.
[639]	Ryu, J.; Park, M.; Cho, J. Advanced technologies for high-energy aluminum-air batteries. *Adv. Mater. 31*, 1804784, **2019**.
[640]	Yadegari, H.; Sun, X.L. Recent advances on sodium-oxygen batteries: a chemical perspective. *Acc. Chem. Res. 51*, 1532-1540, **2018**.
[641]	Yi, J.; Liang, P.C.; Liu, X.Y.; Wu, K.; Liu, Y.Y.; Wang, Y.G.; Xia, Y.Y.; Zhang, J.J. Challenges, mitigation strategies and perspectives in development of zinc-electrode materials and fabrication for rechargeable zinc-air batteries. *Energy Environ. Sci. 11*, 3075-3095, **2018**.
[642]	Zaromb, S. The use and behavior of aluminum anodes in alkaline primary batteries. *J. Electrochem. Soc. 109*, 1125-1130, **1962**.

212

[643]	Ojefors, L., and Carlsson, L. An iron-air vehicle battery. *J. Power Sources 2*, 287-296, **1978**.
[644]	Abraham, K.M.; Jiang, Z. A polymer electrolyte-based rechargeable lithium/oxygen battery. *J. Electrochem. Soc. 143*, 1-5, **1996**.
[645]	Muller, S.; Holzer, F.; Haas, O. Optimized zinc electrode for the rechargeable zinc-air battery. *J. Appl. Electrochem. 28*, 895-898, **1998**.
[646]	Kuboki, T.; Okuyama, T.; Ohsaki, T.; Takami, N. Lithium-air batteries using hydrophobic room temperature ionic liquid electrolyte. *J. Power Sources 146*, 766-769, **2005**.
[647]	Ogasawara, T.; Debart, A.; Holzapfel, M.; Novak, P.; Bruce, P.G. Rechargeable Li_2O_2 electrode for lithium batteries. *J. Am. Chem. Soc. 128*, 1390-1393, **2006**.
[648]	Read, J. Ether-based electrolytes for the lithium/oxygen organic electrolyte battery. *J. Electrochem. Soc. 153*, A96-A100, **2006**.
[649]	Imanishi, N.; Hasegawa, S.; Zhang, T.; Hirano, A.; Takeda, Y.; Yamamoto, O. Lithium anode for lithium-air secondary batteries. *J. Power Sources 185*, 1392-1397, **2008**.
[650]	Peng, Z.Q.; Freunberger, S.A.; Chen, Y.H.; Bruce, P.G. A reversible and higher-rate $Li-O_2$ battery. *Science 337*, 563-566, **2012**.
[651]	Ren, X.D.; Wu, Y.Y. A low-overpotential potassium-oxygen battery based on potassium superoxide. *J. Am. Chem. Soc. 135*, 2923-2926, **2013**.
[652]	Hartmann, P.; Bender, C.L.; Vracar, M.; Durr, A.K., Garsuch, A.; Janek, J.; Adelhelm, P. A rechargeable room-temperature sodium superoxide (NaO_2) battery. *Nat. Mater. 12*, 228-232, **2013**.
[653]	Chen, Y.H.; Freunberger, S.A.; Peng, Z.Q.; Fontaine, O.; Bruce, P.G. Charging a $Li-O_2$ battery using a redox mediator. *Nat. Chem. 5*, 489-494, **2013**.
[654]	Li, B.; Geng, D.S.; Lee, X.S.; Ge, X.M.; Chai, J.W.; Wang, Z.J.; Zhang, J.; Liu, Z.L.; Hor, T.S.A.; Zong, Y. Eggplant-derived microporous carbon sheets: towards mass production of efficient bifunctional oxygen electrocatalysts at low cost for rechargeable Zn-air batteries. *Chem. Commun. (Camb.) 51*, 8841-8844, **2015**.
[655]	Zhang, J.T.; Zhao, Z.H.; Xia, Z.H.; Dai, L.M. A metal-free bifunctional electrocatalyst for oxygen reduction and oxygen evolution reactions. *Nat. Nanotechnol. 10*, 444-452, **2015**.
[656]	Park, J.; Park, M.; Nam, G.; Lee, J.S.; Cho, J. All-solid-state cable-type flexible zinc-air battery. Adv. Mater. 27, 1396-1401, **2015**.
[657]	Dong, Q.; Yao, X.H.; Zhao, Y.Y.; Qi, M.; Zhang, X.Z.; Sun, H.Y.; He, Y.M.; Wang, D.W. Cathodically stable $Li-O_2$ battery operations using water-in-salt electrolyte. *Chem 4*, 1345-1358, **2018**.
[658]	Wang, F.; Borodin, O.; Gao, T.; Fan, X.L.; Sun, W.; Han, F.D.; Faraone, A.; Dura, J.A.; Xu, K.; Wang, C.S. Highly reversible zinc metal anode for aqueous batteries. *Nat. Mater. 17*, 543-549, *2018*.
[659]	Chang, Z.W.; Xu, J.J.; Zhang, X.B. Recent progress in electrocatalyst for $Li-O_2$ batteries. *Adv. Energy Mater. 7*, 1700875, **2017**.
[660]	Pan, J.; Xu, Y.Y.; Yang, H.; Dong, Z.H.; Liu, H.F.; Xia, B.Y. Advanced architectures and relatives of air electrodes in Zn-air batteries. *Adv. Sci. 5*, 1700691, **2018**.
[661]	Park, J.B.; Lee, S.H.; Jung, H.G.; Aurbach, D.; Sun, Y.K. Redox mediators for $Li-O_2$ batteries: status and perspectives. *Adv. Mater. 30*, 1704162, **2018**.
[662]	Zhao, Z.W.; Huang, J.; Peng, Z.Q. Achilles' heel of lithium-air batteries: lithium carbonate. *Angew. Chem. Int. Ed. 57*, 3874-3886, **2018**.
[663]	Fu, J.; Cano, Z.P.; Park, M.G.; Yu, A.P.; Fowler, M.; Chen, Z.W. Electrically rechargeable zinc-air batteries: progress, challenges, and perspectives. *Adv. Mater. 29*, 1604685, **2017**.

[664]	Cao, R.; Lee, J.S.; Liu, M.L.; Cho, J. Recent progress in non-precious catalysts for metal-air batteries. *Adv. Energy Mater. 2*, 816-829, **2012**.
[665]	Lee, D.U.; Xu, P.; Cano, Z.P.; Kashkooli, A.G.; Park, M.G.; Chen, Z.W. Recent progress and perspectives on bi-functional oxygen electrocatalysts for advanced rechargeable metal-air batteries. *J. Mater. Chem. A 4*, 7107-7134, **2016**.
[666]	Busch, M.; Halck, N.B.; Kramm, U.I.; Siahrostami, S.; Krtil, P.; Rossmeisl, J. Beyond the top of the volcano? A unified approach to electrocatalytic oxygen reduction and oxygen evolution. *Nano Energy 29*, 126-135, **2016**.
[667]	Huang, Y.; Wang, Y.; Tang, C.; Wang, J.; Zhang, Q.; Wang, Y.; Zhang, J. Atomic modulation and structure design of carbons for bifunctional electrocatalysis in metal-air batteries. *Adv. Mater. 31*, 1803800, **2019**.
[668]	Li, Y.J.; Cui, L.; Da, P.F.; Qiu, K.W.; Qin, W.J.; Hu, W.B.; Du, X.W.; Davey, K.; Ling, T.; Qiao, S.Z. Multiscale structural engineering of Ni-doped CoO nanosheets for zinc-air batteries with high power density. *Adv. Mater. 30*, e1804653, **2018**.
[669]	Chen, S.; Duan, J.; Zheng, Y.; Chen, X.; Du, X.W.; Jaroniec, M.; Qiao, S.Z. Ionic liquid-assisted synthesis of N/S-double doped graphene microwires for oxygen evolution and Zn-air batteries. *Energy Storage Mater. 1*, 17-24, **2015**.
[670]	Zou, L.L.; Hou, C.C.; Liu, Z.; Pang, H.; Xu, Q. Superlong single-crystal metalorganic framework nanotubes. *J. Am. Chem. Soc. 140*, 15393-15401, **2018**.
[671]	Li, B.Q.; Zhang, S.Y.; Wang, B.; Xia, Z.J.; Tang, C.; Zhang, Q. A porphyrin covalent organic framework cathode for flexible Zn-air batteries. *Energy Environ. Sci. 11*, 1723-1729, **2018**.
[672]	Cheng, C.; Li, S.; Xia, Y.; Ma, L.; Nie, C.X.; Roth, C.; Thomas, A.; Haag, R. Atomic Fe-Nx coupled open-mesoporous carbon nanofibers for efficient and bioadaptable oxygen electrode in Mg-air batteries. *Adv. Mater. 30*, 1802669, **2018**.
[673]	Lyu, Z.Y.; Zhou, Y.; Dai, W.R.; Cui, X.H.; Lai, M.; Wang, L.; Huo, F.W.; Huang, W.; Hu, Z.; Chen, W. Recent advances in understanding of the mechanism and control of Li_2O_2 formation in aprotic $Li-O_2$ batteries. *Chem. Soc. Rev. 46*, 6046-6072, **2017**.
[674]	Feng, N.N.; He, P.; Zhou, H.S. Critical challenges in rechargeable aprotic $Li-O_2$ batteries. *Adv. Energy Mater. 6*, 1502303, **2016**.
[675]	Li, Y.; Wang, X.G.; Dong, S.M.; Chen, X.; Cui, G.L. Recent advances in nonaqueous electrolyte for rechargeable $Li-O_2$ batteries. *Adv. Energy Mater. 6*, 1600751, **2016**.
[676]	Ma, L.; Yu, T.W.; Tzoganakis, E.; Amine, K.; Wu, T.P.; Chen, Z.W.; Lu, J. Fundamental understanding and material challenges in rechargeable nonaqueous $Li-O_2$ batteries: recent progress and perspective. *Adv. Energy Mater. 8*, 1800348, **2018**.
[677]	Song, K.; Jung, J.; Park, M.; Park, H.; Kim, H.J.; Choi, S.I.; Yang, J.; Kang, K.; Han, Y.K.; Kang, Y.M. Anisotropic surface modulation of Pt catalysts for highly reversible $Li-O_2$ batteries: high index facet as a critical descriptor. *ACS Catal. 8*, 9006-9015, **2018**.
[678]	Yui, Y.; Sakamoto, S.; Nohara, M.; Hayashi, M.; Nakamura, J.; Komatsu, T. Electrochemical properties of lithium air batteries with $Pt_{100-x}Ru100_x$ ($0 \leq x \leq 100$) electrocatalysts for air electrodes. *J. Power Sources 340*, 121-125, **2017**.
[679]	Cho, S.A.; Jang, Y.J.; Lim, H.D.; Lee, J.E.; Jang, Y.H.; Nguyen, T.T.H.; Mota, F.M.; Fenning, D.P.; Kang, K.; Shao-Horn, Y., et al. Hierarchical porous carbonized Co_3O_4 inverse opals via combined block copolymer and colloid templating as bifunctional electrocatalysts in $Li-O_2$ battery. *Adv. Energy Mater. 7*, 1700391, **2017**.

[680]	Adpakpang, K.; Oh, S.M.; Agyeman, D.A.; Jin, X.Y.; Jarulertwathana, N.; Kim, I.Y.; Sarakonsri, T.; Kang, Y.M.; Hwang, S.J. Holey 2D nanosheets of low-valent manganese oxides with an excellent oxygen catalytic activity and a high functionality as a catalyst for Li-O$_2$ batteries. *Adv. Funct. Mater. 28*, 1707106, **2018**.
[681]	Bi, R.; Liu, G.X.; Zeng, C.; Wang, X.P.; Zhang, L.; Qiao, S.Z. 3D hollow α-MnO$_2$ framework as an efficient electrocatalyst for lithium-oxygen batteries. *Small 15*, 1804958, **2019**.
[682]	Chen, S.; Liu, G.X.; Yadegari, H.; Wang, H.H.; Qiao, S.Z. Three-dimensional MnO$_2$ ultrathin nanosheet aerogels for high-performance Li-O$_2$ batteries. *J. Mater. Chem. A 3*, 2559-2563, **2015**.
[683]	Gao, R.; Yang, Z.Z.; Zheng, L.R.; Gu, L.; Liu, L.; Lee, Y.L.; Hu, Z.B.; Liu, X.F. Enhancing the catalytic activity of Co$_3$O$_4$ for Li-O$_2$ batteries through the synergy of surface/interface/doping engineering. *ACS Catal. 8*, 1955-1963, **2018**.
[684]	Lau, S.; Archer, L.A. Nucleation and growth of lithium peroxide in the Li-O$_2$ battery. *Nano Lett. 15*, 5995-6002, **2015**.
[685]	Xu, J.J.; Chang, Z.W.; Yin, Y.B.; Zhang, X.B. Nanoengineered ultralight and robust all-metal cathode for high-capacity, stable lithium-oxygen batteries. *ACS Cent. Sci. 3*, 598-604, **2017**.
[686]	Lyu, Z.Y.; Lim, G.J.H.; Guo, R.; Kou, Z.K.; Wang, T.T.; Guan, C.; Ding, J.; Chen, W.; Wang, J. 3D-printed MOF-derived hierarchically porous frameworks for practical high-energy density Li-O$_2$ batteries. *Adv. Funct. Mater. 29*, 1806658, **2019**.
[687]	Song, K.; Agyeman, D.A.; Park, M.; Yang, J.; Kang, Y.M. High-energy-density metal-oxygen batteries: lithium-oxygen batteries vs sodium-oxygen batteries. *Adv. Mater. 29*, 1606572, **2017**.
[688]	Hwang, J.Y.; Myung, S.T.; Sun, Y.K. Recent progress in rechargeable potassium batteries. *Adv. Funct. Mater. 28*, 1802938, **2018**.
[689]	Xia, C.; Black, R.; Fernandes, R.; Adams, B.; Nazar, L.F. The critical role of phase-transfer catalysis in aprotic sodium oxygen batteries. *Nat. Chem. 7*, 496-501, **2015**.
[690]	H. Lei, J. Piao, A. Brouzgou, E. Gorbova, P. Tsiakaras, Z. Liang. Synthesis of nitrogen-doped mesoporous carbon nanosheets for oxygen reduction electrocatalytic activity enhancement in acid and alkaline media. *International journal of hydrogen Energy 44 (9)*, 4423-4431, **2019**.
[691]	Yang, X.Y.; Xu, J.J.; Bao, D.; Chang, Z.W.; Liu, D.P.; Zhang, Y.; Zhang, X.B. High-performance integrated self-package flexible Li-O$_2$ battery based on stable composite anode and flexible gas diffusion layer. *Adv. Mater. 29*, 1700378, **2017**.
[692]	Lee, D.U.; Choi, J.Y.; Feng, K.; Park, H.W.; Chen, Z.W. Advanced extremely durable 3D bifunctional air electrodes for rechargeable zinc-air batteries. *Adv. Energy Mater. 4*, 1301389, **2014**.
[693]	Liu, Z.Q.; Feng, N.N.; Shen, Z.H.; Li, F.J.; He, P.; Zhang, H.G.; Zhou, H.S. Carbon-free O$_2$ cathode with three-dimensional ultralight nickel foam-supported ruthenium electrocatalysts for Li-O$_2$ batteries. *Chem. Sus. Chem. 10*, 2714-2719, **2017**.
[694]	Chang, Y.Q.; Dong, S.M.; Ju, Y.H.; Xiao, D.D.; Zhou, X.H.; Zhang, L.X.; Chen, X.; Shang, C.Q.; Gu, L.; Peng, Z.Q.; et al. A carbon - and binder - free nanostructured cathode for high-performance nonaqueous Li-O$_2$ battery. *Adv. Sci. 2*, 1500092, **2015**.
[695]	Lin, D.C.; Liu, Y.Y.; Cui, Y. Reviving the lithium metal anode for high-energy batteries. *Nat. Nanotechnol. 12*, 194-206, **2017**.
[696]	Sunu, W.G. Transient and failure analyses of the porous zinc electrode I. Theor. *J. Electrochem. Soc. 127*, 2007-2016, **1980**.

[697]	Einerhand, R.E.F.; Visscher, W.; Degoeij, J.J.M.; Barendrecht, E. Zinc electrode shape change II. Process and mechanism. *J. Electrochem. Soc. 138*, 7-17, **1991**.
[698]	Parker, J.F.; Chervin, C.N.; Nelson, E.S.; Rolison, D.R.; Long, J.W. Wiring zinc in three dimensions re-writes battery performance-dendrite-free cycling. *Energy Environ. Sci. 7*, 1117-1124, **2014**.
[699]	Parker, J.F.; Nelson, E.S.; Wattendorf, M.D.; Chervin, C.N.; Long, J.W.; Rolison, D.R. Retaining the 3D framework of zinc sponge anodes upon deep discharge in Zn-air cells. *ACS Appl. Mater. Interfaces 6*, 19471-19476, **2014**.
[700]	Parker, J.F.; Chervin, C.N.; Pala, I.R.; Machler, M.; Burz, M.F.; Long, J.W.; Rolison, D.R. Rechargeable nickel-3D zinc batteries: an energy-dense, safer alternative to lithium-ion. *Science 356*, 414-417, **2017**.
[701]	Kang, L.T.; Cui, M.W.; Jiang, F.Y.; Gao, Y.F.; Luo, H.J.; Liu, J.J.; Liang, W.; Zhi, C.Y. Nanoporous $CaCO_3$ coatings enabled uniform Zn stripping/plating for long-life zinc rechargeable aqueous batteries. *Adv. Energy Mater. 8*, 1801090, **2018**.
[702]	Wu, Y.T.; Zhang, Y.M.; Ma, Y.; Howe, J.D.; Yang, H.C.; Chen, P.; Aluri, S.; Liu, N.A. Ion-sieving carbon nanoshells for deeply rechargeable Zn-based aqueous batteries. *Adv. Energy Mater. 8*, 1802470, **2018**.
[703]	Zhao, K.N.; Wang, C.X.; Yu, Y.H.; Yan, M.Y.; Wei, Q.L.; He, P.; Dong, Y.F.; Zhang, Z.Y.; Wang, X.D.; Mai, L.Q. Ultrathin surface coating enables stabilized zinc metal anode. *Adv. Mater. Interfaces 5*, 7, **2018**.
[704]	Tao, H.S.; Tong, X.; Gan, L.; Zhang, S.Q.; Zhang, X.M.; Liu, X. Effect of adding various carbon additives to porous zinc anode in rechargeable hybrid aqueous battery. *J. Alloy. Compd. 658*, 119-124, **2016**.
[705]	Masri, M.N.; Mohamad, A.A. Effect of adding carbon black to a porous zinc anode in a zinc-air battery. *J. Electrochem. Soc. 160*, A715-A721, **2013**.
[706]	Lee, C.W.; Sathiyanarayanan, K.; Eom, S.W.; Kim, H.S.; Yun, M.S. Effect of additives on the electrochemical behaviour of zinc anodes for zinc/air fuel cells. *J. Power Sources 160*, 161-164, **2006**.
[707]	Feng, Z.B.; Yang, Z.H.; Huang, J.H.; Xie, X.E.; Zhang, Z. Influences of Zn-Sn-Alhydrotalcite additive on the electrochemical performances of ZnO for zinc-nickel secondary cells. *J. Electrochem. Soc. 161*, A1981-A1986, **2014**.
[708]	Yan, Z.; Wang, E.D.; Jiang, L.H.; Sun, G.Q. Superior cycling stability and high rate capability of three-dimensional Zn/Cu foam electrodes for zinc-based alkaline batteries. *RSC Adv. 5*, 83781-83787, **2015**.
[709]	Park, D.J.; Aremu, E.O.; Ryu, K.S. Bismuth oxide as an excellent anode additive for inhibiting dendrite formation in zinc-air secondary batteries. *Appl. Surf. Sci. 456*, 507-514, **2018**.
[710]	Zhou, Z.B.; Zhang, Y.M.; Chen, P.; Wu, Y.T.; Yang, H.C.; Ding, H.R.; Zhang, Y.; Wang, Z.Z.; Du, X.; Liu, N. Graphene oxide-modified zinc anode for rechargeable aqueous batteries. *Chem. Eng. Sci. 194*, 142-147, **2019**.
[711]	Stock, D.; Dongmo, S.; Walther, F.; Sann, J.; Janek, J.; Schroder, D. Homogeneous coating with an anion-exchange ionomer improves the cycling stability of secondary batteries with zinc anodes. *ACS Appl. Mater. Interfaces 10*, 8640-8648, **2018**.
[712]	Otani, T.; Fukunaka, Y.; Homma, T. Effect of lead and tin additives on surface morphology evolution of electrodeposited zinc. *Electrochim. Acta 242*, 364-372, **2017**.

[713]	Jo, Y.N.; Prasanna, K.; Kang, S.H.; Ilango, P.R.; Kim, H.S.; Eom, S.W.; Lee, C.W. The effects of mechanical alloying on the self-discharge and corrosion behavior in Zn-air batteries. *J. Ind. Eng. Chem. 53*, 247-252, **2017**.
[714]	Schmid, M.; Willert-Porada, M. Zinc particles coated with bismuth oxide based glasses as anode material for zinc-air batteries with improved electrical rechargeability. *Electrochim. Acta 260*, 246-253, **2018**.
[715]	Jo, Y.N.; Kang, S.H.; Prasanna, K.; Eom, S.W.; Lee, C.W. Shield effect of polyaniline between zinc active material and aqueous electrolyte in zinc-air batteries. *Appl. Surf. Sci. 422*, 406-412, **2017**.
[716]	Ma, J.L.; Wen, J.B.; Gao, J.W.; Li, Q.A. Performance of Al-1Mg-1Zn-0.1Ga-0.1Sn as anode for Al-air battery. *Electrochim. Acta 129*, 69-75, **2014**.
[717]	Ma, J.L.; Wen, J.B.; Zhu, H.X.; Li, Q.A. Electrochemical performances of Al-0.5Mg-0.1Sn-0.02In alloy in different solutions for Al-air battery. *J. Power Sources 293*, 592-598, **2015**.
[718]	Cheng, X.B.; Peng, H.J.; Huang, J.Q.; Wei, F.; Zhang, Q. Dendrite-free nanostructured anode: entrapment of lithium in a 3D fibrous matrix for ultra-stable lithium-sulfur batteries. *Small 10*, 4257-4263, **2014**.
[719]	Xu, W.; Wang, J.L.; Ding, F.; Chen, X.L.; Nasybutin, E.; Zhang, Y.H.; Zhang, J.G. Lithium metal anodes for rechargeable batteries. *Energy Environ. Sci. 7*, 513-537, **2014**.
[720]	Bruce, P.G.; Freunberger, S.A.; Hardwick, L.J.; Tarascon, J.M. Li-O_2 and Li-S batteries with high energy storage. *Nat. Mater. 11*, 19-29, **2012**.
[721]	Cheng, X.B.; Zhang, R.; Zhao, C.Z.; Zhang, Q. Toward safe lithium metal anode in rechargeable batteries: a review. *Chem. Rev. 117*, 10403-10473, **2017**.
[722]	Yang, S.; He, P.; Zhou, H. Research progresses on materials and electrode design towards key challenges of Li-air batteries. *Energy Storage Mater. 13*, 29-48, **2018**.
[723]	Grande, L.; Paillard, E.; Hassoun, J.; Park, J.B.; Lee, Y.J.; Sun, Y.K.; Passerini, S.; Scrosati, B. The lithium/air battery: still an emerging system or a practical reality? *Adv. Mater. 27*, 784-800, **2015**.
[724]	Assary, R.S.; Lu, J.; Du, P.; Luo, X.Y.; Zhang, X.Y.; Ren, Y.; Curtiss, L.A.; Amine, K. The effect of oxygen crossover on the anode of a Li-O_2 battery using an ether-based solvent: insights from experimental and computational studies. *Chem. Sus. Chem. 6*, 51-55, **2013**.
[725]	Geng, D.S.; Ding, N.; Hor, T.S.A.; Chien, S.W.; Liu, Z.L.; Wuu, D.; Sun, X.L.; Zong, Y. From lithium-oxygen to lithium-air batteries: challenges and opportunities. *Adv. Energy Mater. 6*, 1502164, **2016**.
[726]	Liang, Z.; Lin, D.C.; Zhao, J.; Lu, Z.D.; Liu, Y.Y.; Liu, C.; Lu, Y.Y.; Wang, H.T.; Yan, K.; Tao, X.Y.; et al. Composite lithium metal anode by melt infusion of lithium into a 3D conducting scaffold with lithiophilic coating. *Proc. Natl. Acad. Sci. U S A 113*, 2862-2867, **2016**.
[727]	Xiang, J.W.; Yuan, L.X.; Shen, Y.; Cheng, Z.X.; Yuan, K.; Guo, Z.Z.; Zhang, Y.; Chen, X.; Huang, Y.H. Improved rechargeability of lithium metal anode via controlling lithium-ion flux. *Adv. Energy Mater. 8*, 1802352, **2018**.
[728]	Zhang, R.; Cheng, X.B.; Zhao, C.Z.; Peng, H.J.; Shi, J.L.; Huang, J.Q.; Wang, J.F.; Wei, F.; Zhang, Q. Conductive nanostructured scaffolds render low local current density to inhibit lithium dendrite growth. *Adv. Mater. 28*, 2155-2162, **2016**.
[729]	Zhang, R.; Chen, X.; Shen, X.; Zhang, X.-Q.; Chen, X.-R.; Cheng, X.-B.; Yan, C.; Zhao, C.-Z.; Zhang, Q. Coralloid carbon fiber-based composite lithium anode for robust lithium metal batteries. *Joule 2*, 764-777, **2018**.

[730]	Song, H.; Deng, H.; Li, C.; Feng, N.; He, P.; Zhou, H. (2017). Advances in lithium-containing anodes of aprotic Li-O$_2$ batteries: challenges and strategies for improvements. *Small Methods 1*, 1700135, **2017**.
[731]	Hassoun, J.; Jung, H.G.; Lee, D.J.; Park, J.B.; Amine, K.; Sun, Y.K.; Scrosati, B. A metal-free, lithium-ion oxygen battery: a step forward to safety in lithium-air batteries. *Nano Lett. 12*, 5775-5779, **2012**.
[732]	Guo, Z.Y.; Dong, X.L.; Wang, Y.G.; Xia, Y.Y. A lithium air battery with a lithiated Al-carbon anode. *Chem. Commun. (Camb.) 51*, 676-678, **2015**.
[733]	Xu, R.; Zhang, X.Q.; Cheng, X.B.; Peng, H.J.; Zhao, C.Z.; Yan, C.; Huang, J.Q. Artificial soft-rigid protective layer for dendrite-free lithium metal anode. *Adv. Funct. Mater. 28*, 1705838, **2018**.
[734]	Liao, K.M.; Wu, S.C.; Mu, X.W.; Lu, Q.; Han, M.; He, P.; Shao, Z.; Zhou, H. Developing a ''water-defendable'' and ''dendrite-free'' lithium-metal anode using a simple and promising GeCl$_4$ pretreatment method. *Adv. Mater. 30*, 1705711, **2018**.
[735]	Yan, C.; Cheng, X.B.; Tian, Y.; Chen, X.; Zhang, X.Q.; Li, W.J.; Huang, J.Q.; Zhang, Q. Dual-layered film protected lithium metal anode to enable dendrite-free lithium deposition. *Adv. Mater. 30*, 1707629, **2018**.
[736]	Zhang, X.; Zhang, Q.M.; Wang, X.G.; Wang, C.Y.; Chen, Y.N.; Xie, Z.J.; Zhou, Z. An extremely simple method for protecting lithium anodes in Li-O$_2$ batteries. *Angew. Chem. Int. Ed. 57*, 12814-12818, **2018**.
[737]	Cheng, X.B.; Hou, T.Z.; Zhang, R.; Peng, H.J.; Zhao, C.Z.; Huang, J.Q.; Zhang, Q. (2016). Dendrite-free lithium deposition induced by uniformly distributed lithium ions for efficient lithium metal batteries. *Adv. Mater. 28*, 2888-2895, **2016**.
[738]	Guo, Z.Y.; Wang, F.M.; Li, Z.J.; Yang, Y.; Tamirat, A.G.; Qi, H.C.; Han, J.S.; Li, W.; Wang, L.; Feng, S.H. Lithiophilic Co/Co$_4$N nanoparticles embedded in hollow N-doped carbon nanocubes stabilizing lithium metal anodes for Li-air batteries. *J. Mater. Chem. A 6*, 22096-22105, **2018**.
[739]	Zhang, X.Q.; Cheng, X.B.; Zhang, Q. Advances in interfaces between Li metal anode and electrolyte. *Adv. Mater. Interfaces 5*, 1701097, **2018**.
[740]	McCulloch, W.D.; Ren, X.D.; Yu, M.Z.; Huang, Z.J.; Wu, Y.Y. Potassium-ion oxygen battery based on a high capacity antimony anode. *ACS Appl. Mater. Interfaces 7*, 26158-26166, **2015**.
[741]	Chi, S.S.; Qi, X.G.; Hu, Y.S.; Fan, L.Z. 3D flexible carbon felt host for highly stable sodium metal anodes. *Adv. Energy Mater. 8*, 1702764, **2018**.
[742]	Zhang, Y.M.; Liu, N. Nanostructured electrode materials for high-energy rechargeable Li, Na and Zn batteries. *Chem. Mater. 29*, 9589-9604, **2017**.
[743]	Sun, F.; Gao, R.; Zhou, D.; Osenberg, M.; Dong, K.; Kardjilov, N.; Hilger, A.; Markotter, H.; Bieker, P.M.; Liu, X.F.; et al. (2019). Revealing hidden facts of Li anode in cycled lithium oxygen batteries through X-ray and neutron tomography. *ACS Energy Lett. 4*, 306-316, **2019**.
[744]	Clark, S.; Latz, A.; Horstmann, B. Rational development of neutral aqueous electrolytes for zinc-air batteries. *Chem. Sus. Chem. 10*, 4735-4747, **2017**.
[745]	An, L.; Zhang, Z.Y.; Feng, J.R.; Lv, F.; Li, Y.X.; Wang, R.; Lu, M.; Gupta, R.B.; Xi, P.X.; Zhang, S. Heterostructure-promoted oxygen electrocatalysis enables rechargeable zinc-air battery with neutral aqueous electrolyte. *J. Am. Chem. Soc. 140*, 17624-17631, **2018**.
[746]	Xu, M.; Ivey, D.G.; Xie, Z.; Qu, W. Rechargeable Zn-air batteries: progress in electrolyte development and cell configuration advancement. *J. Power Sources 283*, 358-371, **2015**.

[747]	Manthiram, A.; Li, L.J. Hybrid and aqueous lithium-air batteries. *Adv. Energy Mater. 5*, 1401302, **2015**.
[748]	Hong, W.C.; Jia, Z.J.; Wang, B.G. Influence of cathodic overpotential and zincate concentration on zinc deposition in alkaline solution. *J. Appl. Electrochem. 46*, 1085-1090, **2016**.
[749]	Adler, T.C.; McLarnon, F.R.; Cairns, E.J. Low-zinc-solubility electrolytes for use in zinc/nickel oxide cells. *J. Electrochem. Soc. 140*, 289-294, **1993**.
[750]	Lee, J.; Hwang, B.; Park, M.S.; Kim, K. Improved reversibility of Zn anodes for rechargeable Zn-air batteries by using alkoxide and acetate ions. *Electrochim. Acta 199*, 164-171, **2016**.
[751]	Egan, D.R.; de Leon, C.P.; Wood, R.J.K.; Jones, R.L.; Stokes, K.R.; Walsh, F.C. Developments in electrode materials and electrolytes for aluminium-air batteries. *J. Power Sources 236*, 293-310, **2013**.
[752]	Liu, J.; Wang, D.P.; Zhang, D.Q.; Gao, L.X.; Lin, T. Synergistic effects of carboxymethyl cellulose and ZnO as alkaline electrolyte additives for aluminium anodes with a view towards Al-air batteries. *J. Power Sources 335*, 1-11, **2016**.
[753]	Grishina, E.; Gelman, D.; Belopukhov, S.; Starosvetsky, D.; Groysman, A.; Ein-Eli, Y. Improvement of aluminum-air battery performances by the application of flax straw extract. *Chem. Sus. Chem. 9*, 2103-2111, **2016**.
[754]	Eftekhari, A. High-energy aqueous lithium batteries. *Adv. Energy Mater. 8*, 1801156, **2018**.
[755]	Suo, L.M.; Borodin, O.; Gao, T.; Olguin, M.; Ho, J.; Fan, X.L.; Luo, C.; Wang, C.S.; Xu, K. ''Water-in-salt'' electrolyte enables high-voltage aqueous lithium-ion chemistries. *Science 350*, 938-943, **2015**.
[756]	Yamada, Y.; Usui, K.; Sodeyama, K.; Ko, S.; Tateyama, Y.; Yamada, A. Hydrate-melt electrolytes for high-energy-density aqueous batteries. *Nat. Energy 1*, 16129, **2016**.
[757]	Bryantsev, V.S.; Giordani, V.; Walker, W.; Blanco, M.; Zecevic, S.; Sasaki, K.,;Uddin, J.; Addison, D.; Chase, G.V. Predicting solvent stability in aprotic electrolyte Li-air batteries: nucleophilic substitution by the superoxide anion radical (O_2^{-}). *J. Phys. Chem. A 115*, 12399-12409, **2011**.
[758]	Younesi, R.; Veith, G.M.; Johansson, P.; Edstrom, K.; Vegge, T. Lithium salts for advanced lithium batteries: Li-metal, Li-O_2, and Li-S. *Energy Environ. Sci. 8*, 1905-1922, **2015**.
[759]	Du, P.; Lu, J.; Lau, K.C.; Luo, X.Y.; Bareno, J.; Zhang, X.Y.; Ren, Y.; Zhang, Z.C.; Curtiss, L.A.; Sun, Y.K., et al. Compatibility of lithium salts with solvent of the non-aqueous electrolyte in Li-O_2 batteries. *Phys. Chem. Chem. Phys. 15*, 5572-5581, **2013**.
[760]	Li, F.J.; Zhang, T.; Yamada, Y.; Yamada, A.; Zhou, H.S. Enhanced cycling performance of Li-O_2 batteries by the optimized electrolyte concentration of LiTFSA in glymes. *Adv. Energy Mater. 3*, 532-538, **2013**.
[761]	Luo, W.B.; Gao, X.W.; Chou, S.L.; Kang, Y.M.; Wang, J.Z.; Liu, H.K.; Dou, S.X. Investigation of promising air electrode for realizing ultimate lithium oxygen battery. *Adv. Energy Mater. 7*, 1700234, **2017**.
[762]	Aurbach, D.; McCloskey, B.D.; Nazar, L.F.; Bruce, P.G. Advances in understanding mechanisms underpinning lithium-air batteries. *Nat. Energy 1*, 16128, **2016**.
[763]	Feng, N.N.; He, P.; Zhou, H.S. Enabling catalytic oxidation of Li$_2$O$_2$ at the liquid-solid interface: the evolution of an aprotic Li-O_2 battery. *Chem. Sus. Chem 8*, 600-602, **2015**.
[764]	Xin, X.; Ito, K.; Dutta, A.; Kubo, Y. (2018). Dendrite-free epitaxial growth of lithium metal during charging in Li-O_2 batteries. *Angew. Chem. Int. Ed. 57*, 13206-13210, **2018**.

[765]	Gao, X.W.; Chen, Y.H.; Johnson, L.; Bruce, P.G. Promoting solution phase discharge in Li-O$_2$ batteries containing weakly solvating electrolyte solutions. *Nat. Mater. 15*, 882-888, **2016**.
[766]	Huang, Z.M.; Ren, J.; Zhang, W.; Xie, M.L.; Li, Y.K.; Sun, D.; Shen, Y.; Huang, Y.H. Protecting the Li-metal anode in a Li-O$_2$ battery by using boric acid as an SEI-forming additive. *Adv. Mater. 30*, 1803270, **2018**.
[767]	Zhang, H.; Eshetu, G.G.; Judez, X.; Li, C.M.; Rodriguez-Martinez, L.M.; Armand, M. Electrolyte additives for lithium metal anodes and rechargeable lithium metal batteries: progress and perspectives. *Angew. Chem. Int. Ed. 57*, 15002-15027, **2018**.
[768]	Shiga, T.; Kato, Y.; Hase, Y. Coupling of nitroxyl radical as an electrochemical charging catalyst and ionic liquid for calcium plating/stripping toward a rechargeable calcium-oxygen battery. *J. Mater. Chem. A 5*, 13212-13219, **2017**.
[769]	Thomas, M.L.; Oda, Y.; Tatara, R.; Kwon, H.M.; Ueno, K.; Dokko, K.; Watanabe, M. Suppression of water absorption by molecular design of ionic liquid electrolyte for Li-air battery. *Adv. Energy Mater. 7*, 1601753, **2017**.
[770]	Zhang, J.Q.; Sun, B.; Zhao, Y.F.; Tkacheva, A.; Liu, Z.J.; Yan, K.; Guo, X.; McDonagh, A.M.; Shanmukaraj, D.; Wang, C.Y.; et al. A versatile functionalized ionic liquid to boost the solution-mediated performances of lithium-oxygen batteries. *Nat. Commun. 10*, 602, **2019**.
[771]	Asadi, M.; Sayahpour, B.; Abbasi, P.; Ngo, A.T.; Karis, K.; Jokisaari, J.R.; Liu, C.; Narayanan, B.; Gerard, M.; Yasaei, P.; et al. (2018). A lithium-oxygen battery with a long cycle life in an air-like atmosphere. *Nature 555*, 502-507, **2018**.
[772]	Cheng, X.B.; Zhao, C.Z.; Yao, Y.X.; Liu, H.; Zhang, Q. Recent advances in energy chemistry between solid-state electrolyte and safe lithium-metal anodes. *Chem 5*, 74-96, **2019**.
[773]	Liu, Y.J.; He, P.; Zhou, H.S. Rechargeable solid-state Li-air and Li-S batteries: materials, construction, and challenges. *Adv. Energy Mater. 8*, 1701602, **2018**.
[774]	Cheng, X.L.; Pan, J.; Zhao, Y.; Liao, M.; Peng, H.S. (2018). Gel polymer electrolytes for electrochemical energy storage. *Adv. Energy Mater. 8*, 1702184, **2018**.
[775]	Li, Y.B.; Fu, J.; Zhong, C.; Wu, T.P.; Chen, Z.W.; Hu, W.B.; Amine, K.; Lu, J. Recent advances in flexible zinc-based rechargeable batteries. *Adv. Energy Mater. 9*, 1802605, **2019**.
[776]	Huang, Y.; Li, Z.; Pei, Z.X.; Liu, Z.X.; Li, H.F.; Zhu, M.S.; Fan, J.; Dai, Q.B.; Zhang, M.D.; Dai, L.M.; et al. Solid-state rechargeable Zn//NiCo and Zn-air batteries with ultralong lifetime and high capacity: the role of a sodium polyacrylate hydrogel electrolyte. *Adv. Energy Mater. 8*, 1802288, **2018**.
[777]	Lei, X.F.; Liu, X.Z.; Ma, W.Q.; Cao, Z.; Wang, Y.G.; Ding, Y. Flexible lithium-air battery in ambient air with an in situ formed gel electrolyte. *Angew. Chem. Int. Ed. 57*, 16131-16135, **2018**.
[778]	Zou, X.H.; Lu, Q.; Zhong, Y.J.; Liao, K.M.; Zhou, W.; Shao, Z.P. Flexible, flame-resistant, and dendrite-impermeable gel-polymer electrolyte for Li-O$_2$/air batteries workable under hurdle conditions. *Small 14*, 1801798, **2018**.
[779]	Balaish, M.; Peled, E.; Golodnitsky, D.; Ein-Eli, Y. Liquid-free lithium-oxygen batteries. *Angew. Chem. Int. Ed. 54*, 436-440, **2015**.
[780]	Liu, Y.J.; Li, C.; Li, B.J.; Song, H.C.; Cheng, Z.; Chen, M.R.; He, P.; Zhou, H.S. Germanium thin film protected lithium aluminum germanium phosphate for solid-state Li batteries. *Adv. Energy Mater. 8*, 1702374, **2018**.
[781]	Fan, L.; Wei, S.Y.; Li, S.Y.; Li, Q.; Lu, Y.Y. Recent progress of the solid-state electrolytes for high-energy metal-based batteries. *Adv. Energy Mater. 8*, 1702657, **2018**.

[782]	Wang, J.; Yin, Y.B.; Liu, T.; Yang, X.Y.; Chang, Z.W.; Zhang, X.B. Hybrid electrolyte with robust garnet-ceramic electrolyte for lithium anode protection in lithium-oxygen batteries. *Nano Res. 11*, 3434-3441, **2018**.
[783]	Arora, P.; Zhang, Z.M. Battery separators. *Chem. Rev. 104*, 4419-4462, **2004**.
[784]	Fujiwara, N.; Yao, M.; Siroma, Z.; Senoh, H.; Ioroi, T.; Yasuda, K. Reversible air electrodes integrated with an anion-exchange membrane for secondary air batteries. *J. Power Sources 196*, 808-813, **2011**.
[785]	Stock, D.; Dongmo, S.; Miyazaki, K.; Abe, T.; Janek, J.; Schroder, D. Towards zinc-oxygen batteries with enhanced cycling stability: the benefit of anion-exchange ionomer for zinc sponge anodes. *J. Power Sources 395*, 195-204, **2018**.
[786]	Hwang, H.J.; Chi, W.S.; Kwon, O.; Lee, J.G.; Kim, J.H.; Shul, Y.G. Selective ion transporting polymerized ionic liquid membrane separator for enhancing cycle stability and durability in secondary zinc-air battery systems. *ACS Appl. Mater. Interfaces 8*, 26298-26308, **2016**.
[787]	Kim, H.W.; Lim, J.M.; Lee, H.J.; Eom, S.W.; Hong, Y.T.; Lee, S.Y. Artificially engineered, bicontinuous anion-conducting/-repelling polymeric phases as a selective ion transport channel for rechargeable zinc-air battery separator membranes. *J. Mater. Chem. A 4*, 3711-3720, **2016**.
[788]	Qiao, Y.; He, Y.B.; Wu, S.C.; Jiang, K.Z.; Li, X.; Guo, S.H.; He, P.; Zhou, H.S. MOF-based separator in an Li-O$_2$ battery: an effective strategy to restrain the shuttling of dual redox mediators. *ACS Energy Lett. 3*, 463-468, **2018**.
[789]	Lee, S.H.; Park, J.B.; Lim, H.S.; Sun, Y.K. An advanced separator for Li-O$_2$ batteries: Maximizing the effect of redox mediators. *Adv. Energy Mater. 7*, 1602417, **2017**.
[790]	Liu, Y.D.; Liu, Q.; Xin, L.; Liu, Y.Z.; Yang, F.; Stach, E.A.; Xie, J. Making Li-metal electrodes rechargeable by controlling the dendrite growth direction. *Nat. Energy 2*, 17083, **2017**.
[791]	Hao-Fan, Wang; Qiang, Xu. Materials Design for Rechargeable Metal-Air Batteries. Cell Press Reviews. *Matter 1*, 565-595, **2019**. https://doi.org/10.1016/j.matt.2019.05.008.
[792]	Sayilgan, E.; Kukrer, T.; Civelekoglu, G.; Ferella, F.; Akcil, A.; Veglio, F.; Kitis, M. Hydrometallurgy A review of technologies for the recovery of metals from spent alkaline and zinc – carbon batteries. *Hydrometallurgy 97*, 158-166, **2009**. https://doi.org/10.1016/j.hydromet.2009.02.008.
[793]	Tanong, K.; Tran, L.; Mercier, G.; Blais, J. Recovery of Zn (II), Mn (II), Cd (II) and Ni (II) from the unsorted spent batteries using solvent extraction, electrodeposition and precipitation methods. *J. Clean. Prod. 148*, 233-244, **2017**. https://doi.org/10.1016/j.jclepro.2017.01.158.
[794]	Buzatu, M.; Săceanu, S.; Petrescu, M.I.; Ghica, G.V.; Buzatu, T. Recovery of zinc and manganese from spent batteries by reductive leaching in acidic media. *J. Power Sources 247*, 612-617, **2014**. https://doi.org/10.1016/j.jpowsour.2013.09.001.
[795]	Abid Charef, S.; Affoune, A.M.; Caballero, A.; Cruz-Yusta, M.; Morales, J. Simultaneous recovery of Zn and Mn from used batteries in acidic and alkaline mediums: A comparative study. *Waste Manage. 68*, 518-526, **2017**. https://doi.org/10.1016/j.wasman.2017.06.048.
[796]	Shin, S.; Kang, J.; Yang, D.; Kim, T.; Sohn, J. Comparison of Acid and Alkaline Leaching for Recovery of Valuable Metals from Spent Zinc-carbon Battery. *Geosyst. Eng. 10*, 21-26, **2007**. https://doi.org/10.1080/12269328.2007.10541267.
[797]	Nogueira, C.A.; Margarido, F. Hydrometallurgy Selective process of zinc extraction from spent Zn – MnO$_2$ batteries by ammonium chloride leaching. *Hydrometallurgy 157*, 13-21, **2015**. https://doi.org/10.1016/j.hydromet.2015.07.004.

[798]	Kim, T.-H.; Kang, J.-G.; Sohn, J.; Rhee, K.-I.; Lee, S.-W.; Shin, S.M. Preparation of Mn-Zn Ferrite from Spent Zinc-Carbon Batteries by Alkali Leaching, Acid Leaching and Co-Precipitation. *Met. Mater. Int. 14*, 655-658, **2008**. https://doi.org/10.3365/met.mat.2008.10.655.
[799]	Shin, S.M.; Senanayake, G.; Sohn, J.; Kang, J. Hydrometallurgy Separation of zinc from spent zinc-carbon batteries by selective leaching with sodium hydroxide. *Hydrometallurgy 96*, 349-353, **2009**. https://doi.org/10.1016/j.hydromet.2008.12.010.
[800]	Sadeghi, S.M.; Vanpeteghem, G.; Neto, I.F.F.; Soares, H.M.V.M. Selective leaching of Zn from spent alkaline batteries using environmentally friendly approaches. *Waste Manag. 60*, 696-705, **2017**. https://doi.org/10.1016/j.wasman.2016.12.002.
[801]	Buzatu, T.; Popescu, G.; Birloaga, I.; Sa, S. Study concerning the recovery of zinc and manganese from spent batteries by hydrometallurgical processes. *Waste Manag. 33*, 699-705, **2013**. https://doi.org/10.1016/j.wasman.2012.10.005.
[802]	Senanayake, G.; Shin, S.; Senaputra, A.; Winn, A.; Pugaev, D.; Avraamides, J.; Sohn, J.; Kim, D. Hydrometallurgy Comparative leaching of spent zinc-manganese-carbon batteries using sulfur dioxide in ammoniacal and sulfuric acid solutions. *Hydrometallurgy 105*, 36-41, **2010**. https://doi.org/10.1016/j.hydromet.2010.07.004.
[803]	Ferella, F.; De Michelis, I.; Vegliò, F. Process for the recycling of alkaline and zinc-carbon spent batteries. *J. Power Sources 183*, 805-811, **2008**. https://doi.org/10.1016/j.jpowsour.2008.05.043.
[804]	Deep, A., Kumar, K., Kumar, Parveen, Kumar, Pawan, Sharma, A.L., Gupta, B., Bharadwaj, L.M. Recovery of Pure ZnO Nanoparticles from Spent Zn-MnO_2 Alkaline Batteries. *Environ. Sci. Technol. 45*, 10551-10556, **2011**. https://doi.org/10.1021/es201744t.
[805]	Kursunoglu, S.; Kaya, M. Recovery of manganese from spent batteries using guar meal as a reducing agent in a sulfuric acid medium. *Ind. Eng. Chem. Res. 52*, 18076-18084, **2013**. https://doi.org/10.1021/ie401682f.
[806]	Chen, W.; Liao, C.; Lin, K. Recovery Zinc and Manganese from Spent Battery Powder by Hydrometallurgical Route. Energy Procedia 107, 167-174, **2017**. https://doi.org/10.1016/j.egypro.2016.12.162.
[807]	Kursunoglu, S.; Kaya, M. Dissolution and precipitation of zinc and manganese obtained from spent zinc-carbon and alkaline battery powder. *Physicochem. Probl. Miner. Process. 50*, 41-55, **2014**. https://doi.org/10.5277/ppmp140104.
[808]	Ferella, F.; De Michelis, I.; Beolchini, F.; Innocenzi, V.; Vegliò, F. Extraction of zinc and manganese from alkaline and zinc-carbon spent batteries by citric-sulphuric acid solution. *Int. J. Chem. Eng. 2010*, **2010**. https://doi.org/10.1155/2010/659434.
[809]	Biswas, R.K.; Karmakar, A.K.; Kumar, S.L.; Hossain, M.N. Recovery of manganese and zinc from waste Zn-C cell powder: Characterization and leaching. *Waste Manag. 46*, 529-535, **2015**. https://doi.org/10.1016/j.wasman.2015.09.008.
[810]	Lannoo, S.; Vilas-boas, A.; Sadeghi, S.M.; Jesus, J.; Soares, H.M.V.M. An environmentally friendly closed loop process to recycle raw materials from spent alkaline batteries. *J. Clean. Prod. 236*, **2019**. https://doi.org/10.1016/j.jclepro.2019.117612117612.
[811]	Ibiapinaa, V.F.; Afonso, J.C.; Silva, R.S.; Cláudio Augusto, V.; Mantovano, J.L. Separation of zinc from mangannes by solvent extraction from acidic leachates of spent zinc-MnO_2 dry cells using neutral organophosphorus extractants. *Quim Nov. 41*, 770-777, **2018**. https://doi.org/10.21577/0100-4042.20170249.

[812]	De Michelis, I.; Ferella, F.; Karakaya, E.; Beolchini, F.; Vegliò, F. Recovery of zinc and manganese from alkaline and zinc-carbon spent batteries. *J. Power Sources 172*, 975-983, **2007**. https://doi.org/10.1016/j.jpowsour.2007.04.092.
[813]	Furlani, G.; Moscardini, E.; Pagnanelli, F.; Ferella, F.; Vegliò, F.; Toro, L. Hydrometallurgy Recovery of manganese from zinc alkaline batteries by reductive acid leaching using carbohydrates as reductant. *Hydrometallurgy 99*, 115-118, **2009**. https://doi.org/10.1016/j.hydromet.2009.07.005.
[814]	Maryam Sadeghi, S.; Jesus, J.; Soares, M.V.M., Helena. A critical updated review of the hydrometallurgical routes for recycling zinc and manganese from spent zinc-based batteries. *Waste Management* 113, 342-350, **2020**. https://doi.org/10.1016/j.wasman.2020.05.049.
[815]	T., Zhou; N., Zhang; C., Wu; Y., Xie. Surface/interface nanoengineering for rechargeable Zn-air batteries. *Energy Environ. Sci. 13*, 1132-1153, **2020**.
[816]	J.-C., Dong; X.-G., Zhang; V., Briega-Martos; X., Jin; J., Yang; S., Chen; Z.-L., Yang; D.-Y., Wu; J.M., Feliu; C.T., Williams; Z.-Q., Tian; J.-F., Li. In situ Raman Spectroscopic Evidence for Oxygen Reduction Reaction Intermediates at Platinum Single-crystal Surfaces. *Nat. Energy 4*, 60-67, **2018**.
[817]	D. Gohl, A. Garg, P. Paciok, K.J.J. Mayrhofer, M. Heggen, Y. Shao-Horn, R. E. Dunin-Borkowski, Y. Roman-Leshkov, M. Ledendecker. Engineering stable electrocatalysts by synergistic stabilization between carbide cores and Pt shells. *Nat. Mater. 19*, 287-291, **2020**.
[818]	G.W. Sievers, A.W. Jensen, J. Quinson, A. Zana, F. Bizzotto, M. Oezaslan, A. Dworzak, J.J.K. Kirkensgaard, T.E.L. Smitshuysen, S. Kadkhodazadeh, M. Juelsholt, K.M.O. Jensen, K. Anklam, H. Wan, J. Schafer, K. Cepe, M. Escudero-Escribano, J. Rossmeisl, A. Quade, V. Bruser, M. Arenz. Self-supported Pt-CoO networks combining high specific activity with high surface area for oxygen reduction. *Nat. Mater. 20*, 208-213, **2021**.
[819]	M. Karuppannan, Y. Kim, S. Gok, E. Lee, J.Y. Hwang, J.-H. Jang, Y.-H. Cho, T. Lim, Y.-E. Sung, O.J. Kwon. A highly durable carbon-nanofiber-supported Pt-C core-shell cathode catalyst for ultra-low Pt loading proton exchange membrane fuel cells: facile carbon encapsulation. *Energy Environ. Sci. 12*, 2820-2829, **2019**.
[820]	J. Zhang, J. Zhang, F. He, Y. Chen, J. Zhu, D. Wang, S. Mu, H.Y. Yang. Defect and doping Co-engineered non-metal nanocarbon ORR electrocatalyst. *Nano-Micro Lett. 13*, 65, **2021**.
[821]	H. Cui, M. Jiao, Y.-N. Chen, Y. Guo, L. Yang, Z. Xie, Z. Zhou, S. Guo. Molten-salt-assisted synthesis of 3D holey N-doped graphene as bifunctional electrocatalysts for rechargeable Zn-Air batteries. *Small Methods 2*, 1800144, **2018**.
[822]	J. Luo, K. Wang, X. Hua, W. Wang, J. Li, S. Zhang, S. Chen. Pyridinic-N protected synthesis of 3D nitrogen-doped porous carbon with increased mesoporous defects for oxygen reduction. *Small 15*, 1805325, **2019**.
[823]	Z. Wu, Y. Yu, G. Zhang, Y. Zhang, R. Guo, L. Li, Y. Zhao, Z. Wang, Y. Shen, G. Shao. In situ monitored (N, O)-Doping of Flexible Vertical Graphene Films with High-flux Plasma Enhanced Chemical Vapor Deposition for Remarkable Metal-free Redox Catalysis Essential to Alkaline Zinc-air Batteries. *Adv. Sci. 9*, 2200614, **2022**.
[824]	L. Li, A. Manthiram. O- and N-doped carbon nanowebs as metal-free catalysts for hybrid Li-air batteries. *Adv. Energy Mater. 4*, 1301795, **2014**.
[825]	H. Tabassum, R. Zou, A. Mahmood, Z. Liang, S. Guo. A. Catalyst-free, Synthesis of B, N co-doped graphene nanostructures with tunable dimensions as highly efficient metal free dual electrocatalysts, *J. Mater. Chem. A 4*, 16469-16475, **2016**.

[826] P. Wei, X. Li, Z. He, X. Sun, Q. Liang, Z. Wang, C. Fang, Q. Li, H. Yang, J. Han, Y. Huang. Porous N, B co-doped carbon nanotubes as efficient metal-free electrocatalysts for ORR and Zn-air batteries. *Chem. Eng. J. 422*, 130134, **2021**.

[827] Z. Xing, R. Jin, X. Chen, B. Chen, J. Zhou, B. Tian, Y. Li, D. Fan. Self-templating construction of N, P-co-doped carbon nanosheets for efficient electrocatalytic oxygen reduction reaction. *Chem. Eng. J. 410*, 128015, **2021**.

[828] G.-L. Chai, K. Qiu, M. Qiao, M.-M. Titirici, C. Shang, Z. Guo. Active sites engineering leads to exceptional ORR and OER bifunctionality in P,N Co-doped graphene frameworks. *Energy Environ. Sci. 10*, 1186-1195, **2017**.

[829] X. Zheng, J. Wu, X. Cao, J. Abbott, C. Jin, H. Wang, P. Strasser, R. Yang, X. Chen, G. Wu. N-, P-, and S-doped graphene-like carbon catalysts derived from onium salts with enhanced oxygen chemisorption for Zn-air battery cathodes. *Appl. Catal. B 241*, 442-451, **2019**.

[830] J. Zhu, W. Li, S. Li, J. Zhang, H. Zhou, C. Zhang, J. Zhang, S. Mu. Defective N/S-codoped 3D cheese-like porous carbon nanomaterial toward efficient oxygen reduction and Zn-Air batteries. *Small 14*, 1800563, **2018**.

[831] Y.-N. Sun, J. Yang, X. Ding, W. Ji, A. Jaworski, N. Hedin, B.-H. Han. Synergetic contribution of nitrogen and fluorine species in porous carbons as metal-free and bifunctional oxygen electrocatalysts for zinc-air batteries. *Appl. Catal., B 297*, 120448, **2021**.

[832] J.-P. Zhong, C. Hou, M.-L. Sun, Z.-Y. Yang, D.H. Chen, Y.-J. Fan, W. Chen, H.- G. Liao, S.-G. Sun. A superior electrocatalyst toward oxygen reduction reaction by atomically dispersed copper on N, F co-doped graphene through atomic interface engineering. *J. Mater. Chem. A 10*, 13876-13883, **2022**.

[833] Z. Zhu, H. Yin, Y. Wang, C.H. Chuang, L. Xing, M. Dong, Y.R. Lu, G. Casillas-Garcia, Y. Zheng, S. Chen, Y. Dou, P. Liu, Q. Cheng, H. Zhao. Coexisting single-atomic Fe and Ni sites on hierarchically ordered porous carbon as a highly efficient ORR electrocatalyst. *Adv. Mater. 32*, 2004670, **2020**.

[834] X. Xie, L. Peng, H. Yang, G.I.N. Waterhouse, L. Shang, T. Zhang. MIL-101-derived mesoporous carbon supporting highly exposed Fe single-atom sites as efficient oxygen reduction reaction catalysts. *Adv. Mater. 33*, 2101038, **2021**.

[835] Y. Chen, R. Gao, S. Ji, H. Li, K. Tang, P. Jiang, H. Hu, Z. Zhang, H. Hao, Q. Qu, X. Liang, W. Chen, J. Dong, D. Wang, Y. Li. Atomic-level modulation of electronic density at cobalt single-atom sites derived from metal-organic frameworks: enhanced oxygen reduction performance. *Angew. Chem. Int. Ed. 60*, 3212-3221, **2021**.

[836] Q. Yang, Y. Jia, F. Wei, L. Zhuang, D. Yang, J. Liu, X. Wang, S. Lin, P. Yuan, X. Yao. Understanding the activity of Co-N4–xCx in atomic metal catalysts for oxygen reduction catalysis. *Angew. Chem. Int. Ed. 59*, 6122-6127, **2020**.

[837] J. Li, M. Chen, D.A. Cullen, S. Hwang, M. Wang, B. Li, K. Liu, S. Karakalos, M. Lucero, H. Zhang, C. Lei, H. Xu, G.E. Sterbinsky, Z. Feng, D. Su, K.L. More, G. Wang, Z. Wang, G. Wu. Atomically dispersed manganese catalysts for oxygen reduction in proton-exchange membrane fuel cells. *Nat. Catal. 1*, 935-945, **2018**.

[838] X. Han, T.Y. Zhang, W.X. Chen, B. Dong, G. Meng, L.R. Zheng, C. Yang, X.M. Sun, Z.B. Zhuang, D.S. Wang, A.J. Han, J.F. Liu. Mn-N4 oxygen reduction electrocatalyst: operando investigation of active sites and high performance in zinc-air battery. *Adv. Energy Mater. 11*, 2002753, **2021**.

[839] B. Li, H. Nam, J. Zhao, J. Chang, N. Lingappan, F. Yao, T.H. Lee, Y.H. Lee. Nanoreactor of nickel-containing carbon-shells as oxygen reduction catalyst. *Adv. Mater. 29*, 1605083, **2017**.

[840]	F. Luo, J. Zhu, S. Ma, M. Li, R. Xu, Q. Zhang, Z. Yang, K. Qu, W. Cai, Z. Chen. Regulated coordination environment of Ni single atom catalyst toward high-efficiency oxygen electrocatalysis for rechargeable zinc-air batteries. *Energy Storage Mater. 35*, 723-730, **2021**.
[841]	A.A. Gewirth, J.A. Varnell, A.M. DiAscro. Nonprecious metal catalysts for oxygen reduction in heterogeneous aqueous systems. *Chem. Rev. 118*, 2313-2339, **2018**.
[842]	Y. He, S. Liu, C. Priest, Q. Shi, G. Wu. Atomically dispersed metal-nitrogen-carbon catalysts for fuel cells: advances in catalyst design, electrode performance, and durability improvement. *Chem. Soc. Rev. 49*, 3484-3524, **2020**.
[843]	Y. Shao, J.P. Dodelet, G. Wu, P. Zelenay. PGM-free cathode catalysts for PEM fuel cells: a mini-review on stability challenges. Adv. Mater. 31, 1807615, **2019**.
[844]	W. Huang, J. Li, X. Liao, R. Lu, C. Ling, X. Liu, J. Meng, L. Qu, M. Lin, X. Hong, X. Zhou, S. Liu, Y. Zhao, L. Zhou, L. Mai. Ligand modulation of active sites to promote electrocatalytic oxygen evolution. *Adv. Mater. 34*, 2200270, **2022**.
[845]	X.P. Wang, H.J. Wu, S.B. Xi, W.S.V. Lee, J. Zhang, Z.H. Wu, J.O. Wang, T.D. Hu, L. M. Liu, Y. Han, S.W. Chee, S.C. Ning, U. Mirsaidov, Z.B. Wang, Y.W. Zhang, A. Borgna, J. Wang, Y.H. Du, Z.G. Yu, S.J. Pennycook, J.M. Xue. Strain stabilized nickel hydroxide nanoribbons for efficient water splitting. *Energy Environ. Sci. 13*, 229-237, **2020**.
[846]	F. Li, J. Du, X. Li, J. Shen, Y. Wang, Y. Zhu, L. Sun. Integration of FeOOH and zeolitic imidazolate framework-derived nanoporous carbon as an efficient electrocatalyst for water oxidation. *Adv. Energy Mater. 8*, 1702598, **2018**.
[847]	K. Wang, H. Du, S. He, L. Liu, K. Yang, J. Sun, Y. Liu, Z. Du, L. Xie, W. Ai, W. Huang. Kinetically controlled, scalable synthesis of gamma-FeOOH nanosheet arrays on nickel foam toward efficient oxygen evolution: the key role of in-situ-generated gamma-NiOOH. *Adv. Mater. 33*, 2005587, **2021**.
[848]	W. Luo, C. Jiang, Y. Li, S.A. Shevlin, X. Han, K. Qiu, Y. Cheng, Z. Guo, W. Huang, J. Tang. Highly crystallized α-FeOOH for a stable and efficient oxygen evolution reaction. *J. Mater. Chem. A 5*, 2021-2028, **2017**.
[849]	L.-F. Li, Y.-F. Li, Z.-P. Liu. Oxygen evolution activity on NiOOH catalysts: four-coordinated Ni cation as the active site and the hydroperoxide mechanism. *ACS Catal. 10*, 2581-2590, **2020**.
[850]	H.-Y. Wang, Y.-Y. Hsu, R. Chen, T.-S. Chan, H.M. Chen, B. Liu. Ni^{3+}-induced formation of active NiOOH on the spinel Ni-Co oxide surface for efficient oxygen evolution reaction. *Adv. Energy Mater. 5*, 1500091, **2015**.
[851]	C. Kuai, Y. Zhang, L. Han, H.L. Xin, C.-J. Sun, D. Nordlund, S. Qiao, X.-W. Du, F. Lin. Creating compressive stress at the NiOOH/NiO interface for water oxidation. *J. Mater. Chem. A 8*, 10747-10754, **2020**.
[852]	J. Chen, F. Zheng, S.-J. Zhang, A. Fisher, Y. Zhou, Z. Wang, Y. Li, B.-B. Xu, J.-T. Li, S.-G. Sun. Interfacial interaction between FeOOH and Ni-Fe LDH to modulate the local electronic structure for enhanced OER electrocatalysis. *ACS Catal. 8*, 11342-11351, **2018**.
[853]	S. Ye, J. Wang, J. Hu, Z. Chen, L. Zheng, Y. Fu, Y. Lei, X. Ren, C. He, Q. Zhang, J. Liu. Electrochemical construction of low-crystalline CoOOH nanosheets with short-range ordered grains to improve oxygen evolution activity. *ACS Catal. 11*, 6104-6112, **2021**.
[854]	H. Wang, E.-m Feng, Y.-m Liu, C.-y Zhang. High-performance hierarchical ultrathin sheet-based CoOOH hollow nanospheres with rich oxygen vacancies for the oxygen evolution reaction. *J. Mater. Chem. A 7*, 7777-7783, **2019**.

[855] X. Zheng, Y. Cao, Z. Wu, W. Ding, T. Xue, J. Wang, Z. Chen, X. Han, Y. Deng, W. Hu. Rational design and spontaneous sulfurization of NiCo-(oxy) hydroxysulfides nanosheets with modulated local electronic configuration for enhancing oxygen electrocatalysis. *Adv. Energy Mater. 12*, 2103275, **2022**.

[856] F. Meng, H. Zhong, D. Bao, J. Yan, X. Zhang. In situ coupling of strung Co_4N and intertwined N-C fibers toward free-standing bifunctional cathode for robust, efficient, and flexible Zn-air batteries. *J. Am. Chem. Soc. 138*, 10226-10231, **2016**.

[857] Y. Niu, X. Teng, S. Gong, M. Xu, S.G. Sun, Z. Chen. Engineering two-phase bifunctional oxygen electrocatalysts with tunable and synergetic components for flexible Zn-Air batteries. *Nano-Micro Lett. 13*, 126, **2021**.

[858] P. Liu, J. Ran, B. Xia, S. Xi, D. Gao, J. Wang. Bifunctional oxygen electrocatalyst of mesoporous Ni/NiO nanosheets for flexible rechargeable Zn-air batteries. *Nano-Micro Lett. 12*, 68, **2020**.

[859] P. Liu, D. Gao, W. Xiao, L. Ma, K. Sun, P. Xi, D. Xue, J. Wang. Self-powered water-splitting devices by core-shell NiFe@N-graphite-based Zn-air batteries. *Adv. Funct. Mater. 28*, 1706928, **2018**.

[860] C. Tang, B. Wang, H.F. Wang, Q. Zhang. Defect Engineering toward Atomic Co-Nx-C in Hierarchical Graphene for Rechargeable Flexible Solid Zn-Air Batteries. *Adv. Mater. 29*, 1703185, **2017**.

[861] H. Xu, D. Wang, P. Yang, L. Du, X. Lu, R. Li, L. Liu, J. Zhang, M. An. A hierarchically porous Fe-N-C synthesized by dual melt-salt-mediated template as advanced electrocatalyst for efficient oxygen reduction in zinc-air battery. *Appl. Catal., B 305*, 121040, **2022**.

[862] H. Zhang, M. Zhao, H. Liu, S. Shi, Z. Wang, B. Zhang, L. Song, J. Shang, Y. Yang, C. Ma, L. Zheng, Y. Han, W. Huang. Ultrastable FeCo bifunctional electrocatalyst on Se-doped CNTs for liquid and flexible all-solid-state rechargeable Zn-air batteries. *Nano Lett. 21*, 2255-2264, **2021**.

[863] Y. He, X. Yang, Y. Li, L. Liu, S. Guo, C. Shu, F. Liu, Y. Liu, Q. Tan, G. Wu. Atomically dispersed Fe-Co dual metal sites as bifunctional oxygen electrocatalysts for rechargeable and flexible Zn-Air batteries. *ACS Catal. 12*, 1216-1227, **2022**.

[864] Q. Lu, H. Wu, X. Zheng, Y. Chen, A.L. Rogach, X. Han, Y. Deng, W. Hu. Encapsulating cobalt nanoparticles in interconnected N-doped hollow carbon nanofibers with enriched CoNC moiety for enhanced oxygen electrocatalysis in Zn-air batteries. *Adv. Sci. 8*, 2101438, **2021**.

[865] X. Cui, W. Li, P. Ryabchuk, K. Junge, M. Beller. Bridging homogeneous and heterogeneous catalysis by heterogeneous single-metal-site catalysts. *Nat. Catal. 1*, 385-397, **2018**.

[866] Y. Chen, S. Ji, C. Chen, Q. Peng, D. Wang, Y. Li. Single-atom catalysts: synthetic strategies and electrochemical applications. *Joule 2*, 1242-1264, **2018**.

[867] X. He, Y. Deng, Y. Zhang, Q. He, D. Xiao, M. Peng, Y. Zhao, H. Zhang, R. Luo, T. Gan, H. Ji, D. Ma. Mechanochemical kilogram-scale synthesis of noble metal single-atom catalysts. *Cell Rep. Phys. Sci. 1*, 100004, **2020**.

[868] X. Hai, S. Xi, S. Mitchell, K. Harrath, H. Xu, D.F. Akl, D. Kong, J. Li, Z. Li, T. Sun, H. Yang, Y. Cui, C. Su, X. Zhao, J. Li, J. Perez-Ramirez, J. Lu. Scalable two-step annealing method for preparing ultra-high-density single-atom catalyst libraries. *Nat. Nanotechnol. 17*, 174-181, **2022**.

[869] T. Liu, S. Zhao, Y. Wang, J. Yu, Y. Dai, J. Wang, X. Sun, K. Liu, M. Ni. In situ anchoring Co-N-C nanoparticles on Co_4N nanosheets toward ultrastable flexible self-supported bifunctional oxygen electrocatalyst enables recyclable Zn-air batteries over 10 000 cycles and fast charging. *Small 18*, 2105887, **2021**.

[870]	X. Guo, T. Zheng, G. Ji, N. Hu, C. Xu, Y. Zhang. Core/shell design of efficient electrocatalysts based on $NiCo_2O_4$ nanowires and NiMn LDH nanosheets for rechargeable zinc-air batteries. *J. Mater. Chem. A 6*, 10243-10252, **2018**.
[871]	N. Xu, J.A. Wilson, Y.-D. Wang, T. Su, Y. Wei, J. Qiao, X.-D. Zhou, Y. Zhang, S. Sun. Flexible self-supported Bi-metal electrode as a highly stable carbon- and binder-free cathode for large-scale solid-state zinc-air batteries. *Appl. Catal. B 272*, 118953, **2020**.
[872]	M. Cui, X. Bai, J. Zhu, C. Han, Y. Huang, L. Kang, C. Zhi, H. Li. Electrochemically induced $NiCoSe_2$@NiOOH/CoOOH heterostructures as multifunctional cathode materials for flexible hybrid Zn batteries. *Energy Storage Mater. 36*, 427-434, **2021**.
[873]	Z. Zhao, Z. Yuan, Z. Fang, J. Jian, J. Li, M. Yang, C. Mo, Y. Zhang, X. Hu, P. Li, S. Wang, W. Hong, Z. Zheng, G. Ouyang, X. Chen, D. Yu. In situ activating strategy to significantly boost oxygen electrocatalysis of commercial carbon cloth for flexible and rechargeable Zn-Air batteries. *Adv. Sci. 5*, 1800760, **2018**.
[874]	H. Zhang, T. Wang, A. Sumboja, W. Zang, J. Xie, D. Gao, S.J. Pennycook, Z. Liu, C. Guan, J. Wang. Integrated hierarchical carbon flake arrays with hollow P-Doped $CoSe_2$ nanoclusters as an advanced bifunctional catalyst for Zn-Air batteries. *Adv. Funct. Mater. 28*, 1804846, **2018**.
[875]	B.-Q. Li, S.-Y. Zhang, B. Wang, Z.-J. Xia, C. Tang, Q. Zhang. A porphyrin covalent organic framework cathode for flexible Zn-air batteries. *Energy Environ. Sci. 11*, 1723-1729, **2018**.
[876]	C. Guan, A. Sumboja, H. Wu, W. Ren, X. Liu, H. Zhang, Z. Liu, C. Cheng, S. J. Pennycook, J. Wang. Hollow Co_3O_4 nanosphere embedded in carbon arrays for stable and flexible solid-state zinc-air batteries. *Adv. Mater. 29*, 1704117, **2017**.
[877]	K. Wu, L. Zhang, Y. Yuan, L. Zhong, Z. Chen, X. Chi, H. Lu, Z. Chen, R. Zou, T. Li, C. Jiang, Y. Chen, X. Peng, J. Lu. An iron-decorated carbon aerogel for rechargeable flow and flexible Zn-Air batteries. *Adv. Mater. 32*, 2002292, **2020**.
[878]	D.U. Lee, J.-Y. Choi, K. Feng, H.W. Park, Z. Chen. Advanced extremely durable 3D bifunctional air electrodes for rechargeable zinc-air batteries. *Adv. Energy Mater. 4*, 1301389, **2014**.
[879]	J. Jian, P. Nie, Z. Wang, Y. Qiao, H. Wang, C. Zhang, X. Xue, L. Fang, L. Chang. V^{-5+}-doped potassium ferrite as an efficient trifunctional catalyst for large-current-density water splitting and long-life rechargeable Zn-air battery. *ACS Appl. Mater. Interfaces 14*, 36721-36730, **2022**.
[880]	X. Cai, T. Jiang, M. Wu. Confined growth of NiFe LDH with hierarchical structures on copper nanowires for long-term stable rechargeable Zn-air batteries. *Appl. Surf. Sci. 577*, 151911, **2022**.
[881]	S.S. Shinde, C.H. Lee, J.-Y. Yu, D.-H. Kim, S.U. Lee, J.-H. Lee. Hierarchically designed 3D holey C_2N aerogels as bifunctional oxygen electrodes for flexible and rechargeable Zn-air batteries. *ACS Nano 12*, 596-608, **2017**.
[882]	X. Chen, J. Pu, X. Hu, Y. Yao, Y. Dou, J. Jiang, W. Zhang. Janus hollow nanofiber with bifunctional oxygen electrocatalyst for rechargeable Zn-air battery. *Small 18*, 2200578, **2022**.
[883]	Q. Zhou, S. Hou, Y. Cheng, R. Sun, W. Shen, R. Tian, J. Yang, H. Pang, L. Xu, K. Huang, Y. Tang. Interfacial engineering Co and MnO within N,S co-doped carbon hierarchical branched superstructures toward high-efficiency electrocatalytic oxygen reduction for robust Zn-air batteries. *Appl. Catal. B 295*, 120281, **2021**.
[884]	Y. Chen, S. Hu, F. Nichols, F. Bridges, S. Kan, T. He, Y. Zhang, S. Chen. Carbon aerogels with atomic dispersion of binary iron-cobalt sites as effective oxygen catalysts for flexible zinc-air batteries. *J. Mater. Chem. A 8*, 11649-11655, **2020**.
[885]	D. Yu, Y. Ma, F. Hu, C.C. Lin, L. Li, H.Y. Chen, X. Han, S. Peng. Dual-sites coordination engineering of single atom catalysts for flexible metal-air batteries. *Adv. Energy Mater. 11*, 2101242, **2021**.

[886]	Y. Jiang, Y.-P. Deng, J. Fu, D.U. Lee, R. Liang, Z.P. Cano, Y. Liu, Z. Bai, S. Hwang, L. Yang, D. Su, W. Chu, Z. Chen. Interpenetrating triphase cobalt-based nanocomposites as efficient bifunctional oxygen electrocatalysts for long-lasting rechargeable Zn-air batteries. *Adv. Energy Mater. 8*, 1702900, **2018**.
[887]	Z. Pei, Z. Yuan, C. Wang, S. Zhao, J. Fei, L. Wei, J. Chen, C. Wang, R. Qi, Z. Liu, Y. Chen. A flexible rechargeable zinc-air battery with excellent low-temperature adaptability. *Angew. Chem. Int. Ed. 59*, 4793-4799, **2020**.
[888]	L. Liu, X. Zhang, F. Yan, B. Geng, C. Zhu, Y. Chen. Self-supported N-doped CNT arrays for flexible Zn-air batteries. *J. Mater. Chem. A 8*, 18162-18172, **2020**.
[889]	Z. Xu, J. Zhu, J. Shao, Y. Xia, J. Tseng, C. Jiao, G. Ren, P. Liu, G. Li, R. Chen, S. Chen, F. Huang, H.-L. Wang. Atomically dispersed cobalt in core-shell carbon nanofiber membranes as super-flexible freestanding air-electrodes for wearable Zn-air batteries. *Energy Storage Mater. 47*, 365-375, **2022**.
[890]	W. Zang, A. Sumboja, Y. Ma, H. Zhang, Y. Wu, S. Wu, H. Wu, Z. Liu, C. Guan, J. Wang, S.J. Pennycook. Single Co atoms anchored in porous N-doped carbon for efficient zinc-air battery cathodes. *ACS Catal. 8*, 8961-8969, **2018**.
[891]	Q. Liu, X. Liu, Y. Xie, F. Sun, Z. Liang, L. Wang, H. Fu. N-doped carbon coating enhances the bifunctional oxygen reaction activity of CoFe nanoparticles for a highly stable Zn-air battery. *J. Mater. Chem. A 8*, 21189-21198, **2020**.
[892]	Y. Guo, J. Bae, Z. Fang, P. Li, F. Zhao, G. Yu. Hydrogels and hydrogel-derived materials for energy and water sustainability. *Chem. Rev. 120*, 7642-7707, **2020**.
[893]	M. Hua, S. Wu, Y. Ma, Y. Zhao, Z. Chen, I. Frenkel, J. Strzalka, H. Zhou, X. Zhu, X. He. Strong tough hydrogels via the synergy of freeze-casting and salting out. *Nature 590*, 594-599, **2021**.
[894]	Y.S. Zhang, A. Khademhosseini. Advances in engineering hydrogels. *Science 356*, 3627, **2017**.
[895]	Z. Song, J. Ding, B. Liu, X. Liu, X. Han, Y. Deng, W. Hu, C. Zhong. A rechargeable Zn-Air battery with high energy efficiency and long life enabled by a highly water-retentive gel electrolyte with reaction modifier. *Adv. Mater. 32*, 1908127, **2020**.
[896]	Y. Zhou, J. Pan, X. Ou, Q. Liu, Y. Hu, W. Li, R. Wu, J. Wen, F. Yan. CO_2 ionized poly(vinyl alcohol) electrolyte for CO_2-tolerant Zn-air batteries. *Adv. Energy Mater. 11*, 2102047, **2021**.
[897]	N. Zhao, F. Wu, Y. Xing, W. Qu, N. Chen, Y. Shang, M. Yan, Y. Li, L. Li, R. Chen. Flexible hydrogel electrolyte with superior mechanical properties based on poly (vinyl alcohol) and bacterial cellulose for the solid-state zinc-air batteries. *ACS Appl. Mater. Interfaces 11*, 15537-15542, **2019**.
[898]	Y. Hu, P. Shen, N. Zeng, L. Wang, D. Yan, L. Cui, K. Yang, C. Zhai. Hybrid hydrogel electrolyte based on metal-organic supermolecular self-assembly and polymer chemical cross-linking for rechargeable aqueous $Zn-MnO_2$ batteries. *ACS Appl. Mater. Interfaces 12*, 42285-42293, **2020**.
[899]	M.J. Tan, B. Li, P. Chee, X. Ge, Z. Liu, Y. Zong, X.J. Loh. Acrylamide-derived freestanding polymer gel electrolyte for flexible metal-air batteries. *J. Power Sources 400*, 566-571, **2018**.
[900]	D. Wang, H. Li, Z. Liu, Z. Tang, G. Liang, F. Mo, Q. Yang, L. Ma, C. Zhi. A Nanofibrillated, Cellulose/polyacrylamide electrolyte-based flexible and sewable high-performance $Zn-MnO_2$ battery with superior shear resistance. *Small 14*, 1803978, **2018**.
[901]	N. Ziv, A.N. Mondal, T. Weissbach, S. Holdcroft, D.R. Dekel. Effect of CO_2 on the properties of anion exchange membranes for fuel cell applications. *J. Membr. Sci. 586*, 140-150, **2019**.

[902]	W. Sun, V. Kupers, F. Wang, P. Bieker, M. Winter. A Non-Alkaline, Electrolyte for Electrically Rechargeable Zinc-air Batteries With Long-term Operation Stability In Ambient Air. *Angew. Chem. Int. Ed. 61*, 202207353, **2022**.
[903]	W. Xu, Y. Zhao, Z. Yuan, X. Li, H. Zhang, I.F.J. Vankelecom. Highly stable anion exchange membranes with internal cross-linking networks. *Adv. Funct. Mater. 25*, 2583-2589, **2015**.
[904]	M. Wang, N. Xu, J. Fu, Y. Liu, J. Qiao. High-performance binary cross-linked alkaline anion polymer electrolyte membranes for all-solid-state supercapacitors and flexible rechargeable zinc-air batteries. *J. Mater. Chem. A 7*, 11257-11264, **2019**.
[905]	N. Xu, Y. Zhang, M. Wang, X. Fan, T. Zhang, L. Peng, X.-D. Zhou, J. Qiao. High-performing rechargeable/flexible zinc-air batteries by coordinated hierarchical bi-metallic electrocatalyst and heterostructure anion exchange membrane. *Nano Energy 65*, 104021, **2019**.
[906]	J. Fu, J. Zhang, X. Song, H. Zarrin, X. Tian, J. Qiao, L. Rasen, K. Li, Z. Chen. A flexible solid-state electrolyte for wide-scale integration of rechargeable zinc-air batteries. *Energy Environ. Sci. 9*, 663-670, **2016**.
[907]	W. Wang, M. Tang, Z. Zheng, S. Chen. Alkaline polymer membrane-based ultrathin, flexible, and high-performance solid-state Zn-air battery. *Adv. Energy Mater. 9*, 1803628, **2019**.
[908]	H. Dou, M. Xu, Y. Zheng, Z. Li, G. Wen, Z. Zhang, L. Yang, Q. Ma, A. Yu, D. Luo, X. Wang, Z. Chen. Bioinspired tough solid-state electrolyte for flexible ultralong-life zinc-air battery. Adv. Mater. 34, 2110585, **2022**.
[909]	M. Yu, X. Ji, F. Ran. Chemically building interpenetrating polymeric networks of bi-crosslinked hydrogel macromolecules for membrane supercapacitors. *Carbohydr. Polym. 255*, 117346, **2021**.
[910]	H. Yan, X. Zhang, Z. Yang, M. Xia, C. Xu, Y. Liu, H. Yu, L. Zhang, J. Shu. Insight into the electrolyte strategies for aqueous zinc ion batteries. *Coord. Chem. Rev. 452*, 214297, **2022**.
[911]	Q. Liu, C. Xia, C. He, W. Guo, Z.P. Wu, Z. Li, Q. Zhao, B.Y. Xia. Dual-network structured hydrogel electrolytes engaged solid-state rechargeable Zn-air/iodide hybrid batteries. *Angew. Chem. Int. Ed. 61*, 202210567, **2022**.
[912]	C. Lai, H. Li, Y. Sheng, M. Zhou, W. Wang, M. Gong, K. Wang, K. Jiang. 3D spatial combination of CN vacancy-mediated NiFe-PBA with N-doped carbon nanofibers network toward free-standing bifunctional electrode for Zn-air batteries. *Adv. Sci. 9*, 2105925, **2022**.
[913]	L. Yang, L. Shi, D. Wang, Y. Lv, D. Cao. Single-atom cobalt electrocatalysts for foldable solid-state Zn-Air Battery. *Nano Energy 50*, 691-698, **2018**.
[914]	C. Zhu, Y. Ma, W. Zang, C. Guan, X. Liu, S.J. Pennycook, J. Wang, W. Huang. Conformal dispersed cobalt nanoparticles in hollow carbon nanotube arrays for flexible Zn-air and Al-air batteries. *Chem. Eng. J. 369*, 988-995, **2019**.
[915]	C. Gao, J. Wang, Y. Huang, Z. Li, J. Zhang, H. Kuang, S. Chen, Z. Nie, S. Huang, W. Li, Y. Li, S. Jin, Y. Pan, T. Long, J. Luo, H. Zhou, X. Wang. A high-performance free-standing Zn anode for flexible zinc-ion batteries. *Nanoscale 13*, 10100-10107, **2021**.
[916]	G. Chen, Z. Sang, J. Cheng, S. Tan, Z. Yi, X. Zhang, W. Si, Y. Yin, J. Liang, F. Hou. Reversible and homogenous zinc deposition enabled by in-situ grown Cu particles on expanded graphite for dendrite-free and flexible zinc metal anodes. *Energy Storage Mater. 50*, 589-597, **2022**.
[917]	Q. Guan, Y. Li, X. Bi, J. Yang, J. Zhou, X. Li, J. Cheng, Z. Wang, B. Wang, J. Lu. Dendrite-free flexible fiber-shaped Zn battery with long cycle life in water and air. *Adv. Energy Mater. 9*, 1901434, **2019**.

[918]	S. Qu, J. Liu, X. Han, Y. Deng, C. Zhong, W. Hu. Dynamic stretching-electroplating metal-coated textile for a flexible and stretchable zinc-air battery. *Carbon Energy*, **2022**.
[919]	Q. Yang, G. Liang, Y. Guo, Z. Liu, B. Yan, D. Wang, Z. Huang, X. Li, J. Fan, C. Zhi. Do zinc dendrites exist in neutral zinc batteries: a developed electrohealing strategy to in situ rescue in-service batteries. *Adv. Mater. 31*, 1903778, **2019**.
[920]	Y. He, Y. Cui, W. Shang, Z. Zhao, P. Tan. Insight into the bubble-induced overpotential towards high-rate charging of Zn-air batteries. *Chem. Eng. J. 448*, 137782, **2022**.
[921]	S.S. Shinde, J.Y. Jung, N.K. Wagh, C.H. Lee, D.-H. Kim, S.-H. Kim, S.U. Lee, J.- H. Lee. Ampere-hour-scale zinc-air pouch cells. *Nat. Energy 6*, 592-604, **2021**.
[922]	Q. Wang, Q. Feng, Y. Lei, S. Tang, L. Xu, Y. Xiong, G. Fang, Y. Wang, P. Yang, J. Liu, W. Liu, X. Xiong. Quasi-solid-state Zn-air batteries with an atomically dispersed cobalt electrocatalyst and organohydrogel electrolyte. *Nat. Commun. 13*, 3689, **2022**.
[923]	T. Zhou, H. Shan, H. Yu, C. Zhong, J. Ge, N. Zhang, W. Chu, W. Yan, Q. Xu, H. Wu, C. Wu, Y. Xie. Nanopore confinement of electrocatalysts optimizing triple transport for an ultrahigh-power-density zinc-air fuel cell with robust stability. *Adv. Mater. 32*, 2003251, **2020**.
[924]	Wenzheng, Li; Lukuan, Cheng; Xiaoyang, Chen; Youfa, Liu; Yao, Liu; Qingjiang, Liu; Yan, Huang. Key materials and structural design in flexible and stretchable zinc-air batteries. *Nano Energy 106*, 108039, **2023**. https://doi.org/10.1016/j.nanoen.2022.108039